



Concrete deterioration due to sulfide-bearing aggregates

Thèse

Andreia de Almeida Rodrigues

Doctorat interuniversitaire en sciences de la Terre
Philosophiae doctor (Ph.D.)

Québec, Canada

© Andreia de Almeida Rodrigues, 2016

Concrete deterioration due to sulfide-bearing aggregates

Thèse

Andreia de Almeida Rodrigues

Sous la direction de :

Josée Duchesne, directrice de recherche
Benoit Fournier, codirecteur de recherche

Résumé

Dans la région de Trois-Rivières (Québec, Canada), plus de 1 000 bâtiments résidentiels et commerciaux montrent de graves problèmes de détérioration du béton. Les problèmes de détérioration sont liés à l'oxydation des sulfures de fer incorporés dans le granulat utilisé pour la confection du béton.

Ce projet de doctorat vise à mieux comprendre les mécanismes responsables de la détérioration de béton incorporant des granulats contenant des sulfures de fer, et ce afin de développer une méthodologie pour évaluer efficacement la réactivité potentielle de ce type de granulats.

Un examen pétrographique détaillé de carottes de béton extraites de fondations résidentielles montrant différents degrés d'endommagement a été réalisé. Le granulat problématique contenant des sulfures de fer a été identifié comme un gabbro à hypersthène incorporant différentes proportions (selon les différentes localisations dans les deux carrières d'origine) de pyrrhotite, pyrite, chalcopyrite et pentlandite. Les produits de réaction secondaires observés dans les échantillons dégradés comprennent des formes minérales de "rouille", gypse, ettringite et thaumasite. Ces observations ont permis de déterminer qu'en présence d'eau et d'oxygène, la pyrrhotite s'oxyde pour former des oxyhydroxides de fer et de l'acide sulfurique qui provoquent une attaque aux sulfates dans le béton.

Tout d'abord, la fiabilité de l'approche chimique proposée dans la norme européenne NF EN 12 620, qui consiste à mesurer la teneur en soufre total (S_T , % en masse) dans le granulat pour détecter la présence (ou non) de sulfures de fer, a été évaluée de façon critique. Environ 50% (21/43) des granulats testés, représentant une variété de types de roches/lithologies, a montré une $S_T > 0,10\%$, montrant qu'une proportion importante de types de roches ne contient pas une quantité notable de soufre, qui, pour la plupart d'entre eux, sont susceptibles d'être inoffensifs dans le béton. Ces types de roches/granulats nécessiteraient toutefois d'autres tests pour identifier la présence potentielle de pyrrhotite compte tenu de la limite de S_T de 0,10 % proposée dans les normes européennes.

Basé sur une revue exhaustive de la littérature et de nombreuses analyses de laboratoire, un test accéléré d'expansion sur barres de mortier divisé en deux phases a ensuite été développé pour reproduire, en laboratoire, les mécanismes de détérioration observés à Trois-Rivières. Le test consiste en un conditionnement de 90 jours à 80°C/80% RH, avec 2 cycles de mouillage de trois heures chacun, par semaine, dans une solution d'hypochlorite de sodium (eau de javel) à 6% (Phase I), suivi d'une période pouvant atteindre 90 jours de conditionnement à 4°C/100 % HR (Phase II). Les granulats ayant un potentiel d'oxydation ont présenté une expansion de 0,10 % au cours de la Phase I, tandis que la formation potentielle de thaumasite est détectée par le regain rapide de l'expansion suivi par la destruction des échantillons durant la Phase II.

Un test de consommation d'oxygène a également été modifié à partir d'un test de Drainage Minier Acide, afin d'évaluer quantitativement le potentiel d'oxydation des sulfures de fer incorporés dans les granulats à béton. Cette technique mesure le taux de consommation d'oxygène dans la partie supérieure d'un cylindre fermé contenant une couche de matériau compacté afin de déterminer son potentiel d'oxydation. Des paramètres optimisés pour évaluer le potentiel d'oxydation des granulats comprennent une taille de particule inférieure à 150 µm, saturation à 40 %, un rapport de 10 cm d'épaisseur de granulat par 10 cm de dégagement et trois heures d'essai à 22°C. Les résultats obtenus montrent que le test est capable de discriminer les granulats contenant des sulfures de fer des granulats de contrôle (sans sulfures de fer) avec un seuil limite fixé à 5% d'oxygène consommé.

Finalement, un protocole d'évaluation capable d'estimer les effets néfastes potentiels des granulats à béton incorporant des sulfures de fer a été proposé. Le protocole est divisé en 3 grandes phases: (1) mesure de la teneur en soufre total, (2) évaluation de la consommation d'oxygène, et (3) un test accéléré d'expansion sur barres de mortier. Des limites provisoires sont proposées pour chaque phase du protocole, qui doivent être encore validées par la mise à l'essai d'un plus large éventail de granulats.

Abstract

In the Trois-Rivières area (Quebec, Canada), more than 1 000 houses and commercial buildings are showing serious concrete deterioration problems. The deterioration problems are related to the oxidation of sulfide-bearing aggregates used for concrete manufacturing.

This PhD project aims to better understand the mechanisms responsible for the deterioration of concrete incorporating sulfide-bearing aggregates in order to develop a methodology to efficiently evaluate the potential reactivity of such types of aggregates.

A detailed petrographic examination of core samples extracted from concrete house foundations showing various degrees of severity was carried out. The problematic aggregate was identified as an hypersthene's gabbro incorporating various proportions (according to different locations in the two originating quarries) of pyrrhotite, pyrite, chalcopyrite and pentlandite. Secondary reaction products observed in degraded core samples include “rust” mineral forms, gypsum, ettringite and thaumasite. For those observations, it was concluded that, in presence of water and oxygen, pyrrhotite oxidizes to form iron oxyhydroxides and sulfuric acid that provokes a sulfate attack in concrete.

First, the reliability of the chemical approach proposed in the European Standards NF EN 12 620, which consists in the measurement of the total sulfur content (S_T , % by mass) in the aggregate to detect the presence (or not) of iron sulfide minerals, was critically evaluated. About 50% (21/43) of the aggregate materials tested, representing a variety of rock types / lithologies, showed a $S_T > 0.10\%$, showing that a significant proportion of rock types does contain a noticeable amount of sulfide, which for most of them, are likely to be innocuous in concrete. Such rock types / aggregates would however require further testing to identify the potential presence of pyrrhotite considering the S_T limit of 0.10% proposed in European standards.

Based on extensive literature reviews and laboratory investigations, a two-phase accelerated mortar bar expansion test was then developed to reproduce, in the laboratory, the deterioration mechanisms observed on site. The test consists in 90 days of storage at 80°C/80% RH, with 2 three-hour wetting cycles per week in a 6% sodium hypochlorite

(bleach) solution (Phase I) followed by up to 90 days of storage at 4°C/100% RH (Phase II). Aggregates with oxidation potential presented an expansion over 0.10% during Phase 1, while thaumasite formation potential is detected by rapid regain of expansion followed by destruction of the samples during Phase II.

Also, an oxygen consumption test was modified from research carried out in the context of acid rock drainage, to quantitatively assess the sulfide oxidation potential of concrete aggregates. The technique measures the oxygen consumption rate at the top of a closed cylinder containing a layer of compacted material to determine its oxidation potential. Optimized testing parameters include an aggregate particle size inferior to 150 µm at 40% saturation, a ratio of 10 cm of aggregate material thickness for 10 cm headspace and 3 hours testing at 22°C. The results thus obtained showed that the test is able to discriminate the aggregates containing iron sulfide minerals from the control aggregates with a threshold limit fixed at 5% oxygen consumed.

Finally, an assessment protocol was proposed to evaluate the potential deleterious effects of iron sulfide bearing aggregates when used in concrete. The protocol is divided into 3 major phases: (1) total sulfur content measurement, (2) oxygen consumption evaluation, and (3) an accelerated mortar bar expansion test. Tentative limits are proposed for each phase of the protocol, which still need to be validated through the testing of a wider range of aggregates.

Table of contents

Résumé	iii
Abstract.....	v
Table of contents	vii
List of tables	xv
List of figures	xviii
List of abbreviations	xxiv
Acknowledgements	xxvii
Foreword.....	xxix
Chapter 1	1
Introduction	1
1.1 Problematic.....	1
1.2 Scope, objectives and impact of the investigation.....	4
1.3 Advancement and original contributions.....	5
1.4 Structure of the thesis	6
Chapter 2	8
Literature review.....	8
2.1 The iron sulfide minerals.....	8
2.1.1 Pyrrhotite	8
2.1.2 Pyrite.....	9
2.1.3 Chalcopyrite	9
2.1.4 Pentlandite	9
2.2 Iron sulfides oxidation reaction/process	10
2.2.1 Pyrrhotite oxidation reaction	10
2.2.2 Pyrite oxidation reaction.....	10
2.3 Deterioration process of concrete incorporating sulfide-bearing aggregates	11
2.4 Significant factors in the iron sulfides oxidation process.....	12
2.4.1 Oxygen and water.....	12
2.4.2 Bacteria's presence	13
2.4.3 Crystal structure.....	13
2.4.4 Specific surface area and morphology of the iron sulfide minerals	14
2.4.5 Temperature.....	14
2.4.6 pH system	15
2.4.7 Galvanic interactions between contacting/adjacent sulfide minerals	15

2.5 Deterioration products resulting from an internal sulfate attack due to sulfide-bearing aggregates	17
2.5.1 Gypsum.....	17
2.5.2 Ettringite	18
2.5.3 Thaumasite	18
2.6 Major documented cases of damaged concrete structures involving iron sulfides	20
2.6.1 Oslo, Norway (Moum and Rosenqvist, 1959; Hagelia et al., 2003).....	21
2.6.2 Ottawa, Canada (Quigley and Vogan, 1970).....	22
2.6.3 Ottawa, Canada (Penner et al., 1973)	23
2.6.4 Barcelona, Spain (Pardal, 1975; Vasquez and Toral, 1984; Chinchón et al., 1989, 1990 and 1995)	25
2.6.5 Montreal, Canada (Bérard et al., 1975)	26
2.6.6 Penge, South Africa (Oberholster and Krüger, 1984; Oberholster et al., 1984)	26
2.6.7 Australia, (Shayan, 1988)	27
2.6.8 Cornwall and Devon, England (DEC, 1991; Lugg and Probert, 1996).....	27
2.6.9 Lladorre, Spain (Ayora et al., 1998).....	28
2.6.10 Eastern Canada (Tagnit-Hamou et al., 2005)	29
2.6.11 Switzerland (Schmidt et al., 2011)	30
2.7 Tests involving oxidation of iron sulfide-bearing aggregates when used in concrete.....	31
2.7.1 Sweden (Hagerman and Roosaar, 1955)	31
2.7.2 Montreal (Canada) (Bérard et al., 1975).....	32
2.7.3 South Africa (Oberholster and Kruger, 1984)	33
2.7.4 Spain (Chinchón et al., 1990)	34
2.7.5 Cornwall and Devon, England (Lugg and Probert, 1995; RICS, 2005).....	34
2.7.6 Brazil (Gomides, 2009)	35
2.7.7 Switzerland (Schmidt et al., 2011)	37
2.7.8 Spain (Chinchón-Payá et al., 2012).....	37
2.8 The standardization state face to the problematic of iron sulfides	39
2.9 Research needs	40
Chapter 3	43
Ph.D. research program	43
3.1 General description.....	43
Chapter 4	46
Mineralogical and chemical assessment of concrete damaged by the oxidation of sulfide-bearing aggregates.....	46
4.1 Introduction	46

4.2 Résumé	46
4.3 Scientific publication no. 1	47
Mineralogical and chemical assessment of concrete damaged by the oxidation of sulfide-bearing aggregates: importance of thaumasite formation on reaction mechanisms...	47
4.3.1 Introduction	48
4.3.2 Research significance	50
4.3.3 Materials and methods.....	51
4.3.4. Results	52
4.3.5. Discussion.....	68
4.3.6. Conclusions	70
4.4 Acknowledgments	71
4.5 References	71
Chapter 5	74
Oxygen consumption test	74
5.1 Introduction	74
5.2 Résumé	74
5.3 Scientific publication no. 2.....	75
Quantitative assessment of the oxidation potential of sulfide-bearing aggregates in concrete using an oxygen consumption test	75
Abstract.....	75
5.3.1 Introduction	75
5.3.2. Objectives and Scope of Work	78
5.3.3. Materials and methods.....	78
5.3.4. Results and discussion.....	85
5.3.5. Conclusions	90
5.4 Acknowledgements	91
5.5 References	91
Chapter 6	95
Mortar bar expansion test for aggregates containing.....	95
sulfide-bearing aggregates.....	95
6.1 Introduction	95
6.2 Résumé	95
6.3 Scientific publication no. 3.....	96
A new accelerated mortar bar test to assess the potential deleterious effect of sulfide-bearing aggregates in concrete.	96
Abstract.....	96
6.3.1 Introduction	96

6.3.2 Scope and objective of work	106
6.3.3 Materials and methods.....	107
6.3.4. Results and discussion.....	111
6.3.5. Conclusions	131
6.4 Acknowledgements	133
6.5 References	133
Chapter 7	138
Protocol evaluation.....	138
7.1 Introduction	138
7.2 Résumé	138
7.3 Scientific publication no. 4.....	139
Evaluation protocol for concrete aggregates containing iron sulfide minerals	139
Abstract.....	139
7.3.1 Introduction	139
7.3.2 Research significance	144
7.3.3 Experimental investigation.....	144
7.3.4 Materials	146
7.3.5 Analytical procedure.....	148
7.3.6 Experimental results and discussion.....	151
7.3.7 Protocol for the performance evaluation of sulfide-bearing aggregates.....	159
7.3.8 Conclusions	161
7.4 Acknowledgments	161
7.5 References	162
Chapter 8	165
Conclusion and Recommendations	165
8.1 Conclusions	165
8.2 Recommendations	170
References	172
Appendix A	183
Oxygen consumption test for the quantitative assessment of the oxidation potential of sulfide-bearing aggregate in concrete.....	183
A1. Introduction	184
A.2 Preliminary oxygen consumption tests at (UQAT)	186
A.2.1 Plexiglas columns dimensions: 300 mm in height	186
A.2.2 Test conditions:.....	186

A.2.3 Tested aggregates: Maskimo, B&B, SBR, PKA	186
A.3 Preliminary oxygen consumption tests at Université Laval (Columns 200x147.4mm).....	189
A.3.1 Plexiglas columns dimensions.....	189
A.3.2 Test conditions:.....	189
A.3.4 Results	195
A.4 Preliminary oxygen consumption tests at Université Laval (Columns 300 x 200mm) ..	197
A.4.1 Plexiglas columns dimensions.....	197
A.4.2 Test conditions.....	197
A.4.3 Tested aggregates.....	197
A.4.4 Results	198
A.5. Oxygen consumption tests at Université Laval with optimized parameters	199
A.5.1 Plexiglas columns dimensions.....	199
A.5.2 Test conditions:.....	199
A.5.3 Tested aggregates.....	199
A.5.4 Results	201
A.5.5 Test reproducibility.....	201
Appendix B.....	203
Mortar bar expansion test	203
B1: Introduction.....	204
B2: Concrete core slices	204
B2.1 Test conditions:.....	204
B2.2 Storage conditions.....	204
B2.3 Measurements	205
B2.4 Concrete core slices stored at 4°C, 60% RH, with immersion (three times per week) in bleach (6%) solution.....	207
B2.5 Concrete core slices stored at 4°C, 80% RH, with immersion (three times per week) in bleach (6%) solution.....	208
0 days.....	208
7 days.....	208
26 days.....	208
26 days.....	208
61 days.....	208
61 days.....	208

B2.6 Concrete core slices stored at 4°C, 60% RH, with immersion (three times per week) in peroxide (3%) solution.	209
B2.7 Concrete core slices stored at 4°C, 80% RH, with immersion (three times per week) in peroxide (3%) solution.	210
B2.8 Concrete core slices stored at 4°C, non controlled RH, with immersion (three times per week) in peroxide (3%) solution.....	211
B2.9 Concrete core slices stored at 4°C, non controlled RH, with immersion (three times per week) in bleach (6%) solution.	212
B2.10 Concrete core slices stored at 21°C, 60% RH, with immersion (three times per week) in tap water.....	213
B2.11 Concrete core slices stored at 21°C, 80% RH, with immersion (three times per week) in tap water.....	214
B2.12 Concrete core slices stored at 21°C, non controlled RH, with immersion (three times per week) in tap water.....	215
B2.13 Concrete core slices stored at 21°C, 60% RH, with immersion (three times per week) in peroxide (3%) solution.	216
B2.14 Concrete core slices stored at 21°C, 60% RH, with immersion (three times per week) in bleach (6%) solution.....	217
B2.15 Concrete core slices stored at 21°C, 80% RH, with immersion (three times per week) in peroxide (3%) solution.	218
B2.16 Concrete core slices stored at 21°C, 80% RH, with immersion (three times per week) in bleach (6%) solution.....	219
B2.17 Concrete core slices stored at 21°C, non controlled RH, with immersion (three times per week) in peroxide (3%) solution.....	220
B2.18 Concrete core slices stored at 21°C, non controlled RH, with immersion (three times per week) in bleach (6%) solution.	221
B2.19 Concrete core slices stored at 38°C, 60% RH, with immersion (three times per week) in tap water.....	222
B2.21 Concrete core slices stored at 38°C, 60% RH, with immersion (three times per week) in bleach (6%) solution.....	224
B2.22 Concrete core slices stored at 38°C, 80% RH, with immersion (three times per week) in peroxide (3%) solution.	225
B2.23 Concrete core slices stored at 38°C, 80% RH, with immersion (three times per week) in bleach (6%) solution.....	226
B2.24 Concrete core slices stored at 38°C, non controlled RH, with immersion (three times per week) in tap water.....	227
B2.25 Concrete core slices stored at 38°C, non controlled RH, with immersion (three times per week) in peroxide (3%) solution.....	228
B2.26 Concrete core slices stored at 38°C, non controlled RH, with immersion (three times per week) in bleach (6%) solution.	229
B2.27 Concrete core slices stored at 60°C, 60% RH, with immersion (three times per week) in tap water.....	230
B2.28 Concrete core slices stored at 60°C, 60% RH, with immersion (three times per week) in peroxide (3%) solution.	231
B2.29 Concrete core slices stored at 60°C, 60% RH, with immersion (three times per week) in bleach (6%) solution.....	232

B2.30 Concrete core slices stored at 60°C, 80% RH, with immersion (three times per week) in tap water.....	233
B2.31 Concrete core slices stored at 60°C, 80% RH, with immersion (three times per week) in peroxide (3%) solution.	234
B2.32 Concrete core slices stored at 60°C, 80% RH, with immersion (three times per week) in bleach (6%) solution.....	235
B2.33 Concrete core slices stored at 60°C, non controlled RH, with immersion (three times per week) in tap water.....	236
B2.34 Concrete core slices stored at 60°C, non controlled RH, with immersion (three times per week) in peroxide (3%) solution.....	237
B2.35 Concrete core slices stored at 60°C, non controlled, with immersion (three times per week) in bleach (6%) solution.....	238
 B3: Mortar bars.....	 239
B3.1 Introduction.....	239
B3.2. Conditions tested.....	240
B3.3 Measurements	240
 B4 Preliminary tests: series 1	 240
B4.1 Test conditions:.....	240
B4.2 Aggregates tested:.....	240
B4.3 Storage conditions.....	240
B4.4 Results.....	242
 B5 Preliminary tests: series 2	 261
B5.1 Test conditions:.....	261
B5.2 Aggregates tested:.....	261
B5.3 Storage conditions.....	261
B5.4 Results.....	263
B5.4.2 Expansion as a function of time graphs (second series)	281
 B6 Preliminary tests: series 3	 285
B6.1 Test conditions:.....	285
B6.2 Aggregates tested:.....	285
B6.3 Storage conditions.....	285
B6.5 Results.....	287
 B7 Optimized test conditions	 314
B7.1 Test conditions:.....	314
B7.2 Aggregates tested:.....	314
B7.3 Storage conditions.....	314

B7.4 Results.....	315
Appendix C.....	324
Petrographic description of the rock facies from Maskimo and B&B of Saint-Boniface quarries.	324
C1: Introduction.....	325
C1.1 Rock facies classification: Maskimo quarry	326
C1.2 Rock facies classification: B&B quarry.....	331

List of tables

Chapter 2: Literature review

Table 2.1: Rest potential of some sulfide minerals (adapted from Kwong et al., 2003)	16
--	----

Chapter 5: Oxygen consumption test

Table 5.1: Aggregates mineralogy and total sulfur content.....	81
--	----

Table 5.2: Oxygen consumption values using MSK aggregate with a particle size <1.18mm.....	86
--	----

Table 5.3: Oxygen consumption values using different aggregate particle sizes (compacted ground material thickness of 5 cm at 40% saturation and a headspace of 15 cm).....	87
---	----

Table 5.4: Oxygen consumption and total sulfur values for nine different aggregates.....	89
--	----

Table 5.5: Oxygen consumption test results for material preparation performed by three different operators.....	90
---	----

Table 5.6: Oxygen consumption measured by three different probes.....	90
---	----

Chapter 6: Mortar bar expansion test for aggregates containing sulfidebearing aggregates

Table 6.1: Main properties of aggregates used in this study	108
---	-----

Table 6.2: Cement composition.....	109
------------------------------------	-----

Table 6.3: Expansion of mortar bars subjected to different periods of testing under the same conditions (80°C / 80% RH and 2 weekly cycles in bleach (6%) at 23°C).	116
---	-----

Table 6.4: Statistical values evaluating the reproducibility of the proposed test.	130
---	-----

Chapter 7: Protocol evaluation

Table 7.1: Aggregates used in the different tests and their respective mineralogy	147
---	-----

Table 7.2: Total sulfur values (S_T , % by mass) measured in Lab 1 for aggregate set 1.....	152
--	-----

Table 7.3: Total sulfur values (S_T , % by mass) for all the laboratories, and respective average, Standard deviation (SD) and Coefficient of variation (CV).	153
--	-----

Table 7.4: Oxygen consumption (%) and respective S_T (% by mass) values.....	155
--	-----

Appendix B: Mortar bar expansion test

Table B. 1: Mix design proportions and aggregate particle size.	239
--	-----

Table B. 2: Expansion values (%) of Set 1 (MSK1) mortar specimens stored at 60°C/60% RH, with immersion (twice per week) in bleach (6%) (Bl) or hydrogen peroxide (3%) (Px) solutions. Set 5 (MSK5) mortar specimens are stored at 60°C/60% RH, without immersion (no cycling).	242
--	-----

Table B. 3: Expansion values (%) of Set 2 (MSK2) mortar specimens stored at 60°C/60% RH, with immersion (twice per week) in bleach (6%) (Bl) solution.....	244
--	-----

Table B. 4: Expansion values (%) of Set 2 (MSK2) mortar specimens stored at 60°C/60% RH, with immersion (twice per week) in peroxide (3%) (Px) solution.....	247
--	-----

Table B.5: Expansion values (%) of Set 3 (MSK3) mortar specimens stored at 23°C/60% RH, with immersion (twice per week) in bleach (6%) (Bl) or hydrogen peroxide (3%) (Px) solutions.....	250
---	-----

Table B.6: Expansion values (%) of Set 4 (MSK4) mortar specimens stored at 60°C/80% RH, with immersion (twice per week) in bleach (6%) (Bl) or hydrogen peroxide (3%) (Px) solutions.....	252
---	-----

Table B.7: Expansion values (%) of Set 7 (MSK7) mortar specimens stored at 38°C/60% RH, with immersion (twice per week) in bleach (6%) (Bl) solution.....	255
---	-----

Table B.8: Expansion values (%) of Set 8 (HPL8) mortar specimens stored at 60°C/60% RH, while pursuing the immersion (twice per week) in bleach (6%) (Bl) or hydrogen peroxide (3%) (Px). Set 9 (HPL9): mortar specimens stored at 60°C/60% RH without immersion (no cycling). Set 10 (HPL10): mortar specimens stored at 8°C/60% RH without immersion (no cycling).	256
---	-----

Table B. 9: Expansion values (%) of Set 1 (MSK1) mortar specimens stored at 60°C/80% RH, with immersion (twice per week) in bleach (6%) (Bl) solution.....	263
--	-----

Table B. 10: Expansion values (%) of Set 2 (MSK2) mortar specimens stored at 60°C/80% RH, with immersion (once per week) in bleach (6%) (Bl) solution.....	266
--	-----

Table B.11: Expansion values (%) of Set 3 (MSK3) mortar specimens stored at 80°C/80% RH, with immersion (twice per week) in bleach (Bl) (6%) solution.....	268
--	-----

Table B.12: Expansion values (%) of Set 4 (PKA1) mortar specimens stored at 60°C/80% RH, with immersion (twice per week) in bleach (Bl) (6%) solution.....	270
Table B.13: Expansion values (%) of Set 5 (SBR1) mortar specimens stored at 60°C/80% RH, without immersion (no cycling) or with immersion (twice per week) in bleach (6%) solution.....	273
Table B.14: Expansion values (%) of Set 6 (PKA2) mortar specimens stored at 80°C/80% RH, without immersion (no cycling) or with immersion (twice per week) in bleach (6%) solution.....	276
Table B.15: Expansion values (%) of Set 7 (SBR2) mortar specimens stored at 80°C/80% RH, without immersion (no cycling) or with immersion (twice per week) in bleach (6%) solution.....	279
Table B.16: Expansion values (%) of Set 1 (MSK) mortar specimens stored at 80°C/80% RH, with immersion (once or twice per week) in bleach (Bl) (6%) solution.	287
Table B.17: Expansion values (%) of Set 2 (GGP) mortar specimens stored at 80°C/80% RH, with immersion (once or twice per week) in bleach (Bl) (6%) solution.	295
Table B.18: Expansion values (%) of Set 3 (HPL) mortar specimens stored at 80°C/80% RH with immersion (twice per week) in bleach (Bl) (6%) solution.....	304
Table B. 19: Expansion values (%) of Set 4 PKA mortar specimens stored at 80°C/80% RH with immersion (twice per week) in bleach (Bl) (6%) solution.....	307
Table B. 20: Expansion values (%) of Set 5 SBR mortar specimens stored at 80°C/80% RH with immersion (twice per week) in tap water (Tw) (6%) solution.....	309
Table B.21: Expansion values (%) of mortar specimens stored at 80°C/80% RH, with immersion (twice per week) in bleach (6%) solution.....	315

List of figures

Chapter 1: Introduction

Figure 1.1: A: Concrete foundations showing map-cracking and yellowish / brownish discoloration. B: Cracks filled with caulking material to prevent moisture ingress. C and D: Yellowish and brownish discoloration surrounding the cracks. E and F: Pop-outs showing the presence of oxidized and rusted aggregate particles, as well as whitish/yellowish secondary reaction products. 2

Figure 1. 2: Replacement of the concrete house foundations walls. A: Lifted house with all the brick work removed. B: New foundations being built. 3

Chapter 3: Ph.D. research program

Figure 3.1 Phases of the Ph.D. project «Concrete deterioration incorporating sulfide-bearing aggregates». 43

Chapter 4: Mineralogical and chemical assessment of concrete damaged by the oxidation of sulfide-bearing aggregates

Figure 4. 1: Cracking in housing concrete foundation. Cracks were filled up with sealant materials to prevent water and moisture infiltration..... 52

Figure 4. 2: Features of concrete deterioration. 53

Figure 4. 3Replacement of the concrete foundation walls. 54

Figure 4. 4: Photomicrographs of thin sections of the anorthositic gabbro..... 55

Figure 4. 5: Reflected polarized light views of iron sulfide minerals included in the anorthositic gabbro.. 56

Figure 4. 7: Photomicrographs of thin sections viewed under plane polarized light of the small layer of carbonate mineral surrounding or “coating” the sulfide minerals 58

Figure 4. 8: X-ray microprobe mapping of a sulfide-bearing aggregate particle in the anorthositic gabbro. 59

Figure 4. 9: Broken concrete core sample taken from a deteriorated foundation. Several coarse aggregates are covered with rust. 60

Figure 4. 10: A and B) Stereomicroscopic views of deteriorated polished concrete core with partially disintegrated aggregate particles showing important cracks through the particle and extending into the cement paste.....	61
Figure 4. 11: Overall and stereomicroscopic views of deteriorated concrete foundation block (A) and core (B). A) Aggregate particle covered with iron oxy-hydroxide and surrounded by a whitish halo. B) Crack through an oxidized particle extending into the cement paste.	62
Figure 4. 12: Secondary electron images of ettringite covering the cement paste at the vicinity of sulfide-bearing aggregate particles, with corresponding EDS spectra.	63
Figure 4. 13: Secondary electron images of gypsum observed on broken surfaces of the cement paste surrounding sulfide-bearing aggregate particles, with corresponding EDS spectra.	64
Figure 4. 14: Secondary electron images of thaumasite observed in the cement paste adjacent to sulfide-bearing aggregate particles, with corresponding EDS spectra.....	65
Figure 4. 15: X-ray diffraction pattern of thaumasite/ettringite phases. Sample obtained from whitish haloes surrounding reacted sulfide-bearing aggregate particles.	66
Figure 4. 16: Secondary electron images of iron oxy-hydroxide observed on/next to sulfide-bearing aggregate particles, with corresponding EDS spectra.	67
Figure 4. 17: Back-scattered electron images of thaumasite (T) and gypsum (G) (figures A and B) with corresponding EDS spectra.	68

Chapter 5: Oxygen consumption test

Figure 5. 1: Columns used in the oxygen consumption test.....	83
---	----

Chapter 6: Mortar bar expansion test for aggregates containing sulfide-bearing aggregates

Figure 6. 1: Test conditions of the experimental program flowchart.	110
Figure 6.2: Expansion of mortar specimens stored at 60°C/60% RH, without (no cycling) or with immersion (twice per week) in bleach (6%) or hydrogen peroxide (3%) solutions. HPL is a control sample while MSK is a sample with sulfide-bearing aggregate.....	112
Figure 6.3: Expansion of mortar bars subjected to one or two 3-h immersion period(s) in bleach per week and stored at 80°C and 80% RH the remaining time.	113

Figure 6. 4: Expansion of mortars stored at 60% RH or 80% RH at a temperature of 60°C (MSK aggregate).....	114
Figure 6. 5: Expansion of mortar bars subjected to 80% RH but at different temperatures (2 weekly wetting cycles in bleach).....	115
Figure 6.6: Expansion of companion sets of mortars specimens either kept continuously at 80°C and 80%RH or transferred at 4°C and 80% RH at 90 days.....	118
Figure 6.7: Expansion of mortar bars kept for 90 days at 80°C/80% RH and then transferred to 4°C at 80% or 100% RH, for MSK and GGP sulfide-bearing aggregates.....	120
Figure 6. 8: Expansion of mortar bars kept at 80°C and 80% RH for 90 days and then transferred to 4°C and 80% RH maintaining or not the 2 weekly wetting cycles in 6% bleach solution during the low temperature regime..	121
Figure 6.9: Expansion of mortar bars kept at 80°C and 80% RH for 90 days and then transferred to 4°C and 80% RH with immersion (twice per week) in bleach (6%) solution..	122
Figure 6.10: A: Mortar bar made with MSK aggregate at 90 days before being transferred to low temperature. B and C: Deterioration details of mortar bars at 90 days. D: the same bar at 300 days (i.e. after 210 days at 4°C). E and F: Deterioration details of mortar bars at 300 days.....	123
Figure 6.11: A: MSK mortar bars kept at 80°C/80% RH and then transferred at 4°C/80% RH immediately after rupture at 118 days. B: The same mortar bar series left at 4°C/80% RH for 7 months. The M3-5 bar illustrated in A is the one in the middle of the container.	124
Figure 6.12: A: Mortar bar made with SBR aggregate at 90 days (expansion of 1.31%) before being transferred to low temperature; B and C: Deterioration details of mortar bars at 90 days.	125
Figure 6.13: Mortar bar made with PKA aggregate at 90 days, showing no signs of deterioration for the entire duration of the test. B and C: Deterioration details of mortar bars at 180 days.	125
Figure 6.14: Secondary electron images of the different reaction products observed in the mortar bars and corresponding EDS spectra. A, B: iron oxy/hydroxide; C, D: iron sulfate.	126
Figure 6. 15: Secondary electron images of the different reaction products observed in the mortar bars and corresponding EDS spectra. A, B: ettringite; C, D: ettringite-thaumasite solid solution;	127

Figure 6. 16 Secondary electron images of the general composition of a PKA sample. ... 128

Figure 6. 17: Expansion against time for three sets of mortar bars tested in the same conditions (80°C/80% RH) in order to evaluate the reproducibility at Phase I of the test proposed. 129

Figure 6. 18: Expansion of mortar bars made with MSK aggregate kept at 80°C/80% RH in a temperature and humidity controlled cabinet or in hermetic container with super-saturated salt solution to maintain humidity conditions kept in a oven..... 131

Chapter 7: Protocol evaluation

Figure 7.1: Typical signs of deterioration observed in residential buildings containing iron sulfide-bearing aggregates in the Trois-Rivières area..... 140

Figure 7.2: Typical replacement process of residential concrete foundations in the Trois-Rivières area. A: Stone and brick facing removed. B. Demolition of the concrete foundation. C. House lifted. D. Pouring of new concrete foundation. 141

Figure 7.3: Proposed protocol for determining the potential reactivity of iron sulfide bearing aggregates. 145

Figure 7.4: Procedures for samples preparation schema for the total sulfur (S_T) determination. 149

Figure 7.5: Consumed oxygen (moles/m²/year) for MSK, B&B, GGP, SBR and PKA aggregates using 5cm ground material thickness, 15 cm headspace and 40% degree of saturation. 154

Figure 7.6: Expansion of companion sets of mortars specimens either kept continuously at 80°C [176°F] and 80% RH or transferred at 4°C [39.2°F] and 100% RH at 90 days. 157

Figure 7.7: Expansion of mortar bars subjected to two 3-hour wetting periods in bleach (6%) per week, and kept at 80°C [176°F] /80%RH during 90 days. The bars are transferred after that period to 4°C [39.2°F] /100% RH and exposed to the two 3-hour soaking in bleach per week..... 158

Figure 7.8: Visual condition of mortar bars incorporating the MSK and PKA aggregates during and at the end of the expansion test. 158

Appendix B: Mortar bar expansion test

Figure B.1: Experimental program flowchart - testing conditions for the concrete cores slices. 206

Figure B.2: Experimental program flowchart - testing conditions for the first series.....	241
Figure B.3: Expansion values (%) of Set 1 (MSK1) mortar specimens stored at 60°C/60% RH, with immersion (twice per week) in bleach (6%) (Bl) or hydrogen peroxide (3%) (Px) solutions. Set 5 (MSK5) mortar specimens are stored at 60°C/60% RH, without immersion (no cycling).....	258
Figure B.4: Expansion values (%) of Set 1 (MSK1) mortar specimens stored at 60°C/60% RH, with immersion (twice per week) in bleach (6%) (Bl) or hydrogen peroxide (3%) (Px) solutions. Set 5 (MSK5) mortar specimens are stored at 60°C/60% RH, without immersion (no cycling).....	258
Figure B.5: Expansion values (%) of Set 3 (MSK3) mortar specimens stored at 23°C/60% RH, with immersion (twice per week) in bleach (6%) (Bl) or hydrogen peroxide (3%) (Px) solutions.....	259
Figure B. 6: Expansion values (%) of Set 4 (MSK4) mortar specimens stored at 60°C/80% RH, with immersion (twice per week) in bleach (6%) (Bl) or hydrogen peroxide (3%) (Px) solutions.....	259
Figure B. 7: Expansion values (%) of Set 7 (MSK7) mortar specimens stored at 38°C/60% RH, with immersion (twice per week) in bleach (6%) (Bl) solution.....	260
Figure B.8: Expansion values (%) of Set 8 (HPL8) mortar specimens stored at 60°C/60% RH, while pursuing the immersion (twice per week) in bleach (6%) (Bl) or hydrogen peroxide (3%) (Px). Set 9 (HPL9): mortar specimens stored at 60°C/60% RH without immersion (no cycling). Set 10 (HPL10): mortar specimens stored at 8°C/60% RH without immersion (no cycling).	260
Figure B.9: Experimental program flowchart - testing conditions for the second series. .	262
Figure B. 10: Expansion values (%) of Set 1 (MSK1) mortar specimens stored at 60°C/80% RH, with immersion (twice per week) in bleach (6%) (Bl) solution.....	281
Figure B.11: Expansion values (%) of Set 2 (MSK2) mortar specimens stored at 60°C/80% RH, with immersion (once per week) in bleach (6%) (Bl) solution.	282
Figure B.12: Expansion values (%) of Set 3 (MSK3) mortar specimens stored at 80°C/80% RH, with immersion (twice per week) in bleach (Bl) (6%) solution.....	282
Figure B.13: Expansion values (%) of Set 4 (PKA1) mortar specimens stored at 60°C/80% RH, with immersion (twice per week) in bleach (Bl) (6%) solution.....	283
Figure B.14: Expansion values (%) of Set 5 (SBR1) mortar specimens stored at 60°C/80% RH, without immersion (no cycling) or with immersion (twice per week) in bleach (6%) solution.....	283

Figure B.15: Expansion values (%) of Set 6 (PKA2) mortar specimens stored at 80°C/80% RH, without immersion (no cycling) or with immersion (twice per week) in bleach (6%) solution.....	284
Figure B. 16: Expansion values (%) of Set 7 (SBR2) mortar specimens stored at 80°C/80% RH, without immersion (no cycling) or with immersion (twice per week) in bleach (6%) solution.....	284
Figure B.17: Experimental program flowchart - testing conditions for the third series....	286
Figure B.18: Expansion values (%) of Set 1 (MSK) mortar specimens stored at 80°C/80% RH, with immersion (once or twice per week) in bleach (Bl) (6%) solution. .	311
Figure B.19: Expansion values (%) of Set 2 (GGP) mortar specimens stored at 80°C/80% RH, with immersion (once or twice per week) in bleach (Bl) (6%) solution. .	311
Figure B.20: Expansion values (%) of Set 3 (HPL) mortar specimens stored at 80°C/80% RH with immersion (twice per week) in bleach (Bl) (6%) solution.	312
Figure B.21: Expansion values (%) of Set 4 PKA mortar specimens stored at 80°C/80% RH with immersion (twice per week) in bleach (Bl) (6%) solution.....	312
Figure B.22: Expansion values (%) of Set 5 SBR mortar specimens stored at 80°C/80% RH with immersion (twice per week) in tap water (Tw) (6%) solution.	313
Figure B.23: Expansion of mortar specimens stored at 80°C/80% RH, with immersion (twice per week) in bleach (6%) solution.....	321
Figure B.24: Mortar bars B&B riche after 90 days at 80°C/80%HR and two weekly wet and dry cycles.....	322
Figure B.25: Mortar bars B&B riche at 300 days of testing.	322
Figure B. 26: Mortar bars B&B riche after 438 days of testing.	323
Figure B. 27: Mortar bars B&B riche after 90 days at 80°C/80%HR and two weekly wet and dry cycles	323

List of abbreviations

AAR: alkali-aggregate reaction
AMBT: accelerated mortar bar test
ARD: acid rock drainage
Bio: biotite
Bl: bleach - sodium hypochlorite
BSE: back-scattered electron
Ca: concentration of oxygen in air
Carb: carbonate minerals
Chalco: chalcopyrite
C-S-H: Calcium silicate hydrate
CV: coefficient of variation
Cw: concentration of O₂ in water
DEF: delayed ettringite formation
Eh: redox potential
EPMA: electron probe micro analyser
Ett: ettringite
G: gypsum
Gs: specific gravity
KOH: Potassium hydroxide
M: molar
nc: without immersion
ϕ: particle size
Opc:(opaque): sulfide minerals
Pent: pentlandite
Plg: plagioclase feldspar
Po: pyrrhotite

Px: hydrogen peroxide

Py: pyrite

Pyrx: pyroxene

RH: relative humidity

SEM/EDS: Scanning electron microscopy/Energy-dispersive spectroscopy

SHE/V: Standard hydrogen electrode/ Volt

Sid: siderite

S_T: total sulfur content, in percentage by mass

T: thaumasite

TSA: Thaumasite sulfate attack

Tw: Tap water

w/c: water:cement ratio

XRD: X-ray diffraction

n_{gm}: porosity within the ground material (%) ;

V_{gm} : total volume occupied by the ground material (cm³);

ρ_{agg} :volumetric mass density of the aggregate ;

S_{gm}:degree of saturation (%) of the ground material;

ρ_w :density of water (g/cm³)

*To my brother Tiago for sharing with me all the good and bad moments of my life
and to my niece Tânia, for make me smile even in sad moments.*

*To Catarina, my friend of all times, thank you for always having been there, there are
no words to express my gratitude*

Acknowledgements

It is a great pleasure to address those people who helped me throughout this PhDs project to enhance my knowledge and my practical skills.

My deepest gratitude goes to my supervisor, Josée Duchesne and my co-supervisor Benoît Fournier. The continuous guidance, support, encouragement and patience of them enabled me to approach work positively.

I would also like to express my gratitude to all the partners of this project Benoit Durand, Methat Sheatha and Patrice Rivard for all the support, and the good discussions and shared ideas during our meetings.

I wish to acknowledge the Natural Sciences and Engineering Research Council of Canada (NSERC) for their collaborative research and development grant and all partners (ABQ, ACC, ACRGTQ, APCHQ, Garantie qualité habitation, ACQ, Inspec-sol inc., LVM, RBQ, Exp. Inc., SHQ, Ville de Québec, Ville de Montréal, Hydro-Québec, MTQ, Qualitas).

I want to tank you Bruno Bussière and Olivier Peyronnard from UQAT who shared their expertise and knowledge in the use of oxygen consumption test.

I wish also to tank FCT-Fundação para a Ciência e Tecnologia, Portugal, for my Ph.D. Grant Ref.: SFRH/BD/71203/2010.

A especial thak you to Isabel Fernandes, for being the link between me and Josée Duchesne and Benoît Fournier that allowed me to participate in this project.

I would like to express my gratitude to all the friends, colleagues and trainees ‘La gang du béton’ that had contribute in some way this project (helping, disturbing, annoying): Julie Francoeur, Steve Goyette, Leandro Sanchez, Anthony Allard, Mathieu Turcotte-Robitaille, Charles Lafrenière, Charles-Frédéric Amringer, Alejandra Bustamante Pierre-Luc Fecteau, Sean Beauchemin, Mathieu Labarre, Celestin Fortier, Cédric Drolet, Hubert

Michaud, Roxanne Tremblay, Alexandre Rodrigue, Benoit Mcfaydyen, Marc-André-Gingras, Jean-Benoit Darveau and Isabelle Fily-Paré.

I wish to express my special thanks to Sofie Tremblay, Martin Plante, André Ferland, Marc Choquette, Jean Frenette, Éric David, Edmond Rousseau and Vicky Dodier for the guidance, expertise and the help with the analysis, experiences that had make this project succeed.

An especial thank you to Diana Oliveira, Leandro Sanchez, Maxime Morneau-Pereira and more recently Ian Sanchez, Luciana Garcia, Carla Pozer and Jérôme Imbeault for having received me in Quebec, and for your indispensable friendship.

Thanks to all my friends and family, especially Catarina Almeida, Cristina Almeida, Sandra Rodrigues, Claudia Medeiros, Carla Ribeiro, Pedro Preto, José Miguel Coutinho, Joana Filipe, Violeta Ramos, and all the others (that I certainly forget) for their help and support.

Finally I want to thanks to my mom, for having shown me the meaning of sharing, humility and the importance of studying.

Thank you.

Foreword

The present PhD thesis was elaborated in the context of the project "Study of the concrete deterioration in the presence of sulfide-bearing aggregates".

The body of this thesis is divided into eight chapters. Chapter 1 presents an introduction to the problematic evidenced in this work, the objectives and original contributions. Chapter 2 consists in an extensive literature review and the standardization state regarding the subject of the thesis. Chapter 3 is a summary of the thesis research program.

The Chapters 4 to 7 are the core of the thesis, that is composed of 4 papers published (papers 1, 2, 3) or accepted (paper 4) to international scientific journals with referees. These four papers represent also the evolution of the thesis. In each one of these papers I'm the main author and Josée Duchesne and Benoit Fournier, director and co-director of this thesis, respectively, are co-authors. In the first paper (Chapter 4) and fourth paper (Chapter 7) Benoit Durand (researcher at the Research Institute of Hydro-Québec), Medhat H. Shehata (Professor in the Department of Civil Engineering at Ryerson University) and Patrice Rivard (Professor of civil engineering at the Université de Sherbrooke) are also co-authors.

Chapter 8 includes some final conclusions as well as several recommendations for further research that were also done or supervised by me.

As the author of this thesis I collected the concrete and aggregate samples in the field, excluding the aggregate samples provided from the Quebec aggregate producers (RPPG). The tests performed during each step of this thesis were performed or supervised by myself. Samples preparation, such as gridding, crushing, and milling was done or supervised by me. All the SEM analyses, petrographic analysis at polarizing microscope and stereomicroscope were performed by me as well.

The papers incorporated in this thesis were written entirely or partially by me. Each one of the co-authors has revised all the papers. Graphics, SEM/EDS pictures and graphics,

aggregate photos were produced by me. The photos presented were taken by me or by my supervisors. The analysis of the data produced in this project as drawing of conclusions were performed and achieved by me with my supervisor's collaboration.

The following papers are part of this thesis:

Rodrigues, A., Duchesne, J., Fournier, B., Durand, B., Rivard, P., Shehata, M., "Mineralogical and chemical assessment of concrete damaged by the oxidation of sulfide-bearing aggregates: Importance of thaumasite formation on reaction mechanisms," *Cement and Concrete Research*, V.42, 2012, pp. 1336–1347.

Rodrigues, A., Duchesne, J., Fournier, B., "Quantitative assessment of the oxidation potential of sulfide-bearing aggregates in concrete using an oxygen consumption test," submitted to *Cement and Concrete Composites*.

Rodrigues, A., Duchesne, J., Fournier, B., "A new accelerated mortar bar test to assess the potential deleterious effect of sulfide-bearing aggregates in concrete," *Cement and Concrete Research*, V.73, 2015, pp. 96-110.

Rodrigues, A., Duchesne, J., Fournier, B., Durand, B., Shehata, M., Rivard, P., "Evaluation protocol for concrete aggregates containing iron sulfide minerals," submitted to *ACI Materials Journal*.

The following articles were published during this research program. Although these publications focus on the results obtained in this study, they are not part of this thesis in order to avoid repetition and maintain a logical order in the results presentation.

Rodrigues, A., Duchesne, J., Fournier, B., "Microscopic analysis of the iron sulfide oxidation products used in concrete aggregates," 34th International Conference on Cement Microscopy, 2012, Halle-Saale, Germany.

Rodrigues, A., Duchesne, J., Fournier, B., "Petrographic characterization of the deterioration products of a concrete containing sulfide bearing aggregates; a particular case of internal sulfate attack" 35th International Conference on Cement Microscopy, 2013, Chicago, USA.

Rodrigues A., Duchesne J., Fournier B., “Damage evaluation of two different concrete mix designs containing sulfide-bearing aggregates” 36th International Conference on Cement Microscopy, 2014, Milan, Italy.

Chapter 1

Introduction

1.1 Problematic

In the Trois-Rivières area (Quebec, Canada), more than 1 000 houses and commercial buildings are showing serious concrete deterioration problems. A large number of those house foundations were constructed between 2004 and 2008 and started to show signs of deterioration 3 to 5 years after construction. Recent reports show that some house foundations that were built 15 years ago started to show signs of deterioration.

The signs of concrete deterioration observed in the foundations mainly consist of map-cracking (Fig.1.1A), with some crack openings reaching more than 40 mm. Sometimes, those cracks had been filled with caulking material in order to prevent the moisture to penetrate into the concrete already damaged in an attempt to delay the progress of deterioration (Fig.1.1B). Yellowish and brownish discoloration is often observed surrounding these cracks (Fig.1.1C and D). Pop-outs can be observed on the walls showing the presence of oxidized and rusted aggregate particles (Fig. 1.1E and F). It is also possible to observe small bumps that represent localised sites of expansion and that can be easily detached from the surface thus showing oxidized and rusted aggregate particles. The problematic concrete has a very porous and friable paste and, in many cases, it is possible to observe the breakdown and disintegration of concrete.

In some cases, the deterioration is such that the concrete foundation/element has to be replaced according to the provincial Guarantee Plan for new Residential Buildings (2015) (Fig.1.2)



Figure 1.1: A: Concrete foundations showing map-cracking and yellowish / brownish discoloration. B: Cracks filled with caulking material to prevent moisture ingress. C and D: Yellowish and brownish discoloration surrounding the cracks. E and F: Pop-outs showing the presence of oxidized and rusted aggregate particles, as well as whitish/yellowish secondary reaction products.

A



B



Figure 1. 2: Replacement of the concrete house foundations walls. A: Lifted house with all the brick work removed. B: New foundations being built.

The deterioration problems are related to the coarse aggregate used in the concrete. That coarse aggregate is an intrusive igneous rock consisting of different facies, including a norite or hypersthene's gabbro (plagioclase, pyroxene and biotite) and a garnet's gabbro (plagioclase, pyroxene, biotite and garnet), that contain various proportions of sulfide minerals. The sulfide minerals were mainly pyrrhotite, pyrite, pentlandite and chalcopyrite, disseminated or in veins. The contents of iron sulfides vary from one particle to another, the average being between 2 and 5%; however, some aggregate particles show a sulfide concentration greater than 50%.

The signs of concrete deterioration suggest a case of damage due to the oxidation of iron sulfides (abundance of rust on the fractured surfaces of aggregates) followed by an internal sulfate attack of the concrete.

The chemical reactions that lead to the oxidation of iron sulfides and, in turn, to sulfate attack of the concrete are described in **Chapter 2**, sections 2.2 and 2.3. The main factors influencing the reaction are: temperature, humidity, pH of the system, specific surface area and morphology of the iron sulfides, and the galvanic interactions among contacting sulfides. Some other cases of concrete deterioration due to sulfide bearing aggregates are mentioned in the literature revue (**Chapter 2**), mainly in black shales, schists or sedimentary rocks, known as being porous and mechanically weak (Chinchón et al., 1995; Lugg and Probert, 1996; Schmidt et al., 2011; Moum and Rosenqvist, 1959). A

case using the same kind of rock (gray anorthosite with some amounts of sulfides) was reported by Tagnit-Hamou and coworkers in 2005.

In summary, although the Canadian concrete standards and several publications have identified the risks incurred by the use of sulfide-bearing aggregates in concrete, many questions remain unanswered. The petrographic evidences of concrete deterioration due to such aggregates are well known, but to date no study was able to reproduce the expansion and deterioration of such concretes under laboratory conditions. This lack of understanding of the phenomena, or of the various factors/conditions influencing the deterioration process, is the main reason for the absence of specific guidelines, in the Quebec and Canadian standards, for the evaluation of the deleterious character of sulfide-bearing aggregates for use in concrete infrastructures construction.

1.2 Scope, objectives and impact of the investigation

Regarding the exposed problem, this project seeks globally to better understand the deterioration process in concrete incorporating sulfide-bearing aggregates in the Trois-Rivières area, in order to develop a methodology to efficiently evaluate the potential reactivity of such types of aggregates. This will be done through the following specific objectives:

- assess the mineralogical, chemical and mechanical properties of damaged concretes containing sulfide-bearing aggregates;
- from the above observations, identify and propose the mechanism(s) responsible for concrete deterioration;
- reproduce the deterioration process under laboratory conditions.

This work should contribute significantly to:

- the development of a global evaluation protocol to predict the deleterious potential of aggregates containing iron sulfides, including a performance test or expansion test that can reproduce, under well controlled and reproducible laboratory conditions, the mechanisms responsible for the concrete deterioration and that will enable the identification of problematic aggregates.

- provide recommendations for a global evaluation protocol that can be included in the CSA A23.1/A23.2 standard and / or in the NQ 2621 - 900 BNQ standard (Bureau de normalization du Québec) to control the use of such aggregates in concrete.

1.3 Advancement and original contributions

As documented in the literature, several cases of deterioration of concrete incorporating iron sulfides-bearing aggregates have been documented in recent decades. In the cases analyzed, problematic aggregates consisted mainly of limestone and shales, rocks that are porous and mechanically weak (Bérard et al., 1975; Chinchón et al., 1995; Casanova et al., 1996; Ayora et al., 1998). In the case of the damage observed in the Trois-Rivières area, the rock used is a massive rock. The only case where a similar kind of rock was studied was reported by Tagnit-Hamou and coworkers (2005).

Throughout the published literature, attempts to recreate the mechanisms responsible for the concrete damage due to the oxidation of iron sulfides have unfortunately not been successful (Bérard et al., 1975; Chinchón et al., 1989; Le Roux et al., 2001; Bellaloui et al., 2002) and no test on this type of rock has been developed.

Understanding the origin of the concrete deterioration and the processes of iron sulfides oxidation and internal sulfate attack of concrete is necessary for the development of a test that can reproduce and predict this phenomenon. So far, there is no performance test that can “quantitatively” predict whether the aggregates that contain iron sulfides are harmless or potentially reactive. The iron sulfides analyzed in this case are mainly pyrrhotite and pyrite, the most common iron sulfides in all types of rocks. The development of a reliable and reproducible performance test is therefore essential to ensure that the problem occurring at Trois-Rivières region (Québec, Canada) and elsewhere in the world would not occur again.

This evaluation protocol intended to prevent the use of reactive aggregates in concrete and, as a result, avoid unnecessary spending of millions of dollars in repairs and replacements of the damaged structures.

1.4 Structure of the thesis

The body of this thesis is divided into eight chapters. **Chapter 1** presents an introduction to the problematic to which this work is devoted, the scope of the work, the advancement and original contributions. **Chapter 2** consists of an extensive literature review on the following topics: iron sulfides oxidation reaction/process, products resulting from an internal sulfate attack, the major documented cases of damaged concrete structures involving iron sulfides, the tests involving the oxidation of iron sulfides when used in concrete aggregates and the standardization state in connection with the problematic of iron sulfides. In **Chapter 3**, the thesis research program is presented. **Chapters 4 to 7** are the core of the thesis, each of them corresponding to 1 of 4 papers published in (papers 1, 2 and 3) or submitted and accepted to (paper 4) international scientific refereed journals.

The first paper (*Chapter 4*) deals, in general terms, with the identification of the problem responsible for the concrete deterioration at the Trois-Rivières area (Québec-Canada). Samples from the deteriorated concrete were collected and analysed by petrographic methods to identify the products formed during the deterioration process, as well the aggregates used.

In the second paper (*Chapter 5*), an oxygen consumption test was adapted to evaluate the potential reactivity of iron sulfide aggregates. Several aggregates containing iron sulfides or aggregates that have not iron sulfides or only traces were reduced to different Aggregate particle sizes and the oxygen consumption in a closed space was measured. Different aggregate particle sizes, saturation degrees, compacted ground material thicknesses and headspaces (air) volume/thickness values were investigated in order to reach the optimal test conditions.

The third paper (*Chapter 6*) addresses the development of an accelerated mortar bar test capable to reproduce in laboratory the deterioration observed in the degraded concrete at Trois-Rivières and to predict the deleterious potential of aggregates containing iron sulfides when used in concrete. Different conditions of temperature, humidity, and oxidation solutions were tested in order to identify the optimal conditions.

The fourth paper (*Chapter 7*) proposes a protocol to evaluate concrete aggregates containing iron sulfide mineral. The findings and the tests developed during this project resulted in a three-phase testing protocol using a combination of the above tools and a series of “decision-making points/steps” to identify the potential damaging effects of iron sulfide-bearing aggregates for use in concrete.

Finally, *Chapter 8* draws some final conclusions and issues several recommendations for further research.

Chapter 2

Literature review

This chapter covers the available information on the iron sulfides, the mechanisms that lead to their oxidation and the associated deterioration process when they are used as concrete aggregates, as well as the resulting deterioration products.

This chapter also presents a summary of the major documented cases of damaged concrete structures involving iron sulfides, as well as the results of laboratory investigations involving the oxidation of iron sulfides when used as concrete aggregates.

2.1 The iron sulfide minerals

The iron sulfides are among the most abundant metallic minerals found in nature. They are distributed in all types of rocks from sedimentary to magmatic, and they are commonly present in most sulfide ore deposits. The following sections will focus on the main iron sulfides identified in the rocks from the Maskimo and B&B quarries (Saint-Boniface, Québec, Canada) in previous analyses, i.e. pyrrhotite, pyrite, chalcopyrite and pentlandite (as veins in the pyrrhotite).

2.1.1 Pyrrhotite

Pyrrhotite is one of the most common iron sulfide minerals in nature. Mostly found with pentlandite in basic igneous rocks, as veins in different types of rocks and in metamorphic rocks, pyrrhotite is also found associated with pyrite, marcasite, magnetite and chalcopyrite (Deer et al., 2000; Belzile et al., 2004). In hand sample, this mineral has a metallic luster and bronze brown, yellow or reddish color. Microscopically, pyrrhotite is a mineral with a pink cream or skin color (Deer et al., 2000).

Pyrrhotite has a non-stoichiometric chemical formula (Fe_{1-x}S), with x ranging from 0 (FeS) to 0.125 (Fe_7S_8) (Deer et al., 2000; Thomas et al., 2001; Mikhlin et al., 2002; Belzile et al., 2004; De Villiers and Liles, 2010) or 0 to 0.17 (Korbel and Novák, 2000), or 0 to 0.2 (Berry et al., 1983). Fe_4S_5 is a variant of the formula FeS (troilite), containing often a small percentage of nickel and cobalt, silver or even gold (Buttgenbach, 1953). The formula for

pyrrhotite can also be expressed as $\text{Fe}_{n-1}\text{S}_n$ with $n > 8$, thus giving structures from Fe_7S_8 (monoclinic pyrrhotite) to $\text{Fe}_{11}\text{S}_{12}$ (hexagonal pyrrhotite). Its non-stoichiometry composition is a system of ordered vacancies within the Fe lattice (Thomas et al., 2001; Belzile et al., 2004). Depending on their chemical composition, it can crystallize in the monoclinic (pseudo-hexagonal) or hexagonal systems. The least Fe-deficient forms have hexagonal structures, whereas those with greater iron deficiencies have monoclinic symmetry (Janzen et al., 2000; Thomas et al., 2001). Pyrrhotite has a variable magnetic power, depending on the number of Fe vacancies in the crystal structure.

2.1.2 Pyrite

Pyrite is the most common iron sulfide mineral in nature, as it is present in magmatic, metamorphic and sedimentary rocks. Normally, pyrite can be found in large masses or veins of hydrothermal origin, in the form of both primary and secondary mineral. In hand sample, this mineral has a metallic luster and pale yellow tin color. Microscopically, pyrite is an isotropic mineral with a yellowish-white color in reflected light (Deer et al., 2000).

With the chemical formula FeS_2 , composed by 46.6% in Fe and 53.5% in S, pyrite can also have, in its composition, arsenic, antimony, copper, nickel, cobalt, thallium, silver and gold traces. Pyrite may be well crystallized in the form of cubes, octahedrons and dodecahedrons, but frequently is in the framboidal form or as polyframboids.

2.1.3 Chalcopyrite

Chalcopyrite occurs in all types of rocks. In hand samples, chalcopyrite has a yellow tin color, a metallic luster, and is often superficially altered and iridescent. Microscopically, chalcopyrite is slightly anisotropic with a yellowish-tin color, the chalcopyrite's yellow being brighter than the pyrite's yellow (Deer et al., 2000). The general chemical formula is CuFeS_2 , with 35% in Cu, 30% in Fe and 35% in S. The crystallographic system of chalcopyrite is tetragonal.

2.1.4 Pentlandite

Pentlandite is commonly associated with other sulfide minerals, such as pyrite, chalcopyrite and pyrrhotite, in basic igneous rock intrusions. With the chemical formula $(\text{FeNi})_9\text{S}_8$, pentlandite resembles pyrrhotite, but is slightly paler. Microscopically, it presents a pale creamy yellowish color and is isotropic in reflected light (Deer et al., 2000). According to

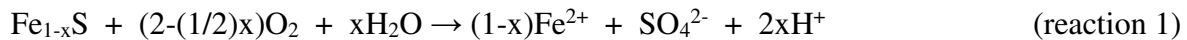
Pearson and Buerger (1956), pentlandite crystallizes in the isometric hexo-octahedral system.

2.2 Iron sulfides oxidation reaction/process

2.2.1 Pyrrhotite oxidation reaction

There are not many studies that explain the factors responsible for the pyrrhotite oxidation. Some authors say that the mechanism is similar to that of pyrite oxidation, mechanism that will be discussed in the next section. The existing studies were mainly carried out in the acid rock drainage context (ARD), which is by far different from the pyrrhotite oxidation process occurring in concrete. In ARD, the pH is like the name says, i.e. “acid”, while the pH in concrete is highly basic, normally higher than 12.5.

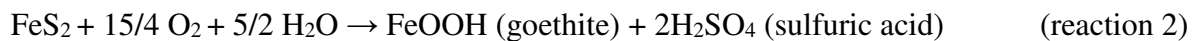
The oxidation of pyrrhotite is highlighted in the following reaction (1) (Janzen et al., 2000; Mikhlin et al., 2002; Belzile et al., 2004), being oxygen and water necessary for the oxidation reaction to occur:



2.2.2 Pyrite oxidation reaction

Pyrite-bearing rocks are increasingly being used for concrete aggregates, because of the decreasing supply of materials with good geological conditions (Wakizaka et al., 2001).

The pyrite oxidation reaction has been described in several studies. This reaction, such as pyrrhotite oxidation reaction, needs water and oxygen to occur (Divet and Davy, 1996; Divet, 2001). According to Divet and Davy (1996), pyrite reacts with oxygen and moisture according to the following reaction (2):



Due to the pyrrhotite and pyrite oxidation process, new products are formed: ferrihydrite ($\text{Fe}^{3+}_2\text{O}_3 \cdot 1/2(\text{H}_2\text{O})$), jarosite ($\text{KFe}^{3+}_3(\text{OH})_6(\text{SO}_4)_2$), limonite ($\text{FeO}(\text{OH}) \cdot n\text{H}_2\text{O}$) and goethite (FeOOH) (Belzile et al., 2004; Duchesne, 2010).

2.3 Deterioration process of concrete incorporating sulfide-bearing aggregates

As mentioned before, iron sulfides have the tendency to be unstable in the presence of oxygen and water. The iron sulfide oxidation-reaction mostly studied in concrete is the pyrite oxidation (reaction 2).

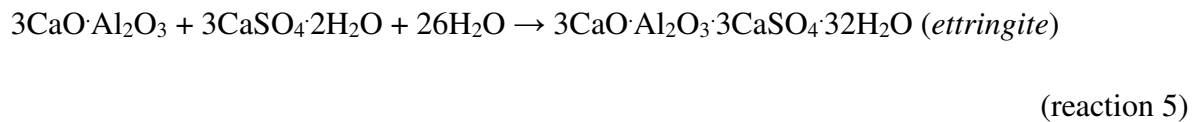
When this oxidation reaction occurs in concrete aggregates, the sulfuric acid thus produced (reaction 2) lowers the pH, but the reduction will be limited by the buffering effect of portlandite, through reaction (3).



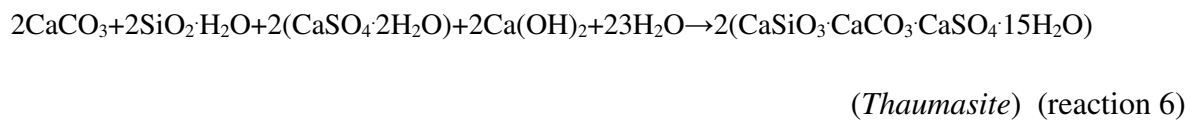
If the reaction (2) occurs in hardened concrete, the sulfuric acid reacts with the portlandite (Ca(OH)_2), which is a product of the hydration of Portland cement, and *gypsum* is formed according to reaction (4).



The gypsum then reacts with the aluminate phases in Portland cement concrete (anhydrous or hydrated), thus leading to the formation of potentially expansive secondary *ettringite* (reaction 5) (Tagnit-Hamou et al., 2005).



If a source of carbonate (CO_3^{2-}) is available in the system (aggregate, cement or other) *thaumasite* can be formed (reaction 6) (Thomas et al., 2003)



The chain of reactions generated after the iron sulfides oxidation in the concrete can thus lead to a deleterious *sulfate attack* (Casanova et al., 1996), like it is observed in the reactions (4), (5) and (6). The extent of the sulfate attack of the paste is controlled by the composition and size of the aggregate particles, the kinetics of sulfide oxidation, the composition of the cement and the mix proportioning of concrete (Casanova et al., 1996).

Besides the above reactions/process, goethite (Moum and Rosenqvist, 1959; Chinchón et al., 1990; Mikhlin et al., 2002), all kind of “rust” as limonite ($\text{FeO}(\text{OH}) \cdot n\text{H}_2\text{O}$), ferrihydrite ($\text{Fe}^{3+}_2\text{O}_3 \cdot 1/2(\text{H}_2\text{O})$), iron hydroxides $\text{Fe}(\text{OH})_2$ [(Moum and Rosenqvist, 1959, Bérard et al., 1975, Bérubé et al., 1986; Chinchón et al., 1990 Mikhlin et al., 2002)] can also be formed through the deleterious oxidation reaction of pyrite.

Many of the minerals identified as final products of the iron sulfide weathering have relatively large molar volumes (or at least, larger than the precursors) and, consequently, their formation is a source for expansive phenomena (Casanova et al., 1996).

The exterior signs of deterioration in concrete structures/elements affected by the sulfide oxidation are staining, spalling and pop-out formation (Seaton, 1948; Mielenz, 1963; Bérard et al., 1975), microcracking (Wakizaka et al., 2001) and map cracking (Bérard et al., 1975; Oberholster and Krüger, 1984; Oberholster et al., 1984; Vasquez and Toral, 1984; Chinchón et al., 1989 and 1990, 1995; Ayora et al., 1998).

2.4 Significant factors in the iron sulfides oxidation process

In addition to water and oxygen (Knipe et al., 1995; Longworth, 2003; Divet and Davy, 1996; Divet, 2001), some authors have described other factors involved in the iron sulfides oxidation process, notably their influence on the reactions kinetic. From the available literature, the bacteria's presence (Bérard, 1970; Bérard et al., 1975; Pye and Miller, 1990; Belzile et al., 2004), the crystal structure (Janzen et al., 2000; Lehmann et al., 2000; Gerson and Jasieniak, 2008), morphology (Divet and Davy, 1996; Divet, 2001) and specific surface area of the iron sulfide mineral (Divet and Davy, 1996; Janzen et al., 2000), temperature (Divet and Davy, 1996; Steger, 1982), the pH of the system (Divet and Davy, 1996; Casanova et al., 1996; Casanova et al., 1997), and the galvanic interactions play also a role in the sulfides oxidation reaction.

2.4.1 Oxygen and water

As observed in the reactions presented in the previous sections, oxygen and water are essential to the sulfide oxidation reaction development. In the study carried out by Steger (1982), about the oxidation of sulfide minerals, the author concluded that the oxidation rate increases directly with increasing relative humidity. In 1995, Knipe and coworkers studied

the interactions between pyrite and pyrrhotite and water vapour. They concluded that the oxygen is the primary oxidant, and when the iron sulfides are exposed to deoxygenated water, they do not oxidize. Divet and Davy (1996) concluded that the rate of pyrite oxidation decreases with the decrease of the dissolved oxygen concentration.

2.4.2 Bacteria's presence

Some studies suggested that the oxidation of pyrite and pyrrhotite can be promoted and catalyzed by the *Thiobacillus ferrooxidans* bacteria (Quigley and Vogan, 1970; Penner et al., 1973; Pye and Miller, 1990; Belzile et al., 2004; Suzuki et al., 1992; Chan and Suzuki, 1993; Suzuki, 1999). These organisms are widely used in the mining industry to recover metals from sulfide ores, especially from the more stable minerals like chalcopyrite and sphalerite (Bérard, 1970). These bacteria develop at low pH (Bérard et al., 1975), in a range 1.0-2.5, deriving their energy from redox reactions where Fe^{2+} or reduced sulfur compounds serve as electron donor and oxygen as electron acceptor. Thiobacilli are most active in temperatures ranging from 20 to 55°C and *T. ferrooxidans* is the dominant organism at temperatures below 40°C (Belzile et al., 2004).

In the case of pyrite and pyrrhotite as components of concrete aggregates, the contribution of these bacteria to those iron sulfides oxidation seems to be unlikely. The action of bacteria (thiobacillus) is not considered probable in an environment with such high pH conditions found in concrete (Bérard et al., 1975). The pH of the concrete pore solution is higher than 12.5, while the optimal conditions for the thiobacillus development and proliferation are, as mentioned before, acidic.

2.4.3 Crystal structure

As previously mentioned, pyrrhotite has a non-stoichiometric composition, $(\text{Fe}_{1-x}\text{S})$, with x ranging from 0 (FeS) to 0.125 (Fe_7S_8), that is responsible for different crystal structure that varies from pure hexagonal to pure monoclinic (Janzen et al., 2000). There is a scarcity of detailed studies on the effect of different crystal structures of pyrrhotite on the oxidation rates (Janzen et al., 2000), and the existing studies are somewhat contradictory. While Orlova et al. (1988) (in Janzen et al., 2000) noted that hexagonal pyrrhotite is more reactive than monoclinic pyrrhotite, Vanyukov and Razumovskaya (1979) (in Janzen et al., 2000) suggested the opposite. Lehmann and coworkers (2000) developed a study to compare the

dissolution of hexagonal and monoclinic pyrrhotites in cyanide solution. They concluded that rate of dissolution of the monoclinic pyrrhotite under the variety of conditions evaluated was greater than that of the hexagonal pyrrhotite. In 2008, Gerson and Jasieniak, also showed that the oxidation rate of monoclinic pyrrhotite was greater than that of hexagonal pyrrhotite.

2.4.4 Specific surface area and morphology of the iron sulfide minerals

Fractures and roughness increase the iron sulfides surface area and consequently the oxidation reaction, because more surface is exposed to moisture and oxygen (Divet and Davy, 1996; Janzen et al., 2000). Pyrite, as it was mentioned before, can crystallize in the form of cubes, octahedron and dodecahedron, but frequently is in the framboidal form or as polyframboïdes.

The iron sulfide morphology can influence the oxidation reaction. In 1996, Divet and Davy studied the oxidation reaction of framboidal and massive pyrite. They concluded that the framboidal pyrite reacts more rapidly (oxidation) than the massive pyrite. The framboidal pyrite shows difficulties in developing active/reaction sites, but the later grow faster. However, the massive pyrite is attacked in numerous locations, but the velocity at which the phenomenon occurs is relatively slow. These observations are true only when the mineral size is superior to 20 μm .

2.4.5 Temperature

According to Steger (1982), Divet and Davy (1996) and Lehmann et al (2000), there is a significant increase in the oxidation rate with increasing temperature. According to Steger (1982), at a constant relative humidity, the temperature will enhance the rate of O_2 diffusion and therefore the formation of ferric oxide (as well as the SO_4^{2-} products). This relation follows the Arrhenius Law. Janzen et al. (2000) studied the oxidation of pyrrhotite at different temperatures (25°C, 35°C and 45°C), and have shown that the rate of oxidation increased with increasing temperature. Lehmann and coworkers (2000) studied the dissolution of both monoclinic and hexagonal forms of pyrrhotite and concluded that, in both cases, the dissolution increases with the increase of temperature.

2.4.6 pH system

One of the studies proving that the pH has a strong influence on the sulfides oxidation process was carried out by Divet and Davy (1996). According to the authors, the parameter that plays the major role in the pyrite's oxidation is the high OH⁻ ion concentration in the alkaline pore solution of concrete. For a pH greater than 12.5, the oxidation rate increases exponentially and reaches about 50 times its initial value at a pH of 13.7.

The pH can also play a significant role in the reactions that occur after the oxidation reaction starts and that are responsible for the production of secondary deterioration products. When the sulfate and hydrogen ions are released into the pore solution, they will react with the paste components (especially tricalcium aluminate and/or portlandite) to form, as mentioned before, expansive phases such as *gypsum* (reaction 4), monosulfoaluminate and eventually *ettringite* (reaction 5). The predominance of one or the other reaction will be controlled by the pH (Casanova et al., 1996, 1997). The formation of gypsum is preferentially occurring at pH<10.5, ettringite will be favoured at 10.5<pH>11.5, calcium aluminate monosulfate at pH>11.5 (Casanova et al., 1996) while a pH greater than 10.5 is ideal for thaumasite formation.

2.4.7 Galvanic interactions between contacting/adjacent sulfide minerals

Several studies indicate that the combined presence of different sulfide minerals is responsible for accelerating the oxidation reaction (Moum and Rosenqvist, 1959; Shuey, 1975; Eglington, 1987; Ekmekçi and Demirel, 1997; Atak et al, 1998; Kwong et al., 2003; Becker, 2009; Azizi et al., 2010, 2011).

Most of metal sulfides are semi-conductors, each characterized by a *rest potential*, which can vary as a function of the sulfide's detailed composition (Shuey, 1975). The rest potential or open circuit potential, is the equilibrium potential of the mineral at zero electric current (Becker, 2009). The ease with which the different sulfide minerals are prone to oxidation can be determined by comparing their rest potential (Becker, 2009). The rest potentials of a few common sulfide minerals measured in 1.0 M H₂SO₄ at room temperature (20–25°C) are given in Table 2.1. Pyrite is the sulfide mineral with the highest

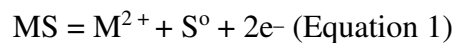
rest potential (V vs. SHE: Standard hydrogen electrode/Volt), thus more stable, while pyrrhotite shows the lowest rest potential and is consequently the most unstable sulfide mineral. In nature, in the presence of an electrolyte, two adjacent sulfides with different rest potentials form a galvanic cell. The sulfide with the highest rest potential becomes the cathode and that with the lowest rest potential, the anode (Kwong et al., 2003).

Table 2.1: Rest potential of some sulfide minerals (adapted from Kwong et al., 2003)

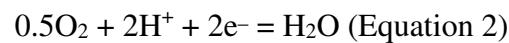
Mineral	Formula	Rest Potential (V vs. SHE)*	References
Pyrite	FeS ₂	0.63	Biegler and Swift 1979
Chalcopyrite	CuFeS ₂	0.52	Warren 1978
Chalcocite	Cu ₂ S	0.44	Chizhikov and Kovylna 1956
Covellite	CuS	0.42	Majima 1969
Galena	PbS	0.28	Chizhikov and Kovylna 1956
Sphalerite	ZnS	-0.24	Chiz-hikov and Kovylna 1956
Pyrrhotite	Fe _(1-x) S	-0.28	Chizhikov and Kovylna 1956

* Standard hydrogen electrode/Volt

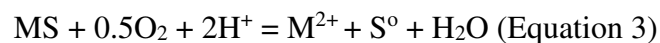
In an oxygenated system, a generalized anodic reaction involving a bivalent metal sulfide (MS) can be represented by Equation 1 (Kwong et al., 2003):



The cathodic reaction, however, relates to the discharge of oxygen adsorbed on the surface of the cathode sulfide, as shown in Equation 2:



In other words, oxidative dissolution of the sulfide with a lower rest potential occurs at the anode while the sulfide with a higher electrode potential is protected from oxidation at the cathode. The overall galvanic reaction characterized by a mixed potential is thus given by:



In the natural environment, the elemental sulfur produced is subsequently converted to sulfate. In addition to the absolute difference in rest potential between two contacting sulfides, the relative surface areas of the galvanic couple greatly affect the rate of oxidative dissolution of the anode sulfide because of the resultant current density generated. The larger the anodic area, the more widely distributed is the current generated by the galvanic cell. The low current density results in a slow dissolution of the anode sulfide (Kwong et al., 2003). For example, if pyrite and pyrrhotite coexist, the pyrite will be the cathode and pyrrhotite will be the anode, so the pyrrhotite will be the one that will be oxidized.

2.5 Deterioration products resulting from an internal sulfate attack due to sulfide-bearing aggregates

As mentioned elsewhere, the oxidation of iron sulfides in concrete can lead initially to the formation of iron oxyhydroxides and, at posteriori, to an internal sulfate attack with formation of different kinds of sulfate minerals such as gypsum, ettringite and thaumasite. These secondary products are normally considered, as well as the secondary products resulting from the iron sulfides oxidation reaction, expansive. Besides expansion, some can also lead to concrete disintegration. These sulfate minerals occur in different conditions of temperature, humidity, and pH solution. In the next sections, the essential conditions to the formation of these sulfates will be presented.

2.5.1 Gypsum

Gypsum is a calcium sulfate dihydrate ($\text{CaSO}_4 \cdot 2(\text{H}_2\text{O})$). In concrete, gypsum can occur as a constituting mineral in the aggregate material, as additive in the cement or as secondary product resulting from sulfate attack.

When sulfate and hydrogen ions are released into the pore solution, they will react with the paste components (especially tricalcium aluminate (C_3A) and/or portlandite) and will form additional expansive phases such as gypsum. Normally, the formation of gypsum occurs at a pH lower than 10.5 (Casanova et al., 1996).

The exact nature of disruption in concrete caused by gypsum formation is not well established (Tian and Cohen, 2000; Santhanam et al., 2003). Softening of the concrete

surface (Cohen and Mather, 1991), rather than expansion (Tian and Cohen, 2000, Neville and Brooks, 2010), has been attributed to the effect of gypsum formation.

2.5.2 Ettringite

Ettringite ($3\text{CaO} \cdot \text{Al}_2\text{O}_3 \cdot 3\text{CaSO}_4 \cdot 32\text{H}_2\text{O}$) is an hydrous calcium trisulfoaluminate. It is produced, in concrete, by a reaction that requires excess of sulfate ions SO_4^{2-} over the aluminate phase in the pore solution (St John et al., 1998). The source of sulfate ions in excess can be either the cement or other constituents of the concrete (Brown and Taylor, 1999), such as the result of the oxidation process of pyrite and/or pyrrhotite present in the aggregates (Divet, 2001; Moum and Rosenqvist, 1959; Chinchón et al., 1989, 1990, 1995; Bérard et al., 1975), late release of sulfates from the clinker, dissolution and re-precipitation of ettringite resulting from normal hydration of cement.

In concrete, ettringite can be formed in two different stages, and the consequences of that formation are completely different (Divet, 2001). Ettringite is generally formed during the early stages of the hydration of Portland cement in a plastic fresh mixture. In this case, it is called early ettringite formation and does not produce any damaging expansion (Colleparidi, 2003). When ettringite occurs at later ages and is related with *heterogeneous* cement paste expansion that can result in excessive cracking and spalling of the hardened concrete, it is called delayed ettringite formation (DEF). This form of internal sulfate attack is generally related to excessive thermal effects during the early stages of the concrete hardening process.

2.5.3 Thaumasite

Thaumasite ($\text{CaSiO}_3 \cdot \text{CaCO}_3 \cdot \text{CaSO}_4 \cdot 15\text{H}_2\text{O}$) is a complex mineral that contains different anions in its composition: carbonate (CO_3^{2-}), sulfate (SO_4^{2-}) and silicate as $\text{Si}(\text{OH})_6^{2-}$. These three anions are associated with the Ca^{2+} cation (Edge and Taylor, 1971).

The internal sulfate attack resulting in thaumasite formation (TSA) has been rarely described in the literature before the 2000's. This is probably due to the fact that the deteriorated concrete is not often subjected to a detailed petrographic examination and also due to the similar appearance of ettringite and thaumasite (needle-like shape) that in many

cases can lead to an erroneous identification. The TSA is potentially more severe than the attack resulting from the gypsum and ettringite formation. In the case of thaumasite formation, the C-S-H phase of the concrete is deleteriously affected, leading to a complete loss of integrity and strength (TEG report, 1999; Chinchón-Payá, 2013).

Conditions normally considered necessary for the formation of the thaumasite are: low temperature ($\approx < 15^{\circ}\text{C}$; the ideal temperature being about 4°C (Crammond, 1985)), constant humidity, a source of carbonate ions, a source of sulfate and a pH greater than 10.5 (Collett et al., 2004; TEG Report, 1999; Köhler et al., 2006; Thomas et al., 2003; Zhou et al., 2006; Newman and Choo, 2003; Skalny et al., 2003).

Even though the majority of the reported cases of thaumasite formation usually occurred under low temperature conditions, some studies and cases studies showed that there are some exceptions. In recent years, cases of TSA have been reported in locations where the average temperatures are above 15°C . In 2011, Torres et al. presented a TSA case that took place in Campina Grande (Brazil), a city where the lowest temperature recorded during the winter was over 20°C . The affected element was a concrete beam used as a top structure of an earth retaining limestone wall. The beam began to show significant signs of deterioration three years after construction.

Another case of thaumasite formation at temperatures exceeding 15°C was reported by Sahu and coworkers in 2003 for residential concrete slabs in Southern California.

In 2011, Day and Middendorf have observed thaumasite formation in the laboratory at room temperature ($\sim 20^{\circ}\text{C}$). Various mortar mixes were cast and subjected to a 0.35 M sodium sulfate solution (in accordance with the test methods CSA A3004-C8/ASTM C1012 for sulfate resistance), with a continuous soaking at room temperature ($\sim 20^{\circ}\text{C}$) or at -5°C in a refrigerator. In both cases (~ 20 and $\sim 5^{\circ}\text{C}$), thaumasite was formed.

A study by Schmidt and colleagues in 2008 demonstrates thaumasite formation both at 8°C and 20°C . The amount of thaumasite formed at 20°C was however found to be lower than at 8°C , mainly due to the increased solubility of the thaumasite with increasing temperature.

Crammond (1985) and TEG report (1999) state that a constantly high humidity is needed for thaumasite formation. This condition seems obvious considering that thaumasite has 15 moles of H₂O in its composition.

The carbonate ions generally originate from carbonate aggregates (limestone, dolomite, etc.). However, some studies reported thaumasite to form in concrete and mortar specimens incorporating a siliceous aggregate. When analyzed in detail, it was concluded that the source of carbonate material for thaumasite formation was the atmospheric CO₂ (Thomas et al., 2003; Collett et al., 2004). Another source of carbonate ions can be the CO₂⁻³ from seawater or the carbonate material used in the manufacture of Portland limestone cements.

The source of sulfate ions is generally considered to be external, usually derived from the groundwater, where it can be associated with a number of different cations, particularly magnesium, calcium and sodium (or a combination of these). Collet and colleagues (2004) reported a case where sulfates originated from sulfate minerals present in bricks, while sulfates could also be derived from the iron sulfides (pyrite and pyrrhotite) existing in concrete aggregates.

According to the report TEG (1999), thaumasite formation is favorable at a pH of 10.5. In 2003, Jallad and colleagues tested the thaumasite formation at pH between 6 and 12 and its stability at pH greater than 12. At pH 6, small amounts of thaumasite were formed. At pH levels of 7 and 8, thaumasite and aragonite were observed and at pH levels of 12 only thaumasite was formed. The same study demonstrated that thaumasite is stable at pH = 13. At pH levels lower than 11, thaumasite reacts with the ions in solution and part is converted to calcium phosphate, calcium silicate and calcium carbonate.

2.6 Major documented cases of damaged concrete structures involving iron sulfides

There are some studies reported in the literature relating damage in concrete structures to the presence of iron sulfides aggregate or granular base materials (Moum and Rosenqvist, 1959; Hagelia et al., 2003, Hagelia and Sibbick, 2009; Pardal, 1975; Vasquez and Toral, 1984; Oberholster et al., 1984; Oberholster and Krüger, 1984; Chinchón et al., 1989; 1990 and 1995; DEC, 1991; Lugg and Probert, 1996; Schmidt et al., 2011). These "problematic"

iron sulfides can be part of the concrete aggregates (Shayan, 1988) or of the bedrock foundations (Quigley and Vogan, 1970; Penner et al., 1973; Grattan-Bellew and Eden, 1975; Grattan-Bellew and and McRostie, 1982).

2.6.1 Oslo, Norway (Moum and Rosenqvist, 1959; Hagelia et al., 2003)

In the Oslo region of Norway, problems of concrete deterioration and foundation heaving seemed to be related to the presence of slightly metamorphosed shales containing pyrrhotite ($\text{FeS}_{1.14}$). In some cases, the concrete structures were transformed into mush after only 9 months.

After World War II, a semi-official “Alum Shale Committee” was set up in Oslo, and the Norwegian Geotechnical Institute was requested to look into the chemical, physical, and mineralogical phases of the problem. This committee started its investigations in a closed tunnel, the Blindtarmen tunnel, where water (with a low pH, sometimes 2.5) entering through the destroyed lining comes directly from one of the most aggressive zones in the alum shale. The tunnel was partially filled with water, with the water level varying somewhat according to precipitation and had air circulation. The water in the upper part was oxidized whereas, in the deeper part, had a low pH. The *Alum Shale Committee* placed some concrete prisms deep below the low-water level (been constantly submerged), and some between the low-water levels (exposed to fluctuation of the ground water level). After 3 to 4 years, the prisms left above the low-water level still had sharp edges and fairly good mechanical properties; however, those left deep in the tunnel were mostly destroyed, except those containing sulfate resistant cement. The "upper" specimens were covered by a brown layer of rust. In the bottom specimens, large amounts of white pulverized material were observed. Petrographic examination showed that the product was mainly *ettringite*. The authors concluded that the deleterious mechanism responsible for the deterioration was a combination of two types of attacks, a typical sulfate attack with production of *ettringite* and an acid attack. In 2001, Hagelia and coworkers (Hagelia et al., 2003; Hagelia and Sibbick, 2009), examining the descriptions of the attack proposed by Moum and Rosenqvist (1959), argued that the deterioration mechanism must represent a severe case of *thaumasite* sulfate attack (TSA). In order to prove their theory, the authors recuperated the samples left in the tunnel since 1959. XRD and petrographic analyses were carried out and

it was concluded that the material that Moum and Rosenqvist (1959) identified as *ettringite* was actually *thaumasite*.

2.6.2 Ottawa, Canada (Quigley and Vogan, 1970)

In this case, Quigley and Vogan (1970) studied the processes involving the heaving of structures sitting directly on pyrite-bearing dark-grey/black shale bedrock.

A lightly loaded building founded directly on drained black shale presented three inches (7.6 cm) of differential heaving over a 20-year period, thus causing severe structural deformations. The heaving was attributed to the oxidation of disseminated iron sulfides in the shale by autotrophic bacteria (*Thiobacillus ferrooxidans* and *Ferrobacillus ferrooxidans*) to produce secondary hydrous sulfates of greater volume. To study the case, logging of a core from the rock foundation, X-ray diffraction on the rock and chemical and bacterial analyses of the water from old boreholes were carried out. The logging showed bands of orange oxidized silty shale and soil like material filling the bedding plane cleavages, and soft white gypsum crystals. Microscopic examinations showed abundant autotrophic bacteria of the *Thiobacillus ferrooxidans* and *Ferrobacillus ferrooxidans* types.

There seem to be two possible heaving mechanisms at the site: 1) hydration and expansion of swelling clay complexes, and 2) geochemical alteration of sulfides to produce secondary sulfates and heaving resulting from pressures of crystallization.

The amount of secondary gypsum that broke apart the bedding plane cleavages in the core is believed to correspond roughly to the magnitude of heaving, which is about 3 in. (7.6 cm).

It is hypothesized, therefore, that the bacteria have oxidized or catalyzed the oxidation of pyrite in the shale, thus producing sulfuric acid. This sulfuric acid then slowly dissolved calcite disseminated in the shale and in the rock cleavages, thus altering into gypsum. The gypsum has migrated through solution, eventually precipitating out as the flat crystals observed in the horizontal and inclined cleavage openings.

2.6.3 Ottawa, Canada (Penner et al., 1973)

At the end of 1969, Penner and coworkers started an investigation on the mechanism responsible for the heaving of the basement floor of a three-storey extension of the Bell Canada Building in Ottawa, founded on shale. The study was initiated when the displacement of the basement floor interfered seriously with the alignment and operation of the power and switching facilities located in this area.

The original building was constructed in 1929, and an extension was added in 1961, with all the corresponding floors located at the same elevation. Heaving of the basement floor in the extension was noticed about 4 years after the addition was completed. The affected area appeared as two rounded domes.

The object of the investigation was to establish the cause of heave and to initiate remedial measures for controlling the heave until the equipment could be relocated.

The building is founded on the Billings formation, a black pyritic, calcareous and fissile shale. The shale formation is about 6m thick at this location and lies conformably on interbedded limestones and shales of the Eastview formation. A minor fault, which appeared to have a strike in the direction of the heaving areas, was observed in an excavation immediately south of the Bell building. This fault was also uncovered during the excavation of the examination pits below the floor slab of the Bell Canada building.

The 30 cm thick reinforced concrete floor slab was placed on a 15 cm layer of crushed limestone. This levelling course, which also contained an under floor drainage tile system, had been placed directly on the shale, at about 1.5 m below the original shale level.

The maximum measured floor displacement was 5.6 cm over a period of about 32 months, which corresponds to a heave rate of approximately 0.18 cm per month. Based on the estimated floor elevation immediately after construction, the maximum total movement was 10.7 cm.

The authors tried to core the affected zone, but the recovery by drilling was poor, so that examination pits were excavated in three locations within the problematic area. The top 40 to 50 cm of shale were extremely soft and crumbly and could be removed with a hand

shovel; below that, excavation was carried out with the aid of a jack hammer. Joint surfaces and shale laminae in the altered zone (top 0.5 to 1 m) were covered with a yellowish brown coating and numerous colourless crystals. The altered zone was found to be acidic and, based on numerous measurements, the pH ranged from 2.8 to 4.4. Below about 1 m, the shale appeared to be sound.

The mineralogical investigations carried out on the reaction products of the altered shale confirmed the presence of gypsum and jarosite. The mineralogical investigation of the unaltered shale showed: pyrite, calcite, illite and quartz; no gypsum or jarosite were observed. The X-ray diffraction analysis that identified the presence of pyrite was unable to determine if other iron sulfides were present.

The existence of extensive pyrite intrusions and general pyritic content in the unaltered shale zone, the type of alterations products identified in the altered zone and the acid conditions in the altered zone, suggested that autotrophic bacteria were probably involved in the weathering and heaving process. The energy for growth and proliferation of autotrophes is obtained by the oxidation of inorganic compounds in the presence of atmospheric oxygen. The autotrophic bacteria that is believed to be responsible of the oxidation is the *Ferrobacillus-Thiobacillus*.

As the shale is calcareous, the formation of gypsum is derived from the neutralization process between the excess sulfuric acid and calcite. Jarosite, also a main reaction product in the altered zone, forms most readily under acid conditions, as found in the altered zone. The potassium content of jarosite is thought to come from the degradation of clay minerals and/or by base exchange reactions in the highly acid environment.

The above reactions caused heaving because the molar volumes of the unaltered components are less than the reaction products. The volume increase from pyrite to jarosite is 115%, and from calcite to gypsum 103%. It is also very apparent that the weathered products formed between the shale laminae, although in the rotted material, gypsum and jarosite were found to exist inside the pores of the laminae.

A remedial treatment had to be implemented to stop the heave. The authors suggested the creation of unfavourable conditions for the growth of the bacteria by neutralizing the

acid conditions in the altered zone with a base and by reducing the air circulation by saturation with water. The decision was, therefore, to keep the treatment concentration below 0.1 N KOH although the exact nature of the dimensional changes resulting from treatment was not well understood.

After about 3 months of treatment, the acid conditions in the shale had been greatly reduced and the cracks were well impregnated with KOH solution although the acidic pH's still persisted near the surface. In the following months, there was a great improvement in the pH in the observation wells and the decision was made to discontinue the KOH treatment but continue to supply water to keep the water table as high as possible and maintain wet conditions beneath the slab. In the period following the start of treatment, floor movements have been controlled satisfactorily.

2.6.4 Barcelona, Spain (Pardal, 1975; Vasquez and Toral, 1984; Chinchón et al., 1989, 1990 and 1995)

Since 1970 (Vasquez and Toral, 1984), studies have been carried out on cases of deterioration of concrete incorporating pyrite-rich aggregates in the Maresme region, near Barcelona (Spain) (Chinchón et al, 1989, 1995). The affected structures consist of public buildings, houses, overpasses and dams. In 1975, more than 30 cases were reported (Pardal, 1975). In all cases, the deterioration started with expansion with resulting cracking leading to the structures destruction (Vasquez and Toral, 1984; Chinchón et al, 1989, 1990). In some cases, where the deterioration was less important, the structures presented large brown spots (Vasquez and Toral, 1984). All the affected concretes contained aggregates from the Mont Palau quarry. These aggregates basically consist of limestones and phyllites, with high content of iron sulfide minerals, mainly pyrite and pyrrhotite (Chinchón et al., 1989, 1990, 1995). The hexagonal pyrrhotite occurs disseminated in the aggregates and the pyrite, formed from the sulfurization of pyrrhotite in “bird eyes” textures that affect all the pyrrhotite, occurs in fracture areas of centimetre-sized range (Chinchón et al., 1989).

In all studies of this problem, liability was associated to the oxidation of pyrite into sulfates, thus causing internal attack in concrete. This attack was the cause of the expansion responsible for cracking and ultimate destruction (Vasquez and Toral, 1984)

2.6.5 Montreal, Canada (Bérard et al., 1975)

In 1971 and 1972, similar cases of distressed concrete structures (bridges, overpasses and houses) were brought to Bérard and coworkers' attention. Some concrete blocks fell down from bridges and overpasses, thus exhibiting fragments of black shale on their surfaces, thus giving the impression that the coarse aggregate was mainly composed of argillaceous shale. All affected structures showed map cracking, pop-outs (with fragments of shale in the center), and, in some cases, iron oxide was seeping out the fractures.

Although the coarse aggregate was composed of three types of crushed rocks, diabase or gabbro, limestone and black shale, only the shale was found to be “reactive”. In the cores drilled from the structures, it was possible to observe the shale fragments surrounded by a whitish rim, 1 or 2 mm in width, of *ettringite*. The petrographic analyses of the shale showed that pyrrhotite was present in a percentage of about 4.5%.

According to the authors, the deterioration process was due to the oxidation of pyrrhotite and the formation of sulfuric acid and rusty secondary minerals, which could be limited to *Jarosite*. The sulfuric acid would then react with the calcite within the shale or with the portlandite of the hydrated cement paste to form more gypsum; the latter was believed to be the main cause of the swelling of the shale.

2.6.6 Penge, South Africa (Oberholster and Krüger, 1984; Oberholster et al., 1984)

In South Africa, damage of concrete made with sulfide-bearing aggregates was noticed. The aggregates consisted of cummingtonite slates incorporating sulfide minerals (pyrrhotite, pyrite, arsenopyrite, and chalcopyrite) and magnetite. The oxidation of iron sulfide minerals was seen in both coarse and fine aggregates. Serious cracking of houses has been encountered where sulfide-bearing aggregates from asbestos mine tailings were used in concrete bricks and floor slabs. Expansion of the concrete floor slabs has pushed the corners of houses outwards and, in some instances, lifted the external walls off the damp proof course. The expansion of concrete bricks containing the sulfide-bearing aggregate has resulted in extensive random cracking in external wall rendering. In some cases, the houses started to show signs of deterioration within two years after construction.

The examination of the concrete bricks revealed the presence of a white powdery material around the black carbonaceous aggregate. Under the SEM, the above secondary material was found to be well-crystallised hexagonal crystals containing calcium, silicon and sulfur (*thaumasite*). The XRD showed the presence of pyrrhotite and the analyses for the mineral sulfur gave a pyrrhotite (with a molar Fe/S ratio of 0.96). The pyrrhotite content in the aggregate was small as 0.5 % by mass.

2.6.7 Australia, (Shayan, 1988)

In Australia, a case of concrete deterioration due to pyritic aggregates (shale) was reported by Shayan (1988). A 10 year-old concrete hospital floor slab, about 150mm in thickness, was laid over a water proofing membrane and covered with conventional vinyl tiles. After a few years, severe blistering occurred over an extensive area of the floor, thus disrupting the vinyl tiles. The blistering was found to be caused by the oxidation of the pyrite in the aggregate particles located near the surface of the slab.

Cores were extracted and analysed by XRD, SEM/EDS and by polarizing microscope. Some affected aggregates contained large amounts of pyrite and produced a large amount of jarosite and smaller amounts of *gypsum*. Some aggregates and mortar were covered by a greenish-yellow material that consisted mainly of *jarosite* and *gypsum* and other blistered zones showed *halotrichite*. In this case, no ettringite was observed.

2.6.8 Cornwall and Devon, England (DEC, 1991; Lugg and Probert, 1996)

Between 1900 and 1950, many buildings were constructed using inferior quality concrete blocks (Lugg and Probert, 1996); the aggregate utilized was found to be at the origin of the concrete failure. The constructors, many of them being the owners of their small building firms, utilized the aggregate that was available in the area and that was cheap, sometimes even available for free. The aggregate mainly consisted of mining tailings, specifically “mundic” and “killas” rocks. “Mundic” is the local name (Cornwall) to designate sulfide-bearing rocks, commonly found in the mining wastes, which may oxidize with the formation of sulfuric acid; the latter attacks the cement paste, thereby causing loss of bond, as well as volumetric expansion. “Killas” is the local name to designate fine-grained sedimentary rocks, containing clay minerals and micas, which undergo cyclic expansions

and contractions in response to changes in moisture content, thereby leading to mechanical weakening of the concrete (Lugg and Probert, 1996).

The deleterious mechanisms involving this type of concrete made with sulfide-bearing aggregates began early after construction, but it was only in the seventies that the mechanisms started to be understood.

The number of affected structures is not known exactly; however, two surveys suggested that approximately 15% of the pre-1959 concrete building stock, in Cornwall, have “mundic” degradation (Lugg and Probert, 1996). In many cases, the strength of the blocks was deteriorated to the point where the walls were structurally unsafe and some houses had to be demolished (DEC, 1991). The sections of the houses that presented the most visible signs of deterioration were the parts most exposed to moisture (DEC, 1991; Lugg and Probert, 1996). The mechanisms that was found to be responsible for this damage are: 1) the aggregate that is very susceptible to swelling and contraction due to changing moisture conditions owing to content of recrystallized clay and related minerals, and 2) oxidation of finely disseminated pyrite causing expansion and adverse resulting effects, including sulfate and acid attack on the cement paste in the concrete.

2.6.9 Lladorre, Spain (Ayora et al., 1998)

In 1998, Ayora and coworkers published cases of two dams presenting significant durability problems. During their service life, the above structures developed map cracking in some surface areas, color changes and expansion. Some cracks had a depth of 30 cm. The aggregates used in the concrete consisted of schists that contained minor amounts of pyrrhotite (Fe_7S_8), as disseminate crystals and veinlets. The total sulfur content of the rock was up to 0.8 wt. % S.

Drilled cores were taken from the two dams and subjected to petrographic analysis, SEM/EDS and XRD. From those analyses, *ettringite* was observed as needle-shape crystals filling cavities and fractures in the cement paste; *gypsum* was found as radial aggregates of needle-shape crystals. In some samples, the pyrrhotite was surrounded by melanterite white halos.

The authors concluded that the principal cause of concrete expansion was pyrrhotite oxidation leading to an acid attack of the components of the cement paste, and the formation of iron sulfates that have a higher molar volume. The second stage of the deterioration process corresponds to the attack of the cement paste, where *ettringite* halos formed and promoted the disintegration of the bounds in the interfacial paste/aggregate zone.

2.6.10 Eastern Canada (Tagnit-Hamou et al., 2005)

Tagnit-Hamou et al. (2005) reported the results of laboratory investigations carried out to elucidate the cause of the premature deterioration of house and building foundations and slabs that occurred in one region of Eastern Canada. The concrete made with the sulfide-bearing grey anorthosite aggregates have caused a large range of damage to the above structures as early as two years after construction. Concrete cores extracted from the deteriorated structures were analysed by XRD, SEM/EDXS, while petrographic examination was conducted using a stereomicroscope.

The observations allowed identifying large deposits of *goethite* around several aggregate particles and a very porous cement paste in some locations. *Ettringite* was identified in all samples, generally very close to the weathered aggregate particles and in the cement paste near sound aggregate particles.

Cracks that reached up to 2 mm in width were observed in the aggregate particles and in the cement paste. Cracks in the cement paste skirt around aggregate particles; however, in some heavily weathered cases, cracks were found to run through the aggregate particles. In the cracked aggregate particles, pyrrhotite exhibits a rusty aspect and, sometimes, the crystals seemed to be completely dissolved. Most of the time, weathered micas are observed within these reacted zones.

In this case, it was shown that the presence of chemically unstable iron sulfides (pyrrhotite) in aggregates would have caused the early cracking of concrete. The oxidation of the iron sulfides provokes a series of chemical reactions leading to the precipitation of iron hydroxides and *ettringite*. The most deteriorated zones were observed where pyrrhotite

was associated to micas, the latter having probably contributed to accelerating and enhancing the deterioration process by absorbing water and oxygen.

2.6.11 Switzerland (Schmidt et al., 2011)

Schmidt et al. (2011) published the results of a study carried out on a concrete dam, constructed in the beginning of the 1970s in Switzerland that was found to suffer from steady expansion since the early 1980s. The overall expansion in the upper part of the dam is estimated to be 0.025%. The authors also reported deposits of “rust” (iron oxides and hydroxides) accumulated in the galleries of the dam, and there was also a smell of sulfurous compounds. The rocks utilized as aggregate in this construction mainly consisted of schists. The foliation layers had a thickness of 0.5–2.0 mm. The schists were mainly composed of feldspar, quartz, biotite, and muscovite. Iron sulfides were found to be randomly dispersed and agglomerated within the aggregates. Pyrite/marcasite (80%) and pyrrhotite (20%) were analysed to be about 0.3 to 0.4% by volume. The ore particles were within a range of 30 to 200µm in size, while minor amounts of ilmenite (FeTiO_3) were also noticed. The concrete was produced with an ordinary Portland cement (equivalent to present day CEM 1 32.5: a blended cement with: $65\% \geq \text{Clinker} \leq 79\%$, $21\% \geq \text{limestone} \leq 35\%$ and calcium sulfate, with the chemical composition in sulfates (SO_3) ≤ 3.5 and chlorides $\leq 0.10\%$), using a water-to-cement ratio in the range 0.5–0.6. The samples (cores of 150 mm in diameter) were taken from the downstream face and from galleries in the inner part of the 40 year-old structure.

The investigations indicated that the deterioration process of the iron sulfide grains in various concrete samples was similar but not uniform. The oxidation or degradation process of both pyrite/marcasite and pyrrhotite usually started from the surface of the grain leading to a layer of oxidation products, which is darker than the unreacted iron sulfide. From the chemical microanalyses, the iron sulfide particles seemed to react to first form iron oxide (Fe_2O_3) and secondly iron hydroxides ($\text{FeO}(\text{OH})$, $\text{Fe}(\text{OH})_3$). The oxidation or degradation reaction was found to usually start from the outside inwards of the iron sulfides grains. The concrete samples showed significant cracking originating from the iron sulfide-containing regions within the aggregate particles, and then extended into the cement paste. Thus, it appears that the degradation can be directly linked to the reaction of iron sulfides, which

leads to an increase in volume within the aggregate particles that, in turn, cause cracking and expansion of the concrete. The formation of secondary *ettringite*, from released sulfate, was observed, but there were no clear signs of expansion associated with the extra sulfate. It is not clear to what extent this may contribute to the macroscopic reactions. It was found that pyrrhotite reacts much faster than pyrite in alkaline concrete environments.

2.7 Tests involving the oxidation of iron sulfide-bearing aggregates when used in concrete

Since it was found that aggregate particles containing iron sulfides can be deleterious to the concrete durability, some laboratory tests have begun to be developed. The aim of these tests has been to determine a limit value of the iron sulfides (pyrite and/or pyrrhotite) content that will be safe to utilize when they are incorporated in concrete aggregates, as well as the influence of different types of cements on the durability of concrete incorporating aggregates with different contents of sulfides. Some studies tried to recreate in the laboratory the field conditions and mechanisms that lead to the concrete deterioration due to sulfide-bearing aggregates.

2.7.1 Sweden (Hagerman and Roosaar, 1955)

After having noticed some concrete deterioration problems involving sulfide-bearing aggregates in Sweden, Hagerman and Roosaar (1955) tried to evaluate the maximum tolerable pyrrhotite content in concrete aggregate.

For their tests, four different types of aggregates containing pyrrhotite, as well as an aggregate produced from crushed Stockholm Granite (without sulfides), were used for comparison purposes. In order to obtain different levels of pyrrhotite contents in the aggregates used in the trial mixes, the rocks were sorted into four series, i.e. in order to obtain samples from Pengfors with pyrrhotite contents of 1%, 5% and 10% (Series 1 to 3), and rocks from Norrforsen with 10 to 15% of pyrrhotite (Series 4). A fifth series was produced with the Stockholm Granite as a control aggregate. This tests involved measurements of the natural frequency in transversal vibrations, length measurements and visual inspections.

The experimental tests were carried out on concrete beams, 80 x 15 x 10 cm and 40 x 15 x 10 cm in size. In the case of the large specimens (80 x 15 x 10 cm), three beams of each series were stored in warm water for 3 days alternating with air storage at 75°C for 4 days, for a total of 7 days for each cycle. Two beams of each series were stored in water for 3 days, alternating with air storage for 4 days, both at room temperature, for a total of 7 days for each cycle. Lastly, three beams from each series were stored outdoors.

In the case of the small specimens (40 x 15 x 10 cm), three beams from each series were subjected to steam curing in an autoclave at 225°C for five hours. After, they were allowed to cool to 100°C in the autoclave, followed by cooling in hot water down to room temperature. This treatment was repeated four times at approximately one week intervals. Between autoclaving, the specimens were stored in air at room temperature.

Visual observations of the test beams were made at 2.5 months, 4.5 months and 7 months. After 7 months of testing, the samples made with pyrrhotite showed the presence of rust, some minor cracks and, in one set of beams (80 x 15 x 10 cm) stored in warm water for 3 days alternating with air at 75°C for 4 days, some aggregate particles close to the surface displayed evidence of swelling thus causing fine cracking in the surrounding concrete.

One of the most deteriorated samples, i.e. those stored in warm water for 3 days alternating with air at 75°C for 4 days, was deliberately broken at the end of the testing period. Upon inspection of the fractured surface, rusty aggregate particles were only present in the first 10 mm from the surface of the prism. The petrographic examination of two thin sections prepared from this sample revealed evidence of oxidation of the sulfides, together with oxidation staining in the cracks. Ettringite was not observed.

2.7.2 Montreal (Canada) (Bérard et al., 1975)

As mentioned before, in 1971 and 1972, similar cases of distressed concrete structures in Montreal were brought to the attention of Bérard and coworkers (Section 3.6.4).

In order to determine the amount of sulfide-bearing shale required to cause the unwanted oxidation reactions, twenty concrete prisms were made. Ten of those prisms were made with shale particles recycled from the deteriorated concrete (maximum aggregate

particle size of 2 cm), while the other ten were made with shale extracted from the quarry (maximum aggregate particle size of 4 cm). The concrete prisms were subjected to cycles of wetting and drying. These cycles consisted of keeping the samples in a moist room at 22.8 °C for a certain period of time, after which the specimens were transferred to another room and allowed to dry for an equal period of time. All the samples suffered shrinkage, while only one specimen showed a longitudinal crack with iron oxide seeping through the crack. Although the test was unable to reproduce the distress observed in the field (expansion/cracking), the deleterious properties of the shale were somewhat highlighted since some shale particles near the surface of the test prisms generated pop-outs through the oxidation of pyrrhotite mainly visible along bedding planes.

Rock expansion tests were also carried out. Five blocks were cut from the shale and expansion measurements were carried out perpendicular to the bedding. Two of the blocks saturated in water expanded by over 0.2% in less than 100 days. Two other test blocks that were kept outdoors (so that variations due to natural weather conditions could be followed) expanded slightly less than the first two blocks. A fifth specimen, kept indoors at room temperature, showed a small shrinkage, mainly because of a small decrease in water content. Oxidation of sulfides was visible and concentrated along thin bedding planes.

2.7.3 South Africa (Oberholster and Kruger, 1984)

Laboratory investigations were carried out using prisms that were cut from bricks and prisms cast using the aggregate from Penge. In the second case, two mix designs were used, namely aggregate-to-cement ratios of 5:1 and 10:1, and these were combined with two manufacturing procedures, i.e. well compacted and poorly compacted. Some prisms were stored at 38°C, either under water or above water in sealed containers.

The prisms cut from the bricks and stored under water expanded by approximately 0.40% after 1000 days; the amount of expansion was however much less than that obtained for the specimens stored above water (more than 1% after 1000 days).

The manufactured prisms started to expand after 22 months. After that period, some of the test prisms stored above water, started expanding at a high rate, while those stored under water did not expand, even after three years. From the above results, it appeared that

only the laboratory prisms cast from the low cement (aggregate-to-cement ratio 10:1) content concrete expanded, and that the well compacted prisms expanded at a higher rate than the poorly compacted ones. Expansions of more than 1% were measured. In the test prisms that were manufactured in the laboratory, no thaumasite was found, instead it was ettringite.

2.7.4 Spain (Chinchón et al., 1990)

Chinchón et al. started a testing program in 1990 in order to study the phase behaviour of aggregate minerals undergoing reaction with water and cement components. Two sets of mortars were made using a P-450 Portland cement. The first set of mortar was composed of limestone (with 4.20% hexagonal pyrrhotite and 0.70% pyrite), cement and water. The second set of mortar was composed of shale (with unknown values of pyrrhotite and pyrite), cement and 20% water. The two types of lithologies had sulfides in their composition, hexagonal pyrrhotite and pyrite 15g-samples of the mortars were separated into porcelain capsules and were maintained at 20°C and 97% of relative humidity and the mortars were monitored over a 140-day period. The formation of ettringite in the mortars made with limestone was slower than in the case of the mortars made with shale. A large production of ettringite and a reduction in the pyrrhotite and pyrite contents was noted in both cases. According to the authors, the results show that the mortar was deteriorated through the formation of ettringite resulting from the iron sulfide oxidation products and the reaction of those with the cement paste products.

2.7.5 Cornwall and Devon, England (Lugg and Probert, 1995; RICS, 2005)

During the 1980s, the market price of houses that were thought to be affected by the “Mundic” problem started to drop and, at that time, there was no effective way to determine whether the houses had the problem or not. In 1985, the Royal Institute of Chartered Surveyors (RICS), commissioned a committee to investigate the problem (Lugg and Probert, 1995). This committee thus developed a guidance note that recommended the use of chemical and petrographic analyses for the identification of the “Mundic” concrete. Besides the chemical and petrographic analyses, the RCIS implemented an experimental program to measure the unrestrained linear expansion of concrete cores taken from the “problematic” houses. This test is an accelerated weathering test where the concrete cores

are subjected to a water-saturated atmosphere (100%HR) at a constant temperature of 38°C and for a period of at least 250 days. Cores showing an average expansion upon wetting exceeding 0.075% at 7 days were considered to have failed the test; on the other hand, if the expansion was less than the above limit, the test had to be pursued up to 250 days. Core specimens showing an expansion lower than 0.025% over the remaining part of the 250 day test period, are likely to remain stable under ambient conditions for many years, provided that normal levels of care are maintained.

2.7.6 Brazil (Gomides, 2009)

In Brazil, some of the bedrocks supporting hydraulic dams and some aggregates available for dams construction contain iron sulfides. Due to the lack of information on the various factors promoting and/or accelerating the oxidation of sulfides and the influence of the type of hydraulic cement on the development of pathological manifestations in concrete made with sulfide-bearing aggregates, a study was launched on this topic (Gomides, 2009). Gomides thus started a PhD to investigate the influence of five types of cements on the durability of concrete incorporating aggregates with different sulfide contents.

The experimental program was separated into two stages. In *stage 1*, the concretes were prepared with a quartz-muscovite-schist aggregate containing 3.89% of sulfides, of these sulfides 3.40% correspond to pyrrhotite, 0.31% correspond to pyrite and 0.17% to marcasite. A water-to-cement ratio of 0.45 was selected for concrete manufacturing. Three types of cements were used; one type of cement was for reference (CP II-F-32), while the other two resulted from the partial replacement of the reference cement by 40% (CP40) and 60% (CP60) of ground granulated blast-furnace slag. In *stage 2*, the concrete specimens were made with three types of cement, specifically: CP II-F-32, CP III-40-RS (sulfate resistant cement) and CP IV-32 (pozzolanic binder (25% to 40%) and 38% of fly ash). The aggregate used in *stage 2* was the same as that used in the *stage 1*, but this aggregate had previously been stored outdoors in steel drums, i.e. subject to all kinds of weathering conditions, during a period of two years. After those two years, the aggregate in question had lost approximately 86% of its sulfide content due to an oxidation process, with a remaining/residual sulfide content of 0.56%. Of this value, 0.29% corresponded to pyrrhotite and 0.27 % corresponded to pyrite.

During the two stages, the concretes specimens used for testing consisted of prisms (75 mm x 75 mm x 285 mm in size) and cylinders (100 mm in diameter x 200 mm in height). After casting, all specimens were stored, for all the time of the experimental program, in a humid chamber where the temperature was maintained between $23^{\circ}\text{C} \pm 2$ and the relative humidity $\geq 90\%$.

The main purpose was to assess the performance of the concretes prepared with these different cements due to internal sulfate attack resulting from the process of sulfide oxidation of the aggregate in a high moisture environment up to approximately five years.

The results showed that pyrrhotite is the most reactive sulfide in the system, i.e. the main mineral responsible for the changes observed in the aggregates extracted from the concretes. It was found that the oxidation promotes the expansion of this material, besides interfering with its elastic-mechanical properties. In the specimens from *stage 1*, external spots of rust, white efflorescence, chipping and breakdown of aggregate particles containing high levels of sulfides were observed. These features of external deterioration resulted from the oxidation of sulfides and were more pronounced in the concrete containing higher proportions of ground granulated blast-furnace slag (CP40 and CP60). The concretes prepared in *stage 2* showed no visual pathological manifestation related with the iron sulfides. In general, the concretes had typical deleterious products of sulfate attack, i.e. ettringite and gypsum. The concrete CP40 and CP60 were those with a higher concentration of these products in *stage 1*. In *stage 2*, no information was obtained about the concentration of ettringite and gypsum. The expansion values calculated after five and a half years of testing reached a maximum value of 0.052% for the CP60 (*stage 1*), and a maximum value of 0.041% for the CPIII after four and a half years of testing (*stage 2*), suggesting that the higher the concentration of sulfides and aluminate ions present in the system, the greater the expansion or the observed levels of deterioration.

It was also verified that the higher the concentration of sulfides, especially pyrrhotite, the more intense and severe was the observed levels of deterioration. A high-moisture environment was an essential parameter to accelerate the oxidation process of these minerals in concrete aggregates.

2.7.7 Switzerland (Schmidt et al., 2011)

In order to recreate the deterioration mechanism responsible for the damage in the dam in Switzerland (section 2.7.11), concrete prisms (70 × 70 × 280 mm in size) were prepared with the same aggregate that was utilized in the dam (Schmidt et al., 2011). The cement utilized was an ordinary Portland cement (CEM I 42.5), with a water-to-cement ratio of 0.50. Those prisms were stored in water for 5 years at 60°C.

The degree of expansion could not be assessed accurately. Petrographic and SEM/EDS analyses of the prisms were performed after 4 years of testing. The laboratory concrete samples had the same appearance and reaction pattern as the dam concrete, but the extent of reaction of the iron sulfides was much lower. The reaction products observed were the same that the ones observed in the dam, i.e. iron oxide, iron hydroxides and ettringite. These observations clearly indicate a very slow reaction rate of the iron sulfide inclusions and the difficulties to reproduce the iron sulfide degradation in the laboratory conditions (immersion) used. Due to the low degree of reaction, it was not possible to assess the influence of temperature on kinetics. These findings indicate the difficulties to reproduce the specific iron sulfide degradation in the laboratory.

2.7.8 Spain (Chinchón-Payá et al., 2012)

Chinchón-Payá and coworkers in the last 20 years have studied samples of concretes from dams in which the metamorphic slate coarse aggregate very often contained oxidizable iron sulfides, usually in the form of pyrrhotite. It has been observed in practice that this combination produces conditions more harmful to concrete than other situations such as for example limestones with pyrite.

The work exposed here is the first step of a more extensive study on the role of different iron sulfide minerals when they form part of aggregates used in concrete dams, and has a twofold objective: firstly, to study the oxidation of pyrite and pyrrhotite samples under the same experimental conditions, seeking to differentiate their respective behaviors; and secondly, to investigate the effects of adding different aggregates to solutions containing pyrite and pyrrhotite in order to check the effect that the host rock has on the speed of reaction and the nature of the reaction products.

Two pyrite and pyrrhotite samples were obtained from the Catalanian Pyrenees (Spain). Approximately 500 g of each sulfide minerals was obtained by separation from the host rock. The pyrite has a composition of S 49.03% and Fe 46.37%, while the composition of the pyrrhotite is S 35.18% and Fe 61.12%. The aggregates used were a Miocene marlstone, a Cretaceous limestone and an Ordovician shale. The three aggregates were chosen taking into account their low content in sulfur. The iron sulfides and aggregate samples were ground in an agate mortar and the fraction with a particle size between 1 mm and 500 μm was used in the experiments.

Two types of experiments were carried out, with and without the addition of coarse aggregates. In the experiment without the addition of aggregates, 10 g of pyrite and 10 g of pyrrhotite were placed in two 500 ml precipitation vessels with 200 ml of water. A constant air flow was applied to the suspension by means of a pump with a pressure of ca. 120 mbar. The pH and solution potential (Eh) values were measured daily for 2 months. At the end, the reaction products were analyzed to determine the sulfate and the total Fe contents.

In the second experimental set-up, binary samples of aggregate and iron sulfide were prepared in proportions of 95% and 5% by mass respectively. The solids were placed in 500 ml precipitation vessels with 200 ml of water; a similar experiment to that described before for the sulfides without aggregates was conducted.

In the case of the dissolution of iron sulfides alone, the Eh (redox potential) during the experiments was almost constant; a significant increase was noted initially only in the case of pyrite and a constant value was reached a few days after the beginning of the experiment. Both solutions present positive potential values, though to a higher extent in the pyrite solution. The pH monitoring showed a fast decrease at the moment of placing the pyrite in contact with water (the pH decrease from 4.5 to almost 3.5), followed by a slight gradual decrease until they reached constant values (pH 3) about 50 days after the beginning of the experiment. The results obtained indicate that the reaction of pyrrhotite generates more sulfates than pyrite.

In the case of exposing the iron sulfides in combination with aggregates, it was noticed, for the three aggregates, a significant increase of pH values (between 6 and 10)

when compared to those obtained for the pure sulfide oxidation experiment. In the case of the iron sulfides combined with marlstone and limestone, there was a buffer effect due to the presence of carbonate minerals. In the iron sulfides with shale case, the pH is controlled by the dissolution of feldspars and micas. The results showed no existence of Fe^{2+} in solution, meaning that the Fe has precipitated in the form of a hydroxide. In the case of SO_4^{2-} concentration, in all three cases, the values were much higher with pyrrhotite than with pyrite.

The results of the various experiments confirmed that aggregates containing pyrrhotite release more sulfates to the solution as a result of the oxidation process than those with pyrite despite the fact that the sulfur content of pyrite (53.4%) was higher than that of pyrrhotite (36.4%).

2.8 The standardization state face to the problematic of iron sulfides

Canadian standards highlight, in the following terms, the risk of using aggregates incorporating iron sulfides in concrete (Clause 4.2.3.6.2, CSA A23.2/A23.2-2014):

Aggregates that produce excessive expansion in concrete through reaction other than alkali reactivity shall not be used for concrete unless preventive measures acceptable to the owner are applied.

Note: *Although rare, significant expansions can occur due to reasons other than alkali-aggregate reaction. Such expansions might be due to the following:*

(a) the presence of sulfides, such as pyrite, pyrrhotite, and marcasite, in the aggregate that might oxidize and hydrate with volume increase or the release of sulfate that produces sulfate attack upon the cement paste, or both (see Annex P for a comprehensive description of the impact of sulfides in concrete aggregate on concrete behaviour);

Back in 1983, the French standard NF P18-301 limited the total sulfur content in concrete aggregates to 1% as SO_3 (0.4% as S). This threshold was further increased/relaxed in the context of European standardization NF EN 12 620 (2003), which specified that the total sulfur content (S) of the aggregates and fillers, must not exceed:

- 1% S by mass for aggregates other than air-cooled blast furnace slag;
- 2% S by mass of S for air-cooled blast furnace slag.

Note: Special precautions need to be taken when pyrrhotite, an unstable form of iron sulfide ($\text{Fe}_{(1-x)}\text{S}$) is present in the aggregate. If the presence of this mineral is proven, a maximum total sulfur content of 0.1% (as S) shall apply.

Despite the fact that the potential problem related to the use of sulfide-bearing aggregates in concrete is highlighted in a number of concrete Standards worldwide, no precise/detailed guidelines have been proposed to evaluate the potential reactivity of such aggregates other than the application of the chemical thresholds mentioned above. While these thresholds could be used as a screening tool for concrete aggregates, they need to be supplemented by other test methods when the total sulfur content is $> 0.10\%$. These tests would identify the type of sulfide mineral(s) present in the aggregate under test. Considering that 0.10% S represents about 0.19% by mass of pyrite or 0.27% by mass of pyrrhotite, the precise identification of such small quantities of material could represent a significant challenge for petrographers. In addition, such quantities are too small to be identified by commonly used X-Ray diffraction analysis. Also, even if the presence of pyrrhotite is identified in the aggregate under investigation, not all forms of pyrrhotite are equally “reactive” (Janzen et al., 2000; Mikhlin et al., 2002; Belzile et al., 2004) thus, other tools are needed for the routine evaluation of aggregates containing iron sulfide-bearing minerals.

2.9 Research needs

As documented in the literature review (section 2), several cases of deterioration of the concrete containing sulfide-bearing aggregates have been documented in the past decades. In the analyzed cases, problematic aggregates consisted mainly of limestone, shale and schist, porous and mechanically weak rocks (Bérard et al., 1975; Chinchón et al., 1995; Casanova et al., 1996; Ayora et al., 1998). In the case of concrete damage observed in the Trois-Rivières area, the rock used is a massive rock. A few cases documenting concrete deterioration using a similar kind of rock were published by Hagerman and Roosaar (1955), Mielenz (1963), Tagnit-Hamou et al. (2005).

In the published literature, attempts to recreate the mechanisms responsible for the oxidation of iron sulfides and damage of concrete have been made, but unfortunately without success. As well no test method capable to evaluate or predict the potential reactivity of such aggregates has been proposed to date.

As previously mentioned (section 2.4), the main parameters that contributes to the oxidation reaction of iron sulfides are presence of oxygen, moisture and high temperature. The data presented in the literature review clearly showed that immersing the mortar or concrete test specimens in water (Schmidt et al., 2011; Oberholster et al., 1984; Hagerman and Roosar, 1955) or keeping them at a high relative humidity of 100% or close to 100% (Lugg and Probert, 1996; Chinchón et al., 1989 and 1990; Gomides, 2009) would not promote expansion or the oxidation reaction will be too slow since, in both cases, the oxygen diffusion is insufficient to accelerate the oxidation of the iron sulfide minerals. Steger (1982) showed that the oxidation of sulfide minerals increases with an increase in relative humidity for values between 37 and 75% RH, while Mbonimpa et al. (2003) stressed that excessive humidity will slow down the reaction. Moreover, samples immersed in water will suffer from a significant decrease of the alkalinity of the concrete pore solution.

The samples submitted to low temperatures (20 to 38°C) (Bérard et al., 1975; Oberholster et al., 1984; Chinchón et al., 1989 and 1990; RICS, 2005; Gomides, 2009) will take long time to react since, as mentioned, sulfides oxidation rate increases significantly with increasing temperature (Steger, 1982; Divet and Davy, 1996). However, generation of ettringite will be eliminated at high temperatures, as tested by Hagerman and Roosar (1955) (225°C) because ettringite is stable up to temperature < 80°C (Zou and Glasser, 2001).

The production of gypsum and/or ettringite was noticed in some studies (Schmidt et al., 2011, Oberholster et al., 1984; Gomides, 2009). Thaumasite, one of the deterioration products identified by Oberholster and Krüger, 1984, and by Oberholster et al., 1984 in problematic concrete was not observed in their laboratory tests; this is not surprising considering that the ideal temperature conditions for thaumasite formation is between 0 and 5°C (Aguilera et al. 2001) while the temperature tested was 38°C.

The development of an evaluation protocol capable to predict the deleterious potential of aggregates containing iron sulfides is necessary. The use of the ideal conditions of temperature and humidity as well as the use of oxidation solutions in the acceleration of the iron-sulfides oxidation and sulfates production will be tested. The development of this evaluation protocol is essential to avoid the use of reactive sulfide-bearing aggregates in concrete and as result avoid the millions of dollars of unnecessary spending in repairs and replacements of damaged structures.

Chapter 3

Ph.D. research program

3.1 General description

Figure 3.1 describes the different phases of the Ph.D. project. As mentioned before, the research program focuses on developing a better understanding of the degradation processes in concrete involving aggregates containing iron sulfide minerals.

To begin, a comprehensive literature review was carried out to determine the state of current knowledge on the mechanisms and main factors responsible for this problem (**Chapter 2**).

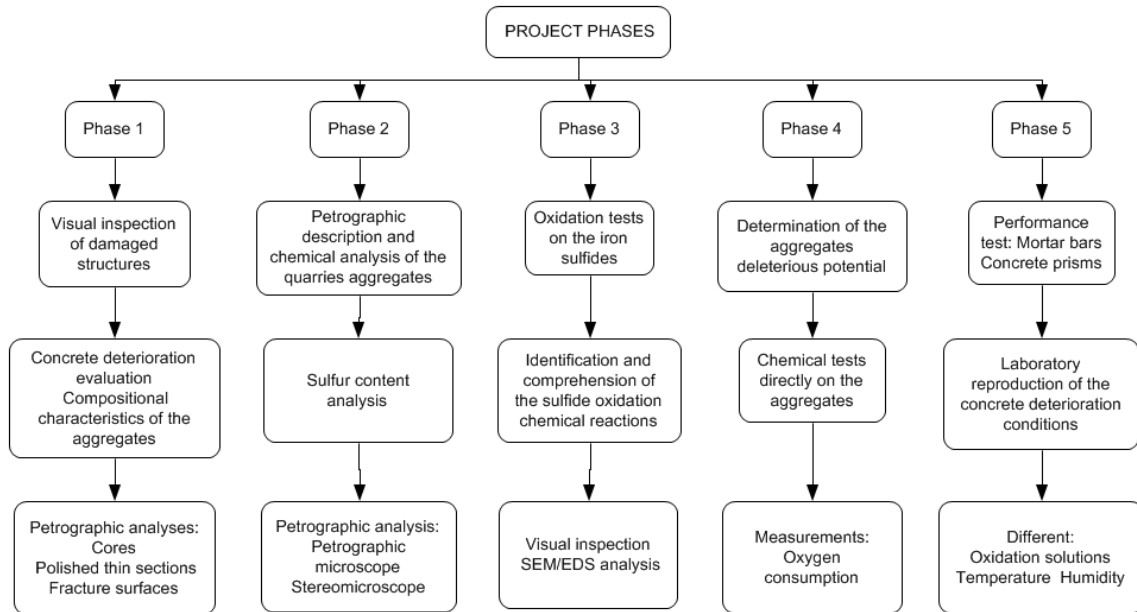


Figure 3.1: Phases of the Ph.D. project «Concrete deterioration incorporating sulfide-bearing aggregates».

The experiments started with the visual inspection of a number of damaged structures in Trois-Rivières and the detailed petrographic analysis of concrete cores extracted from those structures was performed (**Experimental phase 1**) (**Chapter 4**). In order to determine the nature, the relative amount and the spatial distribution of the deterioration products, polished thin sections as well as c fracture surfaces were prepared from the above cores and were analysed using a petrographic microscope (Nikon Eclipse E600 Pol), a scanning electronic microscope (SEM) equipped with an energy dispersive spectrometer

(EDS) (JEOL JSM-840) and an electron probe micro analyser (EPMA CAMECA SX-100). In parallel, the characterization (mineralogical, chemical and textural composition) (Appendix B) of rock samples collected in the Maskimo and B & B quarries (Saint-Boniface), the source of the aggregate materials used in the damaged structures, was performed (**Experimental phase 2**) (**Chapter 4**).

Then, the mechanisms responsible for the weathering of sulfide minerals (pyrite, pyrrhotite, chalcopyrite, pentlandite, Trois-Rivières aggregate) were studied on 1.25 to 2.5 mm particles subjected to different conditions of temperature, humidity and soaked in oxidizing solutions. The aim of this study was to establish favorable oxidation conditions and to study the nature of the resulting secondary products (**Experimental phase 3**). The results obtained in this phase, even if they have contributed to the development and advancement of this Ph.D. program, were published elsewhere (Rodrigues et al., 2012b).

In the sulfide oxidation reaction, oxygen is one of the reactants. Elberling et al. (1994) developed a test to evaluate the rate of oxidation of mine tailings containing sulfide minerals, which consists in the measurement of the oxygen consumption in the headspace at the top of a cylinder containing the rock material placed in favourable oxidizing conditions. When oxygen is consumed, its concentration decreases in the closed volume. The aim of this part of the study (**Experimental phase 4**) was thus to adapt the test conditions to determine whether sulfide-bearing aggregates could be potentially harmful or harmless in concrete (Aggregate particle size, moisture condition, thickness of the compacted aggregate material), and to verify the precision of the test. These tests are detailed in **Chapter 5**.

Tests on mortar bars and concrete specimens were made under different conditions of humidity, temperature and using different oxidizing solutions, so as to establish favorable conditions for the development of a performance test that will reproduce, in the laboratory, the expansive process responsible for the damage of the concrete incorporating sulfide-bearing aggregates (**Experimental phase 5**). This phase is detailed in **Chapter 6**.

Finally, based on the tests developed and the analysis performed (Experimental phases 1 to 5), an **evaluation protocol** for concrete aggregates containing iron sulfide minerals is proposed (**Chapter 7**). The protocol is divided into 3 major phases: (1) total

sulfur content measurement, (2) oxygen consumption evaluation, and (3) accelerated mortar bar expansion test.

Chapter 4

Mineralogical and chemical assessment of concrete damaged by the oxidation of sulfide-bearing aggregates

4.1 Introduction

This paper was published in Cement and Concrete Research journal, Volume 42 (2012), pp. 1136-1347. It was submitted in January 2012 and accepted for publication in June 2012.

4.2 Résumé

La détérioration du béton incorporant des granulats contenant des sulfures de fer a été observée dans la région de Trois-Rivières (Québec, Canada). Un examen pétrographique détaillé d'échantillons de béton a été effectué en utilisant une combinaison d'outils dont l'évaluation au stéréobinoculaire, la microscopie optique, la microscopie électronique à balayage, la diffraction des rayons-x et la microsonde électronique.

Des analyses effectuées on a pu constater que le granulat utilisé était une roche ignée intrusive contenant différents sulfures de fer. Les produits de réaction secondaires observés comprennent différentes formes de 'rouille', du gypse, de l'ettringite et de la thaumasite. En présence d'eau et d'oxygène, la pyrrhotite s'oxyde et forme des oxyhydroxydes de fer et de l'acide sulfurique. L'acide réagit avec les phases de la pâte de ciment et provoque la précipitation de sulfates. La compréhension des deux mécanismes impliqués, oxydation et attaque par les sulfates, est importante de façon à être en mesure de les reproduire en laboratoire, permettant le développement d'un test de performance afin d'évaluer le potentiel d'expansion délétère dans le béton dû aux sulfures de fer présents dans le granulat.

4.3 Scientific publication no. 1

Mineralogical and chemical assessment of concrete damaged by the oxidation of sulfide-bearing aggregates: importance of thaumasite formation on reaction mechanisms

A. Rodrigues, J. Duchesne, B. Fournier, B. Durand, P. Rivard, and M. Shehata

Abstract

Damages in concrete incorporating sulfide-bearing aggregates were recently observed in the Trois-Rivières area (Québec, Canada), characterized by rapid deterioration within 3 to 5 years after construction. A petrographic examination of concrete core samples was carried out using a combination of tools including: stereomicroscopic evaluation, polarized light microscopy, scanning electron microscopy, X-ray diffraction and electron microprobe analysis.

The aggregate used to produce concrete was an intrusive igneous rock with different metamorphism degrees and various proportions of sulfide minerals. In the rock, sulfide minerals were often surrounded by a thin layer of carbonate minerals (siderite). Secondary reaction products observed in the damaged concrete include “rust” mineral forms (e.g. ferric oxyhydroxides such as goethite, limonite ($\text{FeO}(\text{OH})\text{nH}_2\text{O}$) and ferrihydrite), gypsum, ettringite and thaumasite. In presence of water and oxygen, pyrrhotite oxidizes to form iron oxyhydroxides and sulfuric acid. The acid then reacts with the phases of the cement paste/aggregate, and provokes the formation of sulfate minerals. Understanding both mechanisms, oxidation and internal sulfate attack, is important to be able to duplicate the damaging reaction in the laboratory conditions, thus allowing the development of a performance test for evaluating the potential for deleterious expansion in concrete associated with sulfide-bearing aggregates.

Keywords: Petrography; Degradation; Sulfate attack; Thaumasite; Ettringite

4.3.1 Introduction

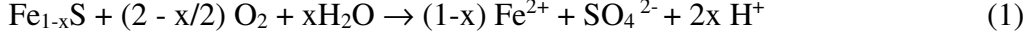
Recently, rapid deterioration of concrete foundations occurred in houses and commercial buildings in the Trois-Rivières area (Québec, Canada). In many cases only three to five years after construction. More than 900 residential owners have faced serious issues related to the deterioration of their concrete housing foundations and slabs. In some cases, the deterioration was such that immediate remedial actions were required.

The distressed concrete structures display map cracking, pop-outs and yellowish discoloration on the surface of the walls. A large number of concrete cores extracted from the above structures were investigated in the laboratory. In all cases, the coarse aggregate used to produce concrete was an intrusive igneous rock showing different degrees of metamorphism, and containing various proportions of sulfide minerals, mainly pyrrhotite (Fe_{1-x}S) and pyrite (FeS_2), among which several particles were covered with rust. A deleterious process involving the oxidation of sulfide minerals is thought to have caused the swelling and cracking of the affected concrete elements. The exact mechanisms involved, as well as the critical factors responsible for the problem, are still open to debate.

Iron sulfides are common minor constituents in many rock types. Consequently, concrete aggregates may contain a certain amount of iron sulfides, mainly pyrite and pyrrhotite. Pyrrhotite is a non-stoichiometric mineral of general formula Fe_{1-x}S , with x varying from 0 (FeS) to 0.125 (Fe_7S_8) [1-2]. These sulfide minerals are unstable in the presence of oxygen and humidity, and pyrrhotite is known as one of the most “reactive” of the sulfide minerals [3]. Belzile et al. 2004 [2] presented a review of pyrrhotite oxidation processes focusing on the main mechanisms and factors controlling the reaction.

Some cases of concrete degradation associated to the oxidation of iron sulfide minerals are reported in the literature for porous and mechanically weak rocks, such as black shales and schists [4-9]. In the present study, the aggregate involved is a massive rock, an anorthositic gabbro. Despite its good mechanical performances (strength, modulus of elasticity, and resistance to abrasion), major features of deterioration were observed in the aggregate particles and the concrete only three to five years after construction.

It is well-known from the literature that sulfide minerals are unstable in oxidizing conditions. Upon exposure to water and oxygen, sulfide minerals oxidize to form acidic, iron and sulfate-rich by-products according to the following equations [2]:

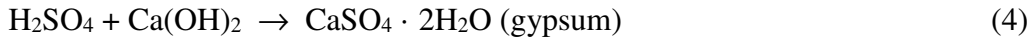


The oxidation of ferrous iron (Fe^{2+}) produces ferric ions (Fe^{3+}) as per Eq. (2) which can precipitate out of solution to form ferric hydroxide, if the pH is higher than 3.5 Fe^{2+} is oxidized and precipitated as ferric oxyhydroxides, principally ferrihydrite ($\text{Fe}_2\text{O}_3 \cdot 0.5(\text{H}_2\text{O})$) and goethite (FeOOH) Eq. (3).

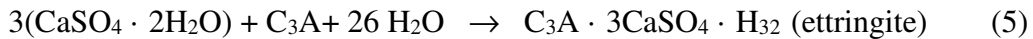


The oxidation reaction of iron sulfides occurs only in the presence of oxygen and humidity, and it generates various mineralogical phases [2, 4]. According to Divet and Davy [10], high pH conditions, as those found in concrete, enhance iron sulfide oxidation.

Steger [11] has shown that the oxidation of pyrrhotite presents two pathways to form goethite and ferric sulfate. According to Grattan-Bellew and Eden [12] and Shayan [13], the sulfuric acid generated through this process reacts with the solids of the cement paste, particularly with the portlandite ($\text{Ca}(\text{OH})_2$), to form gypsum ($\text{CaSO}_4 \cdot 2\text{H}_2\text{O}$) according to the following equation:



The attack of concrete by sulfates resulting from the oxidation of sulfide-bearing aggregates would produce secondary ettringite ($\text{Ca}_6\text{Al}_2(\text{SO}_4)_3(\text{OH})_{12} \cdot 26\text{H}_2\text{O}$) following the reaction with the alumina-bearing phases of the hydrated portland cement paste Eq. (5).



In a general way, secondary products most frequently generated during the oxidation of iron sulfides, are the "rust" in its different forms (ferric oxyhydroxides such as goethite, limonite ($\text{FeO}(\text{OH})\text{nH}_2\text{O}$) and ferrihydrite), sulfates including gypsum and ettringite. The

degradation of concrete is thus due to the combined effects of the oxidation of iron sulfides followed by internal sulfate attack in the cement paste. Both reactions create secondary minerals that can cause expansion, but significant expansion in the aggregate particles has to be attributed to the oxidation of iron sulfides. According to Casanova et al. [6], the reaction of pyrrhotite oxidation forming iron sulfate may generate volume change in the order of 187 cm^3 per mole of sulfide (maximum expansion at reaction completion). The same authors presented volume changes of 42, 183, and 172 cm^3 per mole of sulfide for gypsum, calcium aluminate monosulfate and ettringite, respectively.

In spite of the fact that the reaction mechanisms seem relatively well understood and that rapid deteriorations were observed in the field, no or limited success has been achieved so far in terms of reproducing the damages under laboratory conditions [4, 8, 14, 15]. The goal of this study is to present a detailed characterization of the damaged concrete materials in order to reach a better understanding of the mechanisms involved, thus providing critical information for the development of a performance test for identifying the deleterious character of sulfide-bearing aggregates in concrete.

4.3.2 Research significance

This study is part of an extensive research project which objectives are: 1) to assess the mineralogical, chemical and mechanical properties of damaged concretes containing sulfide-bearing aggregates; 2) to understand the mechanisms responsible for concrete degradation; 3) to reproduce the degradation under laboratory conditions; and finally 4) to develop a performance test (or testing program), as no quality control test currently exists, to enable the identification of potentially deleterious sulfide-bearing aggregates prior to their use in concrete.

This paper presents the results of the detailed mineralogical and chemical assessment of the secondary reaction products found in deteriorated concrete samples incorporating the sulfide-bearing aggregates from the Trois-Rivières area in Quebec, Canada.

4.3.3 Materials and methods

Visual inspection of concrete housing foundations was undertaken to identify any signs of deterioration including deformation, cracking (pattern and intensity), and exposure conditions of the affected concrete elements. Concrete samples (100-mm diameter cores) were drilled through the foundation walls for detailed petrographic examination. Concrete cores were cut or broken for macroscopic and microscopic examinations under the stereomicroscope for any signs of deterioration. Thin sections were then prepared for petrographic analysis in order to determine the nature, spatial sequence/distribution and relative amount of the secondary reaction products. Some cores were selected for further (physical and mechanical) testing. Crushed coarse aggregates were also sampled directly from selected stockpiles in the original quarry, i.e. processed from the anorthositic-gabbro intrusive body occurring in Saint-Boniface (Trois-Rivières area, Quebec, Canada).

The petrographic analysis of the coarse aggregates was carried out on thin sections using transmitted and reflected light microscope (Nikon Eclipse E600 Pol). Polished sections were carbon coated for electron probe micro analysis (EPMA) in a CAMECA SX-100 microprobe equipped with five WDS detectors (LIF, TAP, PET) and one PGT prism EDS detector. Operating conditions were set at 15 kV and 20 nA at high vacuum ($<10^{-5}$ Torr).

Concrete cores were broken or cut with a diamond blade. Some surfaces were polished for stereomicroscope examinations. Selected sub-samples were dried at room temperature and impregnated under vacuum with low viscosity resin (Epofix resin, Struers) and polished for polarizing petrography using SiC (silicon carbide) and loose alumina as abrasive powders. To avoid damage to the concrete during preparation, sections were prepared with isopropyl alcohol as a lubricant and excessive heating was avoided.

The microstructure of broken concrete samples was examined by scanning electron microscopy (SEM - JEOL JSM-840A) using backscattered electron (BSE) and secondary electron (SE) imaging and energy dispersive X-ray spectroscopy (EDS). Operating conditions were set at 15 kV. Prior to SEM observations, concrete samples were heated in an oven kept at 40°C for a minimum of 24 hours and coated with a thin layer of Au-Pd. Thin sections of the deteriorated samples were examined using transmitted and reflected

light microscopy (Nikon Eclipse E600 Pol), as well as under the SEM in the same analytical conditions as for the broken concrete samples.

Samples of secondary reaction products, collected on broken surfaces immediately surrounding oxidized aggregate particles, were analyzed by a Siemens D5000 X-ray diffractometer using Cu K α radiation generated at 20 mA and 40 kV. Specimens were step-scanned as random powder mounts from 6-18° 2 θ at 0.01° 2 θ steps integrated at 9s step⁻¹ in order to obtain detailed spectrum at low angle values.

4.3.4. Results

4.3.4.1 Visual inspection of concrete foundations

Rapid deterioration of concrete foundations occurred in a number of houses in the Trois-Rivières area (Québec, Canada), in most cases only three to five years after construction. Figure 4.1 presents an example of a house affected by this problem. The concrete foundation shows significant cracking and major cracks were filled up with sealer to prevent water ingress.



Figure 4.1: Cracking in housing concrete foundation. Cracks were filled up with sealant materials to prevent water and moisture infiltration

The deteriorated concrete displayed map cracking on the walls, with open cracks typically more pronounced at the corners of the foundation walls (Fig. 4.2A). Crack openings often reach up to 10 mm, and values as high as 40 mm were reported. Major

cracks are often concentrated next to rain gutters, which highlight the role of water or humidity in the reaction and deterioration processes (Fig. 4.2A). The figure also shows yellowish surface coloration often seen on the foundation walls. At some locations, iron hydroxides (or traces or “rust”) were visible in the open cracks. While major problems were observed on the concrete foundation walls, the entrance concrete decks and garage floor slabs were often deteriorated, as illustrated on Fig. 4.2B. Fig.4.2C shows pattern cracking extending to the interior side of the concrete foundation wall. Pop outs are often seen on the interior side of foundation walls, showing oxidized aggregate particle surrounded by a whitish/yellowish powdery deposit (Fig. 4.2D).

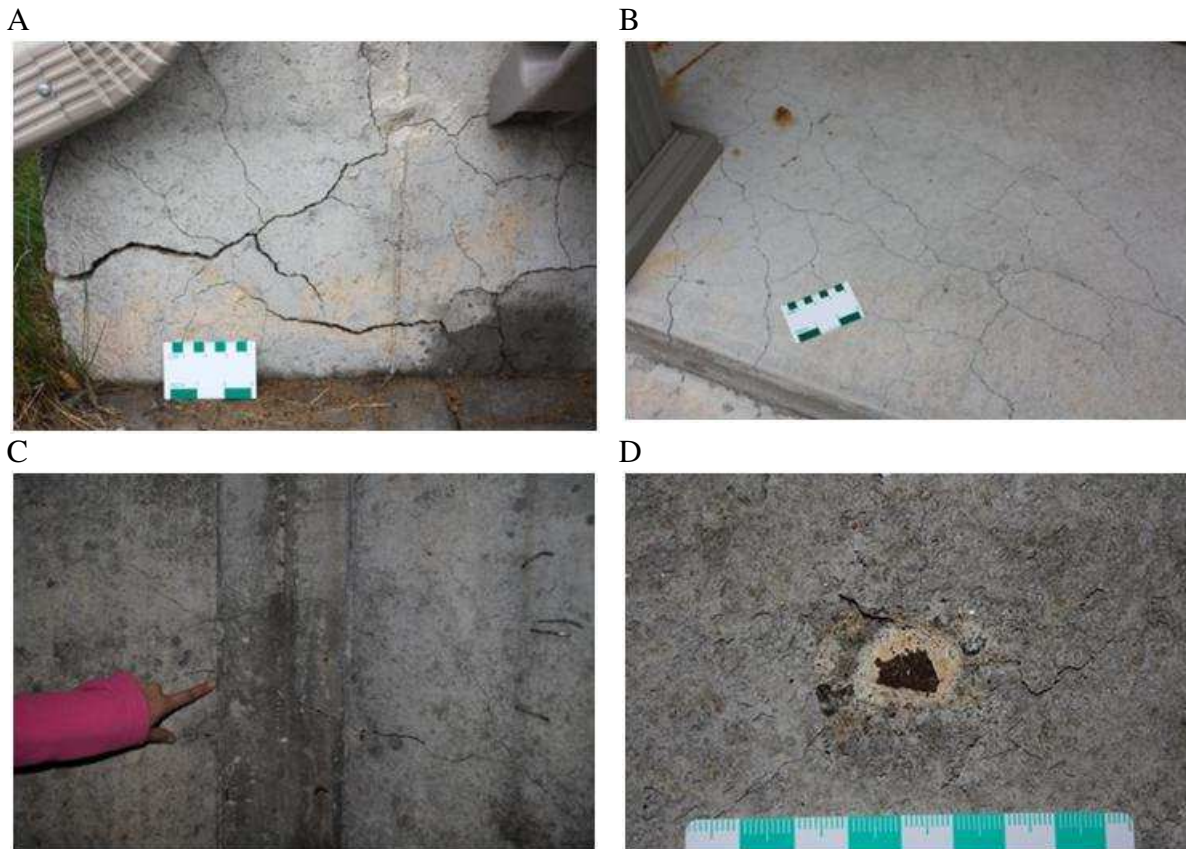


Figure 4.2: Features of concrete deterioration. A - Cracking in housing concrete foundations. Open cracks are typically more pronounced at the corners of the foundation blocks, often next to rain gutters. Yellowish surface coloration is often seen on the exposed foundation walls. B - Map cracking in the entrance concrete deck slab. C - Open cracks seen on the interior side of the concrete foundations. D – Pop outs on the interior side of a wall.

The extent of the deterioration often caused a major threat to the concrete structures and many housing foundations had to be replaced (Fig. 4.3). Typically, because it stands on

the concrete foundations, all the masonry and covering stone works are first removed from the structure. Houses (wood-framed) are then lifted up from their foundations and the later demolished and replaced. The remediation cost was estimated to be close to the original construction cost. More than 900 residential houses and some commercial buildings in the Trois-Rivières area are affected and will be repaired.

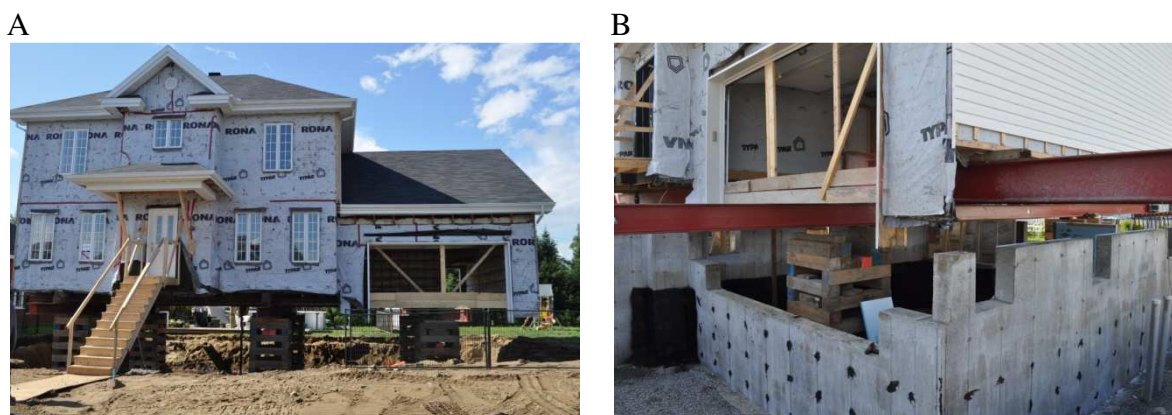


Figure 4.3: Replacement of the concrete foundation walls. All the masonry and covering stones were first removed. Houses (wood-framed) were then lifted up from their foundations. Concrete foundations were then demolished and replaced.

4.3.4.2 Petrographic examination of aggregates

Various samples of damaged concrete examined under a stereomicroscope and a polarizing microscope show that the altered concretes were all made with the same coarse aggregate containing a certain amount of sulfide minerals. The aggregate used to produce the concrete housing foundations is an anorthositic gabbro (*field* identification term), more precisely a norite or an hypersthene's gabbro, containing various proportions of sulfide minerals including pyrite, pyrrhotite, pentlandite ($(\text{Fe,Ni})_9\text{S}_8$) and chalcopyrite (CuFeS_2). Major constituents of this dark-colored coarse-grained dense rock consist of anorthite ($\text{CaAl}_2\text{Si}_2\text{O}_8$), with lesser amounts of biotite ($\text{K}(\text{Mg,Fe})_3\text{AlSi}_3\text{O}_{10}(\text{F,OH})_2$) and pyroxene ($\text{XY}(\text{Si,Al})_2\text{O}_6$).

Figure. 4.4 shows photomicrographs of thin sections of the anorthositic gabbro (norite) aggregate viewed under plane polarized light (Fig. 4.4 A, C).

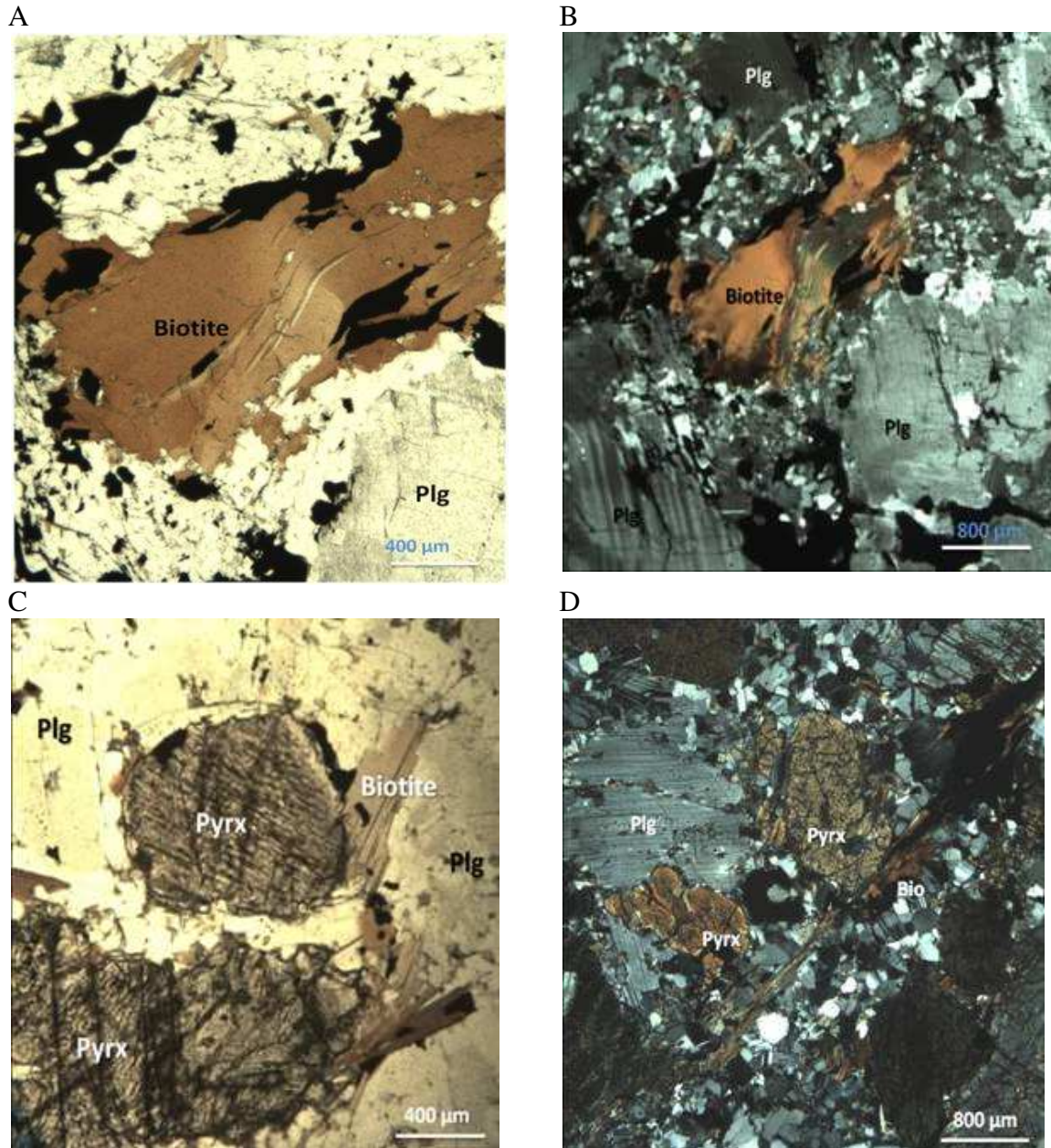


Figure 4.4: Photomicrographs of thin sections of the anorthositic gabbro. A and C: Views under plane polarized light. B and D: Views under crossed polarized light. (Plg: plagioclase feldspar; Pyrx: pyroxene; Bio: biotite; in black: sulfide minerals).

Fig.4.5 presents reflected light microscopy images of the aggregate where iron sulfides, for instance pyrite and pyrrhotite, are closely associated with each other and well disseminated into silicate minerals (Fig. 4.5A). Very fine inclusions of opaque minerals (e.g. sulfides) can be seen throughout silicates. Fig. 4.5B presents oriented blebs of “flame” pentlandite in pyrrhotite. Oriented intergrowths of pentlandite in the form of flames in

pyrrhotite are a common texture of exsolved pentlandite. Pentlandite flames are often oriented perpendicular to cracks or grain boundaries (Fig.4.5B, C, D).

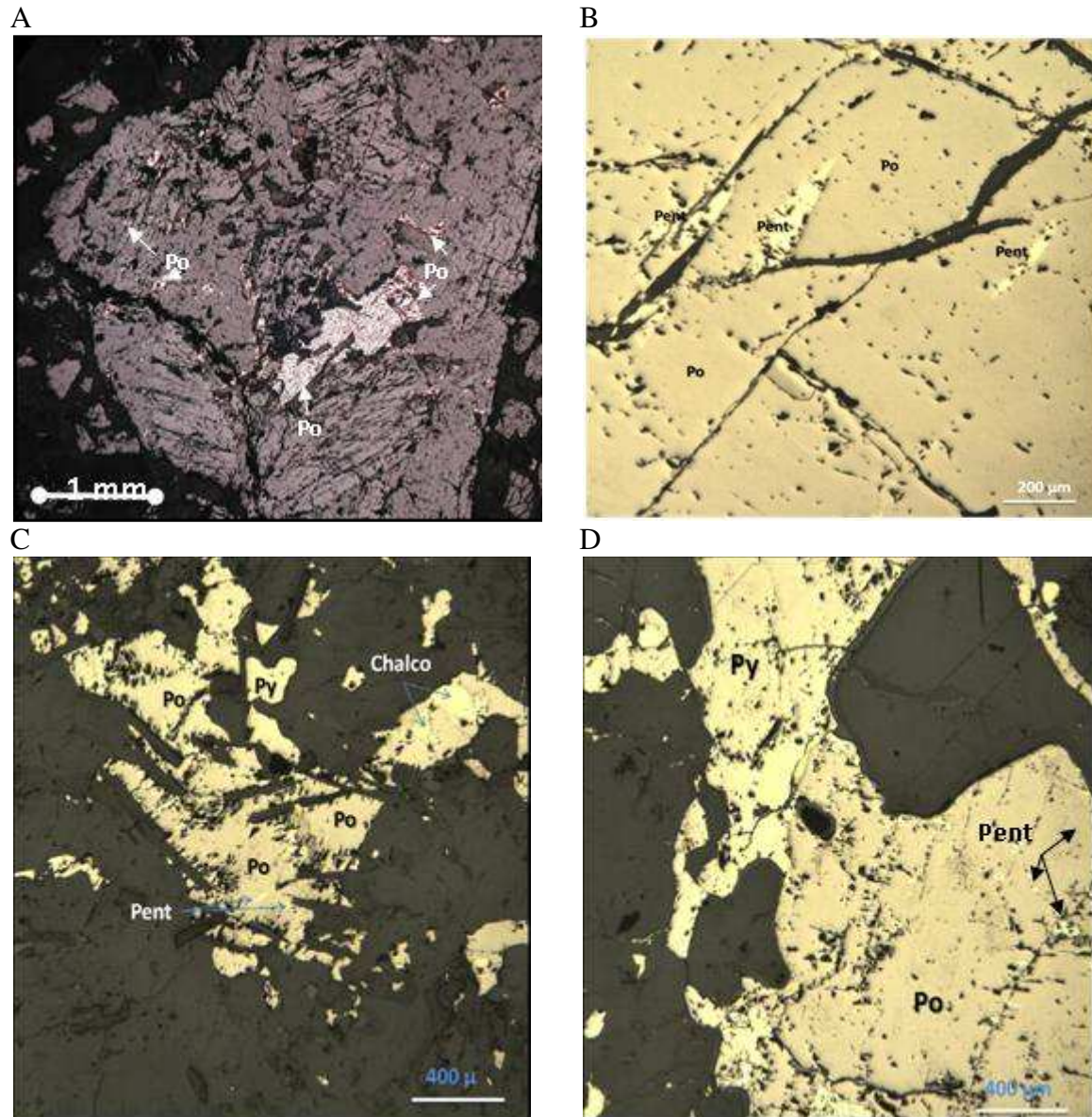


Figure 4.5: Reflected polarized light views of iron sulfide minerals included in the anorthositic gabbro. (Py: pyrite; Po: pyrrhotite; Pent: pentlandite; Chalco: chalcopyrite).

Fig.4.6 presents back-scattered electron (BSE) images of the sulfide minerals taken by EPMA.

Chalcopyrite and pentlandite are found in close contact with pyrrhotite (Fig. 4.6A). Pyrrhotite grains appear darker than pentlandite and chalcopyrite on the BSE image due to its lower atomic density. Fig. 4.6B presents a large grain of pyrrhotite with small inclusions of flame-textured pentlandite oriented perpendicular to grain boundaries or along main

cracks. Black areas in the BSE images correspond to resin or “light” silicate grains. A dark gray-colored phase can be seen surrounding the pyrrhotite grain and filling cracks within pyrrhotite (Fig. 4.6B). X-ray analysis showed that this phase is composed of iron (Fe), carbon (C) and oxygen (O) corresponding to siderite (FeCO_3), a carbonate mineral.

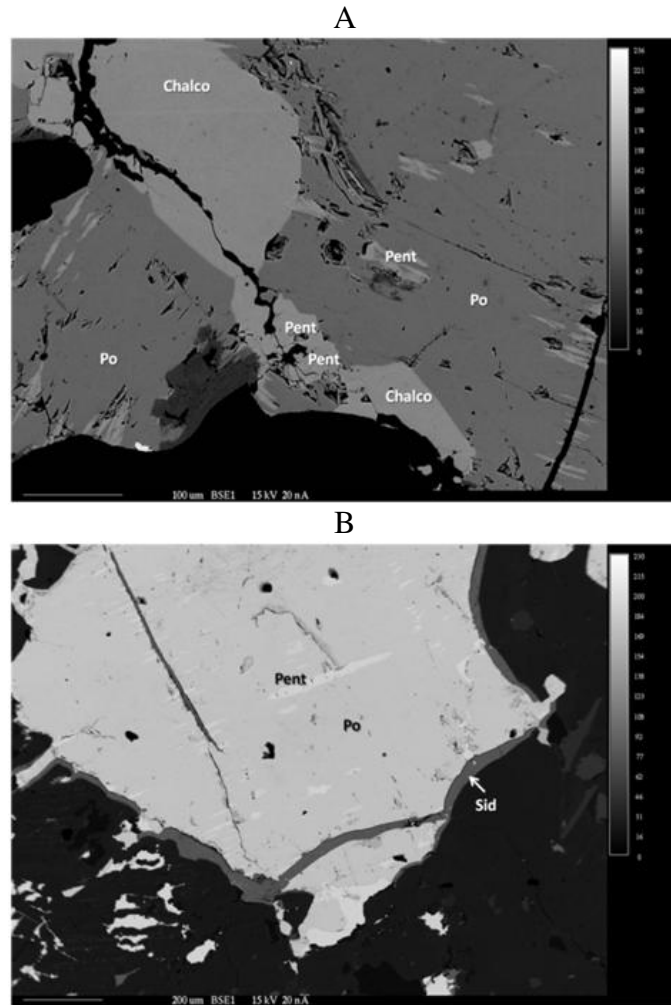


Figure 4.6: Back-scattered electron images (EPMA) of sulfide minerals included in the anorthositic gabbro. (Po: pyrrhotite; Pent: pentlandite; Chalco: chalcopyrite; Sid: siderite).

Fig. 4.7 presents photomicrographs of thin sections of the anorthositic gabbro (norite) viewed under plane polarized light showing the carbonate mineral surrounding the sulfide minerals and filling cracks within the latter phase. The carbonate mineral is present in all samples examined and is not an isolated case.

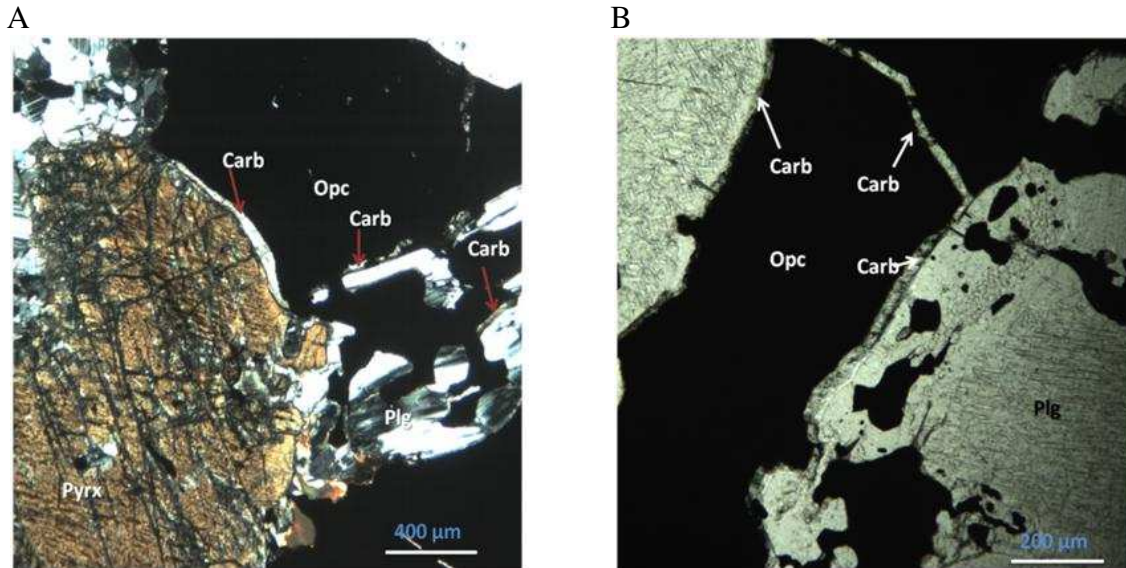


Figure 4.7: Photomicrographs of thin sections viewed under plane polarized light of the small layer of carbonate mineral surrounding or “coating” the sulfide minerals. Plg: plagioclase feldspar; Pyrx: pyroxene; Opc (opaque): sulfide minerals; Carb: carbonate minerals.

Figure 4.8 presents a detailed BSE image and corresponding X-ray microprobe mapping of a “typical” sulfide-bearing aggregate particle of the anorthositic gabbro. X-ray maps are formed by collecting characteristic X-rays from elements in the specimen. This procedure reveals elemental distributions and associations. Fig.4.8 in fact corresponds to a false color reconstruction, for display purposes, of the different phases present. The reconstruction highlights the close association between pentlandite and pyrrhotite. Siderite, the iron carbonate mineral, is present in thin layers “coating” the sulfides minerals and filling up cracks and porosity. Scattered irregular patches of chalcopyrite are found in pyrite and pyrrhotite, the latter being the most abundant sulfide minerals in the anorthositic gabbro under study.

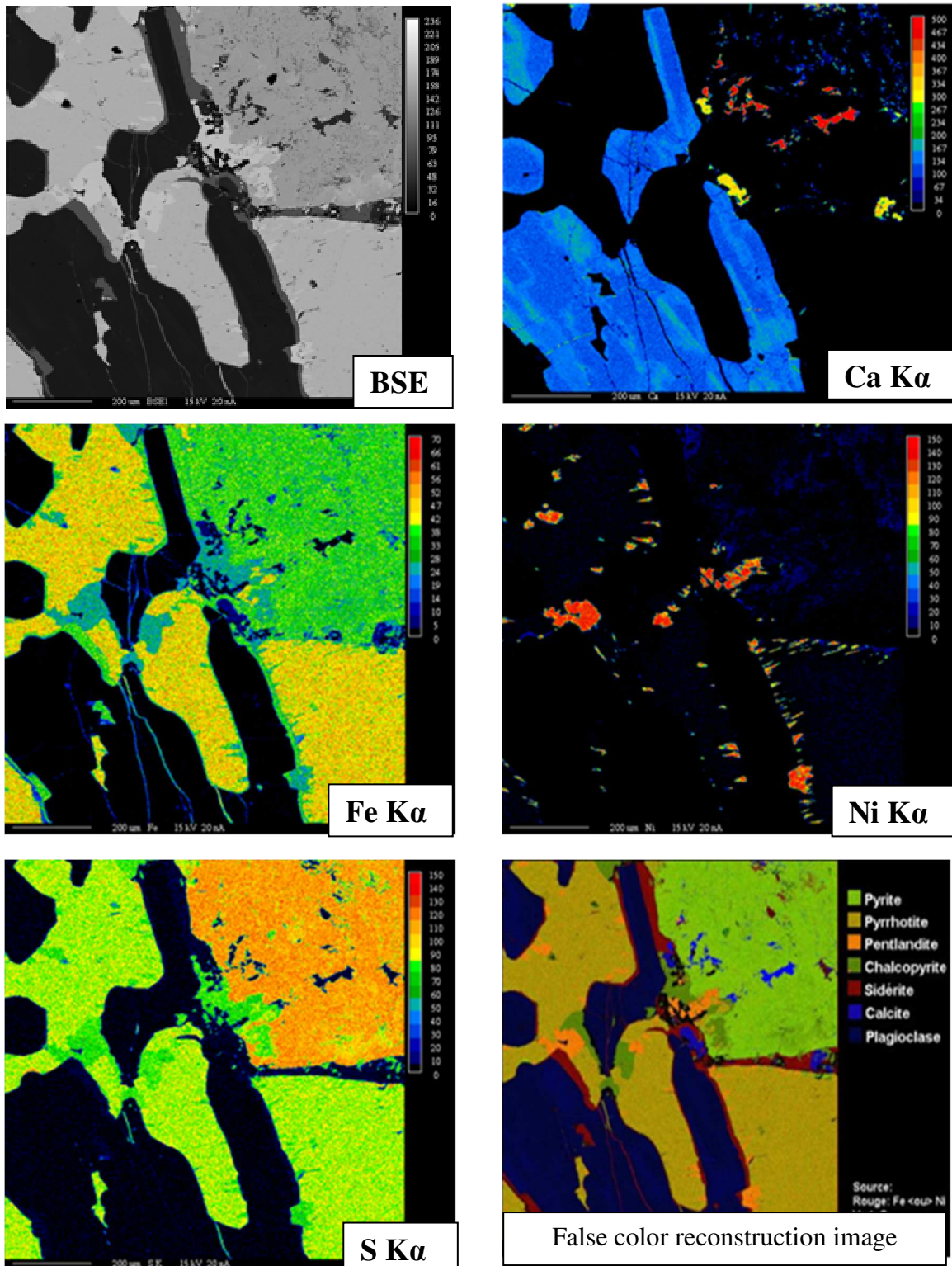


Figure 4.8: X-ray microprobe mapping of a sulfide-bearing aggregate particle in the anorthositic gabbro.

4.3.4.3 Petrographic examination of damaged concrete samples

The macroscopic examination of broken surfaces of concrete cores taken from deteriorated housing foundation walls typically showed “alteration” on sulfide surfaces (Fig. 4.9). Aggregate surfaces were light brown and often covered by rust. Some aggregate particles were completely disintegrated. The bond between the aggregate particles and the cement paste is often weak. Pyrrhotite surfaces are strongly oxidized while pyrite surfaces seem unaltered.

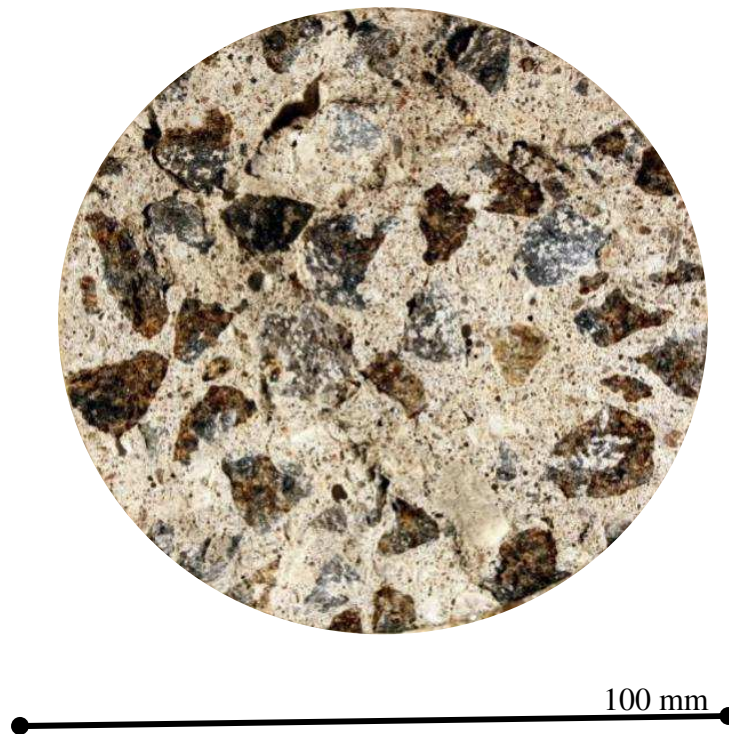


Figure 4.9: Broken concrete core sample taken from a deteriorated foundation. Several coarse aggregates are covered with rust.

The examination of polished concrete core samples under the stereomicroscope revealed that the cement paste is generally highly porous. This is not surprising considering the 15-MPa compressive strength requirements for plain concrete used in residential foundation applications. High water-cement ratio (in the order of 0.7) and relatively low cement contents (about 250 kg/m³ type GU (general use cement)) are often used for such applications. Most of the concrete samples are highly damaged, with important cracking being observed around or through the aggregate particles. Figures 4.10A and B illustrate aggregate particles rich in sulfide minerals. Aggregate particles are often partially

disintegrated with major cracks running through the particle and extending into the cement paste. Figures 4.10 C and D are microscopic views of deteriorated concrete samples with major cracks running through the aggregate particles.

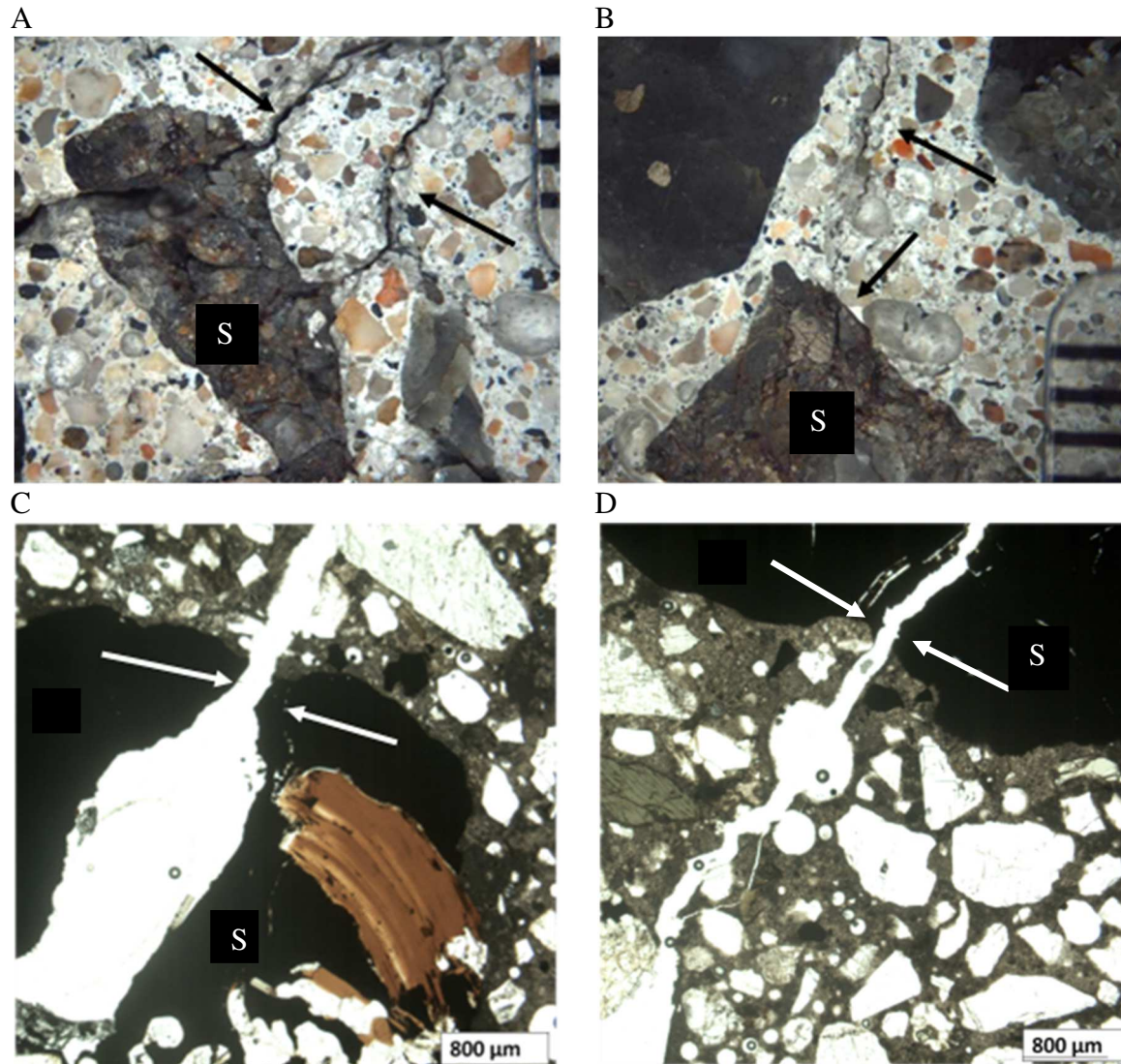


Figure 4.10: A and B) Stereomicroscopic views of deteriorated polished concrete core with partially disintegrated aggregate particles showing important cracks through the particle and extending into the cement paste. C and D) Microscopic views of polished thin sections of deteriorated concrete with crack running through the aggregate particle and extending into the cement paste. (S: sulfide mineral).

The cracks are extending into the cement paste. Reddish to brownish secondary material can be observed covering the surface of several aggregate particles (e.g. Fig. 4.11A). In highly deteriorated concrete specimens, aggregate particles are completely covered with iron oxy-hydroxide and are surrounded by a whitish halo (Fig. 4.11A); also,

cracks can be found running through oxidized aggregate particles and extending into the cement paste (Fig. 4.11B). Most of the time, cracking occurs next to sulfide-rich aggregate particles, thus resulting, in some cases, in aggregate debonding. Results obtained from stereomicroscopic examinations confirm that the pyrrhotite grains were mainly oxidized, while pyrite grains remained practically intact.

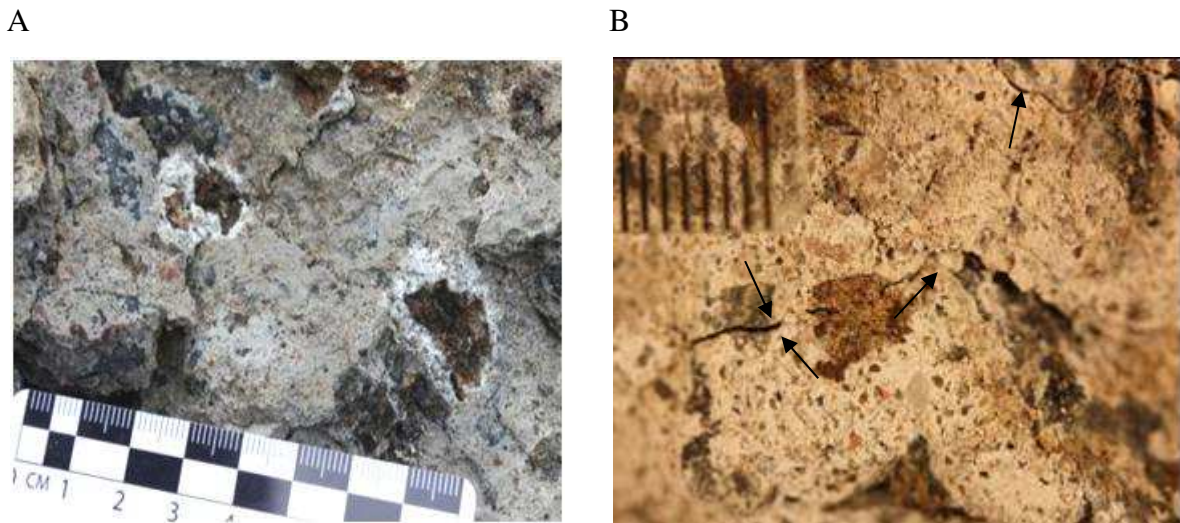


Figure 4.11: Overall and stereomicroscopic views of deteriorated concrete foundation block (A) and core (B). A) Aggregate particle covered with iron oxy-hydroxide and surrounded by a whitish halo. B) Crack through an oxidized particle extending into the cement paste.

The nature and composition of secondary reaction products observed during stereomicroscopic examination was confirmed by SEM observations. The minerals described hereafter are those that were commonly observed during the investigation of a large number of specimens sampled in damaged concrete foundations. Ettringite crystals were often observed close to oxidized aggregate particles on broken surfaces of the concrete core samples (Fig. 4.12A). Fig. 4.12C is a close up view of the striated prismatic ettringite crystals that show hexagonal symmetry. The EDS spectra present the elemental composition of the ettringite, with calcium (Ca), sulfur (S), aluminum (Al) and oxygen (O) X-ray lines. A low intensity line for silicon (Si) was also detected by EDS, which signifies that crystals may represent solid-solution of ettringite/thaumasite instead of ettringite.

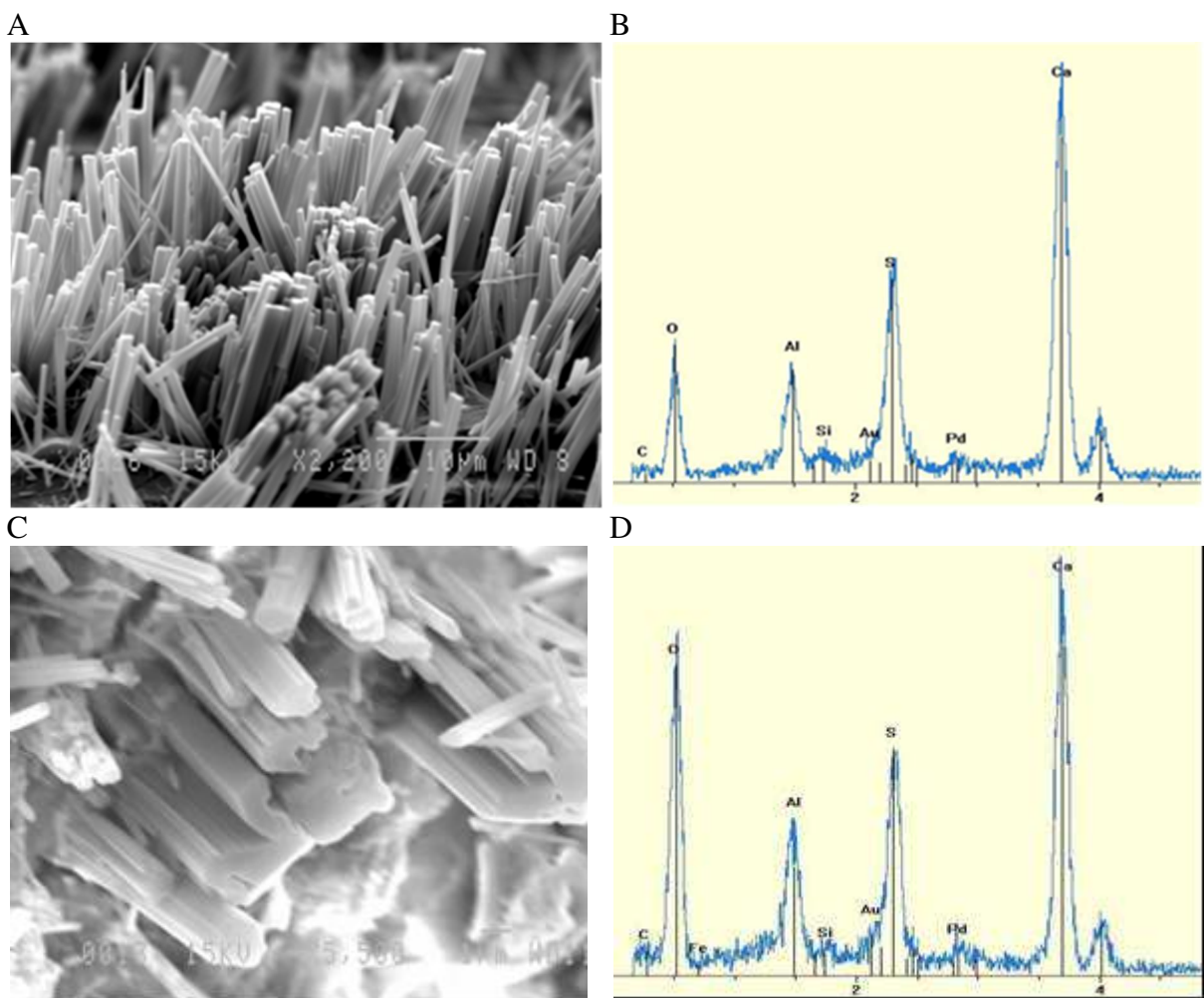


Figure 4.12: Secondary electron images of ettringite covering the cement paste at the vicinity of sulfide-bearing aggregate particles, with corresponding EDS spectra.

Grains of gypsum (calcium sulfate dehydrate - EDS spectrum (Ca – S – O)), were also found on the broken surfaces of the cement paste surrounding oxidized aggregate particles (Fig. 4.13); the two images present different gypsum crystal morphologies, namely a crust of compacted gypsum crystals (4.13A) and a stacking of platy crystals (4.13B).

Short prismatic hexagonal crystals of thaumasite ($\text{Ca}_3\text{Si}(\text{OH})_6(\text{CO}_3)(\text{SO}_4) \cdot 12\text{H}_2\text{O}$) (Fig. 4.14) are observed mainly in the white rims surrounding the oxidized aggregate particles, as seen on Figs. 4.2D and 4.11A. The EDS spectra present the elemental composition of thaumasite, with calcium (Ca), silicon (Si), oxygen (O), carbon (C) and sulfur (S) X-ray lines (Fig. 4.14B, D, H). Low intensity aluminum (Al) line is also present. It is possible that the mineral observed is a thaumasite/ettringite solid-solution as described

by Barnett et al. [16], Crammond [17] and Macphee et al. [18] or simply a mixture of phases, ettringite and thaumasite. According to Barnett et al. [16], a single solid-solution phase is found when SO_4^{2-} is the majority anion, while two phases exist when CO_3^{2-} predominate. Thaumasite presents different morphologies, including bundles of short prismatic hexagonal crystals (Fig. 4.14A, C, G) and massive, dense/ compacted crust/layer of material with map cracking due to water loss in the high vacuum in the SEM (Fig. 4.14E, F).

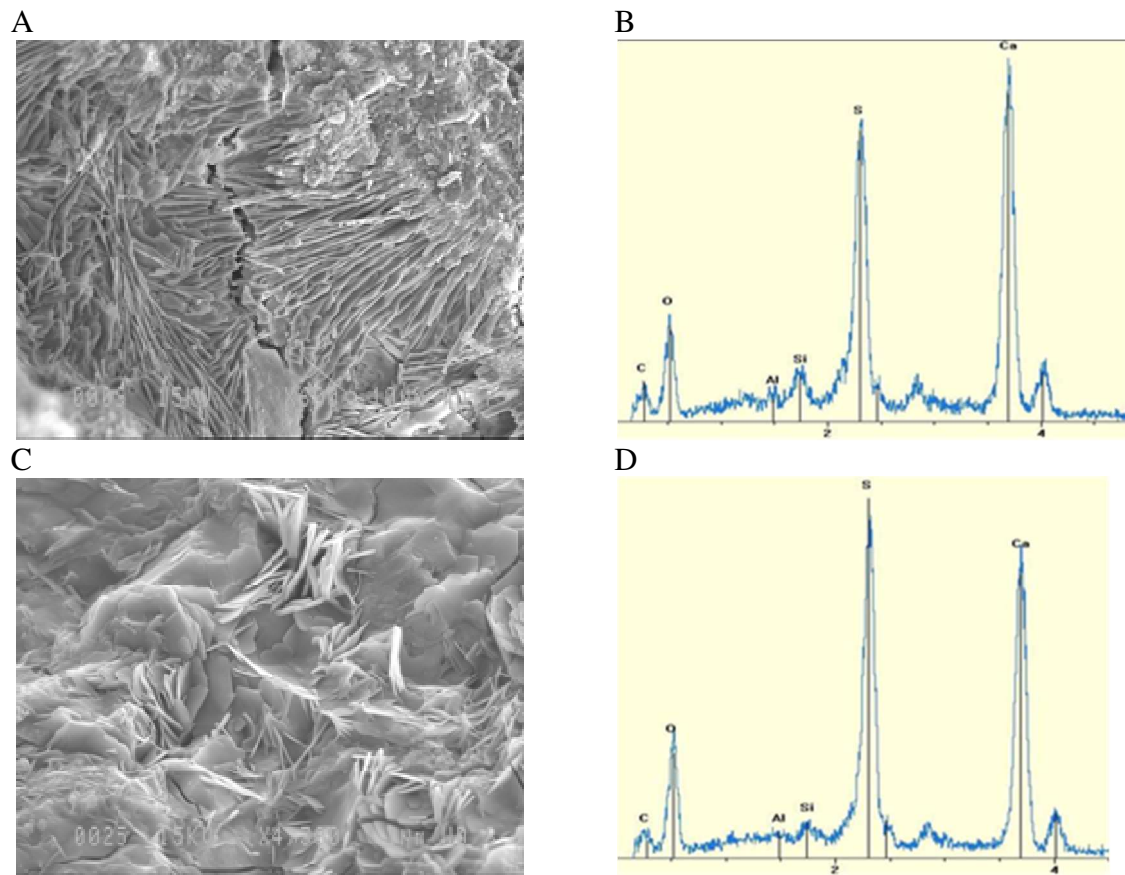


Figure 4.13: Secondary electron images of gypsum observed on broken surfaces of the cement paste surrounding sulfide-bearing aggregate particles, with corresponding EDS spectra.

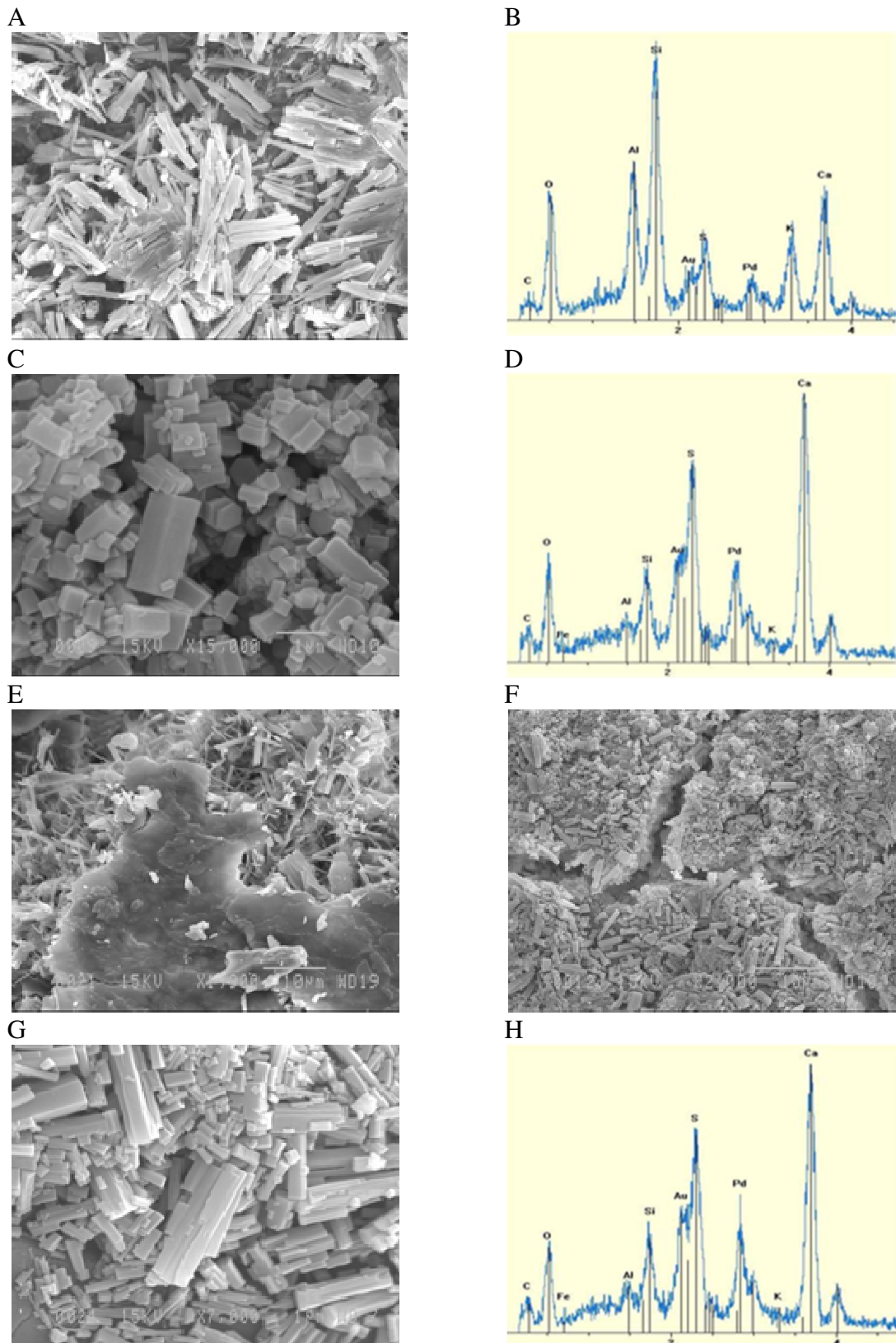


Figure 4.14: Secondary electron images of thaumasite observed in the cement paste adjacent to sulfide-bearing aggregate particles, with corresponding EDS spectra.

The identification of thaumasite may be difficult with the EDS because of its similarity to ettringite. For this reason, X-ray diffraction analysis was undertaken on a powder sample taken in the whitish haloes surrounding oxidized aggregate particles. X-ray diffraction analysis can detect crystalline phases when present in the order of 5% (by mass) or more. However, this method is often not sensitive to the presence of small, but potentially important, quantities of secondary reaction mineral phases. For that reason, X-ray diffraction analysis was scanned at a slow rate (step size 0.01 2θ with a 9 s count per step). Fig. 4.15 presents the XRD trace obtained where both thaumasite and ettringite lines can be seen, as also presented by other authors [16–20].

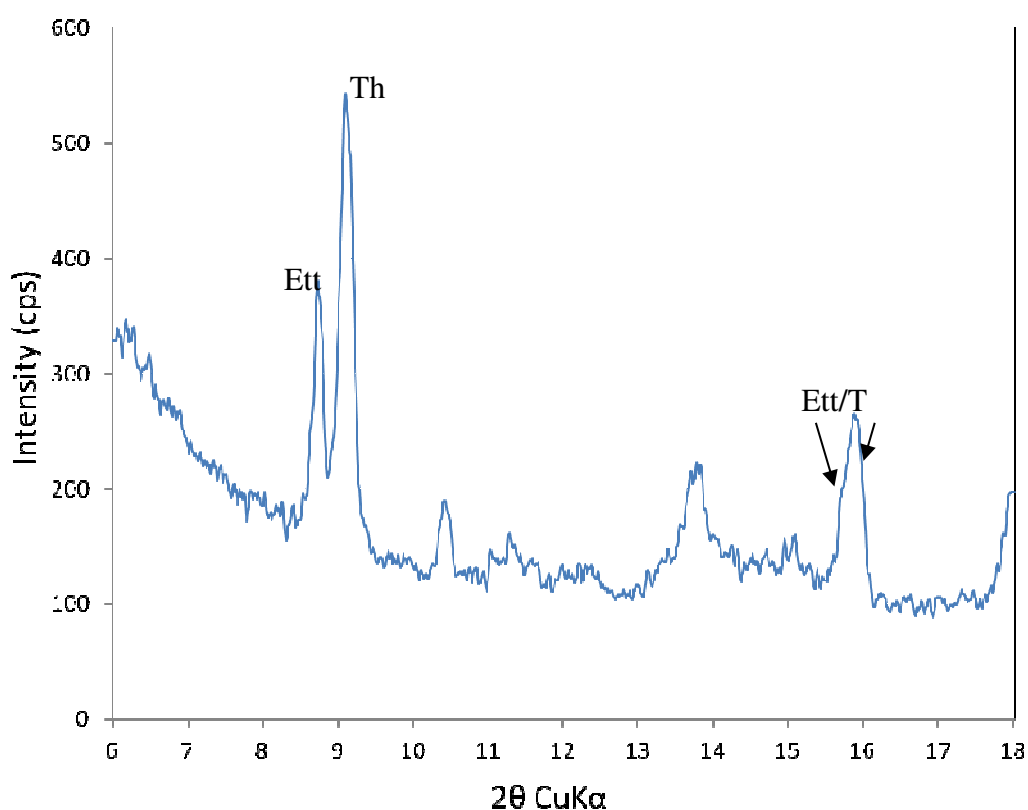


Figure 4.15: X-ray diffraction pattern of thaumasite/ettringite phases. Sample obtained from whitish haloes surrounding reacted sulfide-bearing aggregate particles.

Other types of secondary products are observed covering or in the vicinity of pyrrhotite grains; they are interpreted as iron oxide, hydroxide or oxyhydroxide (Fig. 4.16), despite the fact that their precise nature cannot be determined using EDS since hydrogen is

not detected. Corresponding EDS spectra display iron (Fe) and oxygen (O) X-ray lines. These secondary products are associated to the oxidation of pyrrhotite.

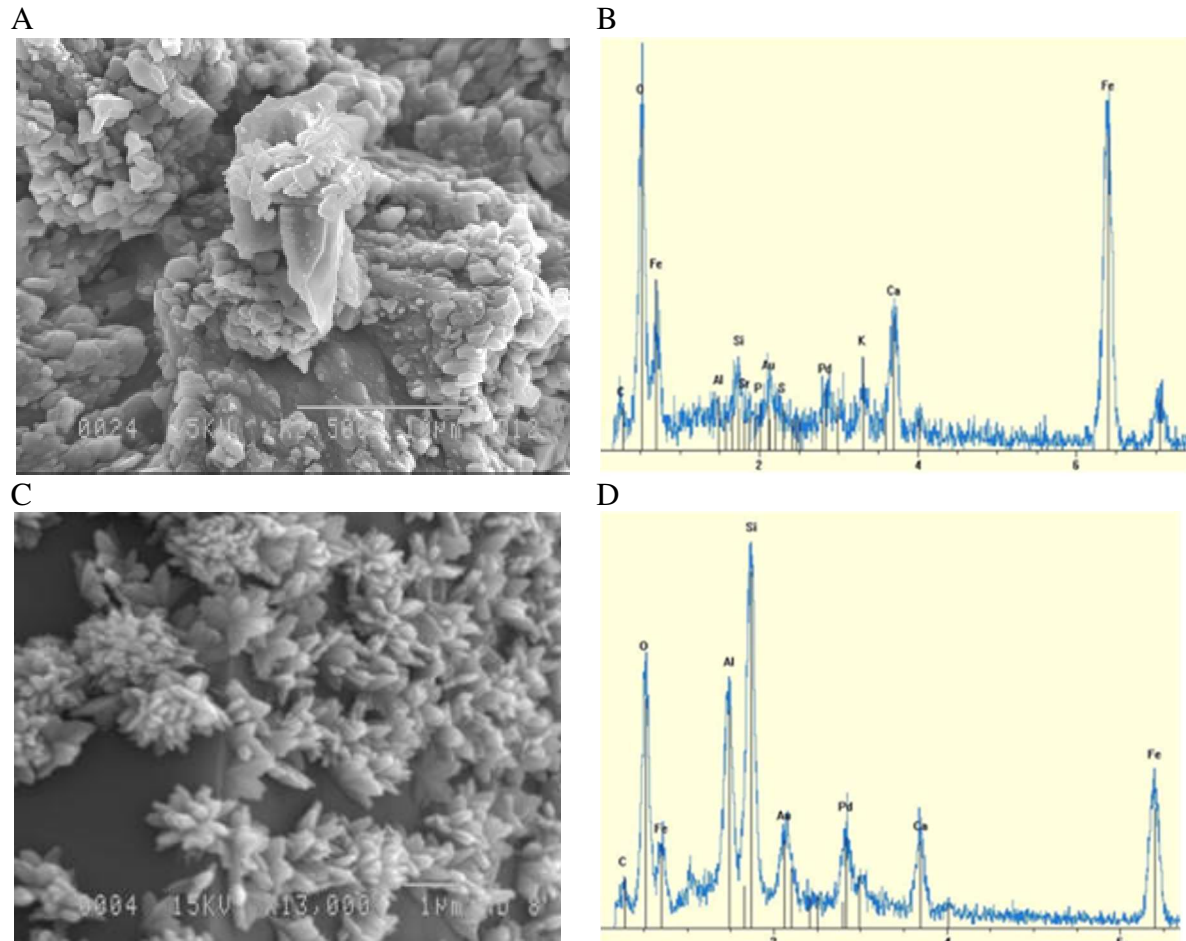


Figure 4.16: Secondary electron images of iron oxy-hydroxide observed on/next to sulfide-bearing aggregate particles, with corresponding EDS spectra.

Figure 4.17 presents images of polished thin sections of deteriorated housing foundation concrete showing the presence of gypsum in the pores of the cement paste, as confirmed by EDS analysis (Fig. 4.17C), and large quantities of thaumasite in the cement paste (Fig. 4.17D). These thin sections came from highly deteriorated concrete samples. Ettringite is almost nonexistent in the sample and seems limited to the ettringite–thaumasite solid solution.

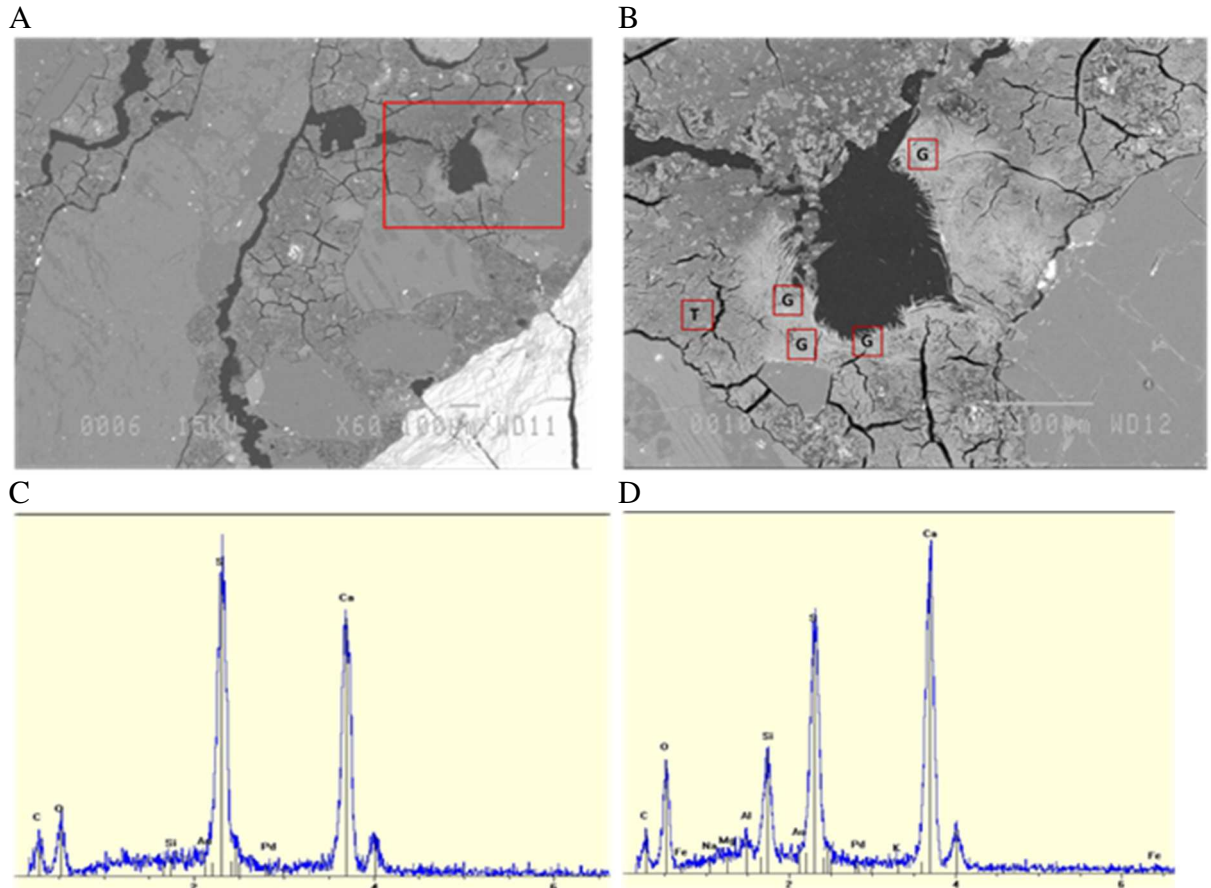


Figure 4.17: Back-scattered electron images of thaumasite (T) and gypsum (G) (figures A and B) with corresponding EDS spectra.

4.3.5. Discussion

Based on petrographic examination, pyrrhotite is determined as the likely “reactive” mineral phase in the aggregate particles of the concrete samples examined. Upon exposure to water and oxygen, sulfide minerals (for instance pyrrhotite since pyrite seems to be largely unreacted) oxidize to form acid, iron and sulfate-rich by-products. SEM and stereomicroscopic observations of damaged concrete samples have shown that secondary products most frequently generated during the oxidation process of iron sulfides are: (i) “rust” with all its forms (goethite (FeOOH), ferrihydrite ($\text{Fe}_2\text{O}_3 \cdot 0.5(\text{H}_2\text{O})$), limonite ($\text{FeO}(\text{OH}) \cdot n\text{H}_2\text{O}$),...), and (ii) sulfates-bearing phases including gypsum, ettringite and thaumasite. Degradation of concrete thus results from the combined effects of the oxidation of iron sulfides followed by the internal sulfate attack of the cement paste. Both reactions create secondary minerals that cause expansion. According to Casanova et al. [6], internal sulfate attack reaction is by far more expansive. In fact, during the formation of gypsum,

the volume of the resulting products represents a little more than double of that of the starting solids. Thaumasite formation is also a significant contributor to concrete deterioration.

The thaumasite sulfate attack (TSA) is characterized by the softening and disintegration of the cement matrix [16]. According to Crammond [17], signs of TSA include: white haloes around aggregate particles; sub-parallel cracks; and white mush compound that loosely holds surrounding aggregate particles. Whitish powdery deposits occurring around aggregate particles were also described by Oberholster et al.[14].

The ettringite appears in the cement paste, filling voids and cracks of the relatively less deteriorated concrete samples. Gypsum is also present in those samples. In the more deteriorated concrete samples, the presence of ettringite is generally less frequent, however ettringite/ thaumasite solid solution, thaumasite and gypsum are the most frequently observed secondary products.

Some aspects of the deterioration process observed in the housing foundations from Trois-Rivières are similar to sulfuric acid attack, i.e. the presence of gypsum, ettringite and thaumasite (Mori et al. [21], and Fernandes et al. [22]). However, in this particular case, the presence of gypsum seems more limited than that of the one reported by the last authors. As mentioned before, the presence of gypsum is mainly limited to air voids and it is not present in substitution of the cement paste. The concrete deterioration was found to be extending to the whole depth of the concrete foundation and not only to the surface area, although the deterioration was more pronounced close to the surface, probably due to increased exposure to moisture.

There was no evidence of “dissolution”, as is frequently found in cases of external acid attack [21, 22]. In addition, clear chemical and mineralogical zonal patterns from the surface to the interior of the concrete element were not observed.

The formation of thaumasite requires a source of carbonate. In the damaged concretes presented here, the carbonate may have been supplied by one or a combination of the following (i) the siderite observed surrounding sulfide minerals, (ii) calcite present in veins and disseminated through the aggregate, (iii) the limestone filler used up to 5% content in

GU cement, and/or (iv) the CO₂ trapped in the carbonated surface of the concrete (Figures 4.6B, 7, 8).

4.3.5.1. Importance of the observations on the development of a performance test

Until now, difficulties were encountered by researchers trying to reproduce the degradation of concrete incorporating iron sulfide-bearing aggregates under laboratory conditions [4,8,14]. In several cases, testing programs using conditions favoring alkali-silica reactivity were used (high-humidity and high-temperature conditions, or complete immersion of mortar or concrete samples in water/lime water) and found unsuccessfully.

The reaction of oxidation needs oxygen (Section 1, Eq. (1); consequently, high humidity conditions do not reproduce field deterioration as diffusion of oxygen through the liquid phase is about 10⁴ times slower than that in the gas phase. On the other hand, the oxidation of iron sulfide is favored by high temperature conditions, while thaumasite usually forms at lower temperatures (lower than 15 °C) [23], although some authors [18] were able to prove that the thaumasite formation is possible at 30 °C and others state that the limit of thermal stability of thaumasite is actually ~45 °C (unpublished cited by [24]). It may thus be necessary to approach the development of a performance test as a two-stage operation, i.e. a first part performed at moderate-to-high temperature and moderate humidity conditions to favor the sulfide oxidation phenomenon and, afterward, a second part involving relatively lower temperature testing for thaumasite formation.

4.3.6. Conclusions

Cases of degradation in concrete incorporating iron sulfide-bearing aggregates were recently observed in the Trois-Rivières area, Quebec, Canada. This study reports the results of site inspections of deteriorated housing foundations, along with concrete core characterization using different petrographic tools. The main results of the above investigation show that:

- Deteriorated housing concrete foundations display map cracking, yellowish surface discoloration, pop-outs and open cracks more pronounced at the corners of the foundation blocks.
- The problematic aggregate is a norite/hypersthene gabbro containing iron sulfide minerals.

- Iron sulfides, which mainly consist of pyrrhotite and pyrite with minor amounts of chalcopyrite and pentlandite, are finely disseminated into silicate minerals.
- Pyrrhotite was found to be oxidized while pyrite was not.
- A thin layer of carbonate mineral (siderite) is often seen “coating” the sulfide minerals. This layer could have served as the source of carbonate required for thaumasite formation.
- Concrete core samples are often highly damaged, with important cracking observed around and through the aggregate particles and the cement paste; some aggregate particles are partially disintegrated or debonded and white haloes are often seen surrounding oxidized sulfide-bearing particles.
- Secondary reaction products/minerals identified consist of iron oxide/hydroxide/oxyhydroxide, ettringite, gypsum and thaumasite.
- The oxidation of pyrrhotite followed by internal sulfate attack of the cement paste seems to be the main mechanisms of concrete deterioration.
- The identification of the different phases associated with the deterioration including thaumasite allows to better understand the degradation mechanisms and to direct future research works aiming to the development of a performance test.

4.4 Acknowledgments

This study has been supported by the National Science and Engineering Research Council of Canada (NSERC) and by the Fonds de recherche sur la nature et les technologies of the Province of Québec (FQRNT). A. Rodrigues benefits from a PhD scholarship financed by FCT—Fundação para a Ciência e Tecnologia, Portugal, Ref.: SFRH/BD/71203/2010. We thank M. Choquette, J. Francoeur and S. Tremblay for their assistance.

4.5 References

- [1] J.P.R. De Villiers, D.C. Liles, The crystal-structure and vacancy distribution in 6C pyrrhotite, *Am. Mineral.* 95 (2010) 148–152.

- [2] N. Belzile, Y.W. Chen, M.F. Cai, Y.R. Li, A review on pyrrhotite oxidation, *J. Geochem. Explor.* 84 (2004) 65–76
- [3] Y.L. Mikhlin, A.V. Kuklinski, N.I. Pavlenko, V.A. Varnek, I.P. Asanov, A.V. Okotrub, G.E. Selyutin, L.A. Solovyev, Spectroscopic and XRD studies of the air degradation of acid-reacted pyrrhotites, *Geochim. Cosmochim. Acta* 66 (2002) 4057–4067.
- [4] J. Bérard, R. Roux, M. Durand, Performance of concrete containing a variety of black shale, *Can. J. Civ. Eng.* 2 (1975) 58–65.
- [5] J.S. Chinchón, C. Ayora, A. Aguado, F. Guirado, Influence of weathering of iron sulfides contained in aggregates on concrete durability, *Cem. Concr. Res.* 25 (1995) 1264–1272.
- [6] I. Casanova, L. Agullo, A. Aguado, Aggregate expansivity due to sulfide oxidation — I. Reaction system and rate model, *Cem. Concr. Res.* 26 (1996) 993–998.
- [7] C. Ayora, S. Chinchón, A. Aguado, F. Guirado, Weathering of iron sulfides and concrete alteration: thermodynamic model and observation in dams from central Pyrenees, Spain, *Cem. Concr. Res.* 28 (1998) 1223–1235.
- [8] T. Schmidt, A. Leemann, E. Gallucci, K. Scrivener, Physical and microstructural aspects of iron sulfide degradation in concrete, *Cem. Concr. Res.* 41 (2011) 263–269.
- [9] J. Moum, I.Th. Rosenqvist, Sulfate attack on concrete in the Oslo region, *J. Am. Concr. Inst.* 56 (1959) 257–264.
- [10] L. Divet, J.P. Davy, Étude des risques d'oxydation de la pyrite dans le milieu basique du béton, *Bull. Lab. Ponts et Chaussées* 204 (1996) 97–107.
- [11] H.F. Steger, Oxidation of sulfide minerals VII. Effect, of temperature and relative humidity on the oxidation of pyrrhotite, *Chem. Geol.* 35 (1982) 281–295.
- [12] P.E. Grattan-Bellew, W.J. Eden, Concrete deterioration and floor heave due to biogeochemical weathering of underlying shale, *Can. Geotech. J.* 12 (1975) 372–378.
- [13] A. Shayan, Deterioration of a concrete surface due to the oxidation of pyrite contained in pyritic aggregates, *Cem. Concr. Res.* 18 (1988) 723–730.

- [14] R.E. Oberholster, P. Du Toit, J.L. Pretonius, Deterioration of concrete containing a carbonaceous sulfide-bearing aggregate, In: Proceedings of the Sixth Int. Conf. on Cement Microscopy, Int. Cement Microscopy Association (ICMA) Eds, March 26–29 1984, Albuquerque, New Mexico, USA.
- [15] A. Le Roux, L. Divet, P. Fasseu, L. Hasni, A.M. Marion, Étude des risques d'oxydation de la pyrite dans le milieu basique du béton, Bull. Lab. Ponts et Chaussées 234 (2001) 79–88.
- [16] S.J. Barnett, D.E. Macphee, E.E. Lachowski, N.J. Crammond, XRD, EDX and IR analysis of solid solutions between thaumasite and ettringite, Cem. Concr. Res. 32 (2002) 719–730.
- [17] N. Crammond, The occurrence of thaumasite in modern construction — a review, Cem. Concr. Compos. 24 (2002) 393–402.
- [18] D.E. Macphee, S.J. Barnett, Solution properties of solids in the ettringite– thaumasite solid solution series, Cem. Concr. Res. 34 (2004) 1591–1598.
- [19] G. Collett, N.J. Crammond, R.N. Swamy, J.H. Sharp, The role of carbon dioxide in the formation of thaumasite, Cem. Concr. Res. 34 (2004) 1599–1612.
- [20] T. Schmidt, B. Lothenbach, M. Romer, K. Scrivener, D. Rentsch, R. Figi, A thermodynamic and experimental study of the conditions of thaumasite formation, Cem. Concr. Res. 38 (2008) 337–349.
- [21] T. Mori, T. Nonaka, K. Tazaki, M. Koga, Y. Hikosaka, S. Noda, Interactions of nutrients, moisture and pH on microbial corrosion of concrete sewer pipes, Water Res. 26 (1992) 29–37.
- [22] I. Fernandes, M. Pericão, P. Hagelia, F. Noronha, M.A. Ribeiro, J. Maia, Identification of acid attack on concrete of a sewage system, 12th Euroseminar on Microscopy Applied to Building Materials, Dortmund, Germany, 2009.
- [23] S. Kohler, D. Heinz, L. Urbonas, Effect of ettringite on thaumasite formation, Cem. Concr. Res. 36 (2006) 697–706.
- [24] F.P. Glasser, J. Marchand, E. Samson, Durability of concrete — degradation phenomena involving detrimental chemical reactions, Cem. Concr. Res. 38 (2008) 226–246.

Chapter 5

Oxygen consumption test

5.1 Introduction

This paper was published in Cement and Concrete Composites Journal, Volume 67 (2016), pp. 93-100. It was submitted in April 2015 and accepted for publication in January 2016.

5.2 Résumé

La détérioration du béton due à l'oxydation des granulats incorporant des sulfures de fer n'est pas un sujet nouveau; toutefois, aucune ligne directrice précise n'est disponible pour le contrôle de la qualité des granulats. En présence d'oxygène et d'humidité, les sulfures de fer s'oxydent pour former différents produits secondaires. Un test de consommation d'oxygène a été modifié afin d'évaluer le potentiel d'oxydation des sulfures de fer dans les granulats à béton. Les paramètres optimisés pour évaluer le potentiel d'oxydation de ces granulats comprennent une granulométrie inférieure à 150 μm , 40% de saturation, un rapport de 10 cm d'épaisseur de granulat pour 10 cm d'espace libre et 3 heures de test à 22°C. Les résultats obtenus montrent que le test est capable de discriminer les granulats contenant des sulfures de fer des granulats de contrôle. Une valeur seuil fixée à 5 % d'oxygène consommé sépare les 2 groupes de granulats.

5.3 Scientific publication no. 2

Quantitative assessment of the oxidation potential of sulfide-bearing aggregates in concrete using an oxygen consumption test

Andreia Rodrigues, Josée Duchesne, and Benoît Fournier

Abstract

In the presence of oxygen and humidity, the iron sulfide minerals present in some concrete aggregates can oxidize creating damage to concrete infrastructure. An oxygen consumption test was developed to assess the oxidation potential of concrete aggregate. A compacted layer of aggregate material is exposed to oxygen (O_2) in a hermetic cell, and the O_2 consumption is monitored. Optimized parameters included a 10 cm compacted layer of aggregate material with particle size $< 150 \mu m$ kept at 40% saturation degree with a 10-cm headspace left at the top of the cell. The consumption of the O_2 present in the headspace is monitored over a 3-hour testing period at 22°C. The test was able to discriminate the eight sulfide-bearing and control aggregates selected when using a threshold limit of 5% O_2 consumed. This draft limit will, however, require to be confirmed through the testing of a larger number of aggregates.

Keywords: iron sulfides oxidation, oxygen consumption, concrete, aggregates, deterioration, testing method

5.3.1 Introduction

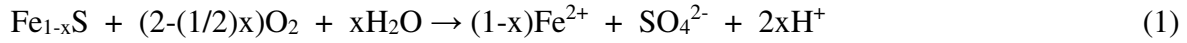
Concrete deterioration due to sulfide-bearing aggregates is not a new subject in the world of civil and geological engineering. Since the 1950's, numerous cases, such as the one reported by Moum and Rosenqvist [1] in the Oslo region (Norway), involving the deterioration of concrete structures due to the presence of iron sulfide minerals (pyrrhotite and pyrite) in the aggregates, have been published [2]. One of the recent cases is the one in the Trois-Rivières area (Quebec, Canada), where the deterioration of concrete foundations and slabs in private houses and commercial buildings was caused by the oxidation of iron

sulfides (mainly pyrrhotite) in coarse aggregates followed by internal sulfate attack leading to thaumasite formation [3], [4], [5], [6].

Even if this problem has been known for many years, there are currently no laboratory tests capable of satisfactorily predicting the potential deleterious character of sulfide-bearing aggregates. A full chemical analysis including the measurement of the total sulfur content, although allowing identifying the presence and, to some extents, the total sulfide mineral content within the aggregate material, will however not differentiate the different mineral forms present, e.g. pyrite from pyrrhotite. This could potentially be done by X-Ray diffraction; however, the method is generally sensitive only for mineral forms in excess of 5% in the rock sample. A detailed petrographic characterization of the aggregates is one of the best ways to identify the various iron sulfides, but various limitations are affecting this technique. For example, in this particular case, the examination needs to be carried out by petrographers with an appropriate experience in reflected light petrography, a challenge that can be even enhanced since sulfide minerals are often sparsely and/or finely disseminated within concrete aggregate particles. Also, unless specific measures are used (e.g. using point-counting methods), the proportions of sulfide minerals in polished thin sections or slabs are often obtained by visual estimate, which can generate significant variations from one petrographer to another. Combined chemical and petrographic characterization of the aggregate material has the potential of providing semi-quantitative or even quantitative (when using advanced methods such as the Mineral Liberation Analysis (MLA) by scanning electron microscopy (SEM) analysis of ground rock/aggregate samples) measurements of the mineral contents within aggregate materials. However, the above still cannot readily assess the deleterious character of the sulfide minerals present since the latter can be influenced by factors such as the mineral types present, the mineral crystallinity and crystallographic characteristics (e.g. for pyrrhotite), porosity, grain size, and galvanic effects between the distinct associated mineral phases [7], [8].

There is consequently an obvious need for a performance test for reliably assessing the oxidation potential of concrete aggregate materials. The mechanisms of iron sulfides oxidation are well-known in the mining environment literature because these reactions are

the source of acid rock drainage (ARD) that is a major concern for the mining industry [9], [10], [11], [12]. It occurs when the iron sulfides are in the presence of oxygen and humidity forming acidic, iron and sulfate-rich by-products as seen in the following equation (1) for the pyrrhotite oxidation:



where x varies between 0.0 and 0.125 depending on the pyrrhotite crystallography [13].

In the sulfide oxidation reaction, the oxygen is one of the reactants and the monitoring of its concentration can be used to determine the oxidation potential of sulfide-bearing aggregates. This process was first proposed by Elberling and coworkers [14] and Elberling and Nicholson [15] to evaluate the rate of oxidation of mine tailings containing sulfide minerals. In the technique developed by Elberling and coworkers [14], the oxygen flux into tailings exposed to the atmosphere is evaluated using oxygen consumption assuming steady state flux prior to making any measurements [16], [17]. The oxygen fluxes are calculated based on the second Fick's law (Equation 2):

$$V \frac{dC}{dt} = AC(kD_{eff})^{0.5} \quad (2)$$

where V is the headspace volume, A is the area of the container, C is oxygen concentration, t is the time, k is the reaction-rate constant for the sulfides and D_{eff} is the effective diffusion coefficient, which is $1.8 \times 10^{-5} \text{ m}^2/\text{s}$ for air at 25°C [14]. Considering the initial condition: $C=C_0$ at $t=0$, the solution of the previous equation will be (Equation 3):

$$\ln\left(\frac{C}{C_0}\right) = -t(kD_{eff})^{0.5} \frac{A}{V} \quad (3)$$

The slope of the graph C/C_0 versus time gives the value of $(kD_{eff})^{0.5}$ when A/V is known.

During the test, the oxygen diffuses through the tailings where it is consumed by the oxidation of sulfide minerals. The progressive decrease of oxygen concentration in the close volume is monitored over time and is used to determine Fick's laws parameters [17]. According to these authors, this interpretation can only be valid for short-duration tests and a more sophisticated approach using numerical modelling is proposed. This is important in the field of ARD where the oxygen consumption test is also used to assess the effectiveness

of remediation schemes involving the use of water covers and engineered soil covers to minimize ingress of oxygen into tailings.

5.3.2. Objectives and Scope of Work

The oxygen consumption method seems to have a great potential to evaluate the oxidation potential of concrete aggregates containing iron sulfide minerals. First, because of the direct measurement of one of the reactants necessary for the oxidation reaction (oxygen) and, second, because the results obtained are quantitative, so less susceptible to erroneous interpretations and variations between operators, as it is the case for petrographic examination.

The present work aims at adapting the oxygen consumption test developed by Elberling and coworkers [14] to evaluate the potential deleterious character of sulfide-bearing aggregates for use in concrete. A parametric testing program was carried out to optimize testing conditions. The "optimized" test was then applied to assess the oxidation potential of ten iron sulphide-bearing and control aggregates. Finally, the precision of the test was evaluated.

5.3.3. Materials and methods

In order to optimize the oxygen consumption test, a series of experiments were carried out to identify the most reliable conditions with respect to the aggregate particle size (obtained by grinding of sulfide-bearing and control aggregates) and moisture condition, as well as the thickness of compacted ground material (Figure 5.1).

Based on the experience of Prof. Bruno Bussière's research team at the Université du Québec en Abitibi-Témiscamingue (UQAT) on the use of the *Oxygen consumption test* for mine tailings, it was decided that all measurements would be performed at atmospheric pressure, room temperature (22°C), and with a 3.5-hour test duration (30 minutes for the probes stabilization plus 3 hours of effective oxygen consumption measurements). Preliminary tests carried out in Prof. Bussière's laboratory indicated that the headspace (air volume) above the compacted ground material had a significant impact on the test results; this parameter was thus further investigated as part of this study (see Figure 5.2).

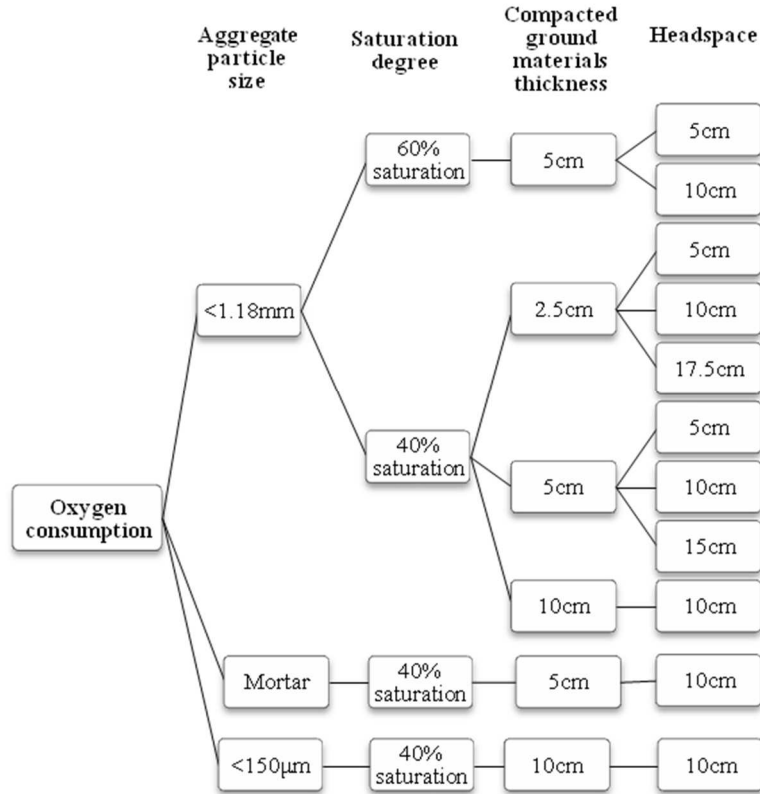


Figure 5. 1: Oxygen consumption testing conditions flowchart.

5.3.3.1 Sulfide-bearing and control aggregates

A total of ten aggregates were used in the different parts of this experiment; their properties are summarized in Table 5.1. They consisted of 7 sulfide-bearing aggregates (MSK, B&B, GGP, SBR, PHS and SW), one mainly composed of iron sulfide minerals (SDBR) and finally three control aggregates with no (PKA, HPL) or only traces of iron sulfides (DLS). A sample of each aggregate tested was taken prior to test in order to analyse the total sulfur (% by mass) content (Table 5.1). MSK, the problematic aggregate used in the construction of the Trois-Rivières house foundations, is a hypersthene gabbro containing various proportions of pyrite $[\text{FeS}_2]$, pyrrhotite $[\text{Fe}_{1-x}\text{S}]$, pentlandite $[(\text{Fe},\text{Ni})_9\text{S}_8]$ and chalcopyrite $[\text{CuFeS}_2]$ [3]. The percentage of sulfur (% S_T by mass) obtained from different MSK sub-samples tested varied from 0.73 to 1.28%.

The B&B is an aggregate with the same characteristics and basically the same mineralogy of MSK aggregate, but with higher sulfur content. In fact, these aggregates come from quarries that are only about 500 meters apart. The B&B sample was obtained by

hand-picking rock fragments (from the 100-mm stockpile) with particularly high sulfide minerals contents.

GGP is a granitic gneiss from Central Quebec (Canada) with a mineralogical composition somewhat similar to the MSK aggregate, especially regarding the iron sulfide minerals present, i.e. pyrrhotite, pyrite and chalcopyrite.

SBR is a fine-grained hornfels from the greater Montreal area (Canada). This aggregate is not used in concrete; however, it was selected due to its mineralogical composition and the presence of iron sulfide minerals (Table 5.1). This aggregate is also an alkali-silica reactive aggregate.

SW is mica schist aggregate from Switzerland. This aggregate was used in the construction of a large concrete dam back in the early 1970s and that started to show signs of expansion in the early 1980s [18]. The dam structure showed signs of concrete elements displacement and deposits of rust in the galleries of the dam. The authors related the concrete deterioration to the oxidation of the iron sulfide minerals present in the aggregate (Table 5.1).

PHS is a phyllite containing iron sulfide minerals. This aggregate has been described in the literature [19], [20], [21], [22], [23], as the source of concrete deterioration in public buildings, houses, overpasses and dams due to the iron sulfide minerals present. The affected concrete showed extensive cracking, iron sulfide stains, and white rims surrounding the aggregate particles. In some cases, the deterioration led to the destruction of the structures [20], [21].

SDBR is a mine waste aggregate, a gabbro at the origin, from the Sudbury area (Canada).

DLS, HPL, and PKA are control aggregates. The first 2 are limestones, while the latter is an anorthosite.

Table 5.1: Aggregates mineralogy and total sulfur content

Aggregate		Rock type	Mineralogy		% S _T by mass *	ρ ** (g/cm ³)
			Main mineral constituents	Iron sulfur minerals		
Sulfide-bearing aggregates	MSK	Norite or hypersthene gabbro	Plagioclase Biotite Pyroxenes Quartz	Pyrrhotite Pyrite Chalcopyrite Pentlandite	0.73-1.28	2.89
	B&B	Gabbro	Pyroxenes Plagioclase Quartz Biotite K Feldspars	Pyrrhotite Pyrite Chalcopyrite Pentlandite	2.13-4.22	3.05
	GGP	Granitic gneiss	Quartz Hornblende Pyroxenes Plagioclase	Pyrrhotite Pyrite Chalcopyrite	0.24-0.33	2.93
	SBR	Hornfels	Feldspars Quartz Clays Organic matter	Pyrrhotite Pyrite Chalcopyrite Sphalerite	0.75-0.87	2.91
	SW	Mica Schist	Quartz Feldspars White mica Amphibole	Pyrrhotite Pyrite Chalcopyrite	0.05-0.07	2.72
	PHS	Phyllite	Quartz Feldspar White mica Chlorite	Pyrrhotite Pyrite Chalcopyrite	0.09-0.32	2.82
	SDBR	Gabbro	Plagioclase Pyroxenes Biotite Epidote Apatite	Pyrrhotite Pyrite Chalcopyrite Pentlandite	13.86-14.46	3.26
Control aggregates	DLS	Limestone	Carbonates	Pyrite (traces)	0.09-0.19	2.78
	PKA	Anorthosite	Plagioclase Hornblende Biotite	–	0.04-0.06	2.87
	HPL	Limestone	Carbonates	–	0.02	2.95

*S_T: Total sulfur in % by mass.**ρ: volumetric mass density of the aggregate in g/cm³

5.3.3.2 Aggregate preparation (various particle sizes)

A representative 5 kg subsample was first prepared by quartering from the original loads of coarse aggregates (5 – 20 mm particle size) selected for the study. Depending on the grain size selected for testing, i.e. mortar bar size fractions (i.e. 5 mm to 150 μm), < 1.18 mm, or

< 150 μm (see Figure 5.1), different approaches of crushing and/or grinding were used. In the case of the samples with a particle size distribution similar to that used in the Accelerated Mortar Bar Test for alkali-aggregate reaction (AAR), progressive crushing and grinding was applied, as specified in ASTM C1260 [24].

The samples prepared to reach a particle size < 1.18 mm were initially introduced in a jaw crusher and then in a roller crusher until all particles passed the 1.18 mm sieve.

For test samples with a particle size < 150 μm , the aggregate was first processed in a jaw crusher followed by a roller crusher until the entire sample passed the 1.18 mm sieve. Finally, a rod mill was used until the entire sample passed the 150 μm sieve.

5.3.3.3 Degree of saturation (S%)

The degree of saturation of the ground material is a key parameter affecting the diffusion of oxygen and, consequently, the rate of oxidation of the iron sulfides within the material. It corresponds to the ratio of the volume of liquid (water) to the total volume of void-space (air and water) in the ground material. Steger [9] indeed reported that the oxidation rate of sulfide minerals increases directly with increasing relative humidity (RH) values between 37 and 75%. The amount of oxygen that can diffuse is limited by the maximum concentration of O_2 in water, ($C_w \approx 9.2 \text{ mg/L}$), which is about 30 times less than the equilibrium concentration of oxygen in air ($C_a \approx 276.7 \text{ mg/L}$) at 20 °C [25]. Consequently, a sample of iron sulfide immersed in water or kept at 100% relative humidity will not oxidize or the oxidation rate will be really slow. Two degrees of saturation, i.e. 40 and 60%, were selected for this study.

5.3.3.4 Column configuration

The oxygen consumption test was performed using Plexiglas columns, 200 mm in height with an internal diameter of 141.7 mm (Figure 5.2). The columns are hermetically sealed with a Plexiglas cap in their upper part allowing a headspace (i.e. above the ground material) that acts as a reservoir for the oxygen. A galvanic-cell type oxygen sensor (Apogee SO-100 & 200 series) is inserted through the Plexiglas cap and connected to a data Logger (OM-CP-IFC200). The sensor measures oxygen gas in air and is capable of measuring 0 to 100% oxygen. The sensor has an integrated heater to compensate for temperature changes and to prevent condensation when used in conditions where relative

humidity can reach up to 100%. The probes contain an internal bridge resistor to provide a mV output linearly proportional to O₂. The probes are calibrated in ambient air and in pure N₂ gas.

During the experiment, the columns are sealed using a layer of high vacuum grease to avoid any leaks or entry of oxygen into the system.



Figure 5.2: Columns used in the oxygen consumption test.

5.3.3.5 Ground aggregate and headspace (air) volumes/thicknesses

The volume of the ground material (corresponding to the aggregate, air void and water) and the headspace above the latter are important parameters to control for the test. In this study, the total volume of ground material was calculated by considering three ground material thicknesses, i.e. 2.5, 5 or 10 cm, within the cell (diameter of 14.17 cm) after compaction, thus giving total ground material volumes of 394, 789 and 1577 cm³. The porosity in the ground material, which corresponds to the ratio of the volume of void-space over the total volume of ground material, was fixed at 50%. Also, as mentioned before, two saturation degrees for the ground material were selected (either 40 or 60%).

So, based on the relative bulk density (dry) of the aggregate, it is possible to calculate the required mass of water and the mass of aggregate based upon the equations (4) and (5).

$$\text{Mass of aggregate (g)} = [(1 - n_{gm}) \times V_{gm} \times \rho_{agg}](4)$$

$$\text{Mass of water (g)} = [(V_{gm} \times n_{gm}) \times S_{gm} \times \rho_w] \quad (5)$$

Where:

n_{gm} : porosity within the ground material (%);

V_{gm} : total volume occupied by the ground material (cm^3);

ρ_{agg} :volumetric mass density of the aggregate ;

S_{gm} :degree of saturation (%) of the ground material;

ρ_w :density of water (g/cm^3)

For example, in the case of the aggregate MSK, the mass of aggregate needed for each experiment ranged from about 570 g for 2.5 cm to 2279 g for 10 cm of ground material (40% saturation).

The material is then placed into the column in 2 layers of equal mass and compacted until it reaches the desired thickness. The consolidation is carried out by using a large and heavy steel pestle. The surface of the second layer must be perfectly flat in order to obtain a good reading by the oxygen sensors.

Finally, the following headspace were tested, i.e. 5, 10, 15 or 17.5 cm. Considering the thickness of compacted ground material tested, the headspace height was achieved by using spacers consisting of plastic rings supporting a Plexiglas disc (with a diameter corresponding to the internal diameter of the column) under the compacted ground material in the bottom part of the columns. For example, in the case of the 2.5 cm of compacted materials and 5 cm headspace, a spacer of 12.5 cm was placed at the bottom of the column.

5.3.3.6 Precision of the test method

A sample of about 20 kg of MSK aggregate was first divided into six equal sub-samples. The precision of the test was then evaluated through two series of experiments. In both cases, the oxygen consumption tests were performed with a ground aggregate particle size of $< 150 \mu\text{m}$, 10 cm of compacted ground material at 40% saturation, 10 cm of headspace, and a test period of 3.5 hours. All oxygen probes used in the precision test had been calibrated prior to testing. The goal was to evaluate the possible variations obtained through sample preparation but also by the utilisation of different oxygen probes.

In the first experiment, three of the above six sub-samples were ground by three different operators. The column preparation, including ground material saturation and compaction, was then performed by one operator. The three O₂ consumption tests were then run using the same column and probe.

In the second experiment, the other three sub-samples were ground separately by the same operator. The column preparation, including ground material saturation and compaction, was also performed by that same operator. The O₂ consumption tests were then run in parallel using three different set-ups (i.e. columns and probes).

5.3.4. Results and discussion

5.3.4.1 Effect of the degree of saturation (40% vs. 60%) and ground material volume, as well as the headspace

The effect of the degree of saturation of the ground material was evaluated using the MSK aggregate. Saturation degrees of 40 and 60% were selected based on the experience acquired in the field of mining environment in order to accelerate the kinetics of oxidation of iron sulfide minerals. The mass of the aggregate (< 1.18 mm) was that required to fill 2.5 and 5 cm in compacted layers. The different headspaces evaluated correspond to 5, 10 or 17.5 cm, and to 5, 10 or 15 cm for 2.5 and 5 cm of compacted ground material, respectively. Table 2 presents the results obtained for the above conditions.

The amount of oxygen consumed by the oxidation reaction is very low for ground materials kept at a 60% saturation, which is not surprising considering that the surface of the material was covered with a water film soon after about 30 minutes following the start of the test. Values of -1 and 8 mole/m²/year were obtained when 5 cm of MSK ground material was tested with 10 and 5 cm headspace, respectively, thus strongly suggesting that the water film formed inhibited the oxygen diffusion. On the other hand, the tests at 40% saturation gave the highest O₂ consumption values (289 moles/ m²/year) when using a compacted ground material thickness of 10 cm and a headspace of 10 cm. The values presented in Table 5.2 showed that for a constant thickness of compacted ground material (e.g. 2.5 or 5 cm), the oxygen consumption values increase with an increasing headspace. Also, for the same headspace (e.g. 10 cm), the use of a larger thickness of compacted ground material results in larger oxygen consumption.

Table 5.2: Oxygen consumption values using MSK aggregate with a particle size < 1.18mm.

	40% saturation							60% saturation	
Ground material thickness	10 cm	5cm			2.5 cm			5cm	
Headspace	10 cm	15 cm	10 cm	5 cm	17.5cm	10 cm	5 cm	10 cm	5 cm
O ₂ consumption (moles/ m ² /year)	289	156	126	83	99	58	27	-1	8

The above results show that a 60% ground material saturation is too high and prevents oxygen from getting to the reaction site. All other tests were then conducted with a 40% saturation degree. Taking into account the results obtained when using different thickness of ground material to headspace ratio, the best ratios were 10 cm of compacted ground material with an headspace of 10 cm (289 moles/ m²/year), followed by 5 cm of compacted ground material with an headspace of 15 cm (156 moles/ m²/year).

5.3.4.2 Effect of the aggregate particle size (mortar vs. <1.18mm vs. <150µm)

In these series of tests, different particle sizes for the ground material were investigated: mortar particle size (5 mm to 150 µm), < 1.18 mm and < 150 µm. The tests were performed using a compacted ground material thickness of 5 cm at 40% saturation and a 15 cm headspace. A total of 8 aggregates were tested. The values obtained for the oxygen consumption test, as well as the total sulfur content (S_T % by mass) measured on representative subsamples ground from each size fractions of the aggregates are summarized in Table 5.3.

The results presented in Table 5.3 show that the particle size distribution has an important impact on the oxidation reaction, the smaller the particle size tested, the higher are the oxygen consumption values obtained. These results agree with the findings of Divet and Davy [8] and Jansen and coworkers [10] who claimed that an increase of the iron sulfides surface area increases the oxidation reaction since a greater surface is exposed to moisture and oxygen.

The data obtained for the sulfide-rich MSK and B&B aggregates indicate that the O₂ consumption is 7 and 4 times higher for samples with particle size < 150 µm compared to

that obtained when using the mortar-bar particle size distribution. Based on the above results, it was decided to adopt a particle size < 150 μm for further testing.

Table 5.3: Oxygen consumption values using different aggregate particle sizes (compacted ground material thickness of 5 cm at 40% saturation and a headspace of 15 cm).

		Sulfide-bearing aggregates						Control aggregates	
		SW	PHS	GGP	SBR	MSK	B&B	PKA	DLS
Mortar	O ₂ consumption (moles/ m ² /year)	---	---	25	35	41	61	0	---
	%S _T by mass	---	---	0.33	0.87	0.84	3.68	0.04	---
Ø <1.18 mm	O ₂ consumption (moles/ m ² /year)	105	40	122	160	156	223	14	31
	%S _T by mass	0.05	0.24	0.30	0.81	1.28	2.13	0.04	0.12
Ø < 150 μm	O ₂ consumption (moles/ m ² /year)	202	75	182	176	267	282	91	92
	%S _T by mass	0.05	0.09	0.29	0.78	0.73	4.22	0.05	0.09

The values presented in Table 5.3 also show the effect of the total sulfur content of the aggregate on the oxidation reaction, higher O₂ consumptions generally being obtained for aggregates with higher sulfur content. However, this applies to the set of aggregates tested and is not a generally applicable rule as it is largely related to the nature of the sulfide minerals present. Also, the difference in the amount of O₂ consumed between the aggregates susceptible to oxidation reaction (i.e. SBR, B&B, SW, MSK) and the control aggregates with very little or no oxidation potential (PKA, DLS) is somewhat small. A higher O₂ consumption was indeed expected for the aggregates with high percentage of total sulfur content, even if the different types of iron sulfide minerals do not react at the same degree or rate.

5.3.4.3 Oxygen consumption with optimized parameters

According to the data obtained in this study, the optimized test parameters include the use of a compacted ground material thickness of 10 cm with a particle size of < 150 μm and a 40% saturation level, 10 cm of headspace, and a test period of 3.5 h (30 minutes for the probes stabilization plus 3 hours of effective oxygen consumption measurements). In order to verify the reliability of this test procedure, nine control and sulfide-bearing aggregates

were tested under those conditions (Table 5.1); the tests were repeated twice for each aggregate.

In the first parts of this paper, the values obtained for the oxygen consumption were reported in moles/m²/year, units typically used in the field of acid rock drainage to reflect the diffusive transport of oxygen through mine tailings or waste rocks. However, since this is not the phenomenon of diffusion that is used here but rather the oxidation potential of the sulfide minerals that is measured by the consumption of one of the reactants, i.e. oxygen, it is more appropriate to introduce this value directly in % of oxygen consumed. Table 5.4 actually compares both consumption values, i.e. in moles/ m²/year and in % of consumed oxygen, and also presents the typical values of S_T (% by mass) for the aggregates investigated.

In general, the highest values of oxygen consumption were obtained for the aggregates with the highest % of S_T. The control samples consumed a very small amount of oxygen with values not exceeding 3%. For those samples, the difference between the two runs is important which is due to the error caused by very low oxygen concentration measured. In the case of SW aggregate, the value of oxygen consumption was expected to be low, since the value of S_T (% by mass) was only 0.07%; however, the oxygen values obtained were higher than, for example, the GGP aggregate that has more than 3 times the value in S_T (% by mass) than the SW. This difference can be explained by different factors, including the mineralogy of the sulfide-bearing phases, their oxidation potential, texture, or others. But, in general, the differences observed between the quantity of the oxygen consumed by the sulfide-bearing aggregates and the control aggregates can be used as discriminatory criteria. Based on results to date, a limit of 5% of oxygen consumed can separate aggregates susceptible to oxidation from “innocuous” ones (for the experimental conditions used). This limit is based on the study of only 9 aggregates and should be refined by the study of a larger number of aggregates. It can also be observed that the results obtained on the two companion specimens are very similar, which is quite encouraging.

Table 5. 4: Oxygen consumption and total sulfur values for nine different aggregates.

Aggregates		Oxygen cons. (moles/ m ² /year)		Oxygen cons. (%)		S _T (% by mass)	
	Tests →	1	2	1	2	1	2
Sulfide-bearing aggregates	PHS	112	111	6.2	6.2	0.32	0.29
	GGP	133	151	5.4	6.0	0.25	0.24
	SW	174	169	8.2	8.2	0.07	0.07
	SBR	226	243	10.7	10.8	0.87	0.75
	MSK	577	558	21.7	21.4	0.99	1.11
	SDBR	2006	1932	57.0	55.5	13.86	14.46
Control aggregates (no sulfide)	DLS	45	6	3.0	0.2	0.12	0.19
	PKA	65	71	2.6	2.8	0.04	0.06
	HPL	13	2.6E ⁻⁵	1.7	0.2	0.02	0.02

3.4.4 Test reproducibility

As described in section 5.3.3, two series of experiments were carried out to evaluate the possible variation obtained through sample preparation as well as from the utilisation of different oxygen probes. In the two cases, the oxygen consumption tests were performed using a compacted MSK ground material thickness of 10 cm with a particle size of < 150 µm and a 40% saturation degree, 10 cm of headspace, and a testing period of 3.5h (30 minutes for the probes stabilization plus 3 hours of effective oxygen consumption measurements).

5.3.4.4.1 Samples prepared by different operators with the same measuring probe

Three different operators prepared each one a sub-sample of aggregate (crushing and grinding) to be used in the oxygen consumption test. The column preparation was then carried out by one single operator and the three O₂ consumption tests performed using the same probe. The very similar values of the percentage of oxygen consumed obtained (Table 5.5) are a good indicator of the reproducibility of the test, with a mean value of 22.4%, a standard deviation value of 0.5 and a coefficient of variation of 2.2%.

Table 5.5: Oxygen consumption test results for material preparation performed by three different operators (MSK aggregate, compacted ground material thickness of 10 cm at 40% saturation, 10 cm headspace, 3.5-h testing period).

	Operator 1	Operator 2	Operator 3
Oxygen cons. (%)	22.7	21.8	22.8
S _T (% by mass)	1.15	1.09	1.13

5.3.4.4.2 Samples prepared by the same operator using different probes

In this second experiment, three sub-samples were prepared by one operator and the oxygen consumption of each sample was measured using three different set-ups (columns and probes). Once again, the values obtained are really close to each other (Table 5.6), with a mean of 22.1%, a standard deviation value of 0.5 and a coefficient of variation of 2.3%.

Table 5.6: Oxygen consumption measured by three different probes (MSK aggregate, compacted ground material thickness of 10 cm at 40% saturation, 10 cm headspace, 3.5-h testing period).

	Probe 1	Probe 2	Probe 3
Oxygen cons. (%)	21.7	21.9	21.8
S _T (% by mass)	0.99	1.07	1.05

Interestingly, the mean value of the six tests carried out on the MSK aggregate was 22.1, with a standard deviation value of 0.50 and a coefficient of variation of 2.2

5.3.5. Conclusions

Sulfide-bearing aggregates can oxidize and cause concrete deterioration. The present work aims at adapting the oxygen consumption test developed by Elberling and coworkers [14] to access the oxidation potential of concrete aggregates. A parametric testing program was carried out to optimize testing conditions using 10 sulfide-bearing and control aggregates. The parameters tested included the Aggregate particle size of the aggregate, the degree of saturation and the thickness of compacted ground material, as well as the headspace above the compacted material.

The experimental conditions that seemed most suitable to discriminate potentially deleterious aggregates from control ones were the use of 40% saturation, a thickness of

compacted ground material of 10 cm with a 10 cm headspace and a particle size $<150\ \mu\text{m}$. Nine aggregates were tested with the optimized conditions, 6 with significant amounts of iron sulfides and 3 controls without or with only traces of iron sulfides. The results obtained on these aggregates tested under the optimized conditions described above showed that the test is able to discriminate the aggregates containing iron sulfide minerals from the control (or sulfide-free) aggregates. A preliminary threshold limit fixed at 5% oxygen consumed separates the 2 groups of samples. In fact, control samples consumed less than 3% oxygen while sulfide-bearing aggregates like the MSK and the sulfide-rich SDBR samples consumed 21.6% and 56.3% in average, respectively. This limit is based only on the study of 9 aggregates and should be refined by the study of a larger number of samples. Finally, the precision of the method was assessed and a very low coefficient of variation of 2.3% was obtained for 8 tests carried out on the MSK aggregate with a mean of 22.0% and a standard deviation value of only 0.50.

5.4 Acknowledgements

The authors wish to acknowledge the Natural Sciences and Engineering Research Council of Canada (NSERC) for their collaborative research and development grant and all partners (ABQ, ACC, ACRGTQ, APCHQ, Garantie qualité habitation, ACQ, Inspec-sol inc., LVM, RBQ, Exp. Inc., SHQ, Ville de Québec, Ville de Montréal, Hydro-Québec, MTQ, Qualitas). Appreciation is also extended to Benoit Durand from IREQ for his implication and for having provided the PKA aggregate and to Methat Shehata for having provided the DLS and the SDBR aggregates. Appreciation is also extended to Bruno Bussière and Olivier Peyronnard from UQAT who shared their expertise and knowledge in the use of oxygen consumption test. A. Rodrigues benefits from a PhD scholarship financed by FCT-Fundação para a Ciência e Tecnologia, Portugal, Ref.: SFRH/BD/71203/2010.

5.5 References

- [1] Moum J, Rosenqvist IT. Sulfate attack on concrete in the Oslo region. J. Am. Concr. Inst. 1959; 56: 257-264.

- [2] Rodrigues A, Duchesne J, Fournier B. A new accelerated mortar bar test to assess the potential deleterious effect of sulfide-bearing aggregate in concrete. *Cem. Concr. Res.* 2015; 73: 96-110.
- [3] Rodrigues A, Duchesne J, Fournier B, Durand B, Rivard P, Shehata M. Mineralogical and chemical assessment of concrete damaged by the oxidation of sulfide-bearing aggregates: Importance of thaumasite formation on reaction mechanisms. *Cem. Concr. Res.* 2012; 42: 1336–1347.
- [4] Rodrigues A, Duchesne J, Fournier B. Microscopic analysis of the iron sulfide oxidation products used in concrete aggregates, 34th International Conference on Cement Microscopy, Halle-Saale, Germany; 2012.
- [5] Rodrigues A, Duchesne J, Fournier B. Petrographic characterization of the deterioration products of a concrete containing sulfide bearing aggregates; a particular case of internal sulfate attack, 35th International Conference on Cement Microscopy, Chicago, USA, 2013.
- [6] Rodrigues A, Duchesne J, Fournier B. Damage evaluation of two different concrete mix designs containing sulfide-bearing aggregates, 36th International Conference on Cement Microscopy, Milan, Italy; 2014.
- [7] Cruz R, Luna-Sanchez RM, Lapidus GT, Gonzalez I, Monroy M. An experimental strategy to determine galvanic interactions affecting the reactivity of sulfide mineral concentrates, *Hydrometallurgy* 2005; 78: 198– 208.
- [8] Divet L, Davy JP. Étude des risques d’oxydation de la pyrite dans le milieu basique du béton, *Bulletin des laboratoires des Ponts et Chaussées*; 1996, 204 : 97-107.
- [9] Steger HF. Oxidation of sulphide minerals VII. Effect, of Temperature and Relative Humidity on the Oxidation of Pyrrhotite, *Chem. Geol.* 1982; 35: 281-295.
- [10] Janzen MP, Nicholson RV, Scharer JM. Pyrrhotite reaction kinetics reaction rates for oxidation by oxygen, ferric iron and for nonoxidative solution, *Geochim. Cosmochim.* 2000; 64: 1511-1522.

- [11] Mikhlin YL, Kuklinski AV, Pavlenko NI, Varnek VA, Asanov IP, Okotrub AV, Selyutin GE, Solovyev LA. Spectroscopic and XRD studies of the air degradation of acid-reacted pyrrhotites. *Geochim. Cosmochim. Acta* 2002; 66: 4057-4067.
- [12] Belzile N, Chen YW, Cai M-F, Li Y. A review on pyrrhotite oxidation, *J. Geochem. Explor.* 2004; 84: 65-76.
- [13] Thomas JE, Skinner MW, Smart RSC. A mechanism to explain sudden changes in rates and products for pyrrhotite dissolution and acid solution», *Geochim. Cosmochim. Acta*, 2001; 65: 1-12.
- [14] Elberling B, Nicholson RV, Reardon EJ, Tibble P. Evaluation of sulfide oxidation rates: a laboratory study comparing oxygen fluxes and rates of oxidation product release, *Can. Geotech. J.* 1994; 31: 375-383.
- [15] Elberling B, Nicholson RV. Field determination of sulphide oxidation rates in mine tailings. *Water Resour. Res.* 1996; 32(6):1773-1784.
- [16] Martin V, Aubertin M, Bussière B, Mbonimpa M, Dagenais AM, Gosselin M. Measurement of oxygen consumption and diffusion in exposed and covered reactive mine tailings, 7th International Conference on Acid Rock Drainage (ICARD), St. Louis MO. R.I. Barnhisel (ed.), Published by the American Society of Mining and Reclamation (ASMR); 2006
- [17] Mbonimpa M, Aubertin M, Bussière B. Oxygen consumption test to evaluate the diffusive flux into reactive tailings: interpretation and numerical assessment, *Can. Geotech. J.* 2011; 48: 878–890.
- [18] Schmidt T, Leemann A, Gallucci E, Scrivener K. Physical and microstructural aspects of iron sulfide degradation in concrete. *Cem. Concr. Res.* 2011; 41: 263-269.
- [19] Pardal MP. Las Piritas del Maresme. Un asunto corrosivo. *Revista de Obras Públicas*; 1975; 3126: 691-693.

- [20] Vasquez E, Toral T. Influence des sulfures de fer des granulats du Maresme (Barcelone) sur les bétons, Bulletin of the International Association of Engineering Geology 1984; 30: 297-300.
- [21] Chinchón JS, Lopez A, Querol X, Ayora C. La Cantera de Mont Palau I: Influència de la mineralogía de los áridos en la durabilidad del hormigón. Ingeniería Civil 1989; 71: 79-88.
- [22] Chinchón J, Lopez A, Soriano J, Vazquez E. La Cantera de Mont Palau II: Formacion de Compuestos Expansivos Generados en la Reaccion Arido-Hormingon, Ingeniería Civil 1990; 72:109-113.
- [23] Chinchón JS, Ayora C, Aguado A, Guirado F. Influence of weathering of iron sulphides contained in aggregates on concrete durability, Cem. Concr. Res. 1995; 25: 1264-1272.
- [24] ASTM C1260 - 14 Standard Test Method for Potential Alkali Reactivity of Aggregates (Mortar-Bar Method). Annual Book of ASTM Standards 04.02, ASTM International, West Conshohocken (USA), 2014.
- [25] Knipe SW., Mycroft JR, Pratt AR, Nesbitt H W, Bancroft GM. X-ray photoelectron spectroscopic study of water adsorption on iron sulphide minerals, Geochim. Cosmochim. Acta 1995; 59: 1075-1090.

Chapter 6

Mortar bar expansion test for aggregates containing sulfide-bearing aggregates

6.1 Introduction

This paper was published in Cement and Concrete Research journal, Volume 73 (2015), pp. 96-110. It was submitted in December 2014, for publication in February 2015 and available online in March 2015.

6.2 Résumé

La détérioration de structures en béton causée par l'oxydation de granulats contenant des sulfures de fer a été rapportée dans la région de Trois-Rivières, Québec, Canada. L'oxydation des sulfures de fer et la génération de sulfates associés sont à l'origine du gonflement et de la fissuration du béton.

L'étude vise à développer un test de performance capable de reproduire, en laboratoire, les mécanismes de détérioration. Un test accéléré sur barres de mortier en deux phases a été élaboré. La phase 1 consiste à accélérer la réaction d'oxydation des sulfures en soumettant les barres de mortier à 2 cycles de mouillage par semaine dans une solution d'hypochlorite de sodium (6%) pour une durée de 3 heures et à conserver les barres à une température de 80°C et une humidité relative de 80% pendant 90 jours. La phase 2 vise à promouvoir la sulfatation interne en conservant les barres à 4°C à une humidité relative de 100%. Les granulats potentiellement réactifs présentent une expansion supérieure à 0,15% (Phase I), alors que la formation potentielle de thaumasite est détectée par un regain de l'expansion suivi par la destruction des échantillons durant la phase II. Les contrôles sans sulfure n'ont montré aucun signe de dégradation au cours des deux phases de l'essai.

6.3 Scientific publication no. 3

A new accelerated mortar bar test to assess the potential deleterious effect of sulfide-bearing aggregates in concrete.

Andreia Rodrigues, Josée Duchesne, and Benoit Fournier

Abstract

Deterioration of concrete structures incorporating sulfide bearing aggregates has been reported in Trois-Rivières area, Québec, Canada. In this case, iron sulfide oxidation and internal sulfate attack were observed.

The present study aims at developing a performance test that will reproduce, in the laboratory, the deterioration mechanisms observed on site. A two-phase accelerated mortar bar test was developed that consists in 90 days of storage at 80°C/80% RH, with 2 3-h wetting cycles per week in a 6% bleach solution (Phase I) followed by up to 90 days of storage at 4°C/100% RH (Phase II). Aggregates with oxidation potential presented an expansion over 0.15% during Phase I, while thaumasite formation potential is detected by rapid regain of expansion followed by destruction of the samples during Phase II. The control aggregates without sulfide mineral did not show any signs of deterioration in both phases of the testing program.

Keywords: Deterioration; Testing method; Internal Sulfate Attack; Pyrrhotite oxidation; Concrete.

6.3.1 Introduction

In the last few years, problems affecting concrete structures incorporating sulfide bearing aggregates have been reported in the Trois-Rivières area (Quebec, Canada). In most cases, the affected structures are house foundations; however, cases involving commercial buildings have also been identified. A large proportion of the house foundations were built between 2004 and 2008 and started to show deterioration within 3-5 years after construction. Visual signs of concrete deterioration consist of map-cracking (with some cracks reaching up to 40 mm in width) often showing yellowish/brownish staining. Pop-outs are also found exposing oxidized aggregate particles sometimes surrounded by a white rim of secondary reaction products [1].

6.3.1.1 Mechanisms of deleterious oxidation reactions and factors influencing the reaction

Recent investigations carried out by the authors [1-4] related the concrete deterioration to the use of a hypersthene gabbro coarse aggregate containing various proportions of sulfide minerals, including pyrrhotite $[\text{Fe}_{1-x}\text{S}]$, pyrite $[\text{FeS}_2]$, pentlandite $[(\text{Fe},\text{Ni})_9\text{S}_8]$ and chalcopyrite $[\text{CuFeS}_2]$. In addition to biotite $[\text{K}(\text{Mg},\text{Fe})_3\text{AlSi}_3\text{O}_{10}(\text{F},\text{OH})_2]$ and plagioclase feldspar $[\text{NaAlSi}_3\text{O}_8 - \text{CaAl}_2\text{Si}_2\text{O}_8]$, a thin layer of an iron carbonate (siderite - FeCO_3) was often found surrounding those sulfide minerals. The petrographic examination of deteriorated concrete specimens obtained from house foundations revealed that the pyrrhotite was often deeply oxidised, while pyrite showed only traces of oxidation or was perfectly sound. The rust products associated to the “unstable” aggregate particles typically consisted of iron oxide/hydroxide/oxyhydroxide; secondary products resulting from subsequent internal sulfate attack, namely gypsum $[\text{CaSO}_4 \cdot 2\text{H}_2\text{O}]$, ettringite $[\text{Ca}_6\text{Al}_2(\text{SO}_4)_3(\text{OH})_{12} \cdot 26\text{H}_2\text{O}]$ and thaumasite $[\text{Ca}_3\text{Si}(\text{OH})_6(\text{CO}_3)(\text{SO}_4) \cdot 12\text{H}_2\text{O}]$, were also identified.

Cases of concrete deterioration involving sulfide bearing black shales, schists or sedimentary rocks were reported in the literature [5-13]. Tagnit-Hamou et al. [13], studied deteriorated concrete house foundations incorporating a sulfide bearing gray anorthosite with some amounts of sulfide minerals very similar to the Trois-Rivières aggregate investigated in this study. Secondary products identified in deteriorated concretes incorporating sulfide-bearing aggregates consisted of jarosite $[\text{KFe}_3(\text{OH})_6(\text{SO}_4)_2]$ [12,14,15], iron oxides and hydroxides [11,13,16], halotrichite $[\text{FeAl}_2(\text{SO}_4)_4 \cdot 22\text{H}_2\text{O}]$ [13], gypsum [10,14,15], ettringite [10,11-13], and thaumasite [15,17,18].

The oxidation of sulfide minerals in the presence of water and oxygen results in the formation of various rust products and sulfuric acid, such as the case presented herein for pyrite (Eq. 1).



Steger [19] concluded that the oxidation rate of sulfide minerals increases directly with increasing relative humidity (RH) values between 37 and 75%. In 1995, Knipe and coworkers [20] studied the interactions between pyrite and pyrrhotite and water vapour.

They concluded that oxygen is the primary oxidant, and that the iron sulfides do not oxidize when exposed to deoxygenated water. The amount of oxygen that can diffuse is limited by the maximum concentration of O₂ in water, ($C_w \approx 9.2$ mg/L), which is about 30 times less than the equilibrium concentration of oxygen in air ($C_a \approx 276.7$ mg/L) at 20 °C [21]. Consequently, a sample of iron sulfide immersed in water or kept at 100% relative humidity will not oxidize or the oxidation rate will be really slow. According to Bussière [22], an expert in the field of mining environment, the optimum relative humidity for sulfide oxidation is between 60 and 80% (personal communication).

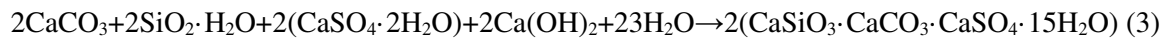
The oxidation of pyrite and pyrrhotite can also be promoted and catalyzed by the *Thiobacillus ferrooxidans* bacteria. These bacteria occur at low pH [6], in the range 1.0 - 2.5, deriving their energy from redox reactions where Fe²⁺ or reduced sulfur compounds serve as electron donor and oxygen as electron acceptor [23]. The specific surface area of the iron sulfides are increased by fracturing and surface roughness that consequently increase the oxidation reaction, because more surface is exposed to moisture and oxygen [24,25]. Divet and Davy [24] and Steger [19] showed that the sulfides oxidation rate increases significantly with increasing temperature, in accordance with the Arrhenius Law. The iron sulfide morphology can also influence the oxidation reaction. Divet and Davy [24] concluded that framboidal pyrite oxidizes much faster than massive pyrite. The authors also found that the high OH⁻ ion concentration in the alkaline pore solution of concrete plays a major role in the pyrite's oxidation. For a pH greater than 12.5, the oxidation rate increases exponentially and reaches about 50 times its initial value for a pH of 13.7.

When the sulfuric acid generated in the Eq. (1) reacts with the solids of the cement paste, mainly with the portlandite [Ca(OH)₂], the formation of gypsum occurs according to the Eq. (2) [14,26].



When the right conditions have been met, such as temperature, pH, humidity, other sulfates such ettringite and thaumasite can also be formed. The resulting internal sulfate attack (causing the formation of gypsum, ettringite and thaumasite), however, requires other conditions and is influenced by factors other than those affecting iron sulfides

oxidation. In the case of internal sulfate attack with thaumasite formation, a source of water, carbonate, sulfate and silicate ions is required (Eq. (3)).



The source of sulfates can be the cement or the aggregates [27-30]. The carbonate source is generally the aggregate [29, 30], the limestone filler in certain cements or the atmospheric CO₂ [30]. The silicate ions are usually provided by the silicates present in the C-S-H, thus leading to the disintegration of cement paste and, consequently, of the concrete [30]. The favourable conditions for thaumasite formation are temperatures below 15°C [30-33], the ideal conditions being between 0 and 5°C [34]. However, cases of thaumasite formation were also reported at room temperature [35].

6.3.1.2 Testing for evaluating the potential for deleterious reaction of sulfide bearing aggregates

Since it was found that sulfide bearing aggregates could affect concrete durability, research was carried out to develop laboratory tests to evaluate their potential deleterious reactivity [5, 11, 17, 36-40]. Some tests aimed at determining a limit value of iron sulfides (e.g. pyrite and/or pyrrhotite) that would make concrete aggregates safe for use [5, 36, 39]. Some studies also tried to recreate in the laboratory, the conditions and mechanisms that lead to concrete deterioration in order to identify deleterious sulfide-bearing aggregates [11, 18, 37, 38, 40]. The following subsections present a summary of the test conditions applied in the above studies and of their main findings.

6.3.1.2.1 Testing by Hagerman and Roosaar [36] in Sweden

Having noticed some concrete deterioration problems involving sulfide-bearing aggregates in Sweden back in the early 1950's, Hagerman and Roosaar tried to determine the maximum tolerable pyrrhotite content in concrete aggregates using rock samples from Pengfors (pyrrhotite contents of 4% and 14%), Norrforsen (21% of pyrrhotite), and Stockholm (control non sulfide-bearing granite). The authors manufactured a series of concrete beams, 80 x 15 x 10 cm and 40 x 15 x 10 cm in size, that they subjected to a range of test conditions, including weekly cycles consisting of 3 days in warm water and 4 days of air storage at 75°C, 3 days in water and 4 days in air both at room temperature, or continuous outdoor exposure. Alternatively, some beams were subjected to steam curing in

an autoclave at 225°C for 5h. The specimens were then allowed to cool to 100°C in the autoclave, and then exposed to warm water to progressively bring their temperature down to 23°C. This treatment was repeated four times at approximately 1 week intervals. Between autoclaving sessions, the specimens were stored in air at room temperature.

After 7 months of testing, the series of beams (80 x 15 x 10 cm) made with rock samples incorporating a higher percentage of pyrrhotite (Pengfors 14% and Norrforsen 21%) and stored in warm water for 3 days followed by 4 days of air exposure at 75°C showed the presence of rust, cracks and bending.. The examination of broken surfaces of the beams made with the Norrforsen rocks (with 21% of pyrrhotite) revealed more damage at the end of testing and also that the rusty aggregate particles were limited to the first 10 mm from the surface; further petrographic examination in thin sections confirmed the presence of sulfide oxidation, together with staining in the cracks. Ettringite was however not observed.

6.3.1.2.2 Testing by Bérard et al. [5] in Montreal (Canada)

The authors studied cases of concrete deterioration related to the presence of sulfide-bearing shale particles (4.5% pyrrhotite) in the coarse aggregate. In order to try reproduce the deleterious reaction in the laboratory, the researchers manufactured 10 concrete prisms with different proportions of shale particles recycled from the deteriorated concrete elements (maximum aggregate particle size of 2 cm), and 10 companion prisms with shale particles obtained from the original quarry (maximum aggregate particle size of 4 cm). They then subjected the concrete prisms to cycles of wetting in a moist room at 23°C for a certain period of time, and drying in air in the laboratory for an equal period of time. All the samples suffered shrinkage, while one specimen showed a longitudinal crack with iron oxide seeping through the crack. Although the test was unable to reproduce the distress observed in the field (expansion/cracking), the deleterious properties of the shale were somewhat highlighted since some shale particles near the surface of the test prisms generated pop-outs through the oxidation of pyrrhotite mainly visible along bedding planes.

In addition, five blocks/cubes, with an initial length of 4 cm and cut from the shale, were subjected to different test conditions and their expansion monitored over time perpendicular to the bedding. Two test cubes immersed in water expanded by more than

0.2% in less than 100 days. Two other test cubes kept outdoors expanded only slightly less than the first two cubes. A fifth specimen, kept indoors at room temperature, showed slight shrinkage. Oxidation of sulfides was visible in all the samples and concentrated along the bedding planes.

6.3.1.2.3 Testing by Gomides [39] in Brazil

Gomides [39] investigated the performance of the concretes incorporating sulfide-bearing aggregates and five types of cements. In *stage 1* of the experimental program, concrete mixtures were prepared with a quartz-muscovite-schist aggregate containing 3.89% of sulfides, i.e. 3.40% pyrrhotite, 0.31% pyrite and 0.17% marcasite. The water-to-cement ratio for the concrete specimens was kept constant at 0.45. Three types of cements were used, i.e. a reference cement (CP II-F-32) and two cements resulting from the partial replacement of CP II-F-32 by 40% (CP40) and 60% (CP60) of ground granulated blast-furnace slag. In *stage 2*, the same aggregate, but with 0.56% of sulfides, was used with three types of cements, specifically: CP II-F-32, CP III-40-RS (sulfate resistant cement) and CP IV-32 (having in its composition: pozzolanic binder (25% to 40%) and 38% of fly ash). The aggregate used in *stage 2* was exactly the same as used in the *stage 1*, but it was stored outdoors in steel drums, i.e. subject to all kinds of weathering conditions, during a period of 2 years. After those 2 years of storage, the aggregate in question had lost approximately 86% of its sulfide content due to an oxidation process, with a remaining/residual sulfide content of 0.56%, i.e. 0.29% pyrrhotite and 0.27% pyrite. Concrete specimens cast in the study consisted of prisms (75 mm x 75 mm x 285 mm in size) and cylinders (100 mm in diameter x 200 mm in height). After casting, all specimens were stored in a humid chamber at $23^{\circ}\text{C} \pm 2$ and relative humidity $\geq 90\%$ for a period of about 5 years.

The results showed that pyrrhotite is the most reactive sulfide in the system. In the specimens from *stage 1*, external spots of rust, white efflorescence, scaling and disintegration of aggregate particles containing high levels of sulfides were observed. These features of deterioration resulted from the oxidation of sulfides and were more pronounced in the concretes containing higher proportions of ground granulated blast-furnace slag (CP40 and CP60). The concretes prepared in *stage 2* showed no visual signs of distress.

In general, the concrete showed the presence of typical deleterious products of sulfate attack, i.e. ettringite and gypsum, higher concentrations of these products being observed in CP 40 and CP 60 concretes. No information was given about the concentration of ettringite and gypsum observed in the *stage 2* specimens. The expansion values calculated after five and a half years of testing reached a maximum value of 0.052% for the CP60, and a maximum value of 0.041% for the CPIII after four and a half years of testing, suggesting that the higher the concentration of sulfides and aluminate ions present in the system, the greater the expansion or the observed levels of deterioration.

6.3.1.2.4 Testing by Oberholster et al [17, 18] in South Africa

In the 1980's, serious problems affecting concrete houses in the mining town of Penge (South Africa) were reported by Oberholster and coworkers. The affected elements (slabs and bricks) were constructed with a carbonaceous, sulfide-bearing, cummingtonite slate aggregate. The main iron sulfide present was pyrrhotite, but pyrite and chalcopyrite were also present. Examination of the concrete bricks revealed a white powdery material around the black carbonaceous aggregate that correspond to thaumasite. In order to recreate the conditions responsible for the deterioration, various sets of test prisms were cut from deteriorating bricks, but also cast using the aggregate from Penge. For the latter, two mix designs were used, namely aggregate-to-cement ratios of 5:1 and 10:1, and these were combined with two manufacturing processes, i.e. well compacted and poorly compacted. Some prisms were stored at 38°C, either under water or above water in sealed containers.

The test prisms that were cut from the bricks and stored under water expanded approximately 0.40% after 1000 days, although the amount of expansion was much less than for those stored above water, i.e. more than 1% after 1000 days. Some manufactured prisms stored above water started expanding at a high rate after 22 months, while those stored under water did not expand even after 3 years. Also, in the case of the laboratory-made concrete prisms, only those incorporating the low cement content (i.e. aggregate: cement ratio of 10:1) expanded, while well compacted prisms expanded at a higher rate than poorly compacted ones. The presence of ettringite was reported in the laboratory-made prisms that expanded.

6.3.1.2.5 Testing by Chinchón et al. [37, 40] in Spain

In 1990, Chinchón and coworkers reported the results of a study aiming at evaluating the phase changes in cement-based mortars incorporating sulfide-bearing rocks. Two sets of mortars were made, consisting of 85% limestone (with 4.20% hexagonal pyrrhotite and 0.70% pyrite) or shale (with values of pyrrhotite and pyrite unknown), 15% P 450 Portland cement and 20% water (by mass). A series of 15g mortar specimens were thus separated into porcelain capsules and maintained at 20°C and 97% R.H. for a 140-day period. A reduction in the pyrrhotite and pyrite contents, along with a large production of ettringite, was noted over that period. The appearance of ettringite was slower in the mortars incorporating the limestone aggregate. The authors concluded that the formation of ettringite, resulting from the reaction between iron sulfide oxidation products and cement paste hydration products, caused the observed mortar deterioration.

6.3.1.2.6 Testing by Lugg and Probert [9] in Cornwall and Devon (England)

From 1900 to 1950, many buildings in Cornwall and Devon (England) were constructed using mine tailing aggregates, mostly sulfide bearing rocks called ‘Mundic rocks’. In the 1980s, the market price of the houses that were thought to be affected by the “Mundic” problem started to drop; however, there was not, at that time, an effective way to determine whether the houses had the problem or not. In 1985, the Royal Institution of Chartered Surveyors (RICS), settled up a committee to investigate the problem [9]. This committee thus developed a guidance note that recommended the use of chemical and petrographic analyses for the identification of the “Mundic” concrete. Besides the chemical and petrographic analyses, the RCIS implemented an experimental program to measure the unrestrained linear expansion of concrete cores extracted from the “problematic” houses. This test [38] consists in subjecting the concrete cores to a water-saturated atmosphere (100% HR) at a constant temperature of 38°C and for a period of at least 250 days. Cores showing an average expansion upon wetting exceeding 0.075% at 7 days were considered to have failed the test; on the other hand, if the expansion was less than the above limit, the test had to be pursued up to 250 days. Core specimens showing an expansion lower than 0.025% over the remaining part of the 250 day test period, are likely to remain stable under ambient conditions for many years, provided that normal levels of care are maintained.

6.3.1.2.7 Testing by Schmidt *et al.* [11] in Switzerland

Schmidt *et al.* [11] reported a case of deterioration in a concrete dam in Switzerland, constructed in the beginning of the 1970s. The authors found that the dam suffered from steady expansion since the early 1980s, now reaching about 0.025% expansion in the upper part of the dam. The authors also reported the presence of “rust” deposits (iron oxides and hydroxides) and a smell of sulfurous compounds in the inspection galleries of the dam. The aggregate used in this construction consists of a schist that is mainly composed of feldspar, quartz, biotite, and muscovite with foliation layers of 0.5–2.0 mm in thickness. Iron sulfides were also found to be randomly dispersed within the aggregate particles, with pyrite/marcasite (80%) and pyrrhotite (20%) representing about 0.3 to 0.4% by volume. The size of the ore inclusions was in the range of about 30 to 200 μm and minor amounts of ilmenite [FeTiO_3] were also noticed. The concrete was produced with an ordinary Portland cement (equivalent to present day CEM I 32.5), using a water-to-cement ratio in the range 0.5–0.6.

Cores samples, 150 mm in diameter, were extracted from the downstream face and the inspection galleries of the 40 year-old structure. The investigations indicated that the deterioration process of the iron sulfide particles was similar but not uniform in the various concrete samples. The oxidation or degradation process of both pyrite/marcasite and pyrrhotite usually started from the surface of the particle forming a layer of oxidation products, which are darker than the unreacted iron sulfide. From the chemical microanalyses, the iron sulfide particles seem to react to form iron oxide [Fe_2O_3] and then iron hydroxides [$\text{FeO}(\text{OH})$, $\text{Fe}(\text{OH})_3$]. The concrete samples showed significant cracking originating from the iron sulfide-containing regions within the aggregate particles, and then extended into the cement paste. Thus, the degradation would be directly linked to the reaction of iron sulfides, leading to an increase in volume within the aggregate particles that, in turn, cause cracking and expansion of the concrete. The formation of secondary ettringite, from released sulfates, was observed, but there were no clear signs of expansion associated with the extra sulfate. It is not clear to what extent this may have contributed to the expansion observed. It was found that pyrrhotite reacts much faster than pyrite in alkaline concrete environments.

In order to recreate the deterioration mechanism responsible for the damage in the dam, concrete prisms, $70 \times 70 \times 280$ mm in size, were prepared with the same aggregate that was utilized in the dam construction. The cement utilized was an ordinary Portland cement (CEM I 42.5), with a water-to-cement ratio of 0.50, with a cement content of 280 kg/m^3 and an aggregate content of about 1900 kg/m^3 . The prisms were stored in water for 5 years at 60°C . Unfortunately, the degree of expansion could not be assessed accurately; however, petrographic and SEM/EDS analyses were performed in the prisms after 4 years of testing. The laboratory concrete specimens had the same appearance and pattern of the reaction as the dam concrete, but the extent of reaction of the iron sulfides was much lower. The reaction products observed were the same in both specimens, i.e. iron oxide, iron hydroxides and ettringite. These observations clearly indicate a very slow reaction rate of the iron sulfide inclusions under the immersion conditions used for testing, and difficulties to identify the right conditions to reproduce the specific iron sulfide degradation in the laboratory.

6.3.1.2.8 Summary

Although there is a significant amount of studies related to the mechanisms of sulfide bearing aggregates oxidation, no test method was able to efficiently reproduce or predict the potential reactivity of aggregate containing sulfide minerals.

As mentioned before, the parameters that influence and accelerate the oxidation of iron sulfides are mainly, high temperature, a somewhat high relative humidity, the pH and a source of oxygen.

The data presented in the scientific literature clearly showed that immersing the mortar or concrete test specimens in water [11, 18, 36] or keeping them at a high relative humidity of 100% or close to 100% [9, 37, 39, 40] would not promote expansion or the oxidation reaction will be too slow since, in both cases, the oxygen diffusion is insufficient to accelerate the oxidation of the iron sulfide minerals. Moreover, samples immersed in water will suffer from a significant decrease of the alkalinity of the concrete pore solution. The samples submitted to low temperatures (20 to 38°C) [5,18,37-40] will take long time to react since, as mentioned before, sulfides oxidation rate increases significantly with increasing temperature [19,24]. Otherwise, generation of ettringite will be eliminated at

high temperatures, as tested by Hagerman and Roosaar [36] (225°C) because ettringite is stable up to temperature < 80°C [41]. Steger [19] showed that the oxidation of sulfide minerals increases with an increase in relative humidity for values between 37 and 75% RH, while Mbonimpa et al. [21] stressed that excessive humidity will slow down the reaction.

The production of gypsum and/or ettringite was noticed in some studies [11, 18, 39]. Thaumassite, one of the deterioration products identified by Oberholster and coworkers [17, 18], was however not observed; this is not surprising considering that the ideal temperature conditions for thaumasite formation is between 0 and 5°C [34](Aguilera et al. 2001) and the temperature tested was 38°C.

In the case of Trois-Rivières concrete deterioration, different deterioration mechanisms are present: the iron sulfides oxidation followed by the internal sulfate attack with thaumasite formation.

6.3.2 Scope and objective of work

The present study aims at developing a performance test that will reproduce, in the laboratory, the expansive process responsible for the damage observed in house foundations in the Trois-Rivières area, i.e. 1) oxidation of iron sulfide minerals with resulting acid formation and sulfate attack of the cement paste, and 2) thaumasite formation. To achieve this goal, an accelerated test on mortar was selected because an increase in the specific surface area of the iron sulfides significantly increases the rate of oxidation [24, 25]. Companion sets of mortar bars were thus made and subjected to different conditions, including various temperatures (4, 23, 38, 60 and 80°C), relative humidity (60, 80 and 100%), immersion (or not) in an oxidizing agent (bleach (6%) and hydrogen peroxide (3%) solutions), and wetting and drying cycles (0, 1 or 2 cycles/week); the expansion of the mortar bars was monitored at specific time over the testing period that reached up to 6 months.

6.3.3 Materials and methods

6.3.3.1 Aggregate materials

Seven aggregate materials were used in this experiment; their properties are summarized in Table 6.1. They consisted of two sulfide-bearing aggregates (MSK and GGP), three sulfide bearing and alkali-silica reactive aggregates (SBR, SW and SPH), and two control aggregates with only traces or no sulfides (PKA and HPL). MSK is the problematic aggregate used in the construction of the Trois-Rivières house foundations; it corresponds to a hypersthene gabbro containing various proportions of pyrite [FeS₂], pyrrhotite [Fe_{1-x}S], pentlandite [(Fe,Ni)₉S₈] and chalcopyrite [CuFeS₂] [1]. The sulfur content (% by mass) measured on a representative aggregate sample of MSK are between 0.73% and 1.28%. Major constituents of this dark-colored coarse-grained rock consist of anorthite [CaAl₂Si₂O₈], with lesser amounts of biotite and pyroxene [XY(Si,Al)₂O₆]. Pyrite and pyrrhotite are closely associated and the pentlandite is found as oriented blebs of “flames” in pyrrhotite areas/grains. Pyrrhotite is the most “reactive” sulfide showing strongly oxidized surfaces, while pyrite surfaces are mostly unaltered. Finally, an iron carbonate mineral (siderite) often forms a thin “coating” around the sulfide minerals and filling up cracks and porosity.

SBR is a fine-grained and hard crushed rock, a hornfels; it was selected because it contains the same types of iron sulfides as MSK but no carbonate minerals. The sulfur content (% by mass) measured on a representative aggregate sample of SBR is between 0.75% and 0.87%. Interestingly, this aggregate is alkali-silica reactive, which will have some impacts on the test results.

GGP is a gneiss of granitic origin containing pyrrhotite and pyrite but without carbonates; the sulfur content (% by mass) measured on representative aggregate sub-sample of GGP is between 0.24% and 0.33%.

PKA (an anorthositic rock) and HPL (High Purity Limestone) are control aggregates without any sulfide minerals. Their sulfur content (% by mass) is close or under 0.06%.

Table 6.1: Main properties of aggregates used in this study

Aggregate	Rock type	Mineralogy			% S _T (by mass)	ASR* reactivity	Density
		Main constituting minerals	Presence of carbonate minerals	Iron sulfurs			
MSK	Norite or hypersthene gabbro	Plagioclase Biotite Pyroxenes Quartz	Yes, siderite (FeCO ₃) surrounding the iron sulfide minerals and calcite	Pyrrhotite Pyrite Chalcopyrite Pentlandite	0.73-1.28	No	2.89
SBR	Hornfels	Feldspars Quartz Clays Organic matter	No	Pyrrhotite Pyrite Chalcopyrite Sphalerite	0.75-0.87	Yes	2.91
SW	Mica Schist	Quartz Feldspars White mica Amphibole	No	Pyrrhotite Pyrite Chalcopyrite	0.07	Yes	2.72
SPH	Phyllite	Quartz Feldspar White mica Chlorite	Yes, calcite in small amounts	Pyrrhotite Pyrite Chalcopyrite	0.29-0.32	Yes	2.82
GGP	Granitic gneiss	Quartz Hornblende Pyroxenes Plagioclase	Traces	Pyrite Pyrrhotite Chalcopyrite	0.24-0.33	No	2.93
PKA (control)	Anorthosite	Plagioclase Hornblende Biotite	No	–	0.04-0.06	No	2.78
HPL (control)	Limestone	Carbonates	Yes – main constituent	–	0.02	No	2.95

*ASR: alkali-silica reactive aggregate

6.3.3.2 Nature and fabrication of the test specimens

With the objective of generating reliable test results in a reasonable time period, the decision was made to work on mortar specimens. Furthermore, in order to minimize the number of parameters involved and for practical reasons, the nature and preparation of aggregate materials and mortar test specimens were modelled in many ways from the commonly-used accelerated mortar bar test (AMBT) for alkali-aggregate reaction (AAR) (ASTM C1260, CSA A23.2-25A) [42, 43], with necessary adjustments considering the scope of this work.

A total of 216 mortar bars, 25 x 25 x 285 mm in size, were manufactured as part of this study. All of these bars were made with a w/c of 0.65 in order to reproduce the porous nature of the housing foundation concretes suffering from iron sulfide oxidation in the Trois-Rivières area (w/c \approx 0.70). A cement-to-aggregate ratio of 1:2.73 (i.e. 440 g of cement for 1200 g of aggregate) was used, i.e. slightly higher than the 1: 2.25 value used in ASTM C1260 due to the higher density of the sulfide-bearing aggregates. However, the types and proportions of the different aggregate size fractions were the same as those

specified in ASTM C1260. All mortar bars were prepared with an ordinary (Type GU) Portland cement (Table 6.2).

The mortar bars were prepared by following the various steps described in ASTM C1260 test procedure. Considering the condition of testing used in this program, titanium studs were used to avoid metal degradation in the presence of oxidizing agents. After casting of the mortar bars, the moulds were placed in a moist curing room at $23 \pm 2^{\circ}\text{C}$, protected with a plastic sheet. Because of the higher water-to-cement ratio selected for this study, the bars were left to cure in their moulds for a period of 72 h. Upon stripping, the bars were weighed, measured longitudinally and then placed into conditions, as will be described hereafter.

Table 6.2: Cement composition

Chemical composition	(%)
SiO ₂	19.8
Al ₂ O ₃	4.7
Fe ₂ O ₃	2.9
CaO	62.1
MgO	2.7
SO ₃	3.8
Loss on ignition (LOI)	2.2
Soluble residue	0.67
Bogue composition	(%)
C ₃ S	56
C ₂ S	15
C ₃ A	8
C ₄ AF	9

6.3.3.3 Testing conditions

Figure 6.1 presents the flowchart adopted for the experimental program. Each set of test specimens is composed of three mortar bars that are subjected to zero, one or two 3-h immersion period(s) per week in bleach (6% sodium hypochlorite solution) or peroxide (3% H₂O₂) solutions at room temperature. After the 3-h soaking period, the mortar bars are left under a hood for a period of 3 h and then stored at different temperature (23°C, 38°C, 60°C and 80°C) and RH conditions (60 or 80%) to promote oxidation reaction. The mass and length variations of the test specimens are monitored regularly, after the wetting cycles.

After 30, 60 or 90 days in the above conditions, some sets of mortar bars are transferred to conditions favorable to thaumasite formation, i.e. 4°C and RH values of either

80 or 100%. During that period of low-temperature storage, the sets of mortar bars were subjected to either 0, 1 or 2 weekly wetting cycle(s) (3 h) in bleach (Fig.6.1); their weight and length were once again monitored regularly during that period of low-temperature storage.

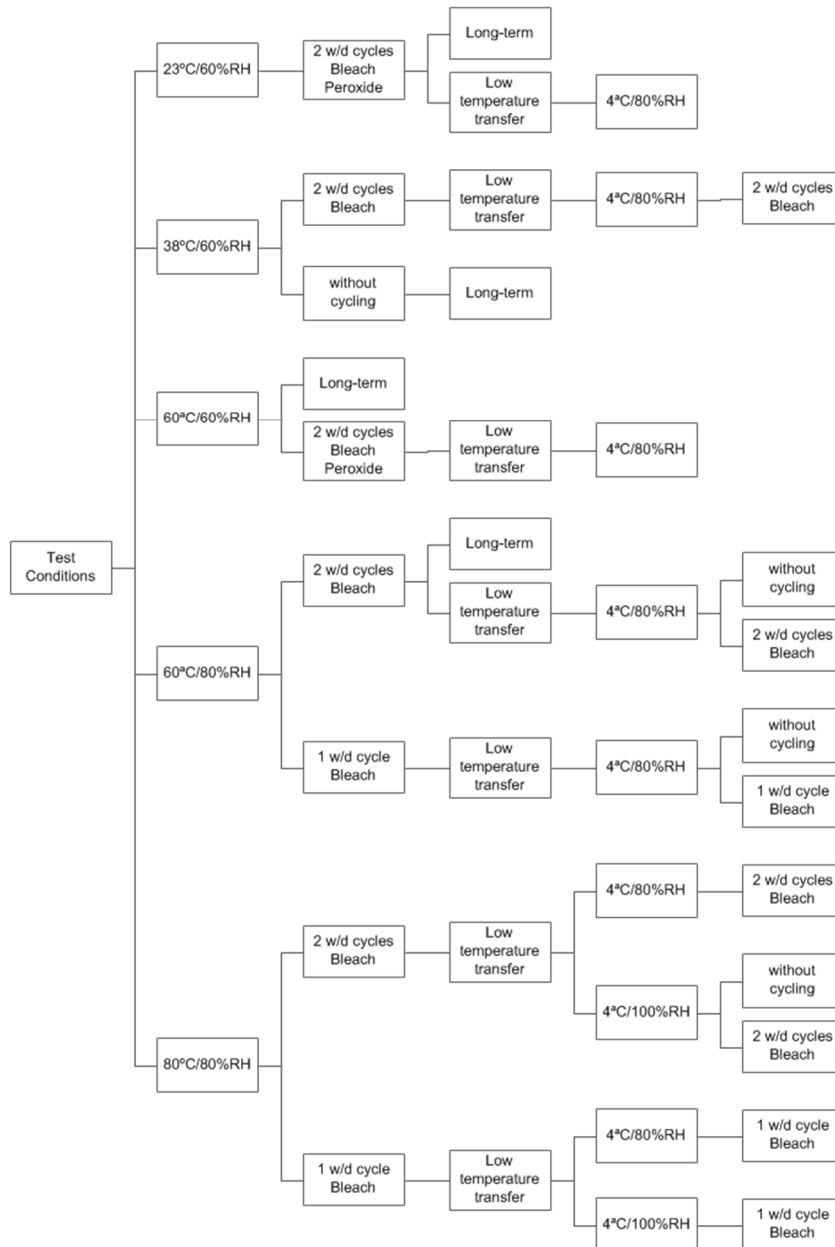


Figure 6. 1: Test conditions of the experimental program flowchart.

The different temperatures and RH values used for the storage of the mortar specimens between the wetting cycles were maintained using environmental (i.e.

temperature and humidity controlled) cabinets (Cincinnati Sub-Zero Z16 and Z44), or by using oversaturated salt solutions at the bottom of hermetic storage containers that were then placed in conventional laboratory ovens maintained at 60 and 80°C. For example, an oversaturated solution of sodium chloride (NaCl) is used to maintain a RH close to 80% at a temperature of 80°C. At 4°C, cane sugar maintains a RH of 80%, while water maintains 100% RH. At 60°C, potassium chloride (KCl) maintains a RH of 80% and sodium nitrate (NaNO₃) a R.H. of 60%. Finally, 60% RH can be obtained using CoCl₂ · 6H₂O at 38°C and Ca(NO₃)₂ · 4H₂O at 23°C [44].

6.3.4. Results and discussion

There are a number of factors contributing to the iron sulfides oxidation resulting in the formation of sulfuric acid and “conventional” internal sulfate attack, but also to thaumasite formation. Although the two types of deterioration mechanisms coexist in the concrete elements of the Trois-Rivières area under study, the approach taken in this study is to separate them by exposing the test specimens to exposure conditions specifically prone to their development. Several factors were thus considered consecutively in order to identify the most influential parameters in the development of a reliable expansion test.

6.3.4.1 Phase one: iron sulfide oxidation resulting in acid formation and internal sulfate attack

The following sections present the results of a parametric testing program aiming to evaluate the effect of, for instance, temperature, relative humidity, and use of oxidizing solutions, on the expansion of companion sets of mortar bars incorporating different control and sulfide-bearing aggregates.

6.3.4.1.1 Effect of the oxidizing agent

Figure 6.2 presents a plot of the expansion against time of mortar specimens incorporating the HPL (control) and the sulfide-bearing aggregate MSK that were subjected to 0 (no cycling) or two, 3-h immersion periods per week in bleach (6%) or in hydrogen peroxide (3%) at 23°C. Between the wetting cycles, the specimens were kept at 60°C and 60% RH. Only MSK mortar specimens soaked in bleach showed significant expansion, reaching an average expansion of 0.09% at the end of the testing period of 230 days; all other specimens presented shrinkage. Soaking in oxidizing solutions had no effect on the control

specimens HPL, while soaking in the peroxide solution did not contribute at inducing expansion for the sulfide-bearing specimens MSK.

The difference between the effectiveness of the two immersion solutions to promote oxidation can likely be explained by the low pH (about 4.5) of the hydrogen peroxide solution. In contact with the mortar bars, the hydrogen peroxide solution is neutralized and quickly loses its oxidizing power. Based on these results, the bleach solution was selected for further work.

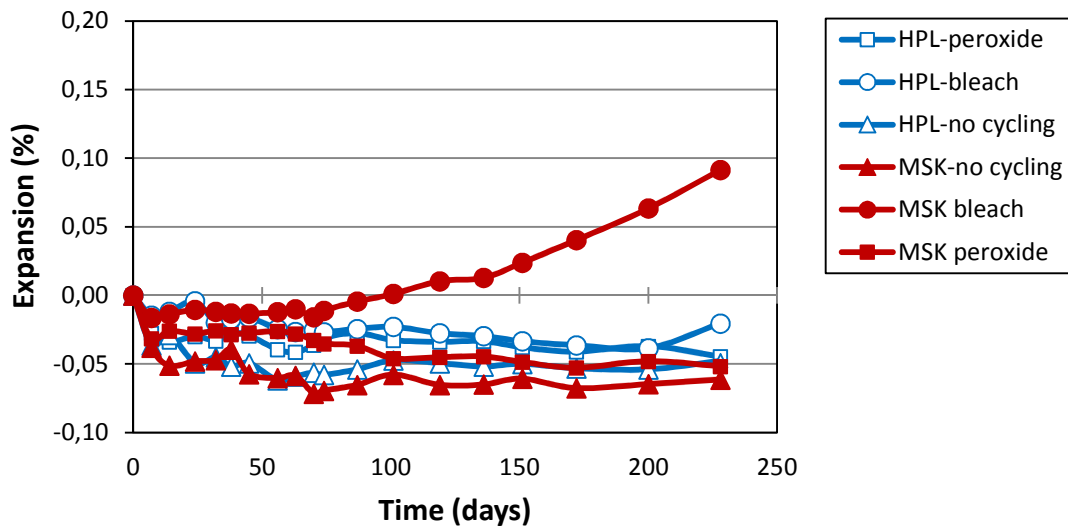


Figure 6.2: Expansion of mortar specimens stored at 60°C/60% RH, without (no cycling) or with immersion (twice per week) in bleach (6%) or hydrogen peroxide (3%) solutions. HPL is a control sample while MSK is a sample with sulfide-bearing aggregate. Each curve in this figure corresponds to the average values obtained from a set of three bars.

6.3.4.1.2 Effect of the number of weekly immersion cycles in bleach

Three aggregates, i.e. the sulfide-bearing aggregates MSK and GGP and the control aggregate HPL, were used in mortar specimens that were subjected to 1 or 2 weekly wetting cycles in bleach (6%) at 23°C. Following each wetting cycle, the specimens were kept at 80°C and 80% RH; the total testing period was 90 days. This was done in order to determine whether there was any benefit in subjecting the test specimens to two wetting cycles in bleach per week (instead of one), considering the additional work/effort involved.

The results presented in Fig. 6.3 show that immersing the test specimens twice per week resulted in higher expansions for both sulfide-bearing aggregates (MSK and GGP) and that the control aggregate (HPL) was unaffected by the immersion treatment. An

induction period of about 30 days was necessary to induce expansion in the mortar specimens incorporating the sulfide-bearing aggregates, and this seemed to be unaffected by the number of wetting cycles. The following testing series were then performed using two weekly immersion cycles in bleach.

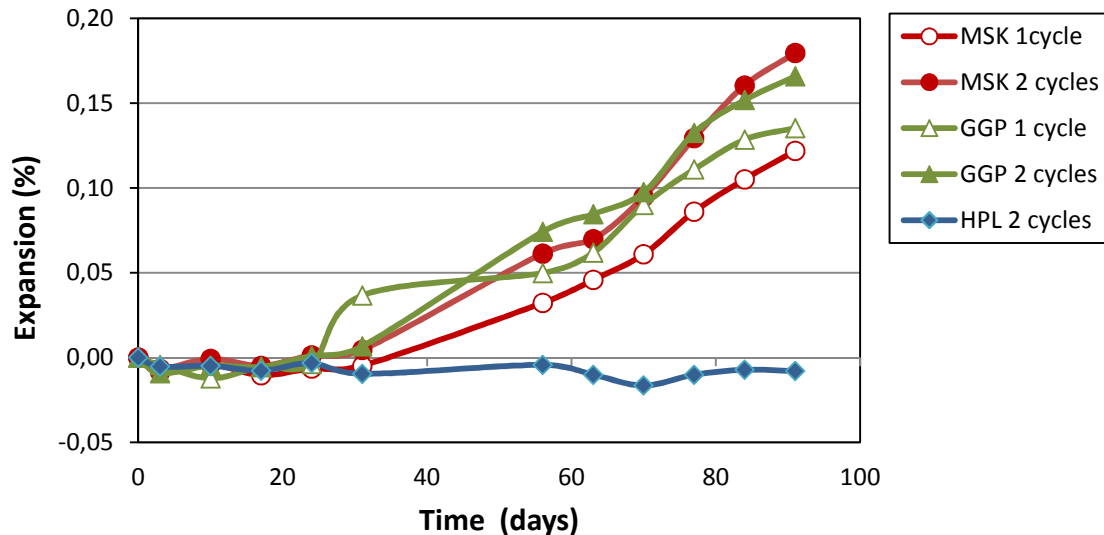


Figure 6.3: Expansion of mortar bars subjected to one or two 3-h immersion period(s) in bleach per week and stored at 80°C and 80% RH the remaining time. Each curve in this figure corresponds to the average values obtained from a set of three bars.

6.3.4.1.3 Effect of the relative humidity conditions (60% RH vs. 80% RH)

As mentioned before, the oxidation of sulfide minerals with the resulting formation of various rust products occurs in the presence of water and oxygen. In order to promote the oxidation in the test specimens, it is thus necessary for oxygen to diffuse through the porosity of the mortar. Since the diffusion rate of oxygen in water is low [2], it will be similarly very slow through the pore space of saturated mortar specimens. This is likely the reason why several attempts to recreate the deleterious oxidation reaction and resulting expansion in the laboratory were largely unsuccessful when specimens were stored in water or in the ASTM C1293 [45] conditions (i.e. 100% RH) (Gomides [39] (RH \geq 90%); Chinchón et al. [37, 40] (97% RH); RICS [38] (100% RH); Schmidt et al. [11] (immersion in water)).

Figure 6.4 illustrates the expansion against time of mortar specimens incorporating the sulfide-bearing aggregate MSK, and that were subjected to two weekly immersion

cycles in bleach at room temperature; between the above wetting sessions, the test specimens were maintained at 60°C, and at 60% or 80% RH. Despite small differences in the results in Fig. 6.4, there are indications that higher expansions can be obtained at 80% RH. It is also interesting to note, from the data presented in Figures 6.2 and 6.3 that much faster and higher expansions were obtained when mortar specimens incorporating the MSK aggregate and immersed twice per week in a 6% bleach solution were exposed to 80°C / 80% RH compared to 60°C / 60% RH. This difference is likely due to the higher temperature but also to the higher RH used for the former test series.

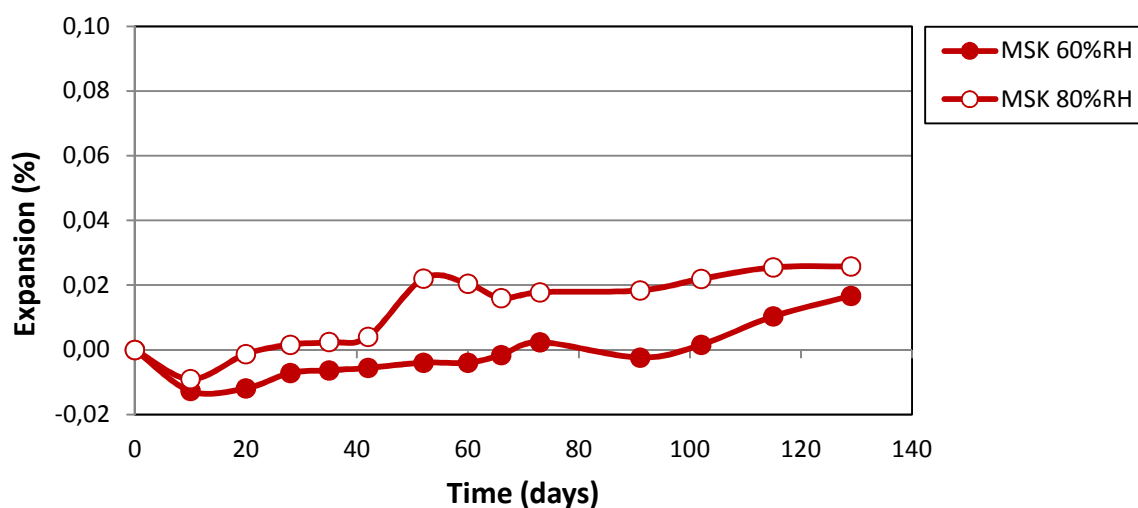


Figure 6. 4: Expansion of mortars stored at 60% RH or 80% RH at a temperature of 60°C (MSK aggregate). Each curve in this figure corresponds to the average values obtained from a set of three bars.

6.3.4.1.4 Effect of the storage temperature (23°C vs. 60°C vs. 80°C)

For this series of tests, all mortar bars were subjected to two weekly immersion cycles in bleach (6%) at 23°C; between the above wetting sessions, all sets of test specimens were maintained at 80% RH, but at different temperatures, i.e. 23°C, 60°C or 80°C for bars incorporating the MSK aggregate, and 60°C and 80°C for those made with the control aggregates PKA and HPL.

Fig. 6.5 clearly shows that an increase in temperature, especially up to 80°C, results in a significant increase in the expansion of mortar bars incorporating the sulfide-bearing aggregates MSK but has no effect on test specimens made with the control aggregates HPL.

and PKA. These results seem consistent with data published by Divet and Davy [24] and Steger [19] showing that the oxidation reaction increases with an increase in temperature, thus resulting in increasing expansion. A temperature of 80°C will thus be preferred for further work.

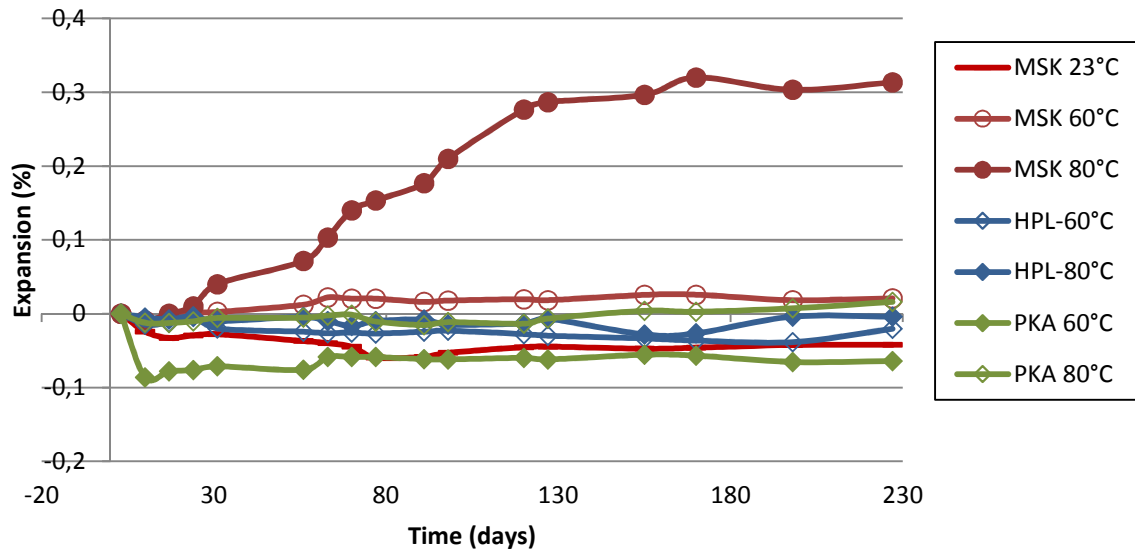


Figure 6. 5: Expansion of mortar bars subjected to 80% RH but at different temperatures (2 weekly wetting cycles in bleach). Each curve in this figure corresponds to the average values obtained from a set of three bars.

6.3.4.1.5 Effect of the period of time under 80°C and 80% RH conditions

The effect of the duration of Phase I testing was evaluated in order to optimize the oxidation reaction and maximize the related expansion, while using a reasonable testing period. Four companion sets of mortar bars incorporating aggregates MSK, GGP, HPL and PKA were thus stored at 80°C and 80% RH for 30, 60 or 90 days, periods during which they were subjected to two weekly wetting cycles in a 6% bleach solution. As seen in Table 6.3, different behaviors are observed for the two groups of aggregates tested. First, the “non reactive” samples, PKA and HPL did not show any expansion. On the other hand, mortar bars incorporating sulfide-bearing aggregates (MSK and GGP) showed a progressive expansion. Actually, two of the three MSK sets of bars showed a more rapid onset of expansion (i.e. 30 and 60-day test series) that reached 0.08% at 60 days, while the third set of mortar bars expanded by about 0.18% at 90 days.

Based on the above results, and considering that Phase I testing period needed to be sufficiently long to reliably differentiate sulfide-bearing aggregates from “non-reactive” (control) ones, but not too long for the test to maintain an “accelerated” character, a period of 90 days of testing was selected for the Phase I of the test.

Table 6.3: Expansion of mortar bars subjected to different periods of testing under the same conditions (80°C / 80% RH and 2 weekly cycles in bleach (6%) at 23°C).

Sample	Expansion (%)		
	30 days	60 days	90 days
MSK	0.01	0.08	0.18
GGP	0.01	0.08	0.17
PKA	-0.01	-0.002	-0.02
HPL	-0.01	-0.01	-0.01

6.3.4.1.6 Conclusions

Based on the results obtained in the first phase of this study, the experimental conditions that appear to most effectively promote the oxidation of the sulfide-bearing aggregates are high temperature (80°C), a relative humidity of 80% and two wetting cycles of 3 h per week in a solution of 6% sodium hypochlorite solution (bleach). A period of 90 days of testing under the above conditions seemed to be effective and sufficiently long to reliably separate between deleterious and control (non reactive) aggregate specimens. Actually, in the case of the evaluation of the potential alkali-reactivity of concrete aggregates, accelerated mortar bar expansions in the order of 0.10% (ASTM C 1260) or 0.15% (CSA A23.2-25A) are proposed for differentiating non-reactive aggregates from potentially reactive ones. It is thus believed that an expansion limit of 0.10 to 0.15% would be desirable in the case of sulfide-bearing aggregates, which “safely” requires about 90 days of testing in the proposed storage conditions. The “external/superficial” condition and the microstructural characteristics of the mortar specimens after completion of this first phase of testing will be described later in the paper (section 6.3.4.4).

6.3.4.2 Phase two: sulfate attack promoting thaumasite formation

As mentioned before, the aim of this research is to reproduce, under accelerated laboratory test conditions, the degradation process observed in the concrete structures of the Trois-Rivières area. The results of laboratory testing presented in the first part of this paper showed that high temperature (80°C) and controlled relative humidity conditions (80% RH) can promote the oxidation of sulfide-bearing minerals in concrete aggregates, with resulting internal sulfate attack and mortar bar expansion. However, thaumasite was also identified in severely deteriorated concrete samples extracted from some housing foundations in the Trois-Rivières area. The conditions that promote thaumasite formation are somewhat different from those contributing to the iron sulfides oxidation, including a low temperature exposure and a source of carbonate material.

In the second phase of this study, an experimental program was developed to identify the most critical parameters and conditions that would contribute to the formation of thaumasite in the test specimens. The following parameters were thus investigated: 1) the effect of transferring the test specimens at low temperature (4°C), 2) the relative humidity conditions (80% or 100%) under low temperature conditioning, and 3) the use of wetting cycles (1 or 2) in a bleach solution during phase II.

6.3.4.2.1 Effect of the samples transfer at low temperature

In order to promote thaumasite formation, a few sets of mortar bars incorporating sulfide bearing and control aggregates were transferred after phase I conditioning to low temperature storage, i.e. 4°C and 80% RH.

In the case of the MSK aggregate, the set of bars continuously subjected to phase I conditions (i.e. MSK 80°C/80%RH) showed a steadily increasing expansion trend from about 30 days on, reaching about 0.50% expansion after 300 days of testing (Fig. 6.6). The companion set of specimens transferred to low-temperature conditions (i.e. MSK 80°C → 4°C) first showed a similar behaviour but the expansion rate slowed down following 4°C transfer (at 90 days), but then increased dramatically after 150 days to reach about 1.5% at 300 days. At 300 days, one of the bars transferred to 4°C was so deteriorated that it broke in pieces. The set of mortar bars incorporating the GGP aggregate and maintained at 80°C

and 80%RH presented a steadily increasing expansion trend similar to that obtained with the MSK bars maintained in the same condition, except that the expansion of the former levelled off at about 0.4% at 210 days. On the other hand, the expansion of the companion set of GGP mortar bars (i.e. GGP 80°C → 4°C) reached about 0.18% at 90 days and then did not progress any further following their transfer at 4°C.

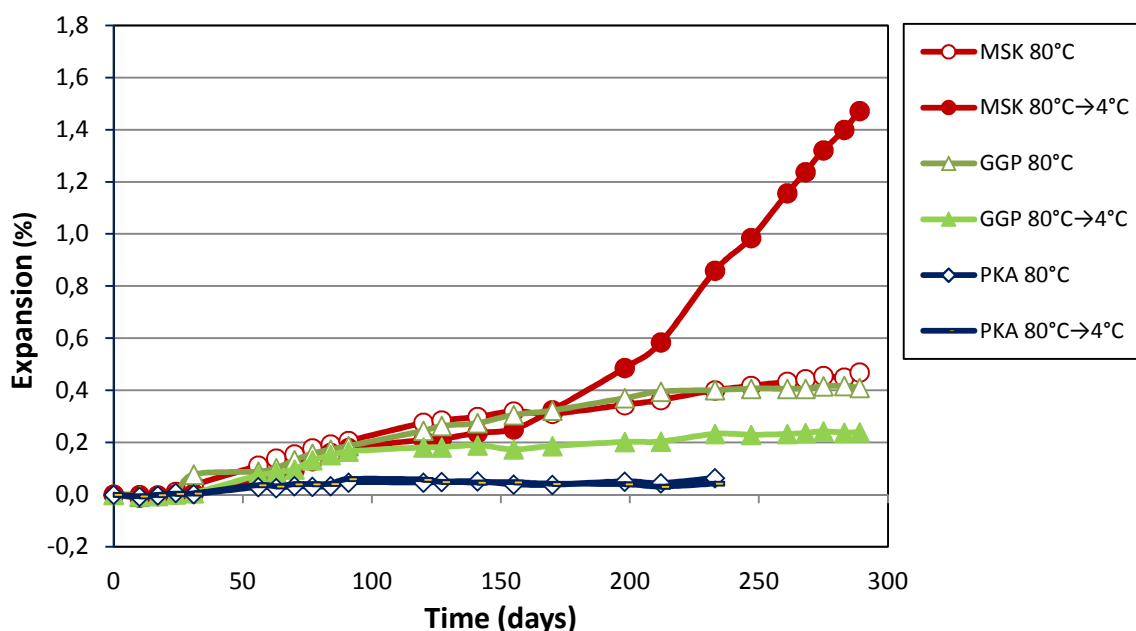


Figure 6.6: Expansion of companion sets of mortars specimens either kept continuously at 80°C and 80%RH or transferred at 4°C and 80% RH at 90 days. MSK, GGP and PKA (control) mortar bars were soaked twice a week for 3 hours in a 6% bleach solution at 23°C, both before and after the transfer to 4°C. Each curve in this figure corresponds to the average values obtained from a set of three bars.

The similar/different behavior of the MSK and GGP aggregates is most interesting and is believed to be due to the compositional differences between the two aggregates. As mentioned before, the MSK aggregate includes pyrrhotite-rich zones that are often surrounded by siderite, an iron carbonate mineral. It is believed that the presence of siderite is critical in thaumasite formation and the development of excessive expansion upon low-temperature transfer. This is supported by the fact that the GGP aggregate continuously maintained at 80°C and 80% RH shows a similar expansive behavior as the MSK bars, but is experiencing no further expansion upon 4°C transfer since it only contains traces of secondary carbonate material.

Finally, the control sample (PKA) presented very low expansion and this for both sets of specimens, i.e. those always maintained at 80°C and 80% RH and those transferred at 4°C after 90 days at 80°C and 80% RH.

6.3.4.2.2 Effect of the relative humidity (80% RH vs. 100% RH) during the low temperature exposure

In addition to low temperature conditions, thaumasite formation is promoted by exposure to a humid environment. After the previously adopted Phase I testing condition (i.e. 90 days at 80°C / 80% RH and 2 weekly 3-h immersion periods in a 6% bleach solution), companion sets of mortar bars manufactured with the MSK and GGP aggregates were transferred at 4°C and maintained at either 80% or 100% RH between the two weekly 3-h wetting cycle in the 6% bleach solution.

The results presented in Fig. 6.7 confirm the advantage of keeping the mortar specimens under high humidity (100% RH) conditions during the 4°C storage period to promote thaumasite formation. This is confirmed by the fact that a change in the RH condition during the low temperature storage did not make any significant difference for the sets of mortar specimens incorporating the GGP aggregate since those bars are not experiencing deleterious expansion related to thaumasite formation during the low temperature storage. In addition, 100% conditioning is very easy to maintain at 4°C (bars above water); this parameter was thus selected for further testing.

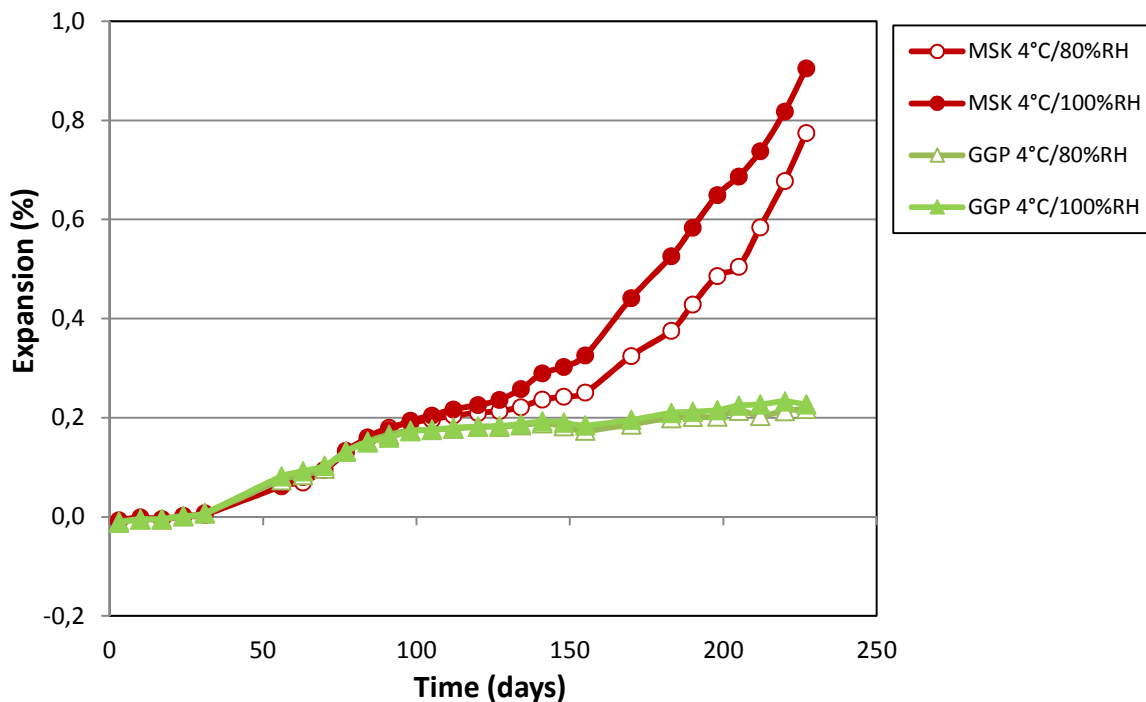


Figure 6.7: Expansion of mortar bars kept for 90 days at 80°C/80% RH and then transferred to 4°C at 80% or 100% RH, for MSK and GGP sulfide-bearing aggregates. Each curve in this figure corresponds to the average values obtained from a set of three bars.

6.3.4.2.3 Cycling effect at low temperature

In order to evaluate the effect/necessity to pursue the wetting cycles in the bleach solution during the low temperature storage, the expansion of companion sets of mortar specimens incorporating the MSK aggregate was evaluated with (MSK 80°C→ 4°C (2 cycles)) or without (MSK 80°C→4°C (no cycling)) immersion periods in the 6% bleach solution at 23°C. The data presented in Fig. 6.8 clearly confirmed that cycles of wetting in an oxidizing solution is very favorable and actually even required for the progress of the reaction and of further expansion at low temperature.

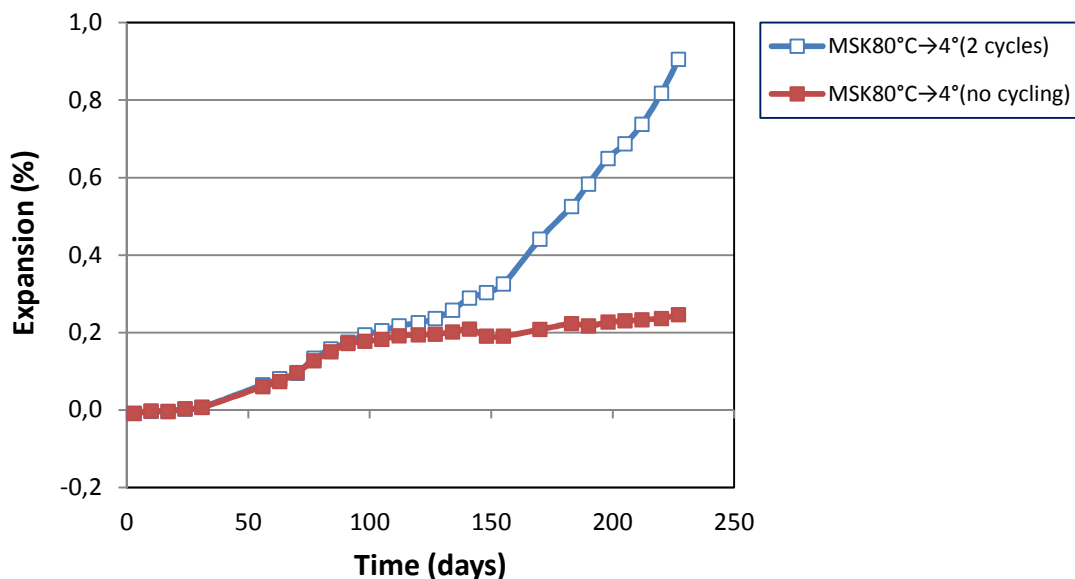


Figure 6. 8: Expansion of mortar bars kept at 80°C and 80% RH for 90 days and then transferred to 4°C and 80% RH maintaining or not the 2 weekly wetting cycles in 6% bleach solution during the low temperature regime. Each curve in this figure corresponds to the average values obtained from a set of three bars.

6.3.4.3 Behaviour of “special” (alkali-reactive and sulfide-bearing) aggregates

Some of the aggregates selected for this study that contains iron sulfide minerals where also found to be alkali-silica reactive (SBR, SW and SPH). The 14-day expansions obtained in the accelerated mortar bar test (CSA A23.2-25A equivalent to the ASTM C1260) were 0.23%, 0.20% and 0.35% for SBR, SW and SPH aggregates, respectively.

These aggregates were also tested for their oxidation potential for 90 days at 80°C and 80% RH followed by a transfer to 4°C/100% RH with 2 wetting cycles per week in a solution of 6% sodium hypochlorite solution (bleach). Figure 6.9 presents the expansion values for these three aggregates, along with MSK and PKA aggregates. The SBR aggregate presents a different behaviour, when compared to MSK, with a very rapid onset of expansion followed by a plateau after about 100 days of testing. This behavior was also observed for the SW and SPH aggregates and can be due to the fact that those three aggregates contain sulfide minerals but are also alkali-silica reactive. Additional work should be done to understand this phenomenon as Phase I conditions used in the present test seem very effective in promoting ASR in an accelerated manner. Another very interesting phenomenon is the fact that there is no further expansion following the transfer

to low temperature for the test specimens incorporating the SBR, SW and SPH aggregates. This is attributed to the low presence of carbonate mineral in these aggregates that in higher amounts would promote the formation of thaumasite at low temperature.

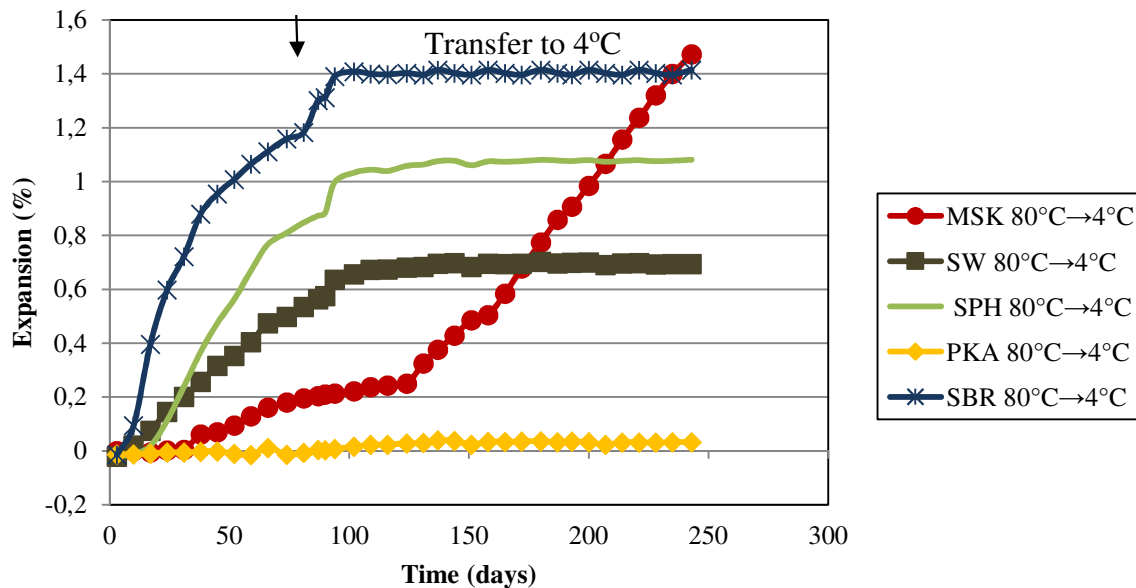


Figure 6.9: Expansion of mortar bars kept at 80°C and 80% RH for 90 days and then transferred to 4°C and 80% RH with immersion (twice per week) in bleach (6%) solution. Each curve in this figure corresponds to the average values obtained from a set of three bars.

6.3.4.4 Visual examination and microstructure of the test specimens

The visual condition of the different sets of mortar bars subjected to the various conditions investigated in this study was evaluated regularly during the expansion monitoring. In addition, specimens from selected sets of mortar bars were characterized under the scanning electron microscope in order to identify the various secondary products developing in the test specimens over different storage conditions. The following subsections present a summary of these findings.

6.3.4.4.1 General condition of the mortar specimens

Figure 6.10A shows the condition of a bar incorporating the MSK aggregate at 90 days (sample tested at 80°C/80% RH and subjected to two wetting cycles per week in a 6% bleach solution) before its transfer to 4°C/100% RH. At that time (expansion of 0.17%), limited macroscopic signs of deterioration were detectable (Fig. 6.10A), but the examination of the test specimens under the stereomicroscope revealed the presence of

microcracks and pop-outs (Fig. 6.10B and 6.10C). At 300 days (expansion of 1.6%), i.e. after 210 days of storage at 4°C, it is easy to observe map cracking, pop-outs, rust covering aggregate particles and deformation on the same bar (Fig. 6.10D, 6.10E and 6.10F).

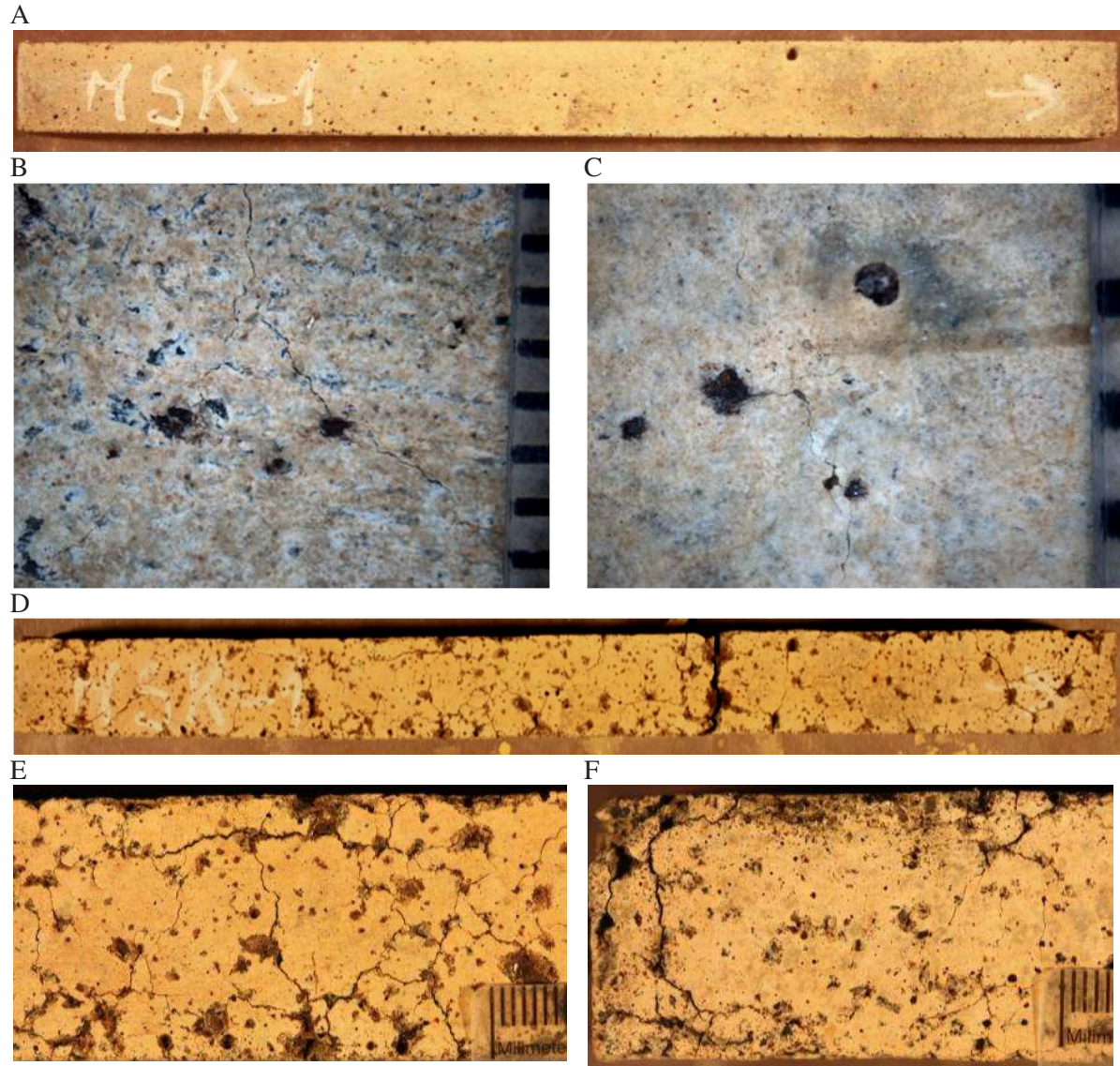


Figure 6.10: A: Mortar bar made with MSK aggregate at 90 days before being transferred to low temperature. B and C: Deterioration details of mortar bars at 90 days. D: the same bar at 300 days (i.e. after 210 days at 4°C). E and F: Deterioration details of mortar bars at 300 days. The scale in Figures 6.10 B, C, E and F is in millimetres.

Some MSK samples that were first stored at 80°C/80%RH for 90 days and then transferred to 4°C/100%RH were left under that condition (4°C/100%RH and no cycling) in the container after the completion of the tests and, as observed in the Figure 6.11A, the deterioration continued leading to the total disintegration of the samples (Fig. 6.11B).



Figure 6.11: A: MSK mortar bars kept at 80°C/80% RH and then transferred at 4°C/80% RH immediately after rupture at 118 days. B: The same mortar bar series left at 4°C/80% RH for 7 months. The M3-5 bar illustrated in A is the one in the middle of the container.

Figure 6.12 illustrates the SBR specimen before the transfer to 4°C (expansion of 1.21%). Samples made with the SBR aggregate show a very rapid rate of expansion early in the experimentation that was responsible for the generation of multiple cracks (Fig. 6.12B and C). Visually, SBR specimens are by far more deteriorated than the MSK samples at the completion of the first 90 days of storage at 80°C and 80% RH, which was expected considering an expansion of 1.31% for SBR (largely due to alkali-silica reaction) and about 0.20% for the bars incorporating the MSK aggregate (Fig. 6.10B and 6.10C).

Figure 6.13 shows the condition of the PKA control samples at the end of the experiment. The low expansion observed for these samples is confirmed by the very good condition of the test specimens during the entire test.

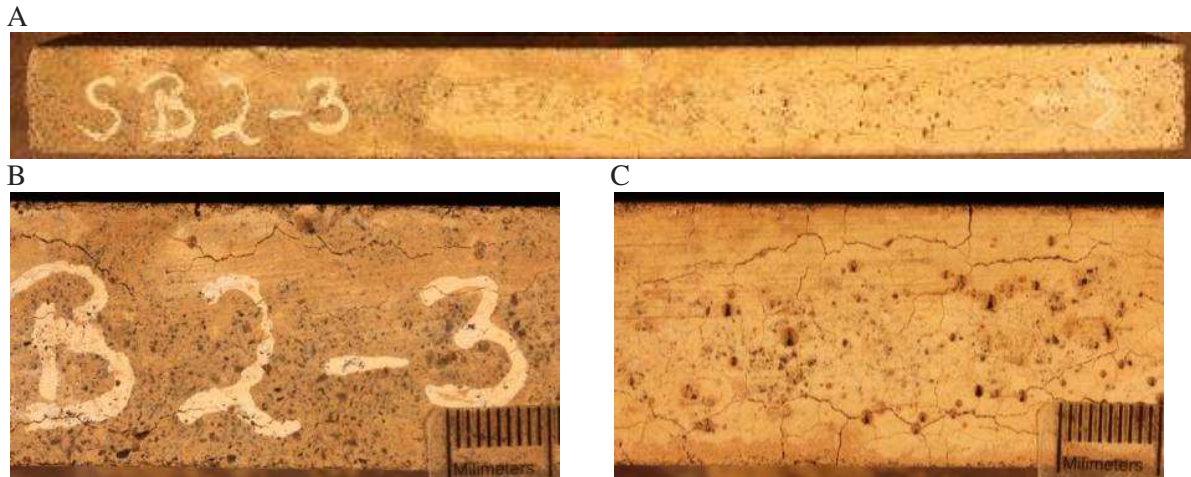


Figure 6.12: A: Mortar bar made with SBR aggregate at 90 days (expansion of 1.31%) before being transferred to low temperature; B and C: Deterioration details of mortar bars at 90 days. The scale in figures B and C is in millimetres.

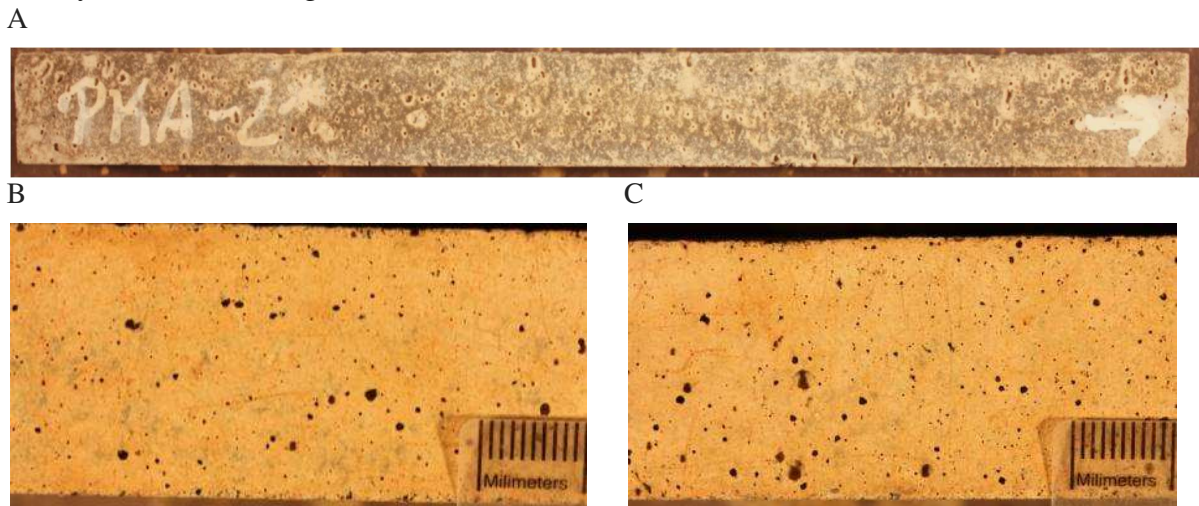


Figure 6.13: Mortar bar made with PKA aggregate at 90 days, showing no signs of deterioration for the entire duration of the test. B and C: Deterioration details of mortar bars at 180 days.

6.3.4.4.2 Microstructural evaluation of the mortar specimens

The nature and composition of secondary products formed during the different phases of the test were analysed by SEM/EDS (gold-palladium alloy (Au-Pd) coating). The analysis of the samples was not an easy task, since the samples were subjected to wetting and drying cycles using bleach as the immersion solution, thus resulting in the precipitation of different kinds of secondary products containing sodium (Na) and chlorine (Cl) on the cracked surfaces of the test specimens. However, despite all the difficulties, some expected secondary products were observed.

Oxidation products were identified in the specimens from the bars incorporating the MSK aggregate, kept at 80°C and 80% RH and subjected to two wetting cycles per week in bleach. Secondary iron oxide, hydroxide or oxyhydroxide (Fig. 6.14 A) phases were observed despite the fact that their precise nature cannot be determined using EDS since hydrogen is not detected. Corresponding EDS spectrum displays main iron (Fe) and oxygen (O) X-ray lines (Fig. 6.14 B). These secondary products are associated to the oxidation of pyrrhotite. Iron sulfates were also observed (Fig. 6.14C). Corresponding EDS spectrum displays sulfur (S), iron (Fe) and oxygen (O) (Fig. 6.14D).

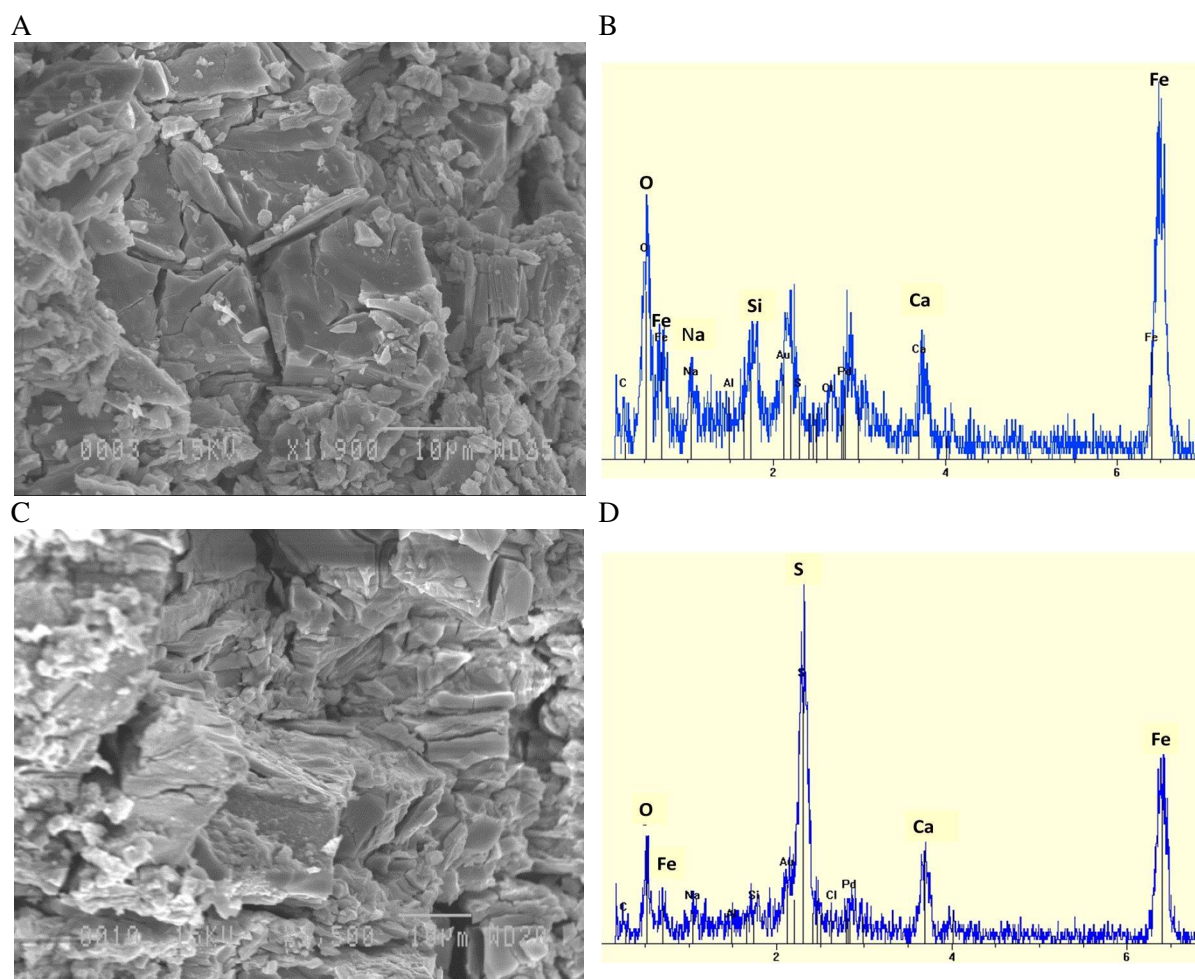


Figure 6.14: Secondary electron images of the different reaction products observed in the mortar bars and corresponding EDS spectra. A, B: iron oxy/hydroxide; C, D: iron sulfate.

The MSK samples that were subjected to 80°C and 80% RH and then transferred to 4°C/80%RH show the presence of ettringite. This secondary product was often found as tiny prismatic crystals, and the elemental composition of the ettringite (Fig. 6.15A) is

observed in the EDS spectrum with calcium (Ca), sulfur (S), aluminum (Al) and oxygen (O) (Fig. 6.15B). The ettringite-thaumasite solid solution was also observed (Fig. 6.15C), the crystals in this case being typically more bulky than the ettringite crystals. The X-ray lines observed were calcium (Ca), sulfur (S), aluminum (Al), silicon (Si) and oxygen (O) (Fig. 6.15D).

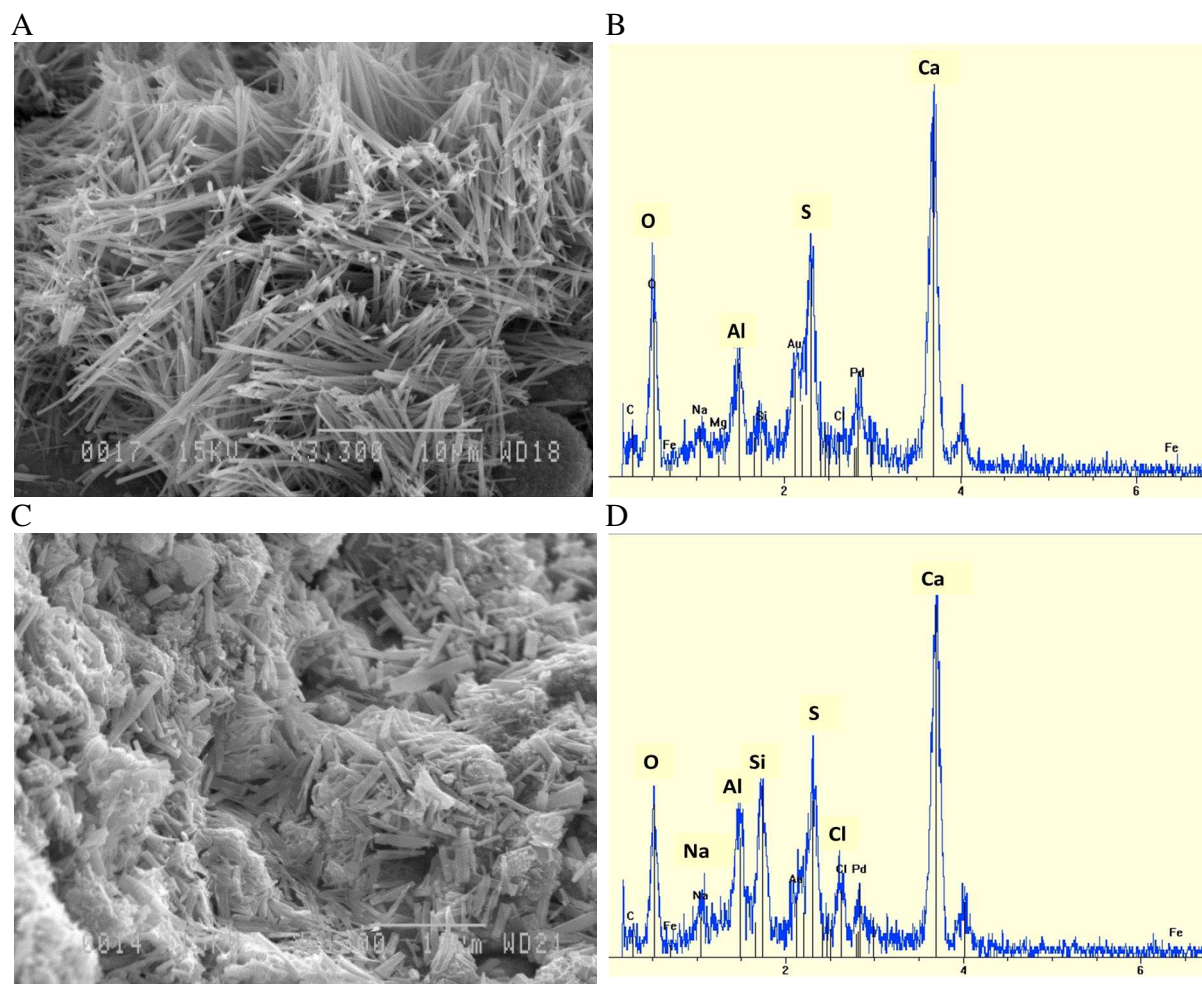


Figure 6. 15: Secondary electron images of the different reaction products observed in the mortar bars and corresponding EDS spectra. A, B: ettringite; C, D: ettringite-thaumasite solid solution; E, F: general composition of a PKA sample.

Besides some secondary products containing sodium (Na) and chlorine (Cl), the control sample PKA did not contain any other kind of secondary products (Fig. 6.16 A and B).

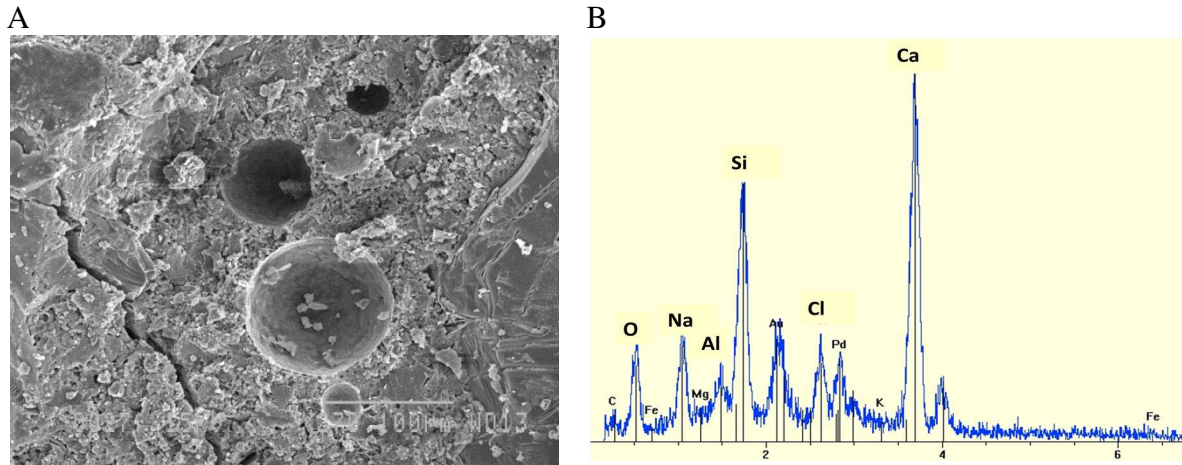


Figure 6.16 Secondary electron images of the general composition of a PKA sample.

6.3.4.5 Description of the proposed accelerated mortar bar test for sulfide-bearing aggregates

6.3.4.5.1 Optimised test parameters

Taking into account the previous results, it seems appropriate to divide the test into the two phases, i.e. a Phase I involving iron sulfide oxidation and sulfuric acid formation resulting into internal sulfate attack, and a Phase II involving the formation of thaumasite.

The Phase 1 consists in exposing mortar bars to high temperature (80°C) and RH (80%) conditions for 90 days with two 3-h immersion periods in a 6% bleach solution per week. This first phase of the test is sufficient to evaluate the oxidation potential of the aggregates. Indeed, the oxidation of sulfide minerals produces a sequence of secondary minerals (iron oxide, hydroxide, oxyhydroxide and iron sulfates), whose volumes are higher than that of the reactants. Obtaining an expansion value greater than about 0.15% at 90 days shows an oxidation potential of the aggregate. However, this limit was established on the basis of limited tests and will need to be validated / adapted through the evaluation of a larger number of aggregate sources. After Phase I, the test can be continued to determine the potential for the formation of thaumasite when a source of carbonate material is available in the system. For this, the samples subjected to Phase I are transferred to low temperature (4°C) at a relative humidity of 100% up to 90 days with two 3-h immersion period in a 6% bleach solution per week. Potential formation of thaumasite is confirmed by the second part of the test with rapid regain of expansion followed by destruction of the samples.

6.3.4.5.2 Test reproducibility

The reproducibility of Phase I of the test was evaluated by testing three sets of mortar bars stored for 90 days at 80°C and 80% RH, with 2 weekly cycles of 3-h in 6% bleach solution. Fig. 6.16 presents the expansion results for the control aggregate PKA, and the sulfide-bearing aggregates MSK and GGP. These results show that the test is reproducible as little change is observed between each series of mortar bars.

The mean expansion values as well as the standard deviation (SD), for each series of bars and the SD and the coefficient of variation (CV) for all the bars made with the same aggregate are given in Table 6.4.

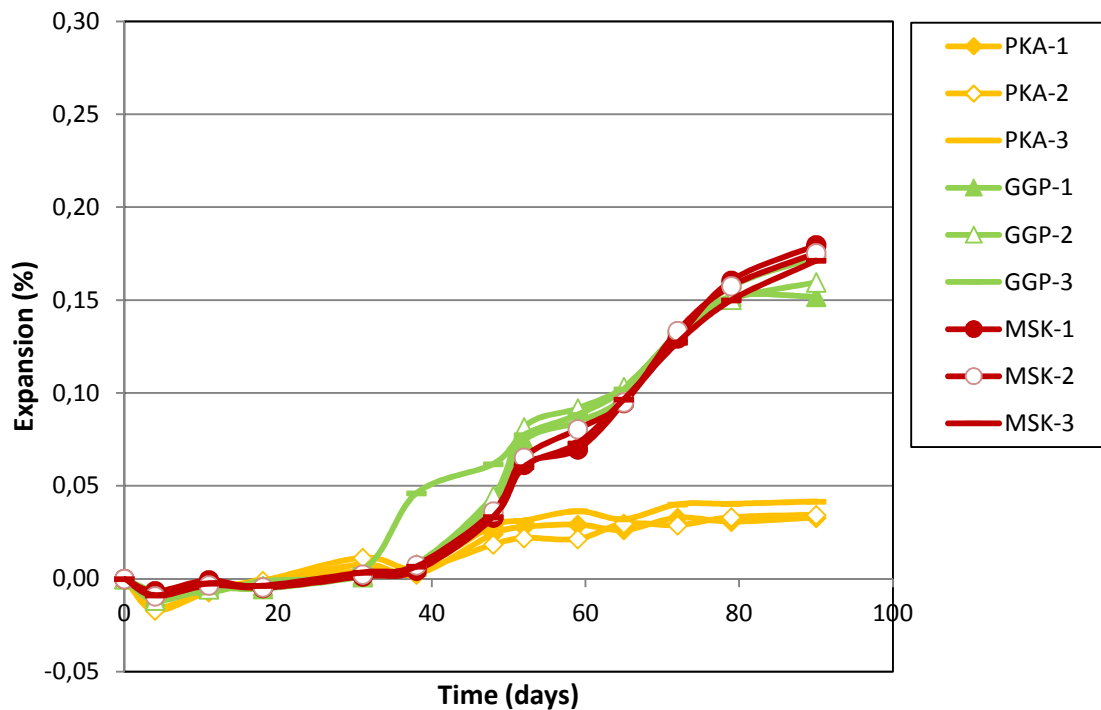


Figure 6. 17: Expansion against time for three sets of mortar bars tested in the same conditions (80°C/80% RH) in order to evaluate the reproducibility at Phase I of the test proposed.

Table 6.4: Statistical values evaluating the reproducibility of the proposed test.

Samples	Mean expansion (%) For the 3 bars of the same set	SD * for the 3 bars of the same set	SD * for the 3 sets made with the same aggregate	CV (%) ** for the 3 sets made with the same aggregate
MSK-1	0.18	0.009	0.0004	0.22
MSK-2	0.18	0.008		
MSK-3	0.17	0.008		
GGP-1	0.17	0.011	0.004	2.58
GGP-2	0.17	0.003		
GGP-3	0.16	0.005		
PKA-1	0.03	0.002	0.006	17.79
PKA-2	0.03	0.01		
PKA-3	0.04	0.004		

*SD: Standard deviation.

**CV: Coefficient of variation

6.3.4.5.3 Technical approaches and precautions

As mentioned before, the conditions of temperature and humidity were maintained either by using environmental chambers or super-saturated salt solutions placed in the bottom of hermetic plastic containers to maintain the relative humidity. In the latter case, the containers are placed in an oven (same type as used for ASR testing) to maintain the temperature. Even if the temperature and humidity controlled chambers are more practical to use, care should be taken because the bleach is an oxidizing agent and its vapors can progressively induce corrosion of the equipment. The same care must be taken to limit the extent of corrosion of the studs used for expansion testing because stainless steel studs are not bleach resistant. In this study, titanium treaded rods were use to manufacture studs and they performed well. Fig. 6.17 compares the expansion obtained for the same mixture tested using both types of set up. Both types of set up provided very similar results; however, considering the high cost of environmental chambers, the use of super-saturated salts for maintaining humidity conditions in a sealed plastic container stored in an oven is a preferred approach, especially considering that many laboratories are used to conduct ASR testing and are thus already using similar equipment to that needed for the sulfide expansion test.

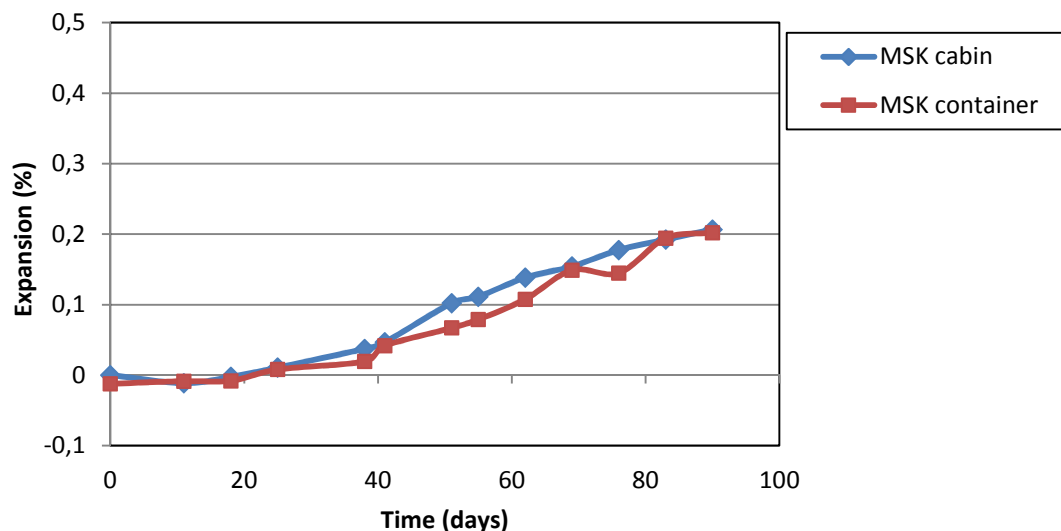


Figure 6. 18: Expansion of mortar bars made with MSK aggregate kept at 80°C/80% RH in a temperature and humidity controlled cabinet or in hermetic container with super-saturated salt solution to maintain humidity conditions kept in a oven.

6.3.5. Conclusions

The rapid and extensive deterioration of concrete structures involving sulfide bearing aggregates has been reported during the past decade in the Trois-Rivières area, Québec (Canada). The extent of the issue triggered the development of an extensive study aiming at developing a performance test/program for evaluating the risk for deleterious oxidation reaction in aggregates prior to their use in concrete. The petrography examination of concrete cores extracted from deteriorated structures, a thorough literature review on cases of concrete deterioration due to the use of sulfide-bearing aggregates, and an extensive laboratory test program, resulted in the development of a two-phase performance test method on mortar bars for sulfide-bearing aggregates.

In the first phase of the test, sets of three mortar bars, 25 by 25 by 285 mm in size, made in accordance with several characteristics used in the accelerated mortar bar test for ASR (ASTM C 1260 or CSA A23.2-25A), are stored for 90 days at 80°C/80% RH, with two 3-h wetting cycles in a 6% bleach solution at 23°C per week. This phase allows for the evaluation of the oxidation potential of the aggregates. Obtaining an expansion value greater than about 0.15% at 90 days shows an oxidation potential of the aggregate. This limit was however established on limited testing and further investigations involving a

larger number of aggregates are required for validation. Phase I can be followed by up to 90 days of storage at 4°C/100% RH, again with two wetting cycles in a 6% bleach solution (Phase II), to determine the potential for thaumasite formation that is confirmed by a rapid regain of expansion followed by destruction of the test specimens during Phase II.

A number of control and sulfide-bearing aggregates were used in this study. For the MSK aggregate, the aggregate that was found to be reactive in the Trois-Rivières structures, the oxidation of sulfide minerals (especially pyrrhotite) present in the aggregate induced mortar bar expansions ranging between 0.18 and 0.21% at the completion of Phase I testing, mainly due to the formation of iron oxides/oxyhydroxides and iron sulfate minerals. Upon transfer to 4°C, the expansion of the MSK mortar specimens first slowed down before showing a large increase in expansion rate until the total disintegration of the bars confirmed by the presence of ettringite and ettringite-thaumasite solid solution in the mortar specimens. The petrographic analysis of the MSK aggregate revealed the presence of siderite (FeCO_3) surrounding the iron sulfide minerals. It is believed that the siderite is the source of the carbonate material necessary for the formation of the ettringite-thaumasite solid solution, causing extensive excessive expansion and eventual disintegration of the mortar bar during the 4°C storage.

The behaviour of the mortar specimens incorporating the GGP aggregate was similar to that of the MSK aggregate during Phase I testing, with expansions ranging from 0.17 to 19%. However, their behaviour differed significantly afterwards since the GGP samples did not show any significant expansion upon transfer to Phase II conditions; this is related to the absence of carbonate material in the GGP aggregate.

The SBR, SW and SPH are sulfide-bearing and alkali-silica reactive aggregates. Those three aggregates showed a rapid onset of expansion that reached levels ranging from 0.58 % (SW) to $\approx 1.31\%$ (SBR) upon 90 days of testing (Phase I), expansion way above that obtained with the MSK aggregate. The observed expansions are a combination of alkali-silica reaction and the iron sulfides oxidation. Interestingly, none of the above three aggregates generated significant expansion upon transfers to 4°C, thus strongly suggesting that the expansion observed in Phase I was mainly related to ASR.

The mortar bars incorporating two control aggregates without sulfide mineral, the PKA anorthosite and the HPL limestone, did not show any expansion nor showed any signs of deterioration during both phases of the testing program.

6.4 Acknowledgements

The authors wish to acknowledge the Natural Sciences and Engineering Research Council of Canada (NSERC) for their collaborative research and development grant and all partners (ABQ, ACC, ACRGTQ, APCHQ, Garantie qualité habitation, ACQ, Inspec-sol inc., LVM, RBQ, Exp. Inc., SHQ, Ville de Québec, Ville de Montréal, Hydro-Québec, MTQ, Qualitas). Appreciation is also extended to Benoit Durand from IREQ for his implication and for having provided the PKA aggregate. A. Rodrigues benefits from a PhD scholarship financed by FCT-Fundação para a Ciência e Tecnologia, Portugal, Ref.: SFRH/BD/71203/2010.

6.5 References

- [1] A. Rodrigues, J. Duchesne, B. Fournier, B. Durand, P. Rivard, M. Shehata, Mineralogical and chemical assessment of concrete damaged by the oxidation of sulfide-bearing aggregates: importance of thaumasite formation on reaction mechanisms, *Cem. Concr. Res.* 42 (2012) 1336–1347.
- [2] A. Rodrigues, J. Duchesne, B. Fournier, Microscopic analysis of the iron sulfide oxidation products used in concrete aggregates, 34th International Conference on Cement Microscopy, 2012 (Halle-Saale, Germany).
- [3] A. Rodrigues, J. Duchesne, B. Fournier, Petrographic characterization of the deterioration products of a concrete containing sulfide bearing aggregates; a particular case of internal sulfate attack, 35th International Conference on Cement Microscopy, 2013 (Chicago, USA,).
- [4] A. Rodrigues, J. Duchesne, B. Fournier, Damage evaluation of two different concrete mix designs containing sulfide-bearing aggregates, 36th International Conference on Cement Microscopy, 2014 (Milan, Italy).

- [5] J. Bérard, R. Roux, M. Durand, Performance of concrete containing a variety of black shale, *Can. J. Civ. Eng.* 2 (1975) 58–65.
- [6] R.M. Quigley, R.W. Vogan, Black shale heaving at Ottawa, Canada, *Can. Geotech. J.* 7 (1970) 106–115.
- [7] J.S. Chinchón, C. Ayora, A. Aguado, F. Guirado, Influence of weathering of iron sulfides contained in aggregates on concrete durability, *Cem. Concr. Res.* 25 (1995) 1264–1272.
- [8] I. Casanova, L. Agulló, A. Aguado, Aggregate expansivity due to sulfide oxidation I. Reaction system and rate model, *Cem. Concr. Res.* 26 (1996) 993–998.
- [9] A. Lugg, D. Probert, “Mundic”-type problems: a building material catastrophe, *Constr. Build. Mater.* 10 (1996) 467–474.
- [10] C. Ayora, S. Chinchón, A. Aguado, F. Guirado, Weathering of iron sulfides and concrete alteration: thermodynamic model and observation in dams from central Pyrenees, Spain *Cem. Concr. Res.* 28 (1998) 1223–1235.
- [11] T. Schmidt, A. Leemann, E. Gallucci, K. Scrivener, Physical and microstructural aspects of iron sulfide degradation in concrete, *Cem. Concr. Res.* 41 (2011) 263–269.
- [12] J. Moum, I.Th. Rosenqvist, Sulfate attack on concrete in the Oslo region, *J. Am. Concr. Inst.* 56 (1959) 257–264.
- [13] A. Tagnit-Hamou, M. Saric-Coric, P. Rivard, Internal deterioration of concrete by the oxidation of pyrrhotitic aggregates, *Cem. Concr. Res.* 35 (2005) 99–107.
- [14] A. Shayan, Deterioration of a concrete surface due to the oxidation of pyrite contained in pyritic aggregates, *Cem. Concr. Res.* 18 (1988) 723–730.
- [15] P. Hagelia, R. Sibbick, N. Crammond, C. Larsen, Thaumasite and secondary calcite in some Norwegian concretes, *Cem. Concr. Compos.* 25 (2013) 1131–1140.

- [16] E. Vasquez, T. Toral, Influence des sulfures de fer des granulats du Maresme (Barcelone) sur les bétons, *Bull. Int. Assoc. Eng. Geol.* 30 (1984) 297–300.
- [17] R.E. Oberholster, J.E. krüger, Investigation of alkali-reactive, sulfide-bearing and by-products aggregates, *Bull. Int. Assoc. Eng. Geol.* 3 (1984) 273–277.
- [18] R.E. Oberholster, P. Du Toit, J.L. Pretonius, Deterioration of concrete containing a carbonaceous sulfide-bearing aggregate, in: *Int. Cement Microscopy Association (ICMA) (Ed.)Sixth Int. Conf. on cement microscopy, 1984 (Albuquerque, New Mexico, USA)*.
- [19] H.F. Steger, Oxidation of sulfide minerals VII Effect, of Temperature and Relative Humidity on the Oxidation of Pyrrhotite, *Chem. Geol.* 35 (1982) 281–295.
- [20] S.W. Knipe, J.R. Mycroft, A.R. Pratt, H.W. Nesbitt, G.M. Bancroft, X-ray photoelectron spectroscopic study of water adsorption on iron sulfide minerals, *Geochim. Cosmochim. Acta* 59 (1995) 1075–1090.
- [21] M.Mbonimpa, M. Aubertin, M. Aachib, B. Bussière, Diffusion and consumption of the oxygen in unsaturated cover materials, *Can. Geotech. J.* 40 (2003) 916–932.
- [22] B. Bussière, personal communication.
- [23] N. Belzile, Y. Chen, M. Cai, Y. Li, A review on pyrrhotite oxidation, *J. Geochem. Explor.* 84 (2004) 65–76.
- [24] L. Divet, J.P. Davy, Étude des risques d'oxydation de la pyrite dans le milieu basique du béton, *Bull. Lab. Ponts Chaussées* 204 (1996) 97–107.
- [25] M. Janzen, Pyrrhotite reaction kinetics reaction rates for oxidation by oxygen, ferric iron and for nonoxidative solution, *Geochim. Cosmochim.* 64 (2000) 1511–1522.
- [26] P.E. Grattan-Bellew, W.J. Eden, Concrete deterioration and floor heave due to biogeochemical weathering of underlying shale, *Can. Geotech. J.* 12 (1975) 372–378.

- [27] The UK Government Thaumasite Expert Group, One-year review, Report of the Thaumasite expert group, Department of the Environment, transport and regions, London, 2000.
- [28] The UK Government Thaumasite Expert Group, Review after three years experience, Report of the Thaumasite expert group, Department of the Environment, transport and regions, London, 2002.
- [29] M.D.A. Thomas, C.A. Rogers, R.F. Bleszynski, Occurrences of thaumasite in laboratory and field concrete, *Cem. Concr. Compos.* 25 (2003) 1045–1050.
- [30] G. Collett, N.J. Crammond, R.N. Swamy, J.H. Sharp, The role of carbon dioxide in the formation of thaumasite, *Cem. Concr. Res.* 34 (2004) 1599–1612.
- [31] The UK Government Thaumasite Expert Group, The thaumasite form of sulfate attack: risks, diagnosis, remedial works and guidance on new construction, Report of the Thaumasite Expert Group, Department of the Environment, transport and regions, London, 1999.
- [32] N.J. Crammond, The thaumasite form of sulfate attack in the UK, *Cem. Concr. Compos.* 25 (2003) 809–818.
- [33] J. Newman, B. Choo, *Cements in Advanced Concrete Technology-Constituent Materials*, Elsevier, Great Britain, 2003. (280 pp.).
- [34] J. Aguilera, M.T. Blanco Varela, T. Vásquez, Procedure of synthesis of thaumasite, *Cem. Concr. Res.* 31 (2001) 1163–1168.
- [35] R. Day, B. Middendorf, Sulfate attack and microstructural change on fly-ash mortars made with ordinary- and limestone-cements, *Proceedings of the 33rd International Conference on Cement Microscopy* (2011) San Francisco, California, USA2011.
- [36] T. Hagerman, H.R. Roosaar, Kismineralens skadeinverkan på betong, *Betonw.* 2 (1955) 151–161.

- [37] J. Chinchón, A. Lopez, J. Soriano, E. Vazquez, La Cantera de Mont Palau II: Formacion de Compuestos Expansivos Generados en la Reaccion Arido-Hormingon, Ing. Civil 72 (1990) 109–113.
- [38] RICS, The “Mundic” Problem Supplement to Second Edition-Stage 3 Expansion Testing, The Royal Institution of Chartered Surveyors, UK, 2005. (59 pp.).
- [39] M.J. Gomides, Investigaç o de Agregados contendo Sulfetos e seus efeitos sobre a durabilidade do concreto, Universidade Federal do Rio Grande do Sul, Brazil, 2009. (PhD. Thesis).
- [40] J.S. Chinch n, A. Lopez, X. Querol, C. Ayora, La Cantera deMont Palau I: influ ncia de la mineralog a de los  ridos en la durabilidad del horming n, Ing. Civil 72 (1990) 79–88.
- [41] Q. Zou, F.P. Glasser, Termal stability and the decomposition mechanisms of ettringite at b120  C, Cem. Concr. Res. 31 (2001) 1333–1339.
- [42] ASTM C1260–14 Standard Test Method for Potential Alkali Reactivity of Aggregates (Mortar-Bar Method), 2014.
- [43] CSA A23.2-25 A D tection des granulats susceptible de r action alcalis-silice par l'expansion acc l r e de barres de mortier.
- [44] F.E.M. O'Brien, The control of humidity by saturated salt solutions, J. Sci. Instrum. 25 (1948) 73–76.
- [45] ASTM C1293 Standard Test Method for Determination of Length Change of Concrete Due to Alkali-Silica Reaction, 2008

Chapter 7

Protocol evaluation

7.1 Introduction

This paper was submitted to the ACI Material Journal in July 2015 and it is presently under revision.

7.2 Résumé

Plusieurs cas de détérioration du béton incorporant des granulats contenant des sulfures de fer ont été rapportés au cours des années. Cependant, il n'y a aucune ligne directrice spécifique disponible pour prendre une décision précise sur le potentiel délétère des granulats contenant des sulfures de fer. Ce document vise à fournir un protocole d'évaluation capable de prédire les effets délétères potentiels des granulats contenant des sulfures de fer lorsqu'ils sont utilisés dans le béton. Les conclusions de ce document sont basées sur des tests développés au cours des dernières années dans le cadre d'un vaste projet de recherche. Le protocole est divisé en 3 grandes phases: (1) mesure de la teneur en soufre total, (2) évaluation de la consommation d'oxygène, et (3) évaluation de l'expansion par un test accéléré sur barres de mortier. Des limites provisoires sont proposées pour chacune des phases du protocole. Ces limites devront être validées en évaluant un plus large éventail de granulats.

7.3 Scientific publication no. 4

Evaluation protocol for concrete aggregates containing iron sulfide minerals

Andreia Rodrigues, Josée Duchesne, Benoit Fournier, Benoit Durand, Medhat Shehata, and Patrice Rivard

Abstract

Several cases of concrete deterioration involving sulfide-bearing aggregates have been reported over the years. However, no specific guidelines are currently available to enable making a precise decision on the deleterious potential of aggregates containing iron sulfide minerals. The aim of this paper is to provide an innovative assessment protocol to evaluate the potential deleterious effects of iron sulfide bearing aggregates prior to their use in concrete. The findings of this paper are based on tests developed within the past few years as part of a major research project. The protocol is divided into 3 major phases: (1) total sulfur content measurement, (2) oxygen consumption evaluation, and (3) an accelerated mortar bar expansion test. Tentative limits are proposed for each phase of the protocol, which still need to be validated through the testing of a wider range of aggregates.

Keywords: Evaluation protocol, deterioration, concrete, testing methods, iron sulfides oxidation, internal sulfate attack.

7.3.1 Introduction

7.3.1.1 General description of the problem

During the last few years, rapid and extensive deterioration of concrete slabs and foundations of residential and commercial buildings have occurred in the Trois-Rivières region (Quebec, Canada) associated with the oxidation of a sulfide-bearing coarse aggregate used for concrete manufacturing. Most of the structures suffering from this problem indeed started to exhibit signs of deterioration only three to five years after construction, mainly consisting of map-cracking, pop-outs and white rims surrounding the aggregate particles, and yellowish discoloration near the cracks (Fig. 7.1).

A



B



C



D



Figure 7.1: Typical signs of deterioration observed in residential buildings containing iron sulfide-bearing aggregates in the Trois-Rivières area. A and B: Concrete foundations showing map-cracking. C: Pop-outs showing the presence of oxidized and rusted aggregate particles, as well as whitish/yellowish secondary reaction products. D: Cracks filled with caulking material to prevent moisture ingress.

In the most advanced cases of deterioration, the concrete was so friable that it could almost be removed by hand. Based on the provincial (Quebec) Guarantee Plan for New Residential Buildings¹, and for cases of excessive deterioration, the affected concrete foundation/element had to be replaced (Fig. 7.2).

A



B



C



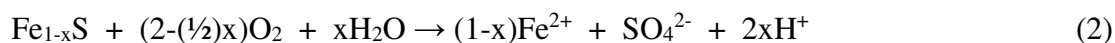
D



Figure 7.2: Typical replacement process of residential concrete foundations in the Trois-Rivières area. A: Stone and brick facing removed. B: Demolition of the concrete foundation. C: House lifted. D: Pouring of new concrete foundation.

Rodrigues et al², in addition to numerous reports from experts involved in the legal case that followed the identification of this problem, related the deterioration to the presence of iron sulfide minerals in the coarse aggregate, a dark-colored coarse-grained and dense hypersthene's gabbro composed mostly of anorthite ($\text{CaAl}_2\text{Si}_2\text{O}_8$), with lesser amounts of biotite ($\text{K}(\text{Mg},\text{Fe})_3\text{AlSi}_3\text{O}_{10}(\text{F},\text{OH})_2$) and pyroxene ($\text{XY}(\text{Si},\text{Al})_2\text{O}_6$). This aggregate also contains various proportions of sulfide minerals, including pyrite (Fe_2S), pyrrhotite (Fe_{1-x}S), pentlandite ($(\text{Fe},\text{Ni})_9\text{S}_8$) and chalcopyrite (CuFeS_2). A rim of siderite (FeCO_3), an iron carbonate, was often observed surrounding those iron sulfides. The pyrrhotite was most of the times heavily oxidized².

Iron sulfides, in presence of oxygen and water, oxidize to form iron oxyhydroxides. Equations (1) and (2) show the reaction for pyrite and pyrrhotite oxidation, respectively^{3, 4}.



The “x” in the equation (2) ranges from 0.0 to 0.125, depending on the pyrrhotite crystallography⁵.

If the oxidation reaction occurs in hardened concrete, the sulfuric acid reacts with the portlandite (Ca(OH)_2), which is a product of hydration of portland cement, and *gypsum* is formed according to equation (3).



The gypsum then reacts with the aluminate phases in portland cement concrete, thus leading to the formation of potentially expansive secondary *ettringite* (equation 4)⁶.



Many of the mineral forms identified above and resulting from iron sulfide oxidation and internal sulfate attack occupy relatively larger molar volumes than their precursors, thus causing deleterious expansion and cracking of the affected concrete⁷. Rodrigues et al^{2, 8, 9} described the microscopic features of deterioration, including the various types of reaction products mentioned above, from the examination of concrete cores extracted from a number of house foundations. Interestingly, the authors also recognized the presence of thaumasite, $\text{Ca}_3\text{Si(OH)}_6(\text{CO}_3)(\text{SO}_4) \cdot 12\text{H}_2\text{O}$, which is likely to be the cause for the extensive degradation of concrete in the advanced stages of deterioration.

7.3.1.2 The standardization state of aggregates containing iron sulfide minerals

Canadian standards highlight, in the following terms, the risk of using aggregates incorporating iron sulfides in concrete (Clause 4.2.3.6.2, CSA A23.2/A23.2-2014)¹⁰:

Aggregates that produce excessive expansion in concrete through reaction other than alkali reactivity shall not be used for concrete unless preventive measures acceptable to the owner are applied.

Note: *Although rare, significant expansions can occur due to reasons other than alkali-aggregate reaction. Such expansions might be due to the following:*

(a) the presence of sulphides, such as pyrite, pyrrhotite, and marcasite, in the aggregate that might oxidize and hydrate with volume increase or the release of sulphate that produces sulphate attack upon the cement paste, or both;

Back in 1983, the French standard NF P18-301¹¹ limited the total sulfur content in concrete aggregates to 1% as SO₃ (0.4% as S). This threshold was further increased/relaxed in the context of European standardization NF EN 12 620 (2003)¹², which specified that the total sulfur content (S) of the aggregates and fillers, must not exceed:

- 1% S by mass for aggregates other than air-cooled blast furnace slag;
- 2% S by mass of S for air-cooled blast furnace slag.

Note: Special precautions need to be taken when pyrrhotite, an unstable form of iron sulfide (Fe_(1-x)S), is present in the aggregate. If the presence of this mineral is proven, a maximum total sulfur content of 0.1% (as S) shall apply.

ASTM C 294-12 (Clause 14)¹³ mentions that: *Marcasite and certain forms of pyrite and pyrrhotite are reactive in mortar and concrete, producing a brown stain accompanied by volume increase that has been reported as one source of pop outs in concrete;* however, ASTM C33/C33M-13¹⁴ does not provide any recommendations/warning regarding the use of sulfide-bearing aggregates in concrete.

Despite the fact that the potential problem related to the use of sulfide-bearing aggregates in concrete is highlighted in a number of concrete Standards worldwide, no precise/detailed guidelines/methods have been proposed to evaluate the potential reactivity of such aggregates other than the application of the chemical thresholds mentioned above. While these tools could be used for basic screening of concrete aggregates, they need to be

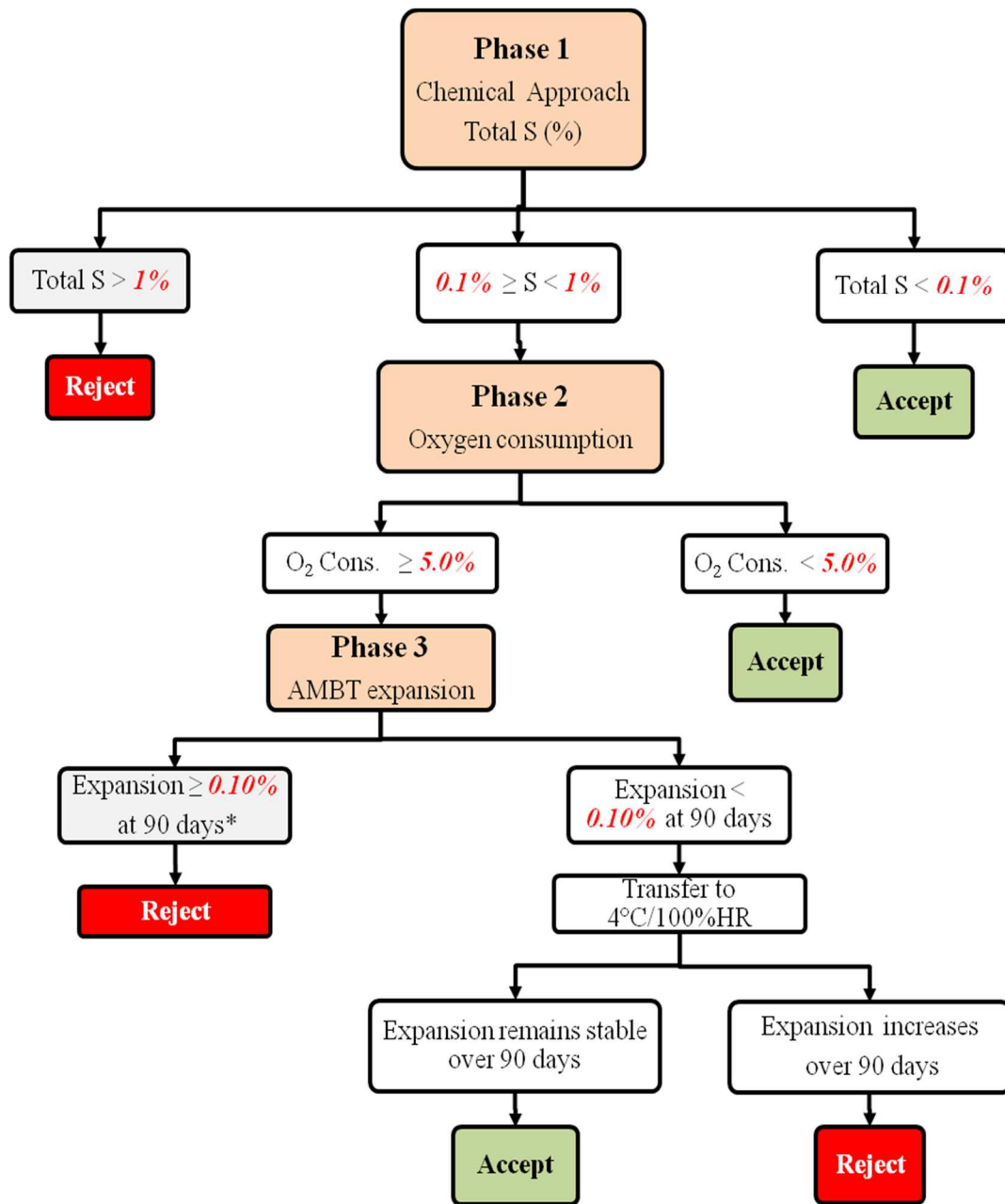
supplemented by other test methods when the total sulfur content is $> 0.10\%$. These tests would not allow identifying the type of sulfide mineral(s) present in the aggregate under test. Also, the precise identification of small quantities of sulfide minerals could represent a significant challenge for petrographers, while being almost impossible by commonly-used X-Ray diffraction analysis. Also, since not all forms of pyrrhotite are equally “reactive”^{3,4}, other tools are needed for the routine evaluation of aggregates containing iron sulfide minerals.

7.3.2 Research significance

An extensive investigation was carried out over the past four years by researchers from four Canadian organizations, aiming at developing an evaluation protocol for iron sulfide-bearing aggregates. The work started with a thorough literature review that allowed identifying the various parameters involved in this deleterious reaction, as well as the reasons for the limited success in developing a reliable approach for identifying this deleterious reaction. The above knowledge was then used to develop a testing program, using a wide range of sulfide-bearing and non-sulfide bearing concrete aggregates.

7.3.3 Experimental investigation

The laboratory work resulted in the development of a three-phase testing protocol illustrated in Fig. 7.3. The approach includes a measurement of the total sulfur content in percentage by mass (S_T) (Phase 1), oxygen consumption by the aggregate tested in a closed space (Phase 2), and finally an accelerated mortar bar expansion test (Phase 3). Details on the development of these various tests are given in the following sections, while a discussion on the combined use of these tools is given in section ‘Protocol for the performance evaluation of sulfide-bearing aggregates’.



* The cause of excessive expansion, i.e. ASR and/or oxidation of sulfide minerals, should be addressed before rejecting the aggregate.

Figure 7.3: Proposed protocol for determining the potential reactivity of iron sulfide bearing aggregates. The numbers in red represent limit values that still need to be validated through the testing of a wider range of aggregate materials.

7.3.4 Materials

In addition to the aggregate responsible for the concrete deterioration in the Trois-Rivières area (MSK), six sulfide-bearing aggregates and four aggregates with no or only traces of iron sulfides (control) were selected for this study (Table 7.1). The B&B aggregate was obtained from a quarry located about 500 m [546.8 yd] away from the MSK quarry. They both show the same mineralogy, but the B&B aggregate was produced from hand-picked rock samples because of their visually high iron-sulfide content. GGP contains similar iron sulfide minerals to those identified in MSK, but it shows only traces of carbonate material. This aggregate is considered as non-potentially alkali silica reactive according to the Accelerated Mortar Bar Test (AMBT) (ASTM C1260)¹⁵. However, Standard Practice CSA A23.2-27A¹⁶ mentions that some granites, gneisses and granodiorites produced expansion lower than the 0.15% limit criterion at 14 days, but were found to cause deterioration of concrete in service. SBR is a fine-grained contact metamorphic rock (hornfels) that was selected for its sulfide-mineral content and its potential alkali-silica reactivity. SW is a mica schist that was reported to have caused the deterioration of a hydraulic dam due to the presence of sulfide minerals; this aggregate is also alkali-silica reactive. SPH is an iron-sulfide bearing metamorphic rock (phyllite) that was the source of concrete deterioration in public buildings, houses, overpasses and dams; it is also an alkali-silica reactive aggregate. SDBR is a mine waste material, originally a gabbro, from the Northern Ontario region. DLS, HPL, PKA, and Spratt are control aggregates with no or only traces of sulfide minerals: three limestones (including the well-known Spratt reactive aggregate) and an anorthosite, (Table 7.1).

In addition, a specific study was carried out for the determination of the S_T of more than 50 aggregates from different geological regions and representing a variety of rock types. This study aimed at evaluating the reproducibility and repeatability of the chemical test adopted in Phase I of the testing protocol.

Table 7.1: Aggregates used in the different tests and their respective mineralogy

Aggregate		Rock type	Mineralogy		Carbonate minerals	ASR* reactivity
			Main mineral constituents	Iron sulfide minerals		
Sulfide-bearing aggregates	MSK	Norite or Hypersthene Gabbro	Plagioclase Biotite Pyroxenes Quartz	Pyrrhotite Pyrite Chalcopyrite Pentlandite	Siderite (FeCO ₃) Calcite (CaCO ₃)	No
	B&B	Gabbro	Pyroxenes Plagioclase Quartz Biotite K Feldspars	Pyrrhotite Pyrite Chalcopyrite	Siderite (FeCO ₃) Calcite (CaCO ₃)	No
	GGP	Granitic Gneiss	Quartz Hornblende Pyroxenes Plagioclase	Pyrrhotite Pyrite Chalcopyrite	Traces	No**
	SBR	Hornfels	Feldspars Quartz Clays Organic matter	Pyrrhotite Pyrite Chalcopyrite Sphalerite	No	Yes
	SW	Mica Schist	Quartz Feldspars White mica Amphibole	Pyrrhotite Pyrite Chalcopyrite	No	Yes
	SPH	Phyllite	Quartz Feldspar White mica Chlorite	Pyrrhotite Pyrite Chalcopyrite	Calcite in small amounts	Yes
	SDBR	Gabbro	Plagioclase Pyroxenes Biotite Epidote Apatite	Pyrrhotite Pyrite Chalcopyrite Pentlandite	No	No
Control aggregates	DLS	Limestone	Carbonates	Pyrite (traces)	Main mineral	No
	PKA	Anorthosite	Plagioclase Hornblende Biotite	–	No	No
	HPL	Limestone	Carbonates	–	Main mineral	No
	Spratt	Limestone	Carbonates	–	Main mineral	Yes

* Potentially alkali silica reactive based on the AMBT (ASTM C1260).

** Contains microcrystalline quartz – may be alkali reactive

7.3.5 Analytical procedure

7.3.5.1 Chemical approach: Total Sulfur content (Phase 1 – Fig. 7.3)

The chemical approach consists in the measurement of the S_T (% by mass) in the aggregate and can serve to detect the presence (or not) of iron sulfide minerals. The proportion of the different iron sulfide minerals present in an aggregate material can theoretically be calculated from the full chemical analysis (including S_T) and the detailed petrographic/mineralogical characterization of the aggregate sample. The proportions of the sulfide minerals are then calculated based on the stoichiometry of the minerals identified. This calculation is somehow theoretical since the majority of minerals are not 100% pure and sometimes, depending on their concentration, cannot be detected.

Even if this technique is not meant to identify the type of sulfide mineral present, the results can be used as a screening test. However, the potential presence of sulfate minerals (e.g. gypsum) in some aggregate materials could significantly influence the results of the S_T determination through this chemical approach.

A 0.3 to 1 g sample is required for the S_T analysis. Since this quantity is very small, special care is needed to obtain a representative sub-sample of the aggregate under test. Based on the existing standard procedures for the chemical analysis of concrete aggregates described in CSA A23.2 26A¹⁷ and in the Annex A of BNQ 2560-500/2003¹⁸, a detailed method for sample preparation was developed (Fig. 4). A representative 4 kg sample of the aggregate, with particles ranging from 5 to 20 mm [0.20 to 0.78 in.] in size, is first obtained following a suitable procedure. This sample is then split into two representative sub-samples of 2 kg. One of those two sub-samples is then progressively crushed, split and pulverized, as explained in Fig.4, until all the particles pass the 80 μm [0.003 in.] sieve. This sub-sample is finally split in 4 sub-samples that will be used for the S_T determination in three different laboratories.

A carbon/sulfur analyser, Model Eltra C-S 800, was used for the analysis performed at Lab1. Laboratories no. 2 and 3 used a LECO, which measures the S_T content using the same principle as the Eltra C-S 800. In the carbon/sulfur analyser induction furnace, the sample is melted in a pure oxygen atmosphere, causing sulfur to react to form sulfur dioxide (SO_2). The SO_2 content is determined by infrared absorption, from which the S_T is

calculated. Each aggregate sample was analysed in three laboratories (Labs 1 to 3) for reproducibility evaluation. In the case of the samples tested in Lab 1, at least two sub-samples were analysed for repeatability testing. Some samples were also tested in duplicates blindly, and standard samples were also analysed.

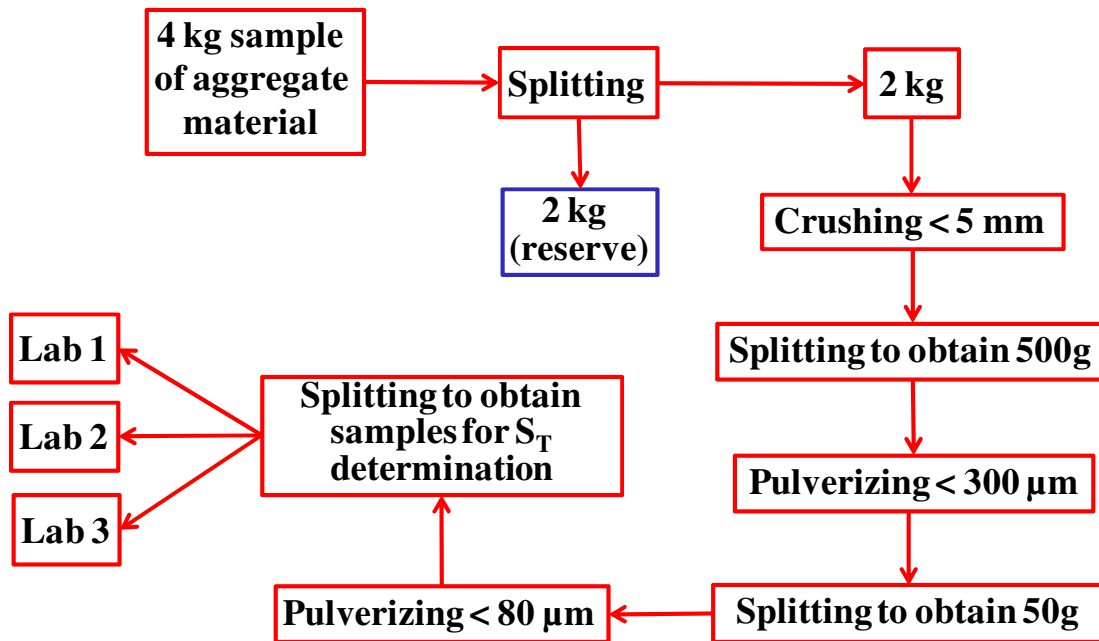


Figure 7.4: Procedures for samples preparation schema for the total sulfur (S_T) determination.

7.3.5.2 Oxygen consumption test (Phase 2 – Fig.7. 3)

Elberling and co-workers in the mid 1990's proposed an oxygen consumption test to evaluate the oxidation potential of sulfide-bearing mine tailings in the context of Acid Rock Drainage (ARD)¹⁹. The technique measures the oxygen consumption rate at the top of a closed cylinder containing a layer of compacted ground material to determine its oxidation potential. Rodrigues et al²⁰ further adapted the method to evaluate the oxidation potential of sulfide-bearing concrete aggregates.

The tests were conducted in sealed Plexiglas columns of 200 mm [7.87 in.] in height and 142 mm [5.59 in.] in internal diameter. The compacted ground material lies in the bottom part of the container, while a galvanic-cell oxygen sensor (able to measure 0 to 100% oxygen) is inserted through the Plexiglas cover at the top of the column and connected to a data-logger. Different parameters were evaluated to find the optimum testing

conditions, such as the particle size (mortar bar size fractions (150 μm to 5 mm [0.006 in. to 0.20 in.]), < 1.18 mm [0.046 in.], or <150 μm [0.006 in.]) of the aggregate, the ground material thickness (2.5, 5 and 10 cm [0.98, 1.97 and 3.94 in.]) and its saturation degree (40% and 60%), and headspace for oxygen consumption measurements (2.5, 5, 10, 15 and 17.5 cm [0.98, 1.97, 3.94, 5.91 and 6.89 in.]). All the measurements were performed at atmospheric pressure, room temperature (22°C [71.6°F]), and using a 3.5-hour test duration (30 minutes for the probes stabilization plus 3 hours of effective oxygen consumption measurements). Two sulfide-bearing aggregates (MSK, and GGP), three sulfide-bearing and alkali-silica reactive aggregates (SBR, SW and SPH), and three control aggregates with no or only traces of sulfides (PKA, HPL and DLS) were selected for this study (Table 7.1).

7.3.5.3 Mortar bar expansion test (Phase 3 – Fig. 7.3)

Mortar bar expansion tests have been used, for decades, for evaluating the potential alkali-silica reactivity of concrete aggregates. When mortar bars are manufactured, coarse aggregates are reduced to sand sizes (5 mm to 150 μm [0.20 to 0.006 in.]). A higher specific surface means that more iron sulfide surfaces can be exposed to oxygen and moisture, thus potentially accelerating the oxidation reaction and the resulting expansion.

Mortar bars, 25 x 25 x 285 mm [0.98 x 0.98 x 11.22 in.] in size, were manufactured, using a General Use high-alkali (0.95% $\text{Na}_2\text{O}_{\text{eq}}$) portland cement, a cement-to-aggregate ratio of 1:2.75, with the proportions of the various aggregate size fractions similar to that used in the accelerated mortar bar test for ASR (ASTM C 1260)¹⁵. A w/c of 0.65 was selected to simulate the characteristics of concrete used for housing foundations in the Trois-Rivières area. The same set of aggregates selected for the development of the oxygen consumption test was used for this part of the investigation (Table 7.1).

The mortar bars were subjected to different storage conditions, including various temperatures (4, 23, 38, 60 and 80°C [39.2, 73.4, 100.4, 140 and 176°F]), relative humidity (60, 80 and 100%), immersion (or not) in an oxidizing agent (sodium hypochlorite solution (bleach 6%) and hydrogen peroxide (3%) solutions), wetting and drying cycles (0, 1 or 2 cycles/week). The low temperature condition was introduced in the test program since thaumasite formation is accelerated at lower temperatures (about 4°C [39.2°F]).

The mortar bars expansion was monitored regularly over the testing period that reached up to 6 months, depending on the storage conditions investigated. Details on the experimental program are given elsewhere²¹.

7.3.6 Experimental results and discussion

The results obtained for the chemical analyses, as well as the oxygen consumption and the accelerated mortar bar tests, are summarized hereafter. The interactions between the above tests are further discussed in section ‘Protocol for the performance evaluation of sulfide-bearing aggregates’.

7.3.6.1 Total Sulfur content

The results of duplicate S_T measurements carried out in Lab 1, for a first set of 21 concrete aggregates, are given in Table 7.2. These results are presented in increasing order of S_T values, ranging from 0.04 to 5.53%, by mass. The measurements obtained from two subsamples produced following the procedure described in Fig. 7.4 show a very good repeatability, with the large majority of the S_T values being within $\pm 0.01\%$ of the average. The variability may seem somewhat higher for S_T values $< 0.10\%$, as they are closer to the detection limit of the apparatus.

Table 7.3 presents the S_T results obtained on a second set of 43 aggregates representing a variety of rock types / lithologies. The materials preparation was performed in Lab 1, which provided subsamples for S_T determination in the two other laboratories mentioned before. The results in Table 7.3 generally show a good multi-laboratory reproducibility, with coefficients of variation (CV) generally less than 10% in the case of aggregates with a $S_T > 0.05\%$. When S_T values $< 0.05\%$ are measured, a high CV is expected since such values are close to the apparatus detection limit. Sample CTV-1 is a standard, whose S_T value is known to be 0.26%; all laboratories obtained very similar S_T (%) values and the data obtained were right on target. It is interesting to note that about 50% (21/43) of the aggregates analysed in this study showed a $S_T > 0.10\%$, confirming that a significant proportion of rock types does contain a noticeable amount of sulfide minerals (thus measurable S_T); however, such rock types / aggregates would require further testing to identify the potential presence of pyrrhotite considering the S_T “limit” of 0.10%

proposed in European standards and for new and unproven sources of concrete aggregates according to the Annex P of CSA A23.1-2014²².

Table 7.2: Total sulfur values (S_T , % by mass) measured in Lab 1 for aggregate set 1. Measurements on two subsamples, average values, Standard deviation (SD), Coefficient of variation (CV), rock type and iron sulfide minerals present.

Sample	S_T (%) by mass		Average	SD	CV (%)	Rock type	Iron sulfur Mineral(s)
	Sub sample 1	Sub sample 2					
S1	0.03	0.04	0.04	0.01	16.24	Tonalitic gneiss	Py
S2	0.04	0.04	0.04	0.00	3.08	Granitic gneiss	Py
S3	0.04	0.04	0.04	0.00	1.15	Granitic gneiss	Py
S4	0.04	0.04	0.04	0.00	2.49	Basalt	Py, Ccp
S5	0.04	0.05	0.05	0.01	14.92	Basalt	Py, Ccp, Bn
PKA	0.05	0.04	0.05	0.00	6.66	Anorthosite	—
S6	0.05	0.05	0.05	0.00	1.38	Diorite	Py, Ccp
S7	0.06	0.05	0.05	0.00	8.62	Limestone	Py
SW	0.07	0.07	0.07	0.01	7.21	Mica schist	Po, Py, Ccp
S8	0.09	0.09	0.09	0.00	1.99	Syenitic gneiss	Py
S9	0.10	0.10	0.10	0.00	2.67	Limestone	Py
S10	0.11	0.11	0.11	0.00	0.12	Diorite	Py, Ccp
DLS	0.13	0.15	0.14	0.01	7.81	Limestone	Pyrite (traces)
S11	0.15	0.16	0.15	0.00	1.75	Limestone	Py, Ccp, Po
S12	0.15	0.16	0.15	0.00	3.04	Limestone	Py, Ccp
S13	0.20	0.21	0.21	0.01	6.25	Limestone	Py
SPH	0.24	0.24	0.24	0.00	0.23	Phyllite	Po, Py, Ccp
GGP	0.34	0.33	0.33	0.01	2.45	Granitic gneiss	Po, Py, Ccp
SBR	0.71	0.73	0.72	0.02	2.68	Hornfels	Po, Py, Ccp, Sp
MSK	1.00	1.00	1.00	0.00	0.00	Norite or gabbro	Po, Py, CCp, Pn
B&B	5.69	5.37	5.53	0.23	4.16	Gabbro	Po, Py, Ccp

¹ Po: Pyrrhotite; Py: Pyrite; Ccp: Chalcopyrite, Pn: Pentlandite; Bn: Bornite; Sp: Sphalerite.

Table 7.3: Total sulfur values (S_T , % by mass) for all the laboratories, and respective average, Standard deviation (SD) and Coefficient of variation (CV).

Samples *	S_T (%) Lab1	S_T (%) Lab2	S_T (%) Lab3	Average	SD	CV	Main rock type	Sulfides ¹
1	0.00	0.00	<0.02	0.00	0.00	17.69	Granite	Py
2	0.00	0.00	<0.02	0.00	0.00	8.14	Sandstone	–
3	0.01	0.01	<0.02	0.01	0.00	14.94	Granite	Py
4	0.01	0.01	<0.02	0.01	0.00	45.39	Sandstone	Py
5	0.01	0.01	<0.02	0.01	0.00	7.69	Sandstone	Py, Ccp
6	0.00	0.01	<0.02	0.01	0.00	50.77	Diorite	–
7	0.02	0.02	0.02	0.02	0.00	8.98	Sandstone	Py
8	0.02	0.02	<0.02	0.02	0.01	27.13	Andesite	Py
9	0.02	0.02	<0.02	0.02	0.00	21.47	Granite	Py
10	0.06	0.02	0.03	0.03	0.02	65.39	Basalt	Ccp
11	0.02	0.02	0.04	0.03	0.01	30.39	Phonolite	–
12	0.03	0.02	0.04	0.03	0.01	43.97	Tuff	Py
13	0.04	0.03	0.03	0.03	0.01	26.05	Sandstone	Py
14	0.03	0.03	0.03	0.03	0.00	9.28	Granite	Py
15	0.03	0.05	0.04	0.04	0.01	14.69	Gneiss	Py, Ccp
16	0.04	0.04	0.04	0.04	0.00	5.79	Diorite	Py
17	0.05	0.04	0.04	0.04	0.01	12.00	Sandstone	Py
18	0.05	0.04	0.04	0.04	0.00	10.33	Sandstone	Py
19	0.04	0.04	0.05	0.04	0.01	12.91	Gabbro	Py, Ccp, Po
20	0.06	0.05	0.06	0.05	0.01	15.26	Limestone	Py
21	0.06	0.05	0.05	0.05	0.00	7.84	Granitic Gneiss	Py
22	0.07	0.08	0.07	0.07	0.00	3.59	Granite	Py, Ccp
23	0.10	0.09	0.10	0.10	0.01	7.73	Andesite	Py
24	0.10	0.09	0.10	0.10	0.01	7.17	Limestone	Py
25	0.10	0.10	<0.02	0.10	0.00	1.28	Syenite	Py
26	0.12	0.12	0.11	0.12	0.01	4.91	Granite	Py, Ccp, Po
27	0.15	0.15	0.14	0.15	0.01	5.03	Limestone	Py
28	0.16	0.15	0.17	0.16	0.01	6.27	Limestone	Py
29	0.15	0.16	0.16	0.16	0.01	3.36	Sandstone	Py
30	0.16	0.17	0.19	0.17	0.01	7.67	Limestone	Py
31	0.22	0.23	0.22	0.22	0.01	3.02	Limestone	Py
32	0.23	0.24	0.26	0.24	0.02	6.60	Diorite	Py
33	0.25	0.23	0.26	0.25	0.02	6.32	Limestone	Py
34	0.26	0.28	0.29	0.28	0.02	6.07	Calcarenite	Py
35	0.26	0.30	0.28	0.28	0.02	6.71	Gabbro	Py
36	0.31	0.29	0.30	0.30	0.01	3.44	Granite	Py, Ccp
37	0.34	0.33	0.34	0.34	0.01	1.50	Gneiss	Py, Apy, Ccp, Po
38	0.35	0.37	0.40	0.37	0.02	6.56	Dolostone	Py
39	0.38	0.40	0.44	0.41	0.03	7.80	Basalt	Py
40	0.46	0.00	0.44	0.45	0.01	2.46	Granitic gneiss	Py, Ccp, Po
41	0.45	0.49	0.54	0.49	0.05	9.40	Dolostone	Py
42	0.58	0.54	0.59	0.57	0.03	4.72	Limestone	Py
43	0.81	0.85	0.91	0.86	0.05	5.76	Dolostone	Py
CVT-1	0.26	0.26	0.25	0.26	0.01	2.18	standard	

¹ Po: Pyrrhotite; Py: Pyrite; Ccp: Chalcopyrite, Apy: Arsenopyrite

*The aggregates tested are not necessary used as aggregates in concrete production.

7.3.6.2 Oxygen consumption test

As mentioned previously, various parameters were tested in order to identify the best conditions for optimum O₂ consumption from sulfide-bearing aggregates. Regarding the particle size, aggregate samples with a particle size < 150 µm [0.006 in.] gave the highest O₂ consumptions (Fig. 7.5). These findings are not surprising considering that a higher specific surface area for the iron sulfides logically results in higher rates of iron sulfide oxidation.

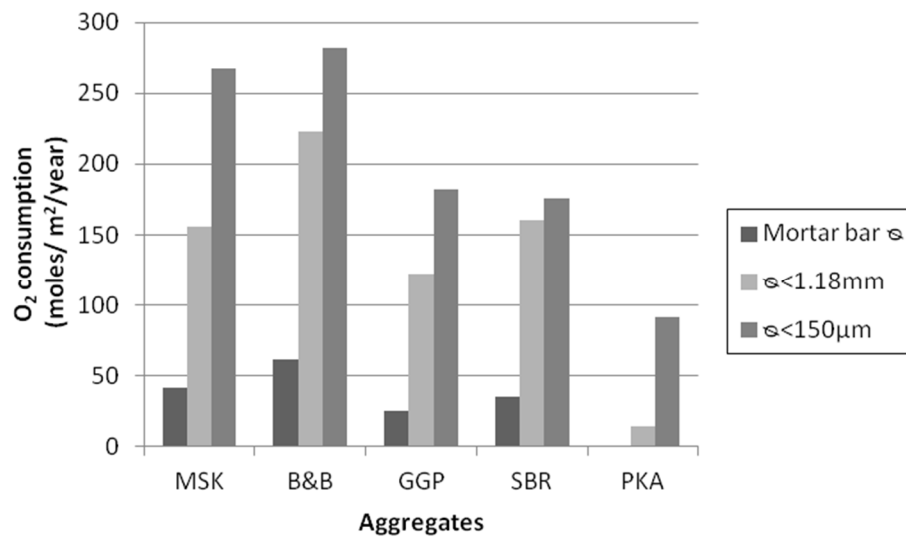


Figure 7.5: Consumed oxygen (moles/m²/year) for MSK, B&B, GGP, SBR and PKA aggregates using 5cm ground material thickness, 15 cm headspace and 40% degree of saturation.

Aggregates with a saturation degree of 60% did not result in a significant O₂ consumption, while much higher values were obtained at 40% saturation (particle sizes material < 1.18 mm [0.05 in.]). Regarding the ground material thickness vs. the headspace in the plexiglass column, the best results were obtained when the ground material thickness was 10 cm [3.94 in.] and the headspace 10 cm [3.94 in.].

Table 7.4 gives the results of duplicate O₂ consumption tests carried out on nine aggregates, when using 10 cm [3.94 in.] of compacted ground material with a particle size of < 150 µm [0.006 in.], a saturation degree of 40% and a headspace of 10 cm [3.94 in.]. These were the optimized conditions for the test and generated repeatable results. Also, the aggregates generally showed a good relationship between the oxygen consumption and the

S_T ; however, all these aggregates had somewhat similar sulfide mineralogy, with the presence of pyrrhotite in all samples. On the other hand, the two control aggregates HPL and PKA, as well as the pyrite-bearing DLS aggregate, induced O_2 consumption values < 5.0%, thus suggesting that this could represent a potential threshold value for this test.

Table 7.4: Oxygen consumption (%) and respective S_T (% by mass) values. The testing was carried out under the following conditions: 10 cm [3.94 in.] of compacted ground material with a particle size of < 150 μm [0.006 in.], a saturation degree of 40% and a headspace of 10 cm [3.94 in.].

Aggregates		Oxygen cons. (%)		S_T (% by mass)		Sulfides present (from Table 1) ¹
	Tests →	1	2	1	2	
Sulfide-bearing aggregates	SPH	6.2	6.2	0.32	0.29	Po, Py, Ccp
	GGP	5.4	6.0	0.25	0.24	Po, Py, Ccp
	SW	8.2	8.2	0.07	0.07	Po, Py, Ccp
	SBR	10.7	10.8	0.87	0.75	Po, Py, Ccp, Pn
	MSK	21.7	21.4	0.99	1.11	Po, Py, Ccp, Sp
	SDBR	57.0	55.5	13.86	14.46	Po, Py, Ccp, Pn
Control aggregates (no sulfide)	DLS	3.0	0.2	0.12	0.19	Py (traces)
	PKA	2.6	2.8	0.04	0.06	---
	HPL	1.7	0.2	0.02	0.02	---

¹ Po: pyrrhotite; Py: pyrite; Ccp: chalcopyrite, Pn: pentlandite; Sp: sphalerite.

7.3.6.3 Mortar bar expansion test (Phase 3)

This two-part mortar bar test consists of: 1) a first part to reproduce the deterioration resulting from the oxidation reaction of the iron sulfides in the aggregates and gypsum formation, and 2) a second part to promote thaumasite formation. The test conditions that were found to best promote the above processes are as follows¹⁵:

Part I: The mortar specimens are stored at 80°C [176°F] and 80% RH with two 3-hour soaking periods at room temperature in a sodium hypochlorite solution (bleach 6%) per week. A testing period of 90 days was found to be sufficient to induce excessive expansion due to the formation of secondary oxidation and sulfate products for the set of aggregates tested.

Part II: Beyond those 90 days, the mortar specimens can be transferred to 4°C [39.2°F] and 100% RH to promote thaumasite formation. The 2 weekly 3-hour soaking periods in bleach (6%) were still maintained during that low-temperature storage period.

As illustrated in Fig. 7.6 and 7.7, different behaviors were observed based on aggregates mineralogy (Table 7.1). Both sets of mortar bars incorporating the MSK and GGP aggregates that were continuously kept at 80°C [176°F] and 80% RH, i.e. MSK 80°C [176°F] and GGP 80°C [176°F] series in Fig. 7.6, displayed a steadily increasing expansion trend that reached between 0.15 and 0.20% at 90 days, and between 0.40 and 0.50% at about 300 days. The companion set of bars incorporating the MSK aggregate that were transferred to 4°C [39.2°F] at 90 days (MSK 80°C → 4°C in Fig. 7.6) continued to expand at a similar rate up to about 150 days, and then the expansion rate increased drastically to finally reach about 1.0% expansion at 243 days. This behavior may be due to the presence of carbonate material (siderite, calcite) in the MSK aggregate that may serve as a potential source of CO₃²⁻ necessary for thaumasite formation. Actually, the GGP aggregate, which contains only traces of carbonate material, stopped expanding when transferred to 4°C [39.2°F] (GGP 80°C → 4°C in Fig. 7.6). The behavior of the GGP aggregate is however not clear regarding its alkali silica reactivity potential, which needs to be further assessed through concrete prism testing.

The mortar bars incorporating the control aggregate PKA did not suffer from significant expansion during both phases of the program (i.e. up to 230 days of testing). This confirms that the somewhat harsh conditions used in the proposed mortar bar method do not in themselves induce excessive expansion in mortars incorporating sulfide-free aggregate materials.

In the case of the sulfide-bearing and alkali-silica reactive aggregates SBR, SPH and SW, a very different expansion pattern, characterised by a rapid onset of expansion that completely stopped shortly after the transfer of the bars at 4°C [39.2°F], was observed (Fig. 7.7). The rapid onset of expansion is suspected to result from the development of ASR in the above mortar specimens; however, additional testing and the detailed petrographic examination of the mortar bars will be required to confirm this hypothesis. It is interesting to note that the mortar bars incorporating the highly alkali-silica reactive Spratt limestone also showed a quick onset of expansion in the particular storage conditions used for testing; however, the expansion level reached at 90 days was much lower than that measured for the SBR, SPH and SW aggregates. The absence of expansion following transfer of the bars at

4°C [39.2°F], however, suggests that thaumasite formation did not occur in the above alkali-silica reactive specimens.

Since all the sulfide-bearing aggregates investigated in this study showed an expansion over 0.10% at the end of Phase 1, this value could be considered as a potential limit to distinguish deleterious sulfide-bearing aggregates from innocuous ones. However, the combined effects of sulfide oxidation and ASR under the storage conditions proposed will require further clarification.

The visual examination of the test specimens incorporating the MSK aggregate showed the progressive development of cracking, pop-outs, traces of rusts, ‘banana shape’ due to excessive expansion and total destruction towards the end of the testing period. On the other hand, the mortar specimens incorporating the PKA aggregate, besides a slight discoloration due to the high temperatures storage, did not show any significant signs of deterioration (Fig. 7.8).

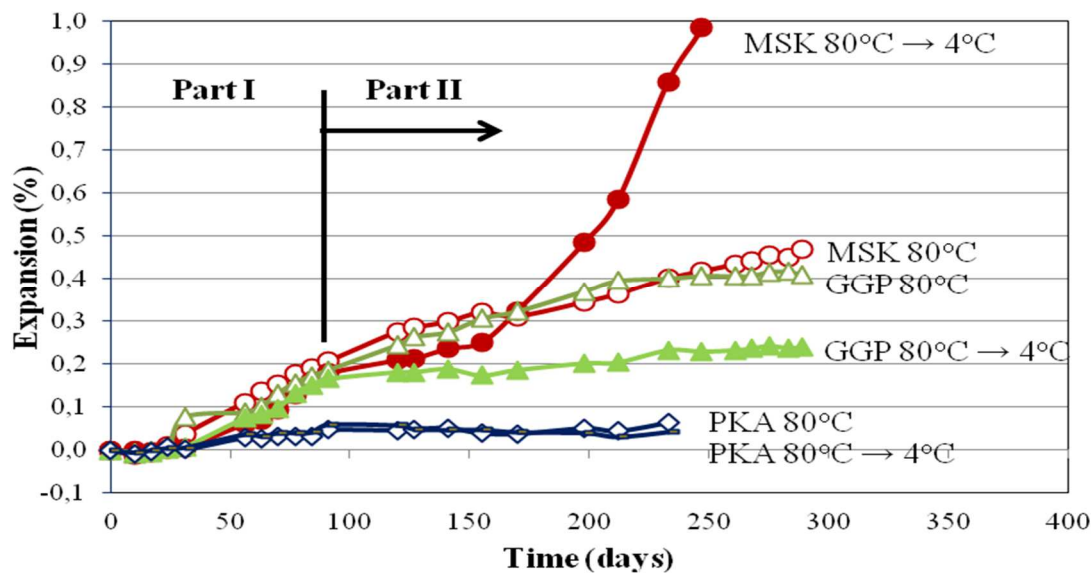


Figure 7.6: Expansion of companion sets of mortars specimens either kept continuously at 80°C [176°F] and 80% RH or transferred at 4°C [39.2°F] and 100% RH at 90 days. The expansion values reported at each age are the average obtained on the 3 bars tested for each aggregate.

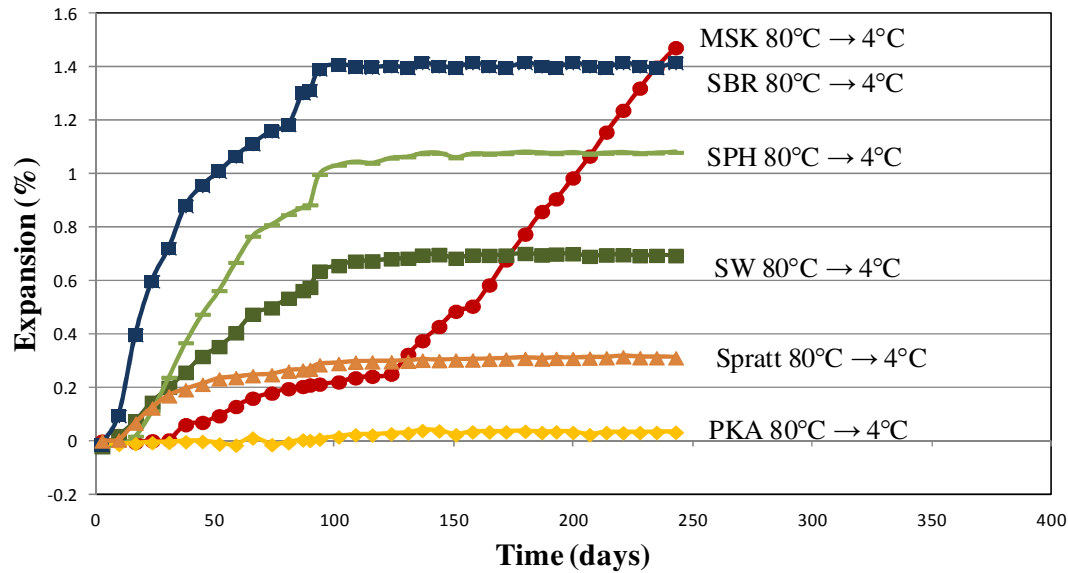


Figure 7.7: Expansion of mortar bars subjected to two 3-hour wetting periods in bleach (6%) per week, and kept at 80°C [176°F] /80%RH during 90 days. The bars are transferred after that period to 4°C [39.2°F] /100% RH and exposed to the two 3-hour soaking in bleach per week. The expansion values reported at each age are the average obtained on the 3 bars manufactured and tested for each aggregate.

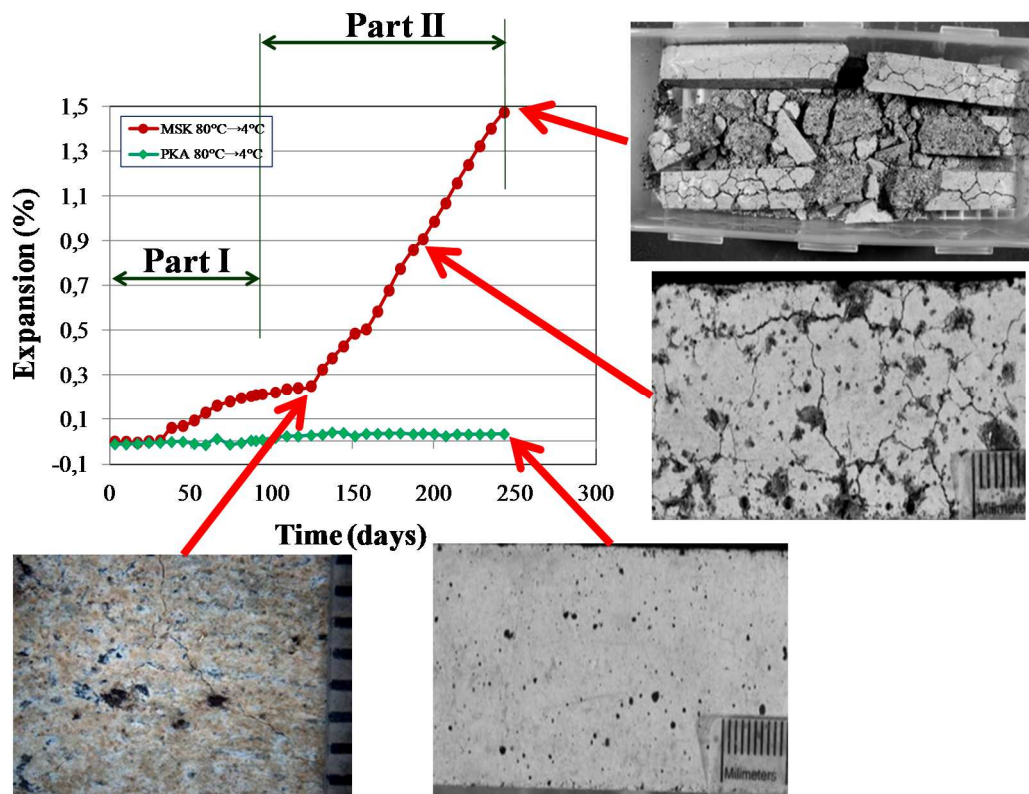


Figure 7.8: Visual condition of mortar bars incorporating the MSK and PKA aggregates during and at the end of the expansion test.

7.3.7 Protocol for the performance evaluation of sulfide-bearing aggregates

Numerous cases of concrete deterioration related to the use of iron-sulfide bearing aggregates have been documented over the past few decades². Based on the knowledge acquired from all these cases, and from the detailed petrographic examination of cores collected from deteriorated concrete foundations from the Trois-Rivières area, a series of tests have been developed by the authors of this paper. All those findings resulted in the development of a three-phase testing protocol using a combination of the above tools and a series of “decision-making points/steps” to help engineers identify the potential damaging effects of iron sulfide-bearing aggregates for use in concrete (Fig. 7.3).

Phase 1 corresponds to a chemical approach, based on the measurement of the S_T of the aggregate material. In accordance to the Annex P of CSA A23.1-2014²² and/or European standards EN 12 620 (2003)¹², aggregates with a S_T higher than 1% should be rejected for concrete applications. In addition, the above standards state that aggregates with a $S_T < 0.10\%$ can be accepted without any further testing. The testing carried out so far in this study did not provide data from O_2 consumption or expansion testing that could confirm the above limits or suggest new ones. Consequently, the S_T limits of 1% and 0.10% are proposed here until the results of further testing are available. At this stage, it is important to mention that the S_T determined in the chemical approach actually corresponds to the total **sulfide** sulfur content within the aggregate material. Appropriate methods should also be applied to determine the **sulfate** sulfur content related to the potential presence, within the aggregate material, of sulfate minerals such as gypsum. The **sulfate** sulfur content should thus be subtracted from the total sulfur content determination in order to apply the selected limit criterion. For aggregates showing a S_T between 1% and 0.1%, further testing is necessary to identify the sulfide minerals present. Further performance evaluation can be carried out on such aggregates through the measurement of the oxygen consumed by the aggregate material under well-controlled temperature and humidity conditions in a closed environment (Phase 2). Based on the testing carried out in this study, a preliminary limit of 5.0% for the O_2 consumed under the test conditions is proposed. Aggregates inducing values $< 5.0\%$ could be accepted for use in concrete applications. On the other hand, aggregates generating oxygen consumption values $\geq 5.0\%$ could potentially

induce deleterious oxidation reaction, which needs to be further investigated through Phase 3 of the protocol.

Phase 3 of the protocol consists of a two-phase mortar bar test, where a set of three mortar bars is first exposed, for 90 days, to high temperature and humidity conditions, with two weekly soaking periods in an oxidizing solution. The testing carried out in this study suggests that an expansion exceeding 0.10% at 90 days could be caused by ASR and/or the oxidation of sulfide phases within the aggregate. Although such aggregates may be deleterious for use in concrete applications anyway, the exact reason for the excessive expansion measured in that test should be clarified before deciding on the use or the rejection of the aggregate because alkali-silica reactive aggregates can be used in concrete provided appropriate preventive actions are taken²³. If the mortar specimens show an expansion lower than 0.10% at 90 days, the mortar bars should be transferred to a second phase of the expansion test, i.e. low temperature and high humidity storage, and this for an additional period of 90 days. If the expansion remains stable during that second phase of testing, the aggregate could be accepted for use in concrete applications. Continuing or increasing expansion rates upon low temperature storage potentially suggests deleterious thaumasite formation, thus causing rejection of the aggregate for use in concrete applications. The expansion testing of a larger number of aggregates should help confirming whether aggregates inducing mortar bar expansions $< 0.10\%$ (or another suitable limit) at 90 days could be accepted for use without the need for further low-temperature testing.

It is important to mention that the protocol illustrated in Fig. 7.3, and the proposed/preliminary test limits, although based on the results of an extensive test program, will need to be further validated through the testing of a larger number of aggregates.

Numerous cases of concrete deterioration related to the use of iron-sulfide bearing aggregates have been documented over the past few decades [2]. Based on the knowledge acquired from all these cases, and from the detailed petrographic examination of core collected from deteriorated concrete foundations from the Trois-Rivières area, a series of tests have been developed by the authors of this paper. All those findings resulted in a three-phase testing protocol using a combination of the above tools and a series of

“decision-making points/steps” to help engineers identify the potential damaging effects of iron sulfide-bearing aggregates for use in concrete (Fig. 7.3).

7.3.8 Conclusions

This study, which covers the work of four research teams, aimed at developing a three-phase evaluation protocol test capable of predicting the damaging potential of aggregates containing iron sulfide minerals prior to their use in concrete. In the first phase, the aggregate total sulfur content (S_T , % by mass) is measured. The values obtained and existing standards lead to proposing: (1) a $S_T > 1\%$ as the value for rejecting the aggregate, (2) $0.10\% \geq S_T < 1\%$ as the interval value for proceeding to the second phase of the protocol, and (3) the $S_T < 0.10\%$ as the limit value of acceptance. The aggregates ($0.10\% \geq S_T < 1\%$) that are directed to Phase 2 are ground to produce a particle size less than $150\ \mu\text{m}$ and then exposed to an oxygen consumption test. Taking into account the limited number of aggregates tested, the tentative acceptance limit was lower than 5.0% of consumed oxygen, while aggregates inducing values equal or higher than 5.0% should be tested in the Phase 3 of the protocol. Phase 3 consists of a two-part mortar bar test. In Part I, mortar bars are subjected to a 90-day storage period at 80°C [176°F] and 80% RH with two 3-hour soaking periods in a 6% sodium hypochlorite solution. It was found that expansions in excess of this limit could be caused by ASR and/or the oxidation of sulfide phases within the aggregate. The exact reason for this excessive expansion should be clarified before deciding on the use or the rejection of the aggregate. If the values are lower than 0.10%, the samples should be transferred to 4°C [39.2°F] and 100% RH for another 90 day-period. If, at the end of those 90 days, the samples expansion remains stable, the aggregates could be accepted. However, if the expansion continues, the aggregate should be rejected. The proposed protocol and preliminary test limits, although based on the results of an extensive test program, will need to be further validated through the testing of a larger number of aggregates.

7.4 Acknowledgments

The authors wish to acknowledge the Natural Sciences and Engineering Research Council of Canada (NSERC) for their collaborative research and development grant and all partners (ABQ, ACC, ACRGTQ, APCHQ, Garantie Qualité Habitation, ACQ, Inspec-sol inc.,

LVM, RBQ, Exp. Inc., SHQ, Ville de Québec, Ville de Montréal, Hydro-Québec, MTQ, Qualitas). The authors also want to thank Bruno Bussière and Olivier Peyronnard from UQAT who shared their expertise and knowledge in the use of oxygen consumption test. A. Rodrigues benefits from a PhD scholarship funded by FCT-Fundação para a Ciência e Tecnologia, Portugal, Ref.: SFRH/BD/71203/2010.

7.5 References

- [1] . Guarantee Plan for New Residential Buildings,
[“http://www2.publicationsduquebec.gouv.qc.ca/”](http://www2.publicationsduquebec.gouv.qc.ca/), July 2015
- [2]. Rodrigues, A., Duchesne, J., Fournier, B., Durand, B., Rivard, P., Shehata, M., “Mineralogical and chemical assessment of concrete damaged by the oxidation of sulfide-bearing aggregates: Importance of thaumasite formation on reaction mechanisms,” *Cement and Concrete Research*, V.42, 2012, pp. 1336–1347.
- [3]. Janzen, M. P., Nicholson, R. V., Scharer, J. M., “Pyrrhotite reaction kinetics reaction rates for oxidation by oxygen, ferric iron and for nonoxidative solution,” *Geochimica et Cosmochimica Acta* , V.64, 2000, pp.1511-1522.
- [4]. Belzile, N., Chen, Y.W., Cai, M-F., and Li, Y., “A review on pyrrhotite oxidation,” *Journal of Geochemical Exploration*, V.84, 2004, pp. 65-76.
- [5]. Thomas, J. E., Skinner, M. W., Smart, R.S.C., “A mechanism to explain sudden changes in rates and products for pyrrhotite dissolution and acid solution,” *Geochimica et Cosmochimica Acta*, V.65, 2001, pp. 1-12.
- [6]. Tagnit-Hamou, A., Saric-Coric, M., Rivard, P., “Internal deterioration of concrete by the oxidation of pyrrhotitic aggregates,” *Cement and Concrete Research*, V.35, 2005, pp. 99-107.
- [7]. Casanova, I., Agullo, L., Aguado, A., “Aggregate expansivity due to sulphide oxidation – I. Reaction system and rate model,” *Cement and Concrete Research*, V.26, 1996, pp. 993-998.

- [8]. Rodrigues, A., Duchesne, J., Fournier, B., “Microscopic analysis of the iron sulfide oxidation products used in concrete aggregates,” 34th International Conference on Cement Microscopy, 2012, Halle-Saale, Germany.
- [9]. Rodrigues, A., Duchesne, J., Fournier, B., “Petrographic characterization of the deterioration products of a concrete containing sulfide bearing aggregates; a particular case of internal sulfate attack,” 35th International Conference on Cement Microscopy, 2013, Chicago, USA.
- [10]. CSA A23.1.14/ A23.2.14 “Concrete materials and methods of concrete construction/Test methods and standard practices for concrete,” Canadian Standards Association, Mississauga, Canada, 2014.
- [11]. French standard NF P18-301: “Granulats naturels pour bétons hydrauliques,” 1983
- [12]. EN-12620: “Aggregates for concrete”, 2003.
- [13]. ASTM C 294-12, "Standard Descriptive Nomenclature for Constituents of Concrete Aggregates," ASTM International, West Conshohocken, PA, 2012, 11p.
- [14]. ASTM C 33/C33M, "Standard Specification for Concrete Aggregates," ASTM International, West Conshohocken, PA, 2012, 11p.
- [15]. ASTM C 1260-14 “Standard Test Method for Potential Alkali Reactivity of Aggregates (Mortar Bar Method),” ASTM International, West Conshohocken, PA, 2012, 5p.
- [16]. CSA A23.2-27A. 2014. “Standard Practice to Identify Degree of Alkali-Reactivity of Aggregates and to Identify Measures to Avoid Deleterious Expansion in Concrete,” Canadian Standards Association, Mississauga, Canada, 691p.
- [17]. CSA A23.2-26A. 2014. “Determination of potential alkali-carbonate reactivity of quarried carbonate rocks by chemical composition,” CSA A23.2-14: Methods of Test and Standard Practices for Concrete,” Canadian Standards Association, Mississauga, Canada, 691p.

- [18]. BNQ 2560-500, "Aggregate Material Sulfate Swelling Potential Petrographic Index Determination – SPPI Evaluation Test Method," BNQ (Bureau de normalisation du Québec), 2003.
- [19]. Elberling, B., Nicholson, R. V., Reardon, E. J., Tibble, P., "Evaluation of sulfide oxidation rates: a laboratory study comparing oxygen fluxes and rates of oxidation product release," Canadian Geotechnical Journal, V.31, 1994, pp. 375-383.
- [20]. Rodrigues, A., Duchesne, J., Fournier, B., "Quantitative assessment of the oxidation potential of sulfide-bearing aggregate in concrete using an oxygen consumption test," Cement and Concrete Composites, V.67, 2016, pp.93-100.
- [21]. Rodrigues, A., Duchesne, J., Fournier, B., "A new accelerated mortar bar test to assess the potential deleterious effect of sulfide-bearing aggregate in concrete," Cement and Concrete Research, V.73, 2015, pp. 96-110.
- [22]. Annex P (informative), "Impact of sulphides in concrete aggregate on concrete behaviour," CSA A23.1-14: Concrete Materials and Methods of Concrete Construction, Canadian Standards Association, Mississauga, Canada, 11p.
- [23]. ASTM C1778-14 "Standard Guide for Reducing the Risk of Deleterious Alkali-Aggregate Reaction in Concrete," ASTM International, West Conshohocken, PA, 2012, 11p.

Chapter 8

Conclusion and Recommendations

8.1 Conclusions

The present Ph.D. project dealt with concrete deterioration involving sulfide-bearing aggregates.

Regarding the exposed problem, this project seeks globally to better understand the deterioration process in concrete incorporating sulfide-bearing aggregates in the Trois-Rivières area in order to develop a methodology to efficiently evaluate the potential reactivity of such types of aggregates. This will be done through the following specific objectives: assess the mineralogical and chemical of damaged concretes containing sulfide-bearing aggregates, propose the mechanism(s) responsible for concrete deterioration, and reproduce the deterioration process under laboratory conditions. The achievement of these objectives has permitted the development of a global evaluation protocol to predict the deleterious potential of aggregates containing iron sulfides.

This project started with the visual inspection of a number of damaged concrete structures in Trois-Rivières area. The detailed petrographic analysis of concrete cores extracted from those structures had permit to conclude that the coarse aggregate used in all the cases was a norite/hypersthene gabbro containing various proportions of sulfide minerals including pyrite, pyrrhotite, pentlandite and chalcopyrite. Major constituents of this dark-colored coarse-grained dense rock consist of anorthite, with lesser amount of biotite and pyroxene. The iron sulfides were found to be finely disseminated into silicate minerals and pyrrhotite was the one showing signs of oxidation. The presence of a thin layer of carbonate mineral (siderite) was often seen “coating” the sulfide minerals. This layer could have served as the source of carbonate required for thaumasite formation.

The detailed petrographic analysis of the concrete core samples showed important cracking around and through the aggregate particles and the cement paste; some aggregate particles were found partially disintegrated or debonded with white haloes surrounding oxidized sulfide-bearing particles. Iron oxide/hydroxide/oxyhydroxide, ettringite, gypsum,

thaumasite and ettringite-thaumasite solid solution were identified by the use of SEM/EDS, EPMA, and X-ray as secondary reaction products/minerals. As mentioned before, iron sulfides have the tendency to be unstable in the presence of oxygen and water leading to oxidation and formation of iron oxyhydroxides and sulfuric acid. When the oxidation reaction occurs in concrete aggregates, the sulfuric acid thus produced lowers the pH, but the reduction will be limited by the buffering effect of portlandite. In concrete, the sulfuric acid reacts with the portlandite and gypsum is formed. The gypsum, then, can react with the aluminate phases in Portland cement concrete (anhydrous or hydrated), thus leading to the formation of potentially expansive secondary ettringite. If a source of carbonate is available in the system (aggregate, cement or other) thaumasite can be formed. Those secondary reaction products/minerals identified, strongly suggested a case of iron sulfides oxidation followed by an internal sulfate attack with thaumasite formation.

The identification of the different phases associated with the deterioration including the presence of thaumasite (**Chapter 4**), along with a thorough literature review on cases of concrete deterioration due to the use of sulfide-bearing aggregates (**Chapter 3**), allowed a better understanding of the degradation mechanisms and lead the development of different tests (oxygen consumption test and accelerated mortar bar test) culminating with the propose of the development of a step by step protocol for predicting the damaging potential of aggregates containing iron sulfide minerals prior to their use in concrete. The set by step protocol had been divided into three phases: (1) total sulfur content measurement, (2) oxygen consumption evaluation, and (3) accelerated mortar bar test expansion measurement.

The total sulfur content measurement consists in the measurement of the S_T (% by mass) on a sample of 0.3 to 1 g passing the 80 μm sieve. The SO_2 content is analysed by a carbon/sulfur analyser by infrared absorption, from which the S_T is calculated. Twenty one concrete aggregates were analysed in one laboratory (Lab1) in duplicate and presented S_T values, ranging from 0.04 to 5.55%, by mass. The measurements obtained show a very good repeatability, with the large majority of the S_T values being within $\pm 0.01\%$ of the average. The variability may seem somewhat higher for S_T values $< 0.10\%$, which is close to the detection limit of the apparatus. Forty-three aggregate materials were analysed in

three laboratories (Labs 1 to 3) for reproducibility evaluation. The results generally show a good multi-laboratory reproducibility, with coefficients of variation (CV) generally less than 10% in the case of aggregate materials with a $S_T > 0.05\%$. When S_T values $< 0.05\%$ are measured, a high CV is expected since such values are close to the apparatus detection limit. About 50% (21/43) of the aggregate materials analysed in this study showed a $S_T > 0.10\%$, confirming that a significant proportion of rock types does contain a noticeable amount of sulfide minerals (thus measurable S_T); however, such rock types / aggregates would require further testing to identify the potential presence of pyrrhotite considering the S_T “limit” of 0.10% proposed in European standards and for new and unproven sources of concrete aggregates according to the Annex P of CSA A23.1-2014.

The adaptation of the oxygen consumption test developed by Elberling and coworkers (1994) to evaluate the oxidation potential of concrete aggregates containing iron sulfide minerals had prove its potential (**Chapter 5**). This technique measures the oxygen consumption rate at the top of a closed cylinder containing a layer of compacted material to determine its oxidation potential. Different experimental conditions were tested to achieve the ideal test conditions. Those ideal conditions were found to be the use of ground aggregate material (particle size $< 150\mu\text{m}$) at a 40% saturation degree, in compacted layer of 10cm in thickness, and with a 10cm headspace in the storage container. The results obtained on nine aggregates tested under the optimized conditions described above showed that the test is able to discriminate the aggregates containing iron sulfide minerals from the control (or sulfide-free) aggregates. A threshold limit fixed at 5% oxygen consumed separates the 2 groups of samples. This threshold value was fixed with some caution; the oxygen consumption values obtained for the control samples were less than 3% oxygen while sulfide-bearing aggregates like the MSK and the sulfide-rich SDBR samples consumed 21.7% and 57%, respectively. Finally, the precision of the method was assessed and a very low coefficient of variation of 2.2% was obtained for 6 tests carried out on the MSK aggregate, with a mean of 22.1% and a standard deviation value of only 0.50.

This mortar bar test consists in a two-phase experiment that will reproduce, in the laboratory, the expansive process observed in house foundations in the Trois-Rivières area,

i.e. 1) oxidation of iron sulfide minerals with resulting acid formation and sulfate attack of the cement paste, and 2) thaumasite formation.

An accelerated test on mortars was selected because an increase in the specific surface area of the iron sulfides significantly increases the rate of oxidation for evaluating the risk for deleterious oxidation reaction in aggregates prior to their use in concrete.

All the experiments were conducted on mortar bars, 25 by 25 by 285 mm in size, and were manufactured in accordance with the procedure described in the CSA A23.2-25A. Several different conditions (temperature, humidity, oxidation solution) were tested (**Chapter 6** and **Appendix B**). For the first phase of the test the ideal conditions found were a 90-day storage period at 80°C/80% RH, with two 3-hr wetting cycles in a 6% sodium hypochlorite (bleach) solution at 23°C per week. This phase allowed the evaluation of the oxidation potential of the aggregates. According to the values obtained, expansion values greater than 0.15% at 90 days are indicative of an oxidation potential of the aggregate. Phase I can be followed by up to 90 days of storage at 4°C/100% RH, again with two wetting cycles in a 6% bleach solution (Phase II), to determine the potential for thaumasite formation that is confirmed by a rapid regain of expansion followed by destruction of the test specimens during Phase II.

A number of control and sulfide-bearing aggregates were tested in this study. For the MSK aggregate, the aggregate that was found to be reactive in the Trois-Rivières structures, the oxidation of sulfide minerals present in the aggregate induced mortar bar expansions ranging between 0.18 and 0.21% at the completion of Phase I testing, mainly due to the formation of iron oxides/oxyhydroxides and iron sulfate minerals. Upon transfer to 4°C, the expansion of the MSK mortar specimens first slowed down before showing a large increase in expansion rate until the total disintegration of the bars confirmed by the presence of ettringite and ettringite-thaumasite solid solution in the mortar specimens. The petrographic analysis of the MSK aggregate revealed the presence of siderite surrounding the iron sulfide minerals. It is believed that the siderite may be the source of the carbonate material necessary for the formation of the ettringite-thaumasite solid solution, causing excessive expansion and eventual disintegration of the mortar bar during the 4°C storage.

The SBR, SW and SPH rock materials are sulfide-bearing and alkali-silica reactive aggregates. Those three aggregates showed a rapid onset of expansion that reached levels ranging from 0.58 % (SW) to $\approx 1.31\%$ (SBR) upon 90 days of testing (Phase I), expansion way above that obtained with the MSK aggregate. The observed expansions are probably a combination of alkali-silica reaction and the iron sulfides oxidation. Interestingly, none of the above three aggregates generated significant expansion upon transfer to 4°C, thus strongly suggesting that the expansion observed in Phase I was significantly related to ASR.

Other aggregate study was the GGP, a granitic gneiss with some amounts of pyrrhotite, pyrite and chalcopryrite. In the AMBT for ASR this aggregate as tested non potentially reactive. The behaviour of the mortar specimens incorporating the GGP aggregate was similar to that of the MSK aggregate during Phase I testing, with expansions ranging from 0.17 to 0.19%. However, their behaviour differed significantly afterwards since the GGP samples did not show any significant expansion upon transfer to Phase II conditions; this can be related to the absence of carbonate material in the GGP aggregate or also to the possibility that this aggregate is alkali-silica reactive, since as it is known some granites, gneisses and granodiorites produced expansion lower than the 0.15% limit criterion at 14 days for the ASTM for ASR, but they were found to cause deterioration of concrete in service.

The mortar bars incorporating the control aggregates without sulfide mineral, the PKA anorthosite and the HPL limestone, did not show any expansion nor showed any signs of deterioration during both phases of the mortar bar testing program.

Finally, as result of this extensive research program, a three-phase evaluation protocol test was proposed for predicting the damaging potential of aggregates containing iron sulfide minerals prior to their use in concrete (**Chapter 7**). The three phases consist in (1) total sulfur content measurement, (2) oxygen consumption evaluation, and (3) accelerated mortar bar test expansion measurement. In the first phase, the aggregate's total sulfur content (S_T , % by mass) is measured and three possibilities are presented, i.e. (1) a $S_T > 1\%$ as the value for rejecting the aggregate, (2) $0.10\% \geq S_T < 1\%$ as the interval value for proceeding to the second phase of the protocol, and (3) the $S_T < 0.10\%$ as the limit value of

acceptance. The aggregates that are directed to Phase 2 are subjected to an oxygen consumption test. The aggregates acceptance limit in this Phase 2 is value lower than 5% of consumed oxygen, while aggregates inducing values equal or higher than 5% should be tested in the Phase 3 of the protocol. Phase 3 consists in the two-phase accelerated mortar bar expansion test. At the end of Phase I, the aggregate can be immediately rejected if the expansion value is higher or equal to 0.10%. If the values are lower than 0.10%, the samples should be transferred to the Part II of the test. If, at the end of those 90 days, the samples expansion remains stable, the aggregates could be accepted. However, if the expansion continues, the aggregate should be rejected.

The proposed protocol and preliminary test limits, although based on the results of an extensive test program, will need to be further validated through the testing of a larger number of aggregates.

8.2 Recommendations

Even if the results obtained from the oxygen consumption test (Chapter 5) and the mortar bar expansion test (Chapter 6) had prove to be effective , additional tests should be performed to confirm the threshold limits proposed. With the aim of consolidating the threshold limits at every phase of the protocol, several aggregate sources should be tested.

The combined presence of different sulfide minerals is responsible for accelerating the oxidation reaction. Most of metal sulfides are semi-conductors, each characterized by a *rest potential*, which can vary as a function of the sulfide's detailed composition. The oxidative dissolution of the sulfide with a lower rest potential occurs at the anode while the sulfide with a higher electrode potential is protected from oxidation at the cathode. Pyrite is the sulfide mineral with the highest rest potential, thus more stable, while pyrrhotite shows the lowest rest potential and is consequently the most unstable sulfide mineral. For example, if pyrite and pyrrhotite coexist, the pyrite will be the cathode and pyrrhotite will be the anode, so the pyrrhotite will be the one that will be oxidized.

Taking into account these galvanic interactions, it is necessary to develop chemical tests with the purpose of establishing the influence of the combined sulfides in the aggregates.

During this PhD research program, all the mortars were manufactured using the same mix design, in order to replicate the one used in the construction of the deteriorated concrete, and to keep the same mix while changing the conditions of temperature, humidity, and the oxidation reaction solutions. It will be important to try different mix designs, mainly mix with a low w/c ratio. The decrease of the w/c ratio will produce a better concrete, meaning, more resistant and less porous. A less porous concrete will be more impermeable, reducing that way availability of water for the sulfides oxidation.

It will be also important try the use of different cement types and/or the supplementary cement materials and its influence in the kinetics of the iron sulfides oxidation reaction, mainly in the sulfates production. As described in **Chapter 2**, the sulfates formation as secondary products in the concrete needs some concrete constituents. The gypsum needs tricalcium aluminate (C_3A) and/or portlandite to form, ettringite requires excess of sulfate ions SO_4^{2-} over the aluminate phases (anhydrous or hydrated) of the portland cement and thaumasite needs source of carbonate (CO_3^{2-}), a source of sulfate (SO_4^{2-}) and silicate as $Si(OH)_6^{2-}$ that is found in the C-S-H of the concrete. The decrease or the substitution of these concrete constituents may prevent the sulfates formation.

During the accelerated mortar bar test (**Chapter 6**) it was found that some aggregates were alkali silica reactive and had in its composition sulfide minerals. One of the questions raised was which one was the principal cause of deterioration, the ASR, the sulfide minerals or both. If, for instance, it is found that it is only the alkali silica reaction that is responsible of the degradation, the aggregate may be used with the preventive measures in use for ASR aggregates. Depending on the level of risk of ASR, preventive measures such limiting the alkali contributed by the Portland cement to the concrete, the use of SCMs or lithium-based admixtures can possibly be used.

References

- Aguilera J., Blanco Varela M.T., Vásquez T., 2001. Procedure of synthesis of thaumasite. *Cement and Concrete Research*, 31: 1163–1168.
- ASTM C1012, 2012. Standard Test Method for Length Change of Hydraulic-Cement Mortars Exposed to a Sulfate Solution.
- Atak, S., Onal, G., Çelik M., 1998. *Innovations in Mineral and Coal Processing*, Taylor & Francis, Netherlands, 992pp.
- Ayora C., Chinchón S., Aguado A., Guirado F., 1998. Weathering of iron sulphides and concrete alteration: thermodynamic model and observation in dams from central Pyrenees, Spain. *Cement and Concrete Research*, 28: 1223–1235.
- Azizi, A., Petre, C., Olsen, C. and Larachi, F., 2010. Electrochemical behavior of gold cyanidation in the presence of a sulfide-rich industrial ore versus its major constitutive sulfide minerals. *Hydrometallurgy*, 101(3-4): 108-119.
- Azizi, A., Petre, C., Olsen, C. and Larachi, F., 2011. Untangling galvanic and passivation phenomena induced by sulfide minerals on precious metal leaching using a new packed-bed electrochemical cyanidation reactor. *Hydrometallurgy*, 107(3-4): 101-111.
- Becker M., 2009. The mineralogy and crystallography of pyrrhotite from selected nickel and PGE ore deposits and its effect on flotation performance. University of Pretoria, South Africa, PhD. Thesis, 253pp.
- Bellaloui, A., Nkurunziza, G., Ballivy, G., 2002. Caractérisation en laboratoire du potentiel expansif de granulats de remblais de fondation. *Canadian Geotechnical Journal*, 39: 141–148.
- Belzile N., Chen Y., Cai M., Li Y., 2004. A review on pyrrhotite oxidation. *Journal of Geochemical Exploration*, 84: 65–76.

- Bérard J., Roux R., Durand M., 1975. Performance of concrete containing a variety of black shale. *Canadian Journal of Civil Engineering*, 2: 58–65.
- Bérard, J., 1970. Black shale heaving at Ottawa, Canada: Discussion, *Canadian Geotechnical Journal*, 7:113-114.
- Berry, L. G., Mason, B. H. I., Dietrich, R. V., 1983. *Mineralogy_ concepts, descriptions, determinations*, 2nd edition, W. H. Freeman and Company, USA, 561pp.
- Bérubé, M. A., Locat, J., Gélinas, P, Gagnon, J. Y., Lefrançois, P., 1986. Black shale heaving at Sainte-Foy, Quebec, Canada *Canadian Journal of Earth Sciences*, 23:1774-1781.
- Biegler T., Swift D. A., 1979. Anodic behaviour of pyrite in acid solutions. *Electrochimica Acta*, 24: 415-420.
- Brown, P.W., Taylor, H.F.W., 1999. The role of ettringite in external sulfate attack. In J. Marchand and J. Skalny (eds) *Materials Science of Concrete Special Volume: Sulfate Attack Mechanisms*, The American Ceramic Society, Westerville, OH, pp. 73–98. Brown and Taylor, 1999
- Buttgenbach, H., 1953. *Les minéraux et les roches: Études Pratiques de Cristallographie Pétrographie et Minéralogie*. H. Vaillant-Carmanne, Belgium, 763pp.
- Casanova I., Aguado A., Agulló L., 1997. Aggregate expansivity due to sulfide oxidation - II. Physico-chemical modeling of sulfate attack. *Cement and Concrete Research*, 27: 1627-1632.
- Casanova I., Agulló L., Aguado A., 1996. Aggregate expansivity due to sulphide oxidation I. Reaction system and rate model. *Cement and Concrete Research*, 26: 993–998.
- Chan C. W., Suzuki I., 1993. Quantitative extraction and determination of elemental sulfur and stoichiometric oxidation of sulfide to elemental sulfur by *Thiobacillus thiooxidans*, *Canadian Journal of Microbiology*, 39: 1166-1168.

- Chinchón J., Lopez A., Soriano J., Vazquez E., 1990. La Cantera de Mont Palau II: Formacion de Compuestos Expansivos Generados en la Reaccion Arido-Hormigon. *Ingeniería Civil*, 72: 109–113.
- Chinchón J.S., Ayora C., Aguado A., Guirado F., 1995. Influence of weathering of iron sulphides contained in aggregates on concrete durability. *Cement and Concrete Research*, 25: 1264–1272.
- Chinchón J.S., Lopez A., Querol X., Ayora C., 1989. La Cantera de Mont Palau I: influència de la mineralogía de los áridos en la durabilidad del hormigón. *Ingeniería Civil*, 72: 79–88.
- Chinchón-Payá S., 2013. Áridos reactivos en hormigones de presa. Reacción sulfática con formación de thaumasite (PhD thesis) Universidad de Alicante, Spain.
- Chinchón-Payá S., Aguado A., Chinchón S., 2012. A comparative investigation of the degradation of pyrite and pyrrhotite under simulated laboratory conditions. *Engineering Geology*, 127: 75–80.
- Chizhikov, D.M., Kovylna, V.N., 1956. Investigation of potentials and anodic polarization of the sulfides and their alloys. *In: 4th Moscow 1956 (Proceedings of the 4th Conference on Electrochemistry, published 1959)*, Izdanja Akademii Nauk SSSR, Trudy Chetvertogo Soveshchaniya po Elektrokhimii, 715–719. (In Kwong et al, 2003).
- Cohen M. D., Mather B., 1991 Sulfate Attack on Concrete - Research Needs. *ACI Materials Journal*. 88 (1): 62- 69
- Collepari M., 2003. A state-of-the-art review on delayed ettringite attack on concrete. *Cement and Concrete Composites*, 25 (4–5): 401-407
- Collett G., Crammond N.J., Swamy R.N., Sharp J.H., 2004. The role of carbon dioxide in the formation of thaumasite. *Cement and Concrete Research*, 34:1599-1612.
- Crammond N. J., 1985. Thaumasite in failed cement mortars and renders from exposed brickwork. *Cement and Concrete Research*, 15: 1039-1050.

- CSA A23.1.14 / A23.2.14, 2014. Concrete materials and methods of concrete construction/Test methods and standard practices for concrete, Canadian Standards Association, Mississauga, Canada.
- CSA A3004-C8/ASTM CSA A3004-C8, 2008. Test Method for Determination of Sulphate Resistance of Mortar Bars Exposed to Sulphate Solution. Canadian Standards Association, Mississauga, Canada.
- Day R., Middendorf B., 2011. Sulfate attack and microstructural change on fly-ash mortars made with ordinary- and limestone-cements. Proceedings of the 33rd International Conference on Cement Microscopy, San Francisco, California, USA.
- De Villiers J.P.R., Liles D.C., 2010. The crystal-structure and vacancy distribution in 6C pyrrhotite, *American Mineralogist*, 95: 148–152.
- DEC, 1991. Advice on certain unsound rock aggregates in concrete in Cornwall and Devon», Department of the Environment, Circular BSC/P (91), DOE, HMSO, London.
- Deer, W., Howie, R., Zussman, J., 2000. *Minerais Constituintes das Rochas - Uma Introdução*. 2nd edition. Fundação Calouste Gulbenkian, Lisbon, 727pp.
- Divet L., Davy J.P., 1996. Étude des risques d'oxydation de la pyrite dans le milieu basique du béton, *Bull. Lab. Ponts Chaussées*. 204: 97–107.
- Divet, L., 2001. Les réactions sulfatiques internes au béton: contribution à l'étude des mécanismes de la formation différée de l'ettringite. Laboratoire Central des Ponts et Chaussées, Paris.
- Duchesne, J., 2010. Projet de recherche sur la détérioration du béton en présence de sulfure de fer. CRIB- Université Laval.
- Edge, R. A., Taylor, B. E. 1971. Crystal Structure of Thaumasite, $[\text{Ca}_3\text{Si}(\text{OH})_6.12\text{H}_2\text{O}](\text{SO}_4)(\text{CO}_3)$. *Acta Crystallographica*, 27: 586-594.

- Eglington M., 1987. Concrete and its Chemical Behaviour. Thomas Telford Ltd, England, 136pp.
- Ekmekçi Z., Demirel H., 1997. Effects of galvanic interaction on collectorless flotation behaviour of chalcopyrite and pyrite. *International Journal of Mineral Processing* 52: 31-48.
- Elberling, B., Nicholson, R. V., Reardon, E. J., Tibble, P., 1994. Evaluation of sulfide oxidation rates: a laboratory study comparing oxygen fluxes and rates of oxidation product release. *Canadian Geotechnical Journal*, 31: 375-383.
- French standard NF P18-301 1983. Granulats naturels pour bétons hydrauliques.
- Gerson A., Jasieniak, M., 2008. The effect of surface oxidation on the Cu activation of pentlandite and pyrrhotite. In: 24th International Mineral Processing Congress 165-174 (Science press: Beijing).
- Gomides M.J., 2009. Investigação de Agregados contendo Sulfetos e seus efeitos sobre a durabilidade do concreto. (PhD. Thesis) Universidade Federal do Rio Grande do Sul, Brazil.
- Grattan-Bellew P.E., Eden, W.J., 1975. Concrete deterioration and floor heave due to biogeochemical weathering of underlying shale. *Canadian Geotechnical Journal*, 12: 372–378.
- Grattan-Bellew, P. E., McRostie, G. C., 1982. Evaluation of heave prevention methods for floors founded on shale in the Ottawa region. *Canadian Geotechnical Journal*, 19(1): 108-111.
- Guarantee Plan for New Residential Buildings (Quebec),
[“http://www2.publicationsduquebec.gouv.qc.ca/”](http://www2.publicationsduquebec.gouv.qc.ca/), July 2015
- Hagelia P., Sibbick R., Crammond N., Larsen C., 2003. Thaumasite and secondary calcite in some Norwegian concretes. *Cement and Concrete Composites*, 25: 1131–1140.

- Hagelia P., Sibbick R.G, Crammond NJ, Grønhaug A, Larsen CK. 2001. Thaumasite and subsequent secondary calcite deposition in sprayed concretes in contact with sulfide bearing Alum Shale, Oslo, Norway. 8th Euroseminar on Microscopy Applied to Building Materials, Athens, Greece, September, pp.131–138.
- Hagelia, P., Sibbick, R.G., 2009. Thaumasite Sulfate Attack, Popcorn Calcite Deposition and acid attack in concrete stored at the «Blindtarmen» test site Oslo, from 1952 to 1982, *Materials Characterization* 60: 686-699.
- Hagerman T., Roosaar H.R., 1955. Kismineralens skadeinverkan på betong, *Betonw* 2: 151-161.
- Jallada K. N., Manu S., Cohen M. D., 2003. Stability and reactivity of thaumasite at different pH levels. *Cement and Concrete Research* 33: 433–437.
- Janzen M., Nicholson R. V., Scharer, J. M. 2000. Pyrrhotite reaction kinetics reaction rates for oxidation by oxygen, ferric iron and for nonoxidative solution, *Geochimica et Cosmochimica Acta*, 64:1511–1522.
- Knipe S.W., Mycroft J.R., Pratt A.R., Nesbitt H.W., Bancroft G.M., 1995. X-ray photoelectron spectroscopic study of water adsorption on iron sulphide minerals, *Geochimica et Cosmochimica Acta*, 59: 1075–1090.
- Köhler, S., Heinz, D. and Urbonas, L., (2006). Effect of ettringite on thaumasite formation. *Cement and Concrete Research*, 36(4): 697-706.
- Kwong Y. T. J., Swerhone G. W., Lawrence J. R., 2003. Galvanic sulphide oxidation as a metal-leaching mechanism and its environmental applications. *Geochemistry: Exploration, Environment, Analysis* 3: 337-343.
- Le Roux A., Divet L., Fasseu P., Hasni L., Marion A.M., 2001. Étude des risques d'oxydation de la pyrite dans le milieu basique du béton. *Bulletin du Laboratoire des Ponts et Chaussées*, 234: 79–88.

- Lehmann M.N., Kaur P., Pennifold R.M., Dunn J.G., 2000. A comparative study of the dissolution of hexagonal and monoclinic pyrrhotites in cyanide solution. *Hydrometallurgy*, 55: 255–273
- Longworth, T. I., 2003. Contribution of construction activity to aggressive ground conditions causing the thaumasite form of sulfate attack to concrete in pyritic grounds. *Cement and Concrete Composites*, 25: 1005-1013.
- Lugg A., Probert D., 1996. Mundic"-type problems: a building material catastrophe. *Construction and Building Materials*, 10: 467-474.
- Majima, H., 1969. How oxidation affects selective flotation of complex sulfide ores. *Canadian Metallurgical Quarterly*, 8: 269-273.
- Mbonimpa M., Aubertin M., Aachib M., Bussière B., 2003. Diffusion and consumption of the oxygen in unsaturated cover materials, *Canadian Geotechnical Journal*, 40: 916–932.
- Mielenz, R. C., 1963. Reactions of aggregates involving solubility, oxidation, sulfates or sulfides. *Highway Research Record*, 43:8-18.
- Mikhlin Y.L., Kuklinski A.V., Pavlenko N.I., Varnek V.A., Asanov I.P., Okotrub A.V., Selyutin G.E., Solovyev L.A., 2002. Spectroscopic and XRD studies of the air degradation of acid-reacted pyrrhotites, *Geochimica et Cosmochimica Acta*, 66: 4057-4067.
- Moum J., Rosenqvist I.Th., 1959. Sulfate attack on concrete in the Oslo region. *Journal of American Concrete Institute*, 56: 257–264.
- Neville A. M., Brooks J. J., 2010. *Concrete Technology*. Harlow, England ; New York : Prentice Hall. 442pp.
- Newman J., Choo B., 2003. *Cements in Advanced Concrete Technology-Constituent Materials*. Elsevier, Great Britain, 280 pp.
- NF EN-12620, 2003. Aggregates for concrete.

- NQ 2621 - 900 BNQ, 2003. Bétons de masse volumique normale et constituants BNQ (Bureau de normalisation du Québec).
- Oberholster R.E., Du Toit P., Pretonius J.L., 1984. Deterioration of concrete containing a carbonaceous sulphide-bearing aggregate. International Cement Microscopy Association (ICMA) (Ed.) Sixth Int. Conf. on cement microscopy. Albuquerque, New Mexico, USA.
- Oberholster R.E., Krüger J.E., 1984. Investigation of alkali-reactive, sulphide-bearing and by-products aggregates. Bulletin of the International Association of Engineering Geology, 3: 273–277.
- Orlova T. A., Stupnikov V. M., and Krestan A. L., 1988. Mechanism of oxidative dissolution of sulphides. Zhurnal Prikladnoi Khimii 61: 2172-2177. In Janzen et al., 2000)
- Pardal, M. P., 1975. Las Piritas del Maresme. Un assunto corrosivo Revista de Obras Públicas. 3126: 691-693.
- Pearson A. D., Buerger M. J., 1956. Confirmation of the crystal structure of pentlandite. American Mineralogist, 41: 804-805.
- Penner, E., Eden, W.J., Gillott, J.E. 1973. Floor Heave Due to Biochemical Weathering of Shale. Proceedings, 8th International Conference on Soil Mechanics and Foundations Engineering, Moscow, 2 (2):151-158.
- Pye, K., Miller, J. A., 1990. Chemical and biochemical weathering of pyritic mudrocks in a shale embankment. Quarterly Journal of Engineering Geology, 23: 365-381
- Quigley R.M., Vogan R.W., 1970. Black shale heaving at Ottawa, Canada, Canadian Geotechnical Journal, 7:106-115.
- RICS, 2005. The “Mundic” Problem Supplement to Second Edition-Stage 3 Expansion Testing. The Royal Institution of Chartered Surveyors, UK. 59 pp.

- Rodrigues, A., Duchesne, J., Fournier, B., 2012. Microscopic analysis of the iron sulfide oxidation products used in concrete aggregates. 34th International Conference on Cement Microscopy, Halle-Saale, Germany.
- Sahu, S., Badger, S., Thaulow, N., 2003. Mechanism of thaumasite formation in concrete slabs on grade in Southern California. *Cement and Concrete Composites*, 25(8): 889-897.
- Santhanam, M., Cohen, M.D., Olek, J., 2003. Effects of gypsum formation on the performance of cement mortars during external sulfate attack. *Cement and Concrete Research*, 33(3): 325-332.
- Schmidt T., Leemann A., Gallucci E., Scrivener K., 2011. Physical and microstructural aspects of iron sulfide degradation in concrete. *Cement and Concrete Research*, 41: 263–269.
- Schmidt, T., Lothenbach, B., Romer, M., Scrivener, K., Rentsch, D. and Figi, R., 2008. A thermodynamic and experimental study of the conditions of thaumasite formation. *Cement and Concrete Research*, 38(3): 337-349
- Seaton, S. G., 1948. Study of causes and prevention of staining and pop-outs in cinder concrete. *Journal of the American Concrete Institute*, 19 (5).
- Shayan A., 1988. Deterioration of a concrete surface due to the oxidation of pyrite contained in pyritic aggregates. *Cement and Concrete Research*, 18: 723-730.
- Shuey, R.T. 1975. *Semiconducting Ore Minerals*. Elsevier, Amsterdam, 415pp.
- Skalny, J., Marchand, J., Odler, I., 2003. *Sulfate attack on concrete*. Spon Press, UK, 217pp.
- St John, D. A., Poole, A. B., Sims, I., 1998. *Concrete Petrography- A handbook of investigative techniques*. Arnold, UK, 474pp.
- Steger H.F., 1982. Oxidation of sulphide minerals VII Effect, of Temperature and Relative Humidity on the Oxidation of Pyrrhotite, *Chemical Geology*, 35:281–295.

- Suzuki I., 1999. Oxidation of inorganic sulfur compounds: Chemical and enzymatic reactions. *Canadian Journal of Microbiology*, 45 (2): 97-105
- Suzuki I., Chan, C. W., Takeuchi, T. L. 1992. Oxidation of elemental sulfur to sulfite by *Thiobacillus thiooxidans* cells. *Applied and Environmental Microbiology*, 58: 3767-3769.
- Tagnit-Hamou A., Saric-Coric M., Rivard P., 2005. Internal deterioration of concrete by the oxidation of pyrrhotitic aggregates,. *Cement and Concrete Research*, 35: 99-107.
- The UK Government Thaumasite Expert Group, 1999. The thaumasite form of sulfate attack: risks, diagnosis, remedial works and guidance on new construction, Report of the Thaumasite Expert Group. Department of the environment, transport and regions, London.
- Thomas M. D. A., Rogers C.A., Bleszynski R.F., 2003. Occurrences of thaumasite in laboratory and field concrete. *Cement and Concrete Composites*, 25 (8): 1045-1050.
- Thomas, J. E., Skinner, M. W., Smart, R. S. C., 2001. A mechanism to explain sudden changes in rates and products for pyrrhotite dissolution and acid solution. *Geochimica et Cosmochimica Acta*, 65: 1-12.
- Tian, B., Cohen M.D., 2000. Does gypsum formation during sulfate attack on concrete lead to expansion? *Cement and Concrete Research*, 30 (1): 117-123.
- Torres, S. M., Leal, A. F., Vieira A. A. P.; Barbosa N. P., 2011. Thaumasite Form of Sulphate Attack in a Tropical Climate Weather. in *Proceedings of the XIII international Congress on the Chemistry of Cement*, Madrid, Spain.
- Vanyukov, A.V., Razumovskaya, N.N., 1979. Hydrothermal oxidation of pyrrhotites. *Izvestiya Visshih Uchebnih Zavedeniy – Tsvetniye Metalli* 6: 605-610 (in Janzen et al., 2000).
- Vasquez E., Toral T., 1984. Influence des sulfures de fer des granulats du Maresme (Barcelone) sur les bétons. *Bulletin of Engineering Geology and the Environment* 1984: 297–300.

- Wakizaka, Y., Ichikawa, K., Nakamura, Y., Anan, S., 2001. Deterioration of concrete due to specific minerals. Proceedings. Aggregate 2001. Environment and Economy, 2: 331-338.
- Warren, G.W. 1978. The electrochemical oxidation of CuFeS_2 . (Ph.D. Thesis, University of Utah, USA.
- Zhou, Q., Hill, J., Byars, E. A., Cripps, J. C., Lynsdale, C. J. and Sharp, J. H., 2006. The role of pH in thaumasite sulfate attack. Cement and Concrete Research, 36(1): 160-170.
- Zou Q., Glasser F.P., 2001. Thermal stability and the decomposition mechanisms of ettringite at $<120^\circ\text{C}$. Cement and Concrete Research, 31: 1333-1339.

Appendix A
Oxygen consumption test for the quantitative assessment of the
oxidation potential of sulfide-bearing aggregate in concrete

A1. Introduction

This appendix presents all the oxygen consumption values obtained during the adaptation and development of the oxygen consumption test.

A total of 10 aggregates were tested in order to reach the optimal conditions. Two degrees of saturation, i.e. 40 and 60%, were selected for this study. Considering these two saturation degrees, a void index of 1, a porosity of 50%, the volumetric mass density (ρ) of the aggregate, and the total volume of the column, it is possible to calculate the mass of water and the mass of the ground material that will be needed to fill up the column at a selected thickness to proceed to the oxygen consumption test at those conditions based upon the following equations.

$$\text{Mass of aggregate (g)} = [(1 - n_{gm}) \times V_{gm} \times \rho_{agg}]$$

$$\text{Mass of water (g)} = [(V_{gm} \times n_{gm}) \times S_{gm} \times \rho_w](5)$$

Where:

n_{gm} : porosity within the ground material (%);

V_{gm} : total volume occupied by the ground material (cm^3);

ρ_{agg} : volumetric mass density of the aggregate;

S_{gm} : degree of saturation (%) of the ground material;

ρ_w : density of water (g/cm^3)

For example, in the case of the aggregate MSK, the mass of aggregate needed for each experiment ranged from about 570g for 2.5 cm to 2279g for 10 cm of ground material (40% saturation).

The material is then placed into the column in 2 layers of equal mass and compacted until it reaches the desired thickness. The consolidation is carried out by using a large and heavy steel pestle. The surface of the second layer must be perfectly flat in order to obtain a good reading by the oxygen sensors.

Notes:

- **Porosity** in the ground material corresponds to the ratio of the volume of void-space over the total volume of ground material
- **Degree of saturation:** It corresponds to the ratio of the volume of liquid (water) to the total volume of void-space (air and water) in the ground material.

A.2 Preliminary oxygen consumption tests at University du Québec en Abitibi-Témiscamingue (UQAT)

A.2.1 Plexiglas columns dimensions: 300 mm in height

Internal diameter: 140mm

A.2.2 Test conditions:

Void ratio: 1

Porosity: 50%

Saturation degree: 40%

Thickness of compacted ground material: 10 or 15 cm

Headspace (air) volume/thickness: 20 or 15 cm

Temperature: 22°C

Testing time: 3h30min

Aggregate particle size: 150µm or 1.18mm

A.2.3 Tested aggregates: Maskimo, B&B, SBR, PKA

Maskimo aggregate	
Aggregate particle size	150 µm
Thickness of compacted ground material	15 cm
Headspace (air) volume/thickness	15 cm
GS	2.89 g/cm ³
Mass of aggregate	3337 g
Mass of water	462 g

Maskimo aggregate	
Aggregate particle size	150 µm
Thickness of compacted ground material	10 cm
Headspace (air) volume/thickness	20 cm
GS	2.89 g/cm ³
Mass of aggregate	2224 g
Mass of water	308 g

Maskimo aggregate	
Aggregate particle size	1.18 mm
Thickness of compacted ground material	10 cm
Headspace (air) volume/thickness	20 cm
GS	2.89 g/cm ³
Mass of aggregate	2224 g
Mass of water	308 g

SBR aggregate	
Aggregate particle size	150 μm
Thickness of compacted ground material	15 cm
Headspace (air) volume/thickness	15 cm
GS	2.91 g/cm ³
Mass of aggregate	3360 g
Mass of water	462 g

SBR aggregate	
Aggregate particle size	150 μm
Thickness of compacted ground material	15 cm
Headspace (air) volume/thickness	15 cm
GS	2.91 g/cm ³
Mass of aggregate	3360 g
Mass of water	462 g

B&B aggregate	
Aggregate particle size	150 μm
Compacted ground materials thickness	15 cm
Headspace (air) volume/thickness	15 cm
GS	3.05 g/cm ³
Mass of aggregate	3524 g
Mass of water	462 g

B&B aggregate	
Aggregate particle size	1.18 mm
Compacted ground materials thickness	15 cm
Headspace (air) volume/thickness	15 cm
GS	3.05 g/cm ³
Mass of aggregate	3524 g
Mass of water	462 g

PKA aggregate	
Aggregate particle size	150 μm
Compacted ground materials thickness	15 cm
Headspace (air) volume/thickness	15 cm
GS	2.78 g/cm ³
Mass of aggregate	3207 g
Mass of water	462 g

PKA aggregate	
Aggregate particle size	1.18 μm
Compacted ground material thickness	15 cm
Headspace (air) volume/thickness	15 cm
GS	2.78 g/cm ³
Mass of aggregate	3207 g
Mass of water	462 g

A.2.4 Results

Aggregate samples	Aggregate particle size	Compacted ground material thickness (cm)	Headspace (air) volume/thickness	O ₂ consumption (moles/m ² /year)
B&B	< 150 μm	15	15	1224
B&B	< 1.18 mm	15	15	265
Maskimo	< 150 μm	10	20	377
Maskimo	< 150 μm	15	15	939
Maskimo	< 1.18 mm	10	20	256
SBR	< 150 μm	15	15	153
SBR	< 1.18 μm	15	15	129
PKA	< 150 μm	15	15	23
PKA	< 1.18 mm	15	15	1

A.3 Preliminary oxygen consumption tests at Université Laval (Columns 200x147.4mm)

A.3.1 Plexiglas columns dimensions: 200 mm in height

Internal diameter: 147.1mm

A.3.2 Test conditions:

Void ratio: 1

Porosity: 50%

Saturation degree: 40% or 60%

Compacted ground material thickness: 2.5, 5 or 10 cm

Headspace (air) volume/thickness: 5, 10, 15, 17.5 cm

Temperature: 22°C

Testing time: 3h30min

Aggregate particle size: 1.18mm, mortar (0.149 mm < ϕ < 4.75mm), 150 μ m

A.3.3 Tested aggregates: Maskimo, B&B, SBR, GGP, PKA, SW, SPH, DLS

Maskimo aggregate (Saturation 40%)	
Aggregate particle size	1.18 mm
Compacted ground material thickness	10 cm
Headspace (air) volume/thickness	10 cm
GS	2.89 g/cm ³
Mass of aggregate	2274 g
Mass of water	315 g

Maskimo aggregate (Saturation 40%)	
Aggregate particle size	1.18 mm
Compacted ground material thickness	5 cm
Headspace (air) volume/thickness	15 cm
GS	2.89 g/cm ³
Mass of aggregate	1139 g
Mass of water	158 g

Maskimo aggregate (Saturation 40%)	
Aggregate particle size	1.18 mm
Compacted ground material thickness	5 cm
Headspace (air) volume/thickness	10 cm
GS	2.89 g/cm ³
Mass of aggregate	1139g
Mass of water	158g

Maskimo aggregate (Saturation 40%)	
Aggregate particle size	1.18 mm
Compacted ground material thickness	5 cm
Headspace (air) volume/thickness	5 cm
GS	2.89 g/cm ³
Mass of aggregate	1139 g
Mass of water	158 g

Maskimo aggregate (Saturation 40%)	
Aggregate particle size	1.18 mm
Compacted ground material thickness	2.5 cm
Headspace (air) volume/thickness	17.5 cm
GS	2.89 g/cm ³
Mass of aggregate	570 g
Mass of water	79 g

Maskimo aggregate (Saturation 40%)	
Aggregate particle size	1.18 mm
Compacted ground material thickness	2.5 cm
Headspace (air) volume/thickness	10 cm
GS	2.89 g/cm ³
Mass of aggregate	570 g
Mass of water	79 g

Maskimo aggregate (Saturation 40%)	
Aggregate particle size	1.18 mm
Compacted ground material thickness	2.5 cm
Headspace (air) volume/thickness	5 cm
GS	2.89 g/cm ³
Mass of aggregate	570 g
Mass of water	79 g

Maskimo aggregate (Saturation 60%)	
Aggregate particle size	1.18 mm
Compacted ground material thickness	5 cm
Headspace (air) volume/thickness	10 cm
GS	2.89 g/cm ³
Mass of aggregate	1139 g
Mass of water	237 g

Maskimo aggregate (Saturation 60%)	
Aggregate particle size	1.18 mm
Compacted ground material thickness	5 cm
Headspace (air) volume/thickness	5 cm
GS	2.89 g/cm ³
Mass of aggregate	1139 g
Mass of water	237 g

Maskimo aggregate (Saturation 40%)	
Aggregate particle size	mortar
Compacted ground material thickness	5 cm
Headspace (air) volume/thickness	15 cm
GS	2.89 g/cm ³
Mass of aggregate	1139 g
Mass of water	158 g

GGP aggregate (Saturation 40%)	
Aggregate particle size	mortar
Compacted ground material thickness	5 cm
Headspace (air) volume/thickness	15 cm
GS	2.93 g/cm ³
Mass of aggregate	1115 g
Mass of water	158 g

SBR aggregate (Saturation 40%)	
Aggregate particle size	mortar
Compacted ground material thickness	5 cm
Headspace (air) volume/thickness	15 cm
GS	2.91 g/cm ³
Mass of aggregate	1148 g
Mass of water	158 g

B&B aggregate (Saturation 40%)	
Aggregate particle size	mortar
Compacted ground material thickness	5 cm
Headspace (air) volume/thickness	15 cm
GS	3.05 g/cm ³
Mass of aggregate	1203 g
Mass of water	158 g

PKA aggregate (Saturation 40%)	
Aggregate particle size	mortar
Compacted ground material thickness	5 cm
Headspace (air) volume/thickness	15 cm
GS	2.78 g/cm ³
Mass of aggregate	1095 g
Mass of water	158 g

DLS aggregate (Saturation 40%)	
Aggregate particle size	mortar
Compacted ground material thickness	5 cm
Headspace (air) volume/thickness	15 cm
GS	2.78g/cm ³
Mass of aggregate	1096 g
Mass of water	158 g

SW aggregate (Saturation 40%)	
Aggregate particle size	<1.18 mm
Compacted ground material thickness	5 cm
Headspace (air) volume/thickness	15 cm
GS	2.72 g/cm ³
Mass of aggregate	1074 g
Mass of water	158 g

SPH aggregate (Saturation 40%)	
Aggregate particle size	<1.18 mm
Compacted ground material thickness	5 cm
Headspace (air) volume/thickness	15 cm
GS	2.82 g/cm ³
Mass of aggregate	1112 g
Mass of water	158 g

GGP aggregate (Saturation 40%)	
Aggregate particle size	<1.18 mm
Compacted ground material thickness	5 cm
Headspace (air) volume/thickness	15 cm
GS	2.93 g/cm ³
Mass of aggregate	1155 g
Mass of water	158 g

SBR aggregate (Saturation 40%)	
Aggregate particle size	<1.18 mm
Compacted ground material thickness	5 cm
Headspace (air) volume/thickness	15 cm
GS	2.91 g/cm ³
Mass of aggregate	1148 g
Mass of water	158 g

B&B aggregate (Saturation 40%)	
Aggregate particle size	<1.18 mm
Compacted ground material thickness	5 cm
Headspace (air) volume/thickness	15 cm
GS	3.05 g/cm ³
Mass of aggregate	1203 g
Mass of water	158 g

PKA aggregate (Saturation 40%)	
Aggregate particle size	<1.18 mm
Compacted ground material thickness	5 cm
Headspace (air) volume/thickness	15 cm
GS	2.78 g/cm ³
Mass of aggregate	1095 g
Mass of water	158 g

DLS aggregate (Saturation 40%)	
Aggregate particle size	<1.18 mm
Compacted ground material thickness	5 cm
Headspace (air) volume/thickness	15 cm
GS	2.78 g/cm ³
Mass of aggregate	1096 g
Mass of water	158 g

SW aggregate (Saturation 40%)	
Aggregate particle size	<150 µm
Compacted ground material thickness	5 cm
Headspace (air) volume/thickness	15 cm
GS	2.72 g/cm ³
Mass of aggregate	1074 g
Mass of water	158 g

SPH aggregate (Saturation 40%)	
Aggregate particle size	<150 μm
Compacted ground material thickness	5 cm
Headspace (air) volume/thickness	15 cm
GS	2.82 g/cm ³
Mass of aggregate	1112 g
Mass of water	158 g

GGP aggregate (Saturation 40%)	
Aggregate particle size	<150 μm
Compacted ground material thickness	5 cm
Headspace (air) volume/thickness	15 cm
GS	2.93 g/cm ³
Mass of aggregate	1155 g
Mass of water	158 g

SBR aggregate (Saturation 40%)	
Aggregate particle size	<150 μm
Compacted ground material thickness	5 cm
Headspace (air) volume/thickness	15 cm
GS	2.91 g/cm ³
Mass of aggregate	1148 g
Mass of water	158 g

MSK aggregate (Saturation 40%)	
Aggregate particle size	<150 μm
Compacted ground material thickness	5 cm
Headspace (air) volume/thickness	15 cm
GS	2.89 g/cm ³
Mass of aggregate	1139 g
Mass of water	158 g

B&B aggregate (Saturation 40%)	
Aggregate particle size	<150 μm
Compacted ground material thickness	5 cm
Headspace (air) volume/thickness	15 cm
GS	3.05 g/cm ³
Mass of aggregate	1203 g
Mass of water	158 g

PKA aggregate (Saturation 40%)	
Aggregate particle size	<150 μm
Compacted ground material thickness	5 cm
Headspace (air) volume/thickness	15 cm
GS	2.87 g/cm ³
Mass of aggregate	1095 g
Mass of water	158 g

DLS aggregate (Saturation 40%)	
Aggregate particle size	<150 μm
Compacted ground material thickness	5 cm
Headspace (air) volume/thickness	15 cm
GS	2.87 g/cm ³
Mass of aggregate	1096 g
Mass of water	1095 g

A.3.4 Results

A.3.4.1 40% saturation vs. 60% saturation

	Maskimo aggregate (Aggregate particle size <1.18mm)								
	40% saturation							60% saturation	
Aggregate thickness	10 cm	5cm			2.5 cm			5cm	
Headspace	10 cm	15 cm	10 cm	5 cm	17.5cm	10 cm	5 cm	10 cm	5 cm
O ₂ consumption (moles/ m ² /year)	289	156	126	83	99	58	27	-1	8

A.3.4.2 Mortar vs. $\phi < 1.18$ mm vs. $\phi < 150\mu\text{m}$; 40% saturation ; aggregate thickness: 5cm; headspace: 15cm

		Sulfide-bearing aggregates					Control aggregates		
		SW	SPH	GGP	SBR	MSK	B&B	PKA	DLS
Mortar	O ₂ consumption (moles/ m ² /year)	---	---	25	35	41	61	0	---
	S _T (% by mass)	---	---	0.33	0.87	0.84	3.68	0.04	---
$\phi < 1.18$ mm	O ₂ consumption (moles/ m ² /year)	105	40	122	160	156	223	14	31
	S _T (% by mass)	0.05	0.24	0.30	0.81	1.28	2.13	0.04	0.12
$\phi < 150\mu\text{m}$	O ₂ consumption (moles/ m ² /year)	202	75	182	176	267	282	91	92
	S _T (% by mass)	0.05	0.09	0.29	0.78	0.73	4.22	0.05	0.09

A.4 Preliminary oxygen consumption tests at Université Laval (Columns 300 x 200mm)

A.4.1 Plexiglas columns dimensions: 310 mm in height

Internal diameter: 200mm

A.4.2 Test conditions:

Void ratio: 1

Porosity: 50%

Saturation degree: 40%

Compacted ground material thickness: 3 cm

Headspace (air) volume/thickness: 28 cm

Temperature: 22°C

Testing time: 3h30 min

Aggregate particle size: 150 µm

A.4.3 Tested aggregates: Maskimo, SBR, PKA

Maskimo aggregate (Saturation 40%)	
Aggregate particle size	<150 µm
Compacted ground material thickness	3 cm
Headspace (air) volume/thickness	20.8 cm
GS	2.89 g/cm ³
Mass of aggregate	1362 g
Mass of water	188 g

SBR aggregate (Saturation 40%)	
Aggregate particle size	<150 µm
Compacted ground material thickness	3 cm
Headspace (air) volume/thickness	20.8 cm
GS	2.91 g/cm ³
Mass of aggregate	1372 g
Mass of water	188 g

PKA aggregate (Saturation 40%)	
Aggregate particle size	<150 μm
Compacted ground material thickness	3 cm
Headspace (air) volume/thickness	20.8 cm
GS	2.87 g/cm ³
Mass of aggregate	1309 g
Mass of water	188 g

A.4.4 Results

	O ₂ consumption (moles/ m ² /year)		
	Maskimo	PKA	SBR
1 st test	174	67	54
S _T (% by mass)	1.01	0.06	0.90
2 nd test	156	-9	-36
S _T (% by mass)	1.016	0.06	0.91

A.5. Oxygen consumption tests at Université Laval with optimized parameters

A.5.1 Plexiglas columns dimensions: 200 mm in height

Internal diameter: 147.1mm

A.5.2 Test conditions:

Void ratio: 1

Porosity: 50%

Saturation degree: 40%

Compacted ground material thickness: 10 cm

Headspace (air) volume/thickness: 10 cm

Temperature: 22°C

Testing time: 3h30min

Aggregate particle size: <150 μm

A.5.3 Tested aggregates: Maskimo, SPH, GGP, SW, SBR, SDBR, DLS, PKA, HPL

Maskimo aggregate	
Aggregate particle size	150 μm
Compacted ground material thickness	10 cm
Headspace (air) volume/thickness	10 cm
GS	2.89 g/cm ³
Mass of aggregate	2279 g
Mass of water	315 g

SPH aggregate	
Aggregate particle size	150 μm
Compacted ground material thickness	10 cm
Headspace (air) volume/thickness	10 cm
GS	2.82 g/cm ³
Mass of aggregate	2224 g
Mass of water	315 g

GGP aggregate	
Aggregate particle size	150 μm
Compacted ground material thickness	10 cm
Headspace (air) volume/thickness	10 cm
GS	2.93 g/cm ³
Mass of aggregate	2310 g
Mass of water	315 g

SW aggregate	
Aggregate particle size	150 μm
Compacted ground material thickness	10 cm
Headspace (air) volume/thickness	10 cm
GS	2.72 g/cm ³
Mass of aggregate	2145 g
Mass of water	315 g

SBR aggregate	
Aggregate particle size	150 μm
Compacted ground material thickness	10 cm
Headspace (air) volume/thickness	10 cm
GS	2.91 g/cm ³
Mass of aggregate	2295 g
Mass of water	315 g

SDBR aggregate	
Aggregate particle size	150 μm
Compacted ground material thickness	10 cm
Headspace (air) volume/thickness	10 cm
GS	3.26 g/cm ³
Mass of aggregate	2570 g
Mass of water	315 g

DLS aggregate	
Aggregate particle size	150 μm
Compacted ground material thickness	10 cm
Headspace (air) volume/thickness	10 cm
GS	2.78 g/cm ³
Mass of aggregate	2192 g
Mass of water	315 g

PKA aggregate	
Aggregate particle size	150 μm
Compacted ground material thickness	10 cm
Headspace (air) volume/thickness	10 cm
GS	2.78 g/cm ³
Mass of aggregate	2192 g
Mass of water	315 g

HPL aggregate	
Aggregate particle size	150 μm
Compacted ground material thickness	10 cm
Headspace (air) volume/thickness	10 cm
GS	2.95 g/cm ³
Mass of aggregate	2326 g
Mass of water	315 g

A.5.4 Results

Aggregates		Oxygen cons. (moles/ m ² /year)		Oxygen cons. (%)		S _T (% by mass)	
	Tests →	1	2	1	2	1	2
Sulfide-bearing aggregates	SPH	112	111	6.2	6.2	0.32	0.29
	GGP	133	151	5.4	6.0	0.25	0.24
	SW	174	169	8.2	8.2	0.07	0.07
	SBR	226	243	10.7	10.8	0.87	0.75
	MSK	577	558	21.7	21.4	0.99	1.11
	SDBR	2006	1932	57.0	55.5	13.86	14.46
Control aggregates (no sulfide)	DLS	45	6	3.0	0.2	0.12	0.19
	PKA	65	71	2.6	2.8	0.04	0.06
	HPL	13	2.6E ⁻⁵	1.7	0.2	0.02	0.02

A.5.5 Test reproducibility

A.5.5.1 Samples prepared by different operators with the same measuring probe

Maskimo aggregate	
Aggregate particle size	150 μm
Compacted ground material thickness	10 cm
Headspace (air) volume/thickness	10 cm
GS	2.89 g/cm ³
Mass of aggregate	2279 g
Mass of water	315 g

	Maskimo (40% saturation)		
	Operator 1	Operator 2	Operator 3
Oxygen cons. (%)	22.7	21.8	22.8
S (% by mass)	1.15	1.09	1.13

A.5.5.2 Samples prepared by the same operator using different probes

	Maskimo (40% saturation)		
	Probe 1	Probe 2	Probe 3
Oxygen cons. (%)	21.7	21.9	21.8
S (% by mass)	0.99	1.07	1.05

Appendix B

Mortar bar expansion test

B1: Introduction

This appendix presents all the expansion values and respective graphics obtained during the development of the mortar bar expansion test.

Preliminary tests were conducted on concrete core slices, of 10 cm diameter and 2.5 cm of thickness, cut and polished from concrete cores from the problematic house foundations of the Trois-Rivières region, whose aggregate came from St. Boniface. The purpose of these tests was to identify and better understand the various parameters (e.g. exposure conditions) that may influence the iron sulfides oxidation reactions (Section B2). These preliminary tests have as main purpose to guide the test conditions for the performance test on mortar bars.

After the results obtained in the section B2, an experimental program was developed to determine the conditions favoring the deterioration of concrete containing aggregates rich in sulfide minerals using mortar bars expansion test (section B3).

B2: Concrete core slices

B2.1 Test conditions:

- Temperature: 4°C, 21°C, 38°C, 60°C
- Relative humidity (RH): 60%, 80%, non controlled
- Immersion solutions: bleach (6%), peroxide (3%), tap water

B2.2 Storage conditions

- 4°C/60% RH: concrete core slices stored above oversaturated solution of cane sugar in air-tight container.
- 4°C/80% RH: concrete core slices stored above oversaturated solution of NaCl in air-tight container.
- 4°C, non controlled RH: concrete core slices stored inside a fridge.
- 21°C/80% RH: concrete core slices stored above oversaturated solution of $\text{Co}(\text{NH}_2)_2$ in air-tight container.
- 21°C/60% RH: concrete core slices stored above oversaturated solution of $\text{Ca}(\text{NO}_3)_2 \cdot 4\text{H}_2\text{O}$ in air-tight container.

- 21°C, non controlled RH: concrete core slices stored at room temperature
- 38°C/60% RH: concrete core slices above oversaturated solution of $\text{CoCl}_2 \cdot 6\text{H}_2\text{O}$ in air-tight container
- 38°C/80% RH: concrete core slices stored above oversaturated solution of KBr in an air-tight container.
- 38°C, non controlled RH: concrete core slices stored in a chamber at 38°C
- 60°C/60% RH: concrete core slices stored above oversaturated solution of $\text{CaCl}_2 \cdot 6\text{H}_2\text{O}$ in an air-tight container.
- 60°C/80% RH: concrete core slices stored above oversaturated solution of KCl in an air-tight container.
- 60°C, non controlled RH: concrete core slices stored in a oven at 60°C.

B2.3 Measurements

- Measurements of mass and diameter were taken three times per week.
- After immersing the concrete core slices in the respective solution (bleach, peroxide or tap water) for a period of 3 hours, the bars are removed and placed on a tray over a cloth.
- The mass and diameter measurements are taken within 5 minutes following the previous step. The measurements are taken three times a week.
- Then, the concrete core slices are placed on egg crate plastic pieces, exposed to air, under the hood ($21 \pm 2^\circ\text{C}$) for a period of 3 hours (± 5 minutes).
- Finally, the concrete core slices are replaced in their respective storage conditions.

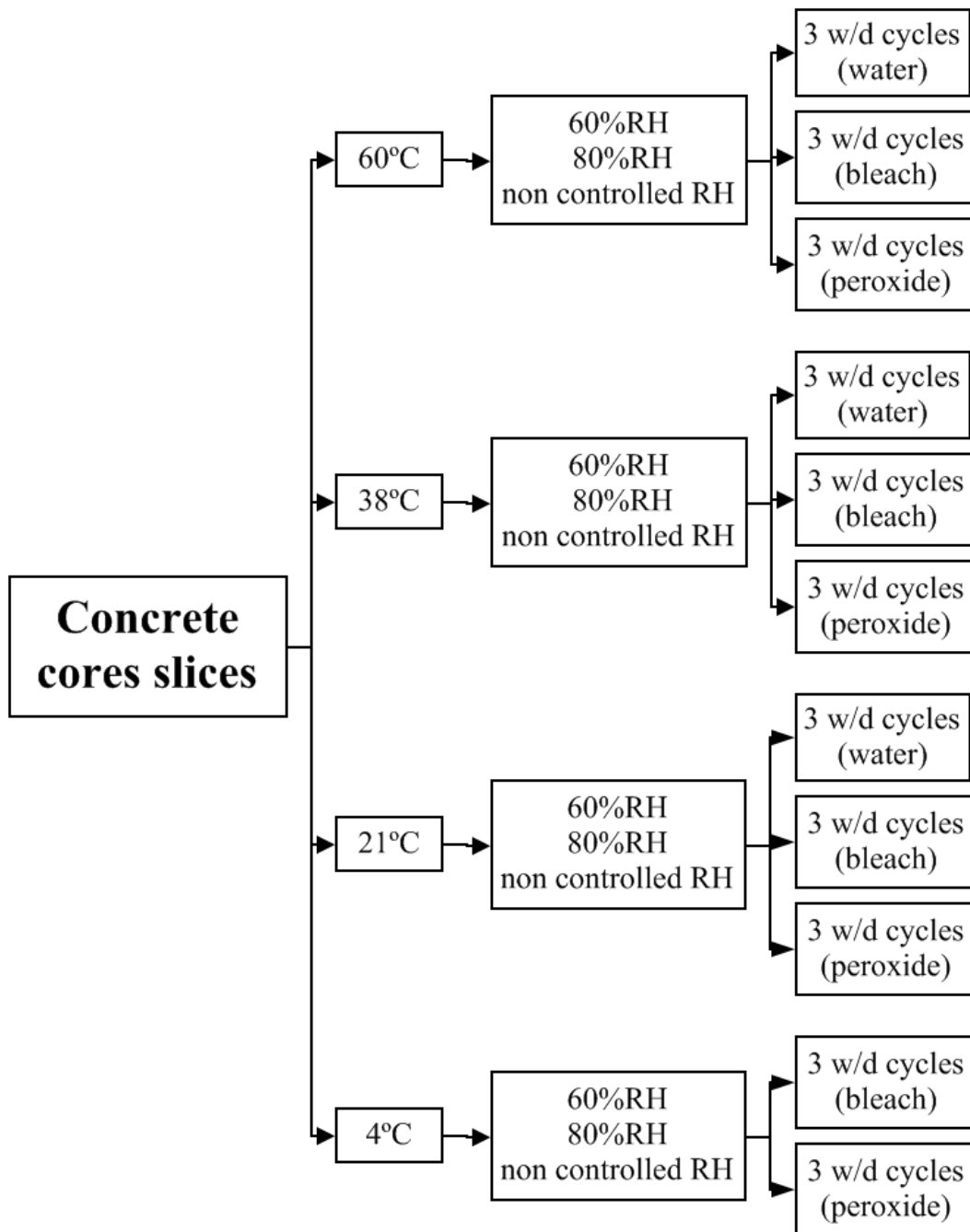


Figure B.1: Experimental program flowchart - testing conditions for the concrete cores slice.

B2.4 Concrete core slices stored at 4°C, 60% RH, with immersion (three times per week) in bleach (6%) solution.



0 days



7 days



26 days



26 days



68 days



68 days

B2.5 Concrete core slices stored at 4°C, 80% RH, with immersion (three times per week) in bleach (6%) solution.



0 days



7 days



26 days



26 days



61 days



61 days

B2.6 Concrete core slices stored at 4°C, 60% RH, with immersion (three times per week) in peroxide (3%) solution.



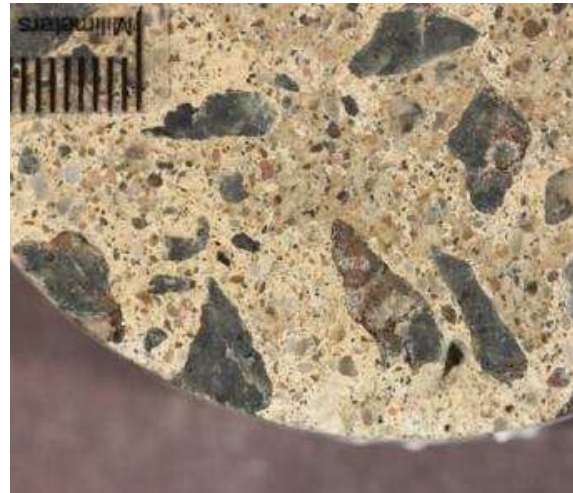
0 days



7 days



339 days



339 days

B2.7 Concrete core slices stored at 4°C, 80% RH, with immersion (three times per week) in peroxide (3%) solution.



0 days



7 days



339 days



339 days

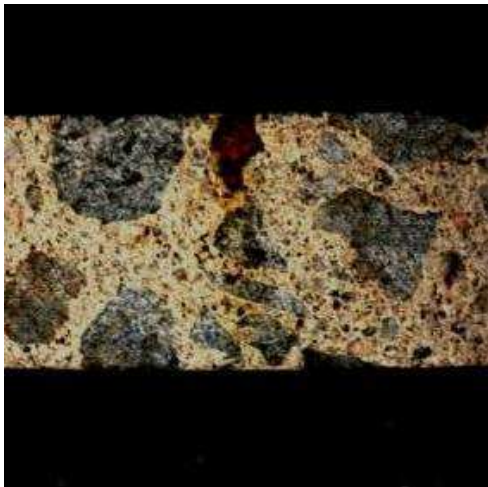
B2.8 Concrete core slices stored at 4°C, non controlled RH, with immersion (three times per week) in peroxide (3%) solution.



0 days



7 days



185 days



185 days



339 days



339 days

B2.9 Concrete core slices stored at 4°C, non controlled RH, with immersion (three times per week) in bleach (6%) solution.



0 days



7 days



26 days



26 days



68 days



82 days

B2.10 Concrete core slices stored at 21°C, 60% RH, with immersion (three times per week) in tap water.



0 days



7 days



339 days

B2.11 Concrete core slices stored at 21°C, 80% RH, with immersion (three times per week) in tap water



0 days



339 days

B2.12 Concrete core slices stored at 21°C, non controlled RH, with immersion (three times per week) in tap water.



0 days



7 days



339 days

B2.13 Concrete core slices stored at 21°C, 60% RH, with immersion (three times per week) in peroxide (3%) solution.



0 days



7 days



339 days



339 days

B2.14 Concrete core slices stored at 21°C, 60% RH, with immersion (three times per week) in bleach (6%) solution.



0 days



7 days



26 days



26 days



54 days

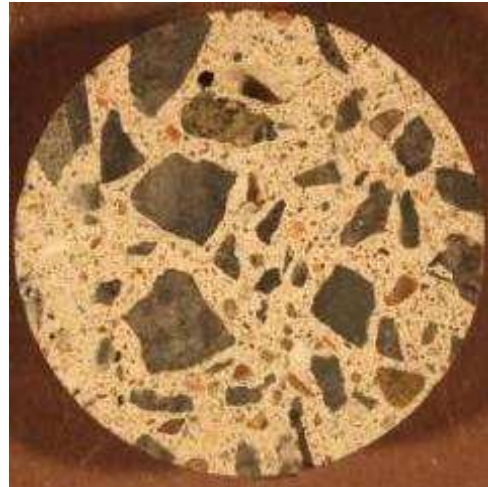


68 days

B2.15 Concrete core slices stored at 21°C, 80% RH, with immersion (three times per week) in peroxide (3%) solution.



0 days



7 days



185 days



339 days



339 days



339 days

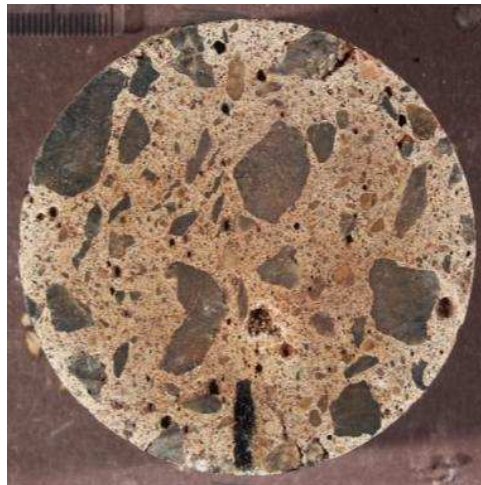
B2.16 Concrete core slices stored at 21°C, 80% RH, with immersion (three times per week) in bleach (6%) solution.



0 days



7 days



26 days



54 days



61 days



68 days

B2.17 Concrete core slices stored at 21°C, non controlled RH, with immersion (three times per week) in peroxide (3%) solution.



0 days



7 days



185 days



185 days



339 days



339 days

B2.18 Concrete core slices stored at 21°C, non controlled RH, with immersion (three times per week) in bleach (6%) solution.



0 days



7 days



26 days



54 days



61 days



68 days

B2.19 Concrete core slices stored at 38°C, 60% RH, with immersion (three times per week) in tap water.



0 days



7 days



339 days

B2.20 Concrete core slices stored at 38°C, 60% RH, with immersion (three times per week) in peroxide (3%) solution.



0 days



7 days



339 days



339 days

B2.21 Concrete core slices stored at 38°C, 60% RH, with immersion (three times per week) in bleach (6%) solution.



0 days



7 days



26 days



26 days



61 days



61 days

B2.22 Concrete core slices stored at 38°C, 80% RH, with immersion (three times per week) in peroxide (3%) solution.



0 days



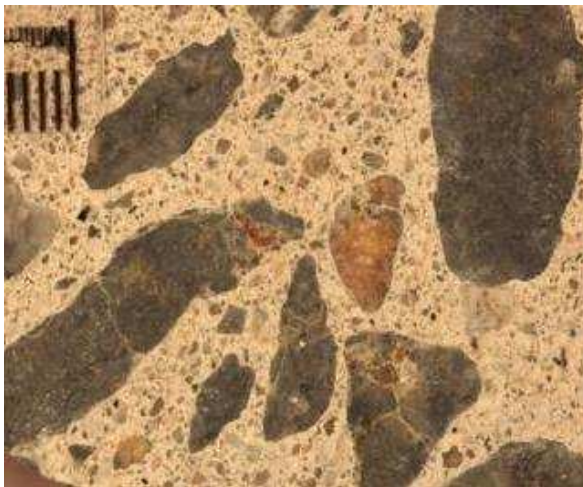
7 days



339 days



339 days



339 days

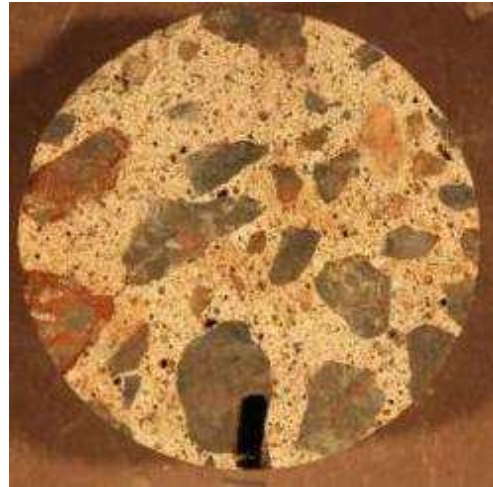


339 days

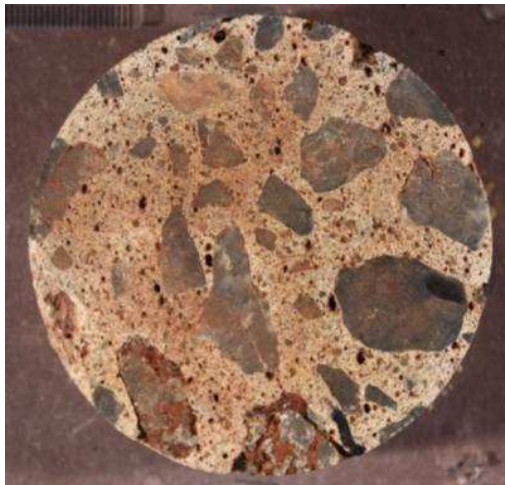
B2.23 Concrete core slices stored at 38°C, 80% RH, with immersion (three times per week) in bleach (6%) solution.



0 days



7 days



26 days



26 days



61 days



68 days

B2.24 Concrete core slices stored at 38°C, non controlled RH, with immersion (three times per week) in tap water.



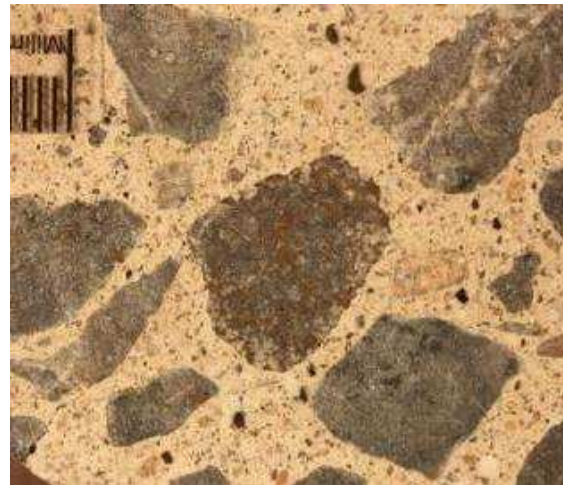
0 days



7 days



339 days



339 days

B2.25 Concrete core slices stored at 38°C, non controlled RH, with immersion (three times per week) in peroxide (3%) solution.



0 days



7 days



185 days



185 days



339 days



339 days

B2.26 Concrete core slices stored at 38°C, non controlled RH, with immersion (three times per week) in bleach (6%) solution.



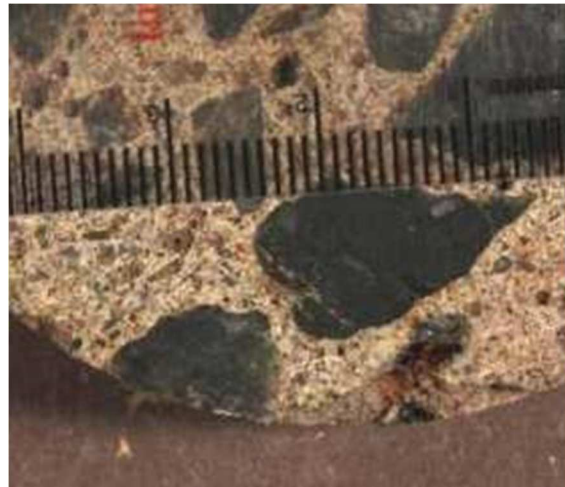
0 days



7 days



26 days



26 days



61 days



61 days

B2.27 Concrete core slices stored at 60°C, 60% RH, with immersion (three times per week) in tap water.



0 days

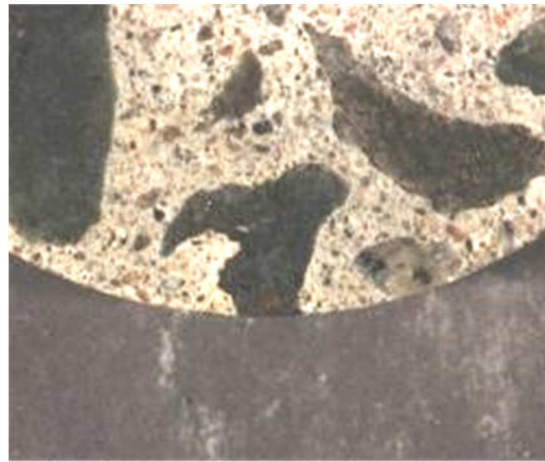


339 days

B2.28 Concrete core slices stored at 60°C, 60% RH, with immersion (three times per week) in peroxide (3%) solution.



0 days



185 days



339 days



339 days

B2.29 Concrete core slices stored at 60°C, 60% RH, with immersion (three times per week) in bleach (6%) solution.



0 days



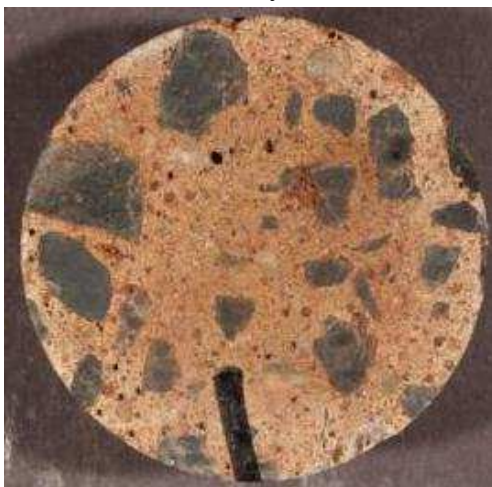
54 days



54 days



68 days

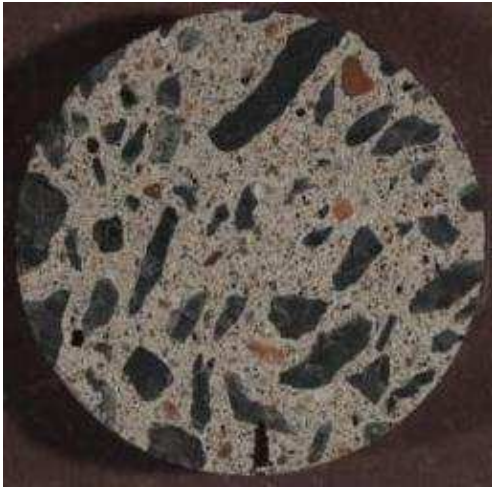


119 days



119 days

B2.30 Concrete core slices stored at 60°C, 80% RH, with immersion (three times per week) in tap water



0 days



339 days



339 days

B2.31 Concrete core slices stored at 60°C, 80% RH, with immersion (three times per week) in peroxide (3%) solution.



0 days

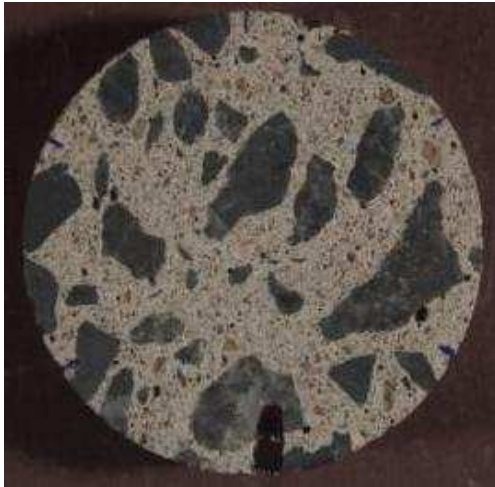


339 days



339 days

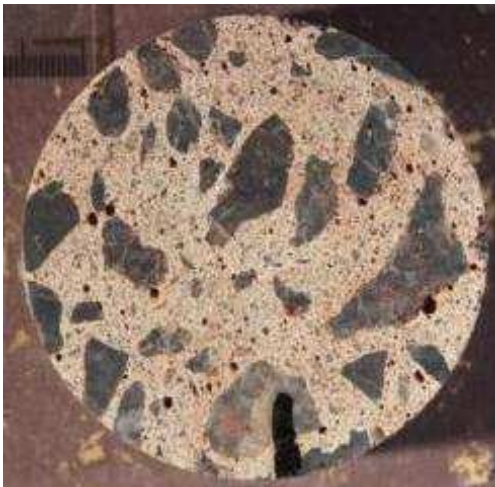
B2.32 Concrete core slices stored at 60°C, 80% RH, with immersion (three times per week) in bleach (6%) solution.



0 days



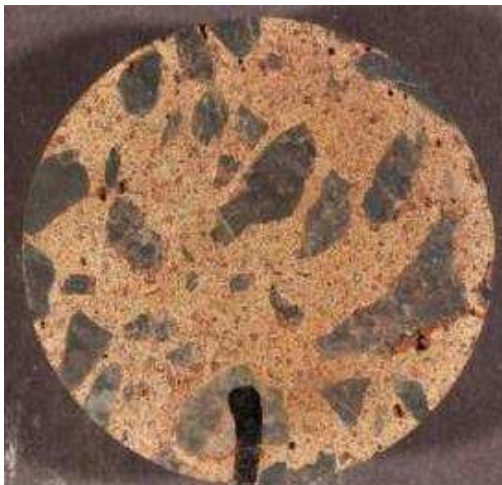
7 days



68 days



82 days



119 days



119 days

B2.33 Concrete core slices stored at 60°C, non controlled RH, with immersion (three times per week) in tap water.



0 days



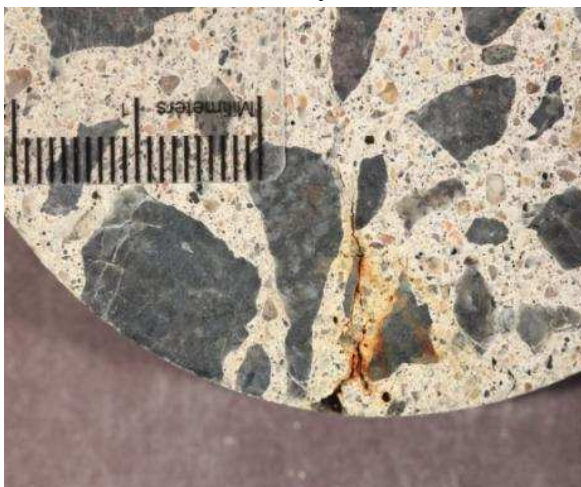
49 days



339 days



339 days



339 days

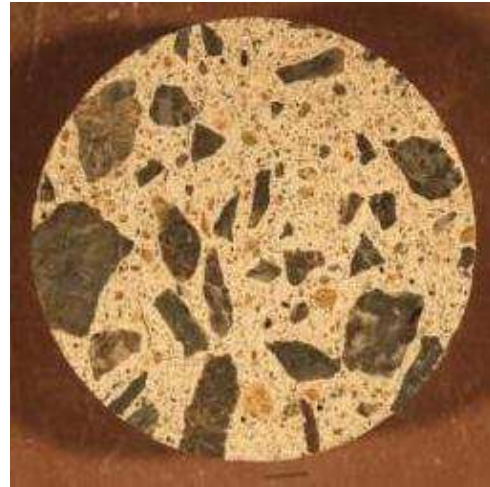


339 days

B2.34 Concrete core slices stored at 60°C, non controlled RH, with immersion (three times per week) in peroxide (3%) solution.



0 days



7 days



185 days



339 days



339 days



339 days

B2.35 Concrete core slices stored at 60°C, non controlled, with immersion (three times per week) in bleach (6%) solution.



0 days



7 days



26 days



82 days



101 days



101days

B3: Mortar bars

B3.1 Introduction

All aggregates used in these tests were separated into the various sieve sizes (Table B1). Each size fraction was then washed with a water spray over the “retaining” sieve to remove adhering dust and fine particles from the aggregate. The material retained on the various sieves was then dried at 80°C overnight and, unless used immediately, stored in a clean and air-tight bag.

The mortar bars were manufactured in accordance with the procedure described in the CSA A23.2-25A test procedure (Accelerated Mortar Bar Test). Then, the mortar bars were kept in their moulds for 48 hours, covered with wet burlap and a plastic sheet, and the bars were stripped. After that, the bars were placed in a moist chamber (23°C) protected from excess (water dripping) moisture, for another 24 hours.

The mix design proportions were kept constant for all the conditions and aggregates tested (Table B1). All mortar bars, 25 x 25x 285 mm in size, were made with a w/c of 0.65 in order to reproduce the porous nature of the housing foundation concretes suffering from iron sulfide oxidation in the Trois-Rivières area. A cement-to-aggregate ratio of 1: 2.73 was used, i.e. slightly higher than the 1: 2.25 value used in CSA A23.2-25A due to the higher density of the sulfide-bearing aggregates. However, the types and proportions of the different aggregate size fractions were the same as those specified in CSA A23.2-25A. All mortar bars were made with an ordinary (Type GU) portland cement.

In order to achieve the proper conditions selected for this study, the samples were kept under controlled temperature and humidity conditions using environmental chambers or using oversaturated solutions of salts into hermetic containers.

Table B. 1: Mix design proportions and aggregate particle size.

		Mass (g)
Cement type: GU		440
Water		268
Aggregate sieve sizes	Proportions	Mass
particles -4 +8	10%	120g
particles -8 +16	25%	300g
particles -16 +30	25%	300g
particles -30 +50	25%	300g
particles -50 + 100	15%	180g

B3.2. Conditions tested

- Temperature: 4°C, 8°C, 23°C, 38°C, 60°C and 80°C
- Relative humidity (RH): 60%, 80% and 100%
- Immersion solutions: 6% sodium hypochlorite (bleach) solution, peroxide (3%), tap water

B3.3 Measurements

- After immersing the bars in the respective solution (bleach, peroxide or tap water) for a period of 3 hours, the bars are removed and placed on a tray over a cloth.
- The studs are dried/ cleaned with a cloth.
- The mass and length measurements are taken within 5 minutes following the previous step. The measurements are taken one or twice a week.
- Then, the bars are placed on egg crate plastic pieces, exposed to air, under the hood ($23 \pm 2^\circ\text{C}$) for a period of 3 hours (± 5 minutes).
- Finally, the bars are replaced in their respective storage conditions.

B4 Preliminary tests: series 1

B4.1 Test conditions:

- Temperature: 8°C, 23°C, 38°C, 60°C
- Relative humidity (RH): 60%
- Immersion solutions: bleach (6%), peroxide (3%)

B4.2 Aggregates tested:

- MSK
- HPL (control aggregate)

B4.3 Storage conditions

- 8°C/60% RH: bars stored in an environmental test chamber
- 23°C/60% RH: bars stored above oversaturated solution of $\text{Ca}(\text{NO}_3)_2 \cdot 4\text{H}_2\text{O}$ in air-tight container
- 38°C/60% RH: bars stored above oversaturated solution of $\text{CoCl}_2 \cdot 6\text{H}_2\text{O}$ in air-tight container
- 60°C/60% RH: bars stored in an environmental test chamber

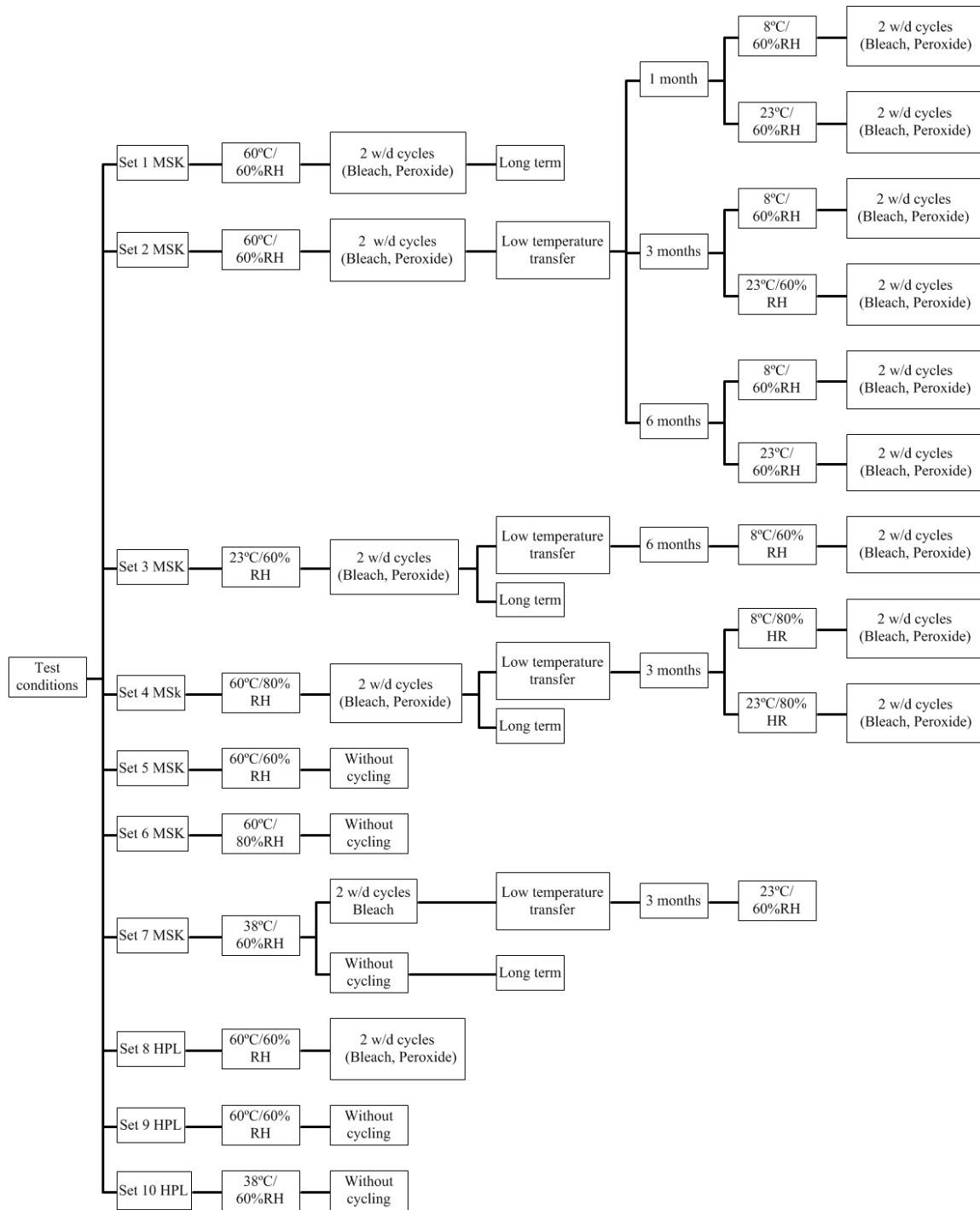


Figure B.2: Experimental program flowchart - testing conditions for the first series

B4.4 Results

B4.4.1 Expansion values (%); first series

Table B. 2: Expansion values (%) of Set 1 (MSK1) mortar specimens stored at 60°C/60% RH, with immersion (twice per week) in bleach (6%) (Bl) or hydrogen peroxide (3%) (Px) solutions. Set 5 (MSK5) mortar specimens are stored at 60°C/60% RH, without immersion (no cycling). Average values for each series of 3 bars in grey.

Mortar bars	Expansion (%) as function as time (days)								
	0	7	10	20	28	35	42	52	60
MSK1-1	0	-0.02	-0.01	-0.01	-0.01	-0.01	-0.01	0.00	0.00
MSK1-2	0	-0.02	-0.02	-0.01	-0.01	-0.01	-0.02	-0.02	-0.02
MSK1-3	0	-0.02	-0.02	-0.02	-0.02	-0.02	-0.02	-0.02	-0.02
MSK1 (2 cycles Bl)	0	-0.02	-0.02	-0.01	-0.01	-0.01	-0.01	-0.01	-0.01
MSK1-4	0	-0.03	-0.03	-0.03	-0.03	-0.03	-0.03	-0.03	-0.04
MSK1-5	0	-0.03	-0.03	-0.02	-0.02	-0.02	-0.02	-0.02	-0.02
MSK1-6	0	-0.03	-0.04	-0.03	-0.03	-0.03	-0.03	-0.03	-0.03
MSK1 (2 cycles Px)	0	-0.03	-0.03	-0.03	-0.03	-0.03	-0.03	-0.03	-0.03
MSK5-1	0	-0.05	-0.04	-0.05	-0.05	-0.05	-0.04	-0.06	-0.06
MSK5-2	0	-0.04	-0.04	-0.05	-0.05	-0.05	-0.04	-0.06	-0.06
MSK5-3	0	-0.05	-0.04	-0.05	-0.05	-0.04	-0.04	-0.05	-0.05
MSK5 (no cycling)	0	-0.05	-0.04	-0.05	-0.05	-0.05	-0.04	-0.06	-0.06

Table B.2 (continued): Expansion values (%) of Set 1 and Set 5 mortar bars.

Mortar bars	Expansion (%) as function as time (days)								
	66	73	91	102	115	129	147	164	200
MSK1-1	0.00	0.00	0.00	0.00	0.01	0.02	0.03	0.03	0.05
MSK1-2	-0.02	-0.01	-0.02	-0.01	0.00	0.00	0.01	0.02	0.04
MSK1-3	-0.02	-0.02	-0.03	-0.03	-0.02	-0.02	-0.02	-0.01	0.04
MSK1 (2 cycles Bl)	-0.01	-0.01	-0.02	-0.01	0.00	0.00	0.01	0.01	0.04
MSK1-4	-0.03	-0.03	-0.04	-0.04	-0.04	-0.05	-0.05	-0.05	-0.06
MSK1-5	-0.02	-0.02	-0.03	-0.03	-0.03	-0.04	-0.04	-0.04	-0.05
MSK1-6	-0.03	-0.03	-0.03	-0.04	-0.04	-0.04	-0.04	-0.04	-0.05
MSK1 (2 cycles Px)	-0.03	-0.03	-0.03	-0.04	-0.04	-0.05	-0.05	-0.04	-0.05
MSK5-1	-0.06	-0.06	-0.07	-0.07	-0.07	-0.07	-0.07	-0.07	-0.07
MSK5-2	-0.06	-0.06	-0.07	-0.07	-0.07	-0.06	-0.06	-0.06	-0.07
MSK5-3	-0.05	-0.05	-0.07	-0.06	-0.06	-0.05	-0.07	-0.06	-0.07
MSK5 (no cycling)	-0.06	-0.06	-0.07	-0.07	-0.07	-0.06	-0.07	-0.06	-0.07

Table B2 (continued): Expansion values (%) of Set 1 and Set 5 mortar bars.

Mortar bars	Expansion (%) as a function of time (days)	
	228	250
MSK1-1	0.06	0.08
MSK1-2	0.05	0.07
MSK1-3	0.08	0.13
MSK1 (2 cycles Bl)	0.06	0.09
MSK1-4	-0.05	-0.05
MSK1-5	-0.05	-0.06
MSK1-6	-0.05	-0.05
MSK1 (2 cycles Px)	-0.05	-0.05
MSK5-1	-0.07	-0.07
MSK5-2	-0.07	-0.06
MSK5-3	-0.06	-0.06
MSK5 (no cycling)	-0.06	-0.06

Table B. 3: Expansion values (%) of Set 2 (MSK2) mortar specimens stored at 60°C/60% RH, with immersion (twice per week) in bleach (6%) (Bl) solution. The different sub-sets of bars were transferred at either 8°C/60% RH or 23°C/60% after 1, 3 or 6 months, while pursuing the immersion (twice per week) in bleach (6%) (i.e. same immersion solution as before the temperature transfer). Average values for each series of 3 bars in grey.

Mortar bars	Expansion (%) as a function of time (days)							
	0	3	6	10	20	28	35	42
MSK2-1	0.00	-0.02	-0.01	-0.01	-0.01	0.00	0.00	0.00
MSK2-2	0.00	-0.02	-0.02	-0.01	-0.01	-0.01	-0.01	0.00
MSK2-3	0.00	-0.02	-0.02	-0.01	-0.01	0.00	-0.01	0.00
MSK2 (2 cycles Bl→1 m 8°C)	0.00	-0.02	-0.01	-0.01	-0.01	0.00	0.00	0.00
MSK2-4	0.00	-0.01	-0.01	-0.02	0.03	0.06	0.07	0.06
MSK2-5	0.00	-0.02	-0.02	-0.01	0.00	0.00	0.00	0.00
MSK2-6	0.00	-0.01	-0.02	-0.02	-0.01	-0.01	-0.06	-0.07
MSK2 (2 cycles Bl→1 m 23°C)	0.00	-0.01	-0.02	-0.01	0.01	0.02	0.00	0.00
MSK2-7	0.00	-0.02	-0.02	-0.01	-0.01	-0.01	-0.01	-0.01
MSK2-8	0.00	-0.02	-0.02	-0.01	-0.01	-0.01	-0.01	-0.01
MSK2-9	0.00	-0.01	-0.02	-0.01	-0.01	-0.01	-0.01	-0.01
MSK2 (2 cycles Bl→3 m 8°C)	0.00	-0.02	-0.02	-0.01	-0.01	-0.01	-0.01	-0.01
MSK2-10	0.00	-0.01	-0.02	-0.02	-0.02	-0.02	-0.02	-0.01
MSK2-11	0.00	-0.01	-0.02	-0.01	-0.01	-0.01	-0.01	-0.01
MSK2-12	0.00	-0.02	-0.02	-0.01	-0.01	-0.01	-0.01	-0.01
MSK2 (2 cycles Bl→3 m 23°C)	0.00	-0.01	-0.02	-0.01	-0.01	-0.01	-0.01	-0.01
MSK2-13	0.00	-0.01	-0.02	-0.01	-0.02	-0.02	-0.02	-0.02
MSK2-14	0.00	-0.02	-0.02	-0.01	-0.01	-0.01	-0.01	-0.01
MSK2-15	0.00	-0.01	-0.02	-0.01	-0.01	0.01	0.01	0.02
MSK2 (2 cycles Bl→6 m 8°C)	0.00	-0.01	-0.02	-0.01	-0.01	-0.01	-0.01	-0.01
MSK2-16	0.00	-0.02	-0.02	-0.01	-0.01	-0.01	-0.01	-0.01
MSK2-17	0.00	-0.02	-0.02	-0.02	-0.01	-0.02	-0.02	-0.02
MSK2-18	0.00	-0.02	-0.02	-0.01	-0.01	-0.01	-0.01	-0.01
MSK2 (2 cycles Bl→6 m 23°C)	0.00	-0.02	-0.02	-0.01	-0.01	-0.01	-0.01	-0.01

Table B3 (continued): Expansion values (%) of Set 2 mortar bars with immersion (twice per week) in bleach (6%) (Bl) solution.

Mortar bars	Expansion (%) as a function of time (days)							
	52	60	66	73	91	102	115	129
MSK2-1	0.00	0.00	0.01	0.01	0.01			
MSK2-2	0.00	0.00	0.01	0.01	0.00	0.01	0.02	0.03
MSK2-3	0.00	0.00	0.01	0.01	0.00	0.01	0.02	0.02
MSK2 (2 cycles Bl→1 m 8°C)	0.00	0.00	0.01	0.01	0.01	0.01	0.02	0.02
MSK2-4	0.06	0.05	0.05	0.06	0.05	0.05	0.06	0.06
MSK2-5	0.00	-0.01	0.00	0.00	0.00	0.00	0.01	0.01
MSK2-6	-0.07	-0.09	-0.09	-0.09	-0.09	-0.09	-0.09	-0.08
MSK2 (2 cycles Bl→1 m 23°C)	-0.01	-0.02	-0.01	-0.01	-0.02	-0.01	-0.01	0.00
MSK2-7	-0.01	-0.01	0.00	0.00	-0.01	0.00	0.02	0.03
MSK2-8	-0.01	-0.01	-0.01	0.00	-0.01	0.00	0.01	0.02
MSK2-9	-0.01	-0.01	0.00	0.00	-0.01	0.00	0.02	0.03
MSK2 (2 cycles Bl→3 m 8°C)	-0.01	-0.01	-0.01	0.00	-0.01	0.00	0.02	0.03
MSK2-10	-0.01	-0.01	0.00	0.01	0.06	0.07	0.09	0.09
MSK2-11	0.03	0.04	0.05	0.05	0.09	0.10	0.12	0.12
MSK2-12	-0.01	-0.01	0.00	0.00	0.00	0.00	0.01	0.01
MSK2 (2 cycles Bl→3 m 23°C)	0.00	0.01	0.02	0.02	0.05	0.06	0.07	0.08
MSK2-13	-0.01	-0.03	-0.02	-0.02	-0.01	0.01	0.04	0.06
MSK2-14	-0.01	-0.01	0.00	0.00	-0.01	0.00	0.01	0.02
MSK2-15	0.01	0.01	0.01	0.01	0.02	0.05	0.09	0.13
MSK2 (2 cycles Bl→6 m 8°C)	-0.01	-0.01	-0.01	0.00	0.00	0.02	0.05	0.07
MSK2-16	-0.01	-0.01	0.00	0.00	0.00	0.00	0.01	0.02
MSK2-17	-0.02	-0.02	0.00	0.02	0.11	0.12		
MSK2-18	-0.01	-0.01	0.00	0.00	-0.01	0.00	0.01	0.02
MSK2 (2 cycles Bl→6 m 23°C)	-0.01	-0.01	0.00	0.01	0.03	0.04	0.01	0.02

Table B3 (continued): Expansion values (%) of Set 2 mortar bars with immersion (twice per week) in bleach (6%) (Bl) solution.

Mortar bars	Expansion (%) as a function of time (days)							
	147	164	179	200	228	256	277	312
MSK2-1								
MSK2-2	0.04	0.05	0.07	0.10	0.17	0.23	0.29	0.43
MSK2-3	0.03	0.03	0.03	0.04	0.06	0.08	0.10	0.14
MSK2 (2 cycles Bl→1 m 8°C)	0.03	0.04	0.05	0.07	0.12	0.16	0.19	0.28
MSK2-4	0.06	0.07	0.09	0.11	0.12	0.15	0.16	0.18
MSK2-5	0.02	0.02	0.02	0.02	0.02	0.03	0.04	
MSK2-6	-0.08	-0.08	-0.08	-0.09	-0.08	-0.08	-0.08	-0.08
MSK2 (2 cycles Bl→1 m 23°C)	0.00	0.00	0.01	0.02	0.02	0.03	0.04	0.05
MSK2-7	0.06	0.11						
MSK2-8	0.05	0.13						
MSK2-9	0.08	0.32						
MSK2 (2 cycles Bl→3 m 8°C)	0.06	0.19						
MSK2-10	0.11	0.13						
MSK2-11	0.13	0.15						
MSK2-12	0.01	0.01						
MSK2 (2 cycles Bl→3 m 23°C)	0.08	0.10						
MSK2-13	0.08	0.12						
MSK2-14	0.02	0.03						
MSK2-15	0.15	0.20						
MSK2 (2 cycles Bl→6 m 8°C)	0.08	0.12						
MSK2-16	0.03	0.03						
MSK2-17								
MSK2-18	0.03	0.03						
MSK2 (2 cycles Bl→6 m 23°C)	0.03	0.03						

Table B. 4: Expansion values (%) of Set 2 (MSK2) mortar specimens stored at 60°C/60% RH, with immersion (twice per week) in peroxide (3%) (Px) solution. The different subsets of bars were transferred at either 8°C/60% RH or 23°C/60% after 1, 3 or 6 months, while pursuing the immersion (twice per week) in peroxide (3%) (i.e. same immersion solution as before the temperature transfer). Average values for each series of 3 bars in grey.

Mortar bars	Expansion (%) as a function of time (days)							
	0	3	6	10	20	28	35	42
MSK2-19	0.00	0.00	0.00	0.00	0.00	0.00	0.00	0.01
MSK2-20	0.00	-0.02	-0.03	-0.03	-0.03	-0.03	-0.02	-0.02
MSK2-21	0.00	-0.02	-0.03	-0.03	-0.03	-0.03	-0.02	-0.02
MSK2 (2 cycles Px→1 m 8°C)	0.00	-0.01	-0.02	-0.02	-0.02	-0.02	-0.01	-0.01
MSK2-22	0.00	-0.02	-0.02	-0.03	-0.03	-0.03	-0.02	-0.02
MSK2-23	0.00	-0.03	-0.03	-0.03	-0.03	-0.03	-0.03	-0.03
MSK2-24	0.00	-0.02	-0.03	-0.03	-0.03	-0.03	-0.02	-0.03
MSK2 (2 cycles Px→1 m 23°C)	0.00	-0.02	-0.03	-0.03	-0.03	-0.03	-0.02	-0.03
MSK2-25	0.00	-0.02	-0.02	-0.03	-0.03	-0.02	-0.02	-0.03
MSK2-26	0.00	-0.03	-0.03	-0.03	-0.03	-0.03	-0.02	-0.03
MSK2-27	0.00	-0.02	-0.03	-0.03	-0.03	-0.03	-0.03	-0.03
MSK2 (2 cycles Px→3 m 8°C)	0.00	-0.02	-0.03	-0.03	-0.03	-0.03	-0.03	-0.03
MSK2-28	0.00	-0.02	-0.03	-0.03	-0.02	-0.03	-0.02	-0.02
MSK2-29	0.00	-0.02	-0.03	-0.03	-0.02	-0.03	-0.02	-0.02
MSK2-30	0.00	-0.02	-0.03	-0.03	-0.03	-0.03	-0.02	-0.03
MSK2 (2 cycles Px→3 m 23°C)	0.00	-0.02	-0.03	-0.03	-0.02	-0.03	-0.02	-0.02
MSK2-31	0.00	-0.02	-0.03	-0.03	-0.03	-0.03	-0.03	-0.04
MSK2-32	0.00	-0.02	-0.03	-0.03	-0.03	-0.04	-0.03	-0.04
MSK2-33	0.00	-0.02	-0.02	-0.03	-0.02	-0.03	-0.02	-0.02
MSK2 (2 cycles Px→6 m 8°C)	0.00	-0.02	-0.03	-0.03	-0.03	-0.03	-0.03	-0.03
MSK2-34	0.00	-0.02	-0.02	-0.03	-0.02	-0.03	-0.03	-0.03
MSK2-35	0.00	-0.02	-0.03	-0.03	-0.03	-0.03	-0.03	-0.03
MSK2-36	0.00	-0.02	-0.03	-0.03	-0.03	-0.03	-0.03	-0.03
MSK2 (2 cycles Px→6 m 23°C)	0.00	-0.02	-0.03	-0.03	-0.03	-0.03	-0.03	-0.03

Table B4 (continued): Expansion values (%) of Set 2 mortar bars with immersion (twice per week) in peroxide (3%) (Px) solution.

Mortar bars	Expansion (%) as a function of time (days)							
	52	60	66	73	91	102	115	129
MSK2-19	0.01	0.01	0.01	0.01	0.00	0.00	0.01	0.01
MSK2-20	-0.02	-0.03	-0.02	-0.02	-0.03	-0.02	-0.02	-0.02
MSK2-21	-0.02	-0.02	-0.01	-0.01	-0.02			
MSK2 (2 cycles Px→1 m 8°C)	-0.01	-0.01	-0.01	-0.01	-0.02	-0.01	-0.01	-0.01
MSK2-22	-0.02	-0.03	-0.02	-0.02	-0.04	-0.03	-0.03	-0.03
MSK2-23	-0.03	-0.02	-0.02	-0.02	-0.03	-0.02	-0.02	-0.03
MSK2-24	-0.02	-0.02	-0.02	-0.02	-0.03	-0.02	-0.02	-0.03
MSK2 (2 cycles Px→1 m 23°C)	-0.02	-0.03	-0.02	-0.02	-0.03	-0.03	-0.02	-0.03
MSK2-25	-0.02	-0.03	-0.02	-0.02	-0.03	-0.01	-0.01	-0.01
MSK2-26	-0.02	-0.04	-0.03	-0.04	-0.05	-0.03	-0.03	-0.03
MSK2-27	-0.03	-0.04	-0.02	-0.03	-0.04	-0.02	-0.02	-0.02
MSK2 (2 cycles Px→3 m 8°C)	-0.03	-0.04	-0.02	-0.03	-0.04	-0.02	-0.02	-0.02
MSK2-28	0.00	-0.03	-0.02	-0.03	-0.05	-0.03	-0.02	-0.03
MSK2-29	-0.01	-0.02	-0.01	-0.02	-0.03	-0.01	-0.01	-0.01
MSK2-30	-0.01	-0.02	-0.03	-0.03	-0.03	-0.03	-0.03	-0.03
MSK2 (2 cycles Px→3 m 23°C)	-0.01	-0.02	-0.02	-0.03	-0.04	-0.02	-0.02	-0.02
MSK2-31	-0.02	-0.02	-0.03	-0.03	-0.04	-0.04	-0.03	-0.04
MSK2-32	-0.03	-0.03	-0.03	-0.03	-0.04	-0.03	-0.03	-0.04
MSK2-33	0.00	0.00	-0.01	-0.01	-0.02	-0.02	-0.02	-0.03
MSK2 (2 cycles Px→6 m 8°C)	-0.02	-0.02	-0.02	-0.02	-0.04	-0.03	-0.03	-0.04
MSK2-34	-0.03	-0.03	-0.03	-0.03	-0.05	-0.04	-0.04	-0.05
MSK2-35	-0.03	-0.03	-0.02	-0.03	-0.05	-0.04	-0.04	-0.05
MSK2-36	-0.03	-0.03	-0.02	-0.04	-0.05	-0.04	-0.04	-0.05
MSK2 (2 cycles Px→6 m 23°C)	-0.03	-0.03	-0.03	-0.03	-0.05	-0.04	-0.04	-0.05

Table B4 (continued): Expansion values (%) of Set 2 mortar bars with immersion (twice per week) in peroxide (3%) (Px) solution.

Mortar bars	Expansion (%) as a function of time (days)							
	147	164	179	200	228	256	277	312
MSK2-19	0.01	0.01	0.00	0.00	0.01	0.00	0.01	0.01
MSK2-20	-0.02	-0.02	-0.02	-0.03	-0.02	-0.03	-0.02	-0.02
MSK2-21								
MSK2 (2 cycles Px→1 m 8°C)	-0.01	-0.01	-0.01	-0.01	-0.01	-0.02	-0.01	-0.01
MSK2-22	-0.03	-0.03	-0.04	-0.04	-0.04	-0.04	-0.03	-0.03
MSK2-23	-0.02	-0.02	-0.03	-0.03	-0.03	-0.03	-0.02	-0.02
MSK2-24	-0.03	-0.03	-0.03	-0.03	-0.03	-0.03	-0.02	-0.02
MSK2 (2 cycles Px→1 m 23°C)	-0.03	-0.03	-0.03	-0.03	-0.03	-0.03	-0.02	-0.02
MSK2-25	-0.02	-0.01	-0.02	-0.02	-0.01	-0.02	-0.02	-0.02
MSK2-26	-0.03	-0.03	-0.03	-0.03	-0.03	-0.04	-0.04	-0.03
MSK2-27	-0.02	-0.02	-0.02	-0.02	-0.02	-0.02	-0.02	-0.02
MSK2 (2 cycles Px→3 m 8°C)	-0.02	-0.02	-0.02	-0.02	-0.02	-0.03	-0.03	-0.02
MSK2-28	-0.03	-0.03	-0.03	-0.04	-0.03	-0.04	-0.03	-0.02
MSK2-29	-0.02	-0.01	-0.02	-0.02	-0.02	-0.03	-0.02	-0.02
MSK2-30	-0.03	-0.03	-0.04	-0.04	-0.04	-0.05	-0.04	-0.03
MSK2 (2 cycles Px→3 m 23°C)	-0.03	-0.02	-0.03	-0.03	-0.03	-0.04	-0.03	-0.02
MSK2-31	-0.05	-0.05	-0.05	-0.04	-0.03	-0.04	-0.04	-0.03
MSK2-32	-0.04	-0.04	-0.04	-0.03	-0.02	-0.03	-0.03	-0.02
MSK2-33	-0.03	-0.03	-0.03	-0.03	-0.02	-0.03	-0.03	-0.02
MSK2 (2 cycles Px→6 m 8°C)	-0.04	-0.04	-0.04	-0.03	-0.02	-0.03	-0.03	-0.02
MSK2-34	-0.05	-0.05	-0.05	-0.05	-0.04	-0.05	-0.04	-0.04
MSK2-35	-0.04	-0.04	-0.05	-0.04	-0.03	-0.04	-0.04	-0.03
MSK2-36	-0.04	-0.04	-0.05	-0.04	-0.04	-0.05	-0.04	-0.03
MSK2 (2 cycles Px→6 m 23°C)	-0.04	-0.05	-0.05	-0.04	-0.04	-0.05	-0.04	-0.03

Table B.5: Expansion values (%) of Set 3 (MSK3) mortar specimens stored at 23°C/60% RH, with immersion (twice per week) in bleach (6%) (Bl) or hydrogen peroxide (3%) (Px) solutions. Two sub-sets of mortar bars were kept for long-term monitoring in the above conditions. The other two sub-sets of bars were transferred at 8°C/60% RH after 6 months, while pursuing the immersion (twice per week) in bleach (6%) or hydrogen peroxide (3%) (i.e. same immersion solution as before the temperature transfer). Average values for each series of 3 bars in grey.

Mortar bars	Expansion (%) as a function of time (days)							
	0	7	15	22	29	39	47	53
MSK3-1	0.00	-0.03	-0.04	-0.03	-0.03	-0.03	-0.04	-0.04
MSK3-2	0.00	-0.02	-0.03	-0.03	-0.03	-0.03	-0.04	-0.04
MSK3-3	0.00	-0.02	-0.03	-0.03	-0.03	-0.03	-0.04	-0.04
MSK3 (2 cycles Bl 23°C)	0.00	-0.02	-0.03	-0.03	-0.03	-0.03	-0.04	-0.04
MSK3-4	0.00	0.00	-0.01	0.00	0.00	-0.01	-0.03	-0.02
MSK3-5	0.00	-0.01	-0.02	-0.02	-0.02	-0.02	-0.03	-0.03
MSK3-6	0.00	0.03	0.02	0.02	0.01	0.01	0.00	0.00
MSK3 (2 cycles Bl→6 m 8°C)	0.00	0.01	-0.01	0.00	0.00	-0.01	-0.02	-0.02
MSK3-10	0.00	-0.02	-0.03	-0.02	-0.02	-0.02	-0.02	-0.02
MSK3-11	0.00	-0.02	-0.03	-0.02	-0.02	-0.02	-0.02	-0.02
MSK3-12	0.00	-0.02	-0.04	-0.02	-0.02	-0.02	-0.02	-0.02
MSK3 (2 cycles Px 23°C)	0.00	-0.02	-0.03	-0.02	-0.02	-0.02	-0.02	-0.02
MSK3-13	0.00	-0.02	-0.02	-0.02	-0.02	-0.02	-0.02	-0.01
MSK3-14	0.00	-0.02	-0.02	-0.02	-0.01	-0.01	0.00	-0.01
MSK3-15	0.00	-0.02	-0.03	-0.03	-0.02	-0.02	-0.03	-0.02
MSK3 (2 cycles Px→6 m 8°C)	0.00	-0.02	-0.02	-0.02	-0.02	-0.02	-0.02	-0.01

Table B5 (continued): Expansion values (%) of Set 3 mortar bars.

Mortar bars	Expansion (%) as a function of time (days)							
	60	71	78	89	102	116	134	151
MSK3-1	-0.05	-0.06	-0.07	-0.06	-0.05	-0.05	-0.05	-0.05
MSK3-2	-0.04	-0.06	-0.05	-0.05	-0.04	-0.04	-0.05	-0.04
MSK3-3	-0.04	-0.06	-0.05	-0.05	-0.04	-0.04	-0.04	-0.04
MSK3 (2 cycles Bl 23°C)	-0.04	-0.06	-0.06	-0.05	-0.05	-0.04	-0.05	-0.05
MSK3-4	-0.03	-0.04	-0.05	-0.05	-0.04	-0.04	-0.05	-0.05
MSK3-5	-0.03	-0.04	-0.05	-0.04	-0.03	-0.03	-0.03	-0.04
MSK3-6	0.00	-0.01	-0.02	0.00	0.00	0.01	0.00	0.00
MSK3 (2 cycles Bl→6 m 8°C)	-0.02	-0.03	-0.04	-0.03	-0.02	-0.02	-0.03	-0.03
MSK3-10	-0.03	-0.03	-0.05	-0.04	-0.05	-0.06	-0.06	-0.07
MSK3-11	-0.03	-0.04	-0.05	-0.05	-0.05	-0.06	-0.06	-0.07
MSK3-12	-0.03	-0.04	-0.06	-0.05	-0.05	-0.06	-0.06	-0.08
MSK3 (2 cycles Px 23°C)	-0.03	-0.03	-0.05	-0.04	-0.05	-0.06	-0.06	-0.07
MSK3-13	-0.02	-0.03	-0.05	-0.04	-0.04	-0.06	-0.06	-0.07
MSK3-14	-0.02	-0.03	-0.05	-0.04	-0.05	-0.05	-0.06	-0.07
MSK3-15	-0.03	-0.04	-0.05	-0.05	-0.05	-0.06	-0.06	-0.07
MSK3 (2 cycles Px→6 m 8°C)	-0.02	-0.03	-0.05	-0.04	-0.05	-0.06	-0.06	-0.07

Table B5 (continued): Expansion values (%) of Set 3 mortar bars.

Mortar bars	Expansion (%) as a function of time (days)						
	166	187	215	246	264	299	327
MSK3-1	-0.05	-0.05	-0.05	-0.06	-0.06	-0.04	-0.04
MSK3-2	-0.04	-0.04	-0.04	-0.04	-0.04	-0.03	-0.02
MSK3-3	-0.04	-0.04	-0.03	-0.04	-0.03	-0.02	-0.01
MSK3 (2 cycles Bl 23°C)	-0.04	-0.04	-0.04	-0.05	-0.04	-0.03	-0.03
MSK3-4	-0.04	-0.04	-0.03	-0.04	-0.03	-0.03	-0.01
MSK3-5	-0.03	-0.02	-0.01	0.00	0.01	0.01	0.02
MSK3-6	0.01	0.01	0.02	0.03	0.04	0.04	0.06
MSK3 (2 cycles Bl→6 m 8°C)	-0.02	-0.02	0.00	0.00	0.01	0.01	0.02
MSK3-10							
MSK3-11	-0.07	-0.07	-0.07	-0.07	-0.06	-0.05	-0.04
MSK3-12	-0.07	-0.08	-0.07	-0.07	-0.06	-0.05	-0.04
MSK3 (2 cycles Px 23°C)	-0.07	-0.07	-0.07	-0.07	-0.06	-0.05	-0.04
MSK3-13	-0.07	-0.07	-0.04	-0.05	-0.04	-0.03	-0.03
MSK3-14	-0.07	-0.07	-0.04	-0.05	-0.04	-0.04	-0.03
MSK3-15	-0.07	-0.08	-0.05	-0.05	-0.04	-0.03	-0.03
MSK3 (2 cycles Px→6 m 8°C)	-0.07	-0.07	-0.04	-0.05	-0.04	-0.03	-0.03

Table B.6: Expansion values (%) of Set 4 (MSK4) mortar specimens stored at 60°C/80% RH, with immersion (twice per week) in bleach (6%) (Bl) or hydrogen peroxide (3%) (Px) solutions. Two sub-sets of mortar bars were kept for long-term monitoring in the above conditions. The other series of bars were transferred at either 8°C/60% RH or at 23°C/60% after 3 months, while pursuing the immersion (twice per week) in bleach (6%) or hydrogen peroxide (3%) (i.e. same immersion solution as before the temperature transfer). Set 6 (MSK6): mortar specimens stored at 60°C/80% RH without immersion (no cycling). Average values for each series of 3 bars in grey.

Mortar bars	Expansion (%) as a function of time (days)							
	0	7	15	22	29	39	47	53
MSK4-1	0.00	-0.01	0.00	0.00	0.00	0.00	0.00	0.01
MSK4-2	0.00	-0.01	0.00	0.00	0.00	0.00	0.00	0.01
MSK4-3	0.00	-0.01	0.00	0.00	0.00	0.00	0.00	0.00
MSK4 (2 cycles Bl)	0.00	-0.01	0.00	0.00	0.00	0.00	0.00	0.01
MSK4-4	0.00	-0.01	0.04	0.07	0.06	0.05	0.02	0.02
MSK4-5	0.00	-0.01	0.00	0.01	0.00	0.00	0.00	0.00
MSK4-6	0.00	0.01	0.06	0.06	0.06	0.06	0.07	0.09
MSK4 (2 cycles Bl→3 m 8°C)	0.00	0.00	0.03	0.05	0.04	0.04	0.03	0.04
MSK4-7	0.00	-0.01	0.00	-0.01	0.00	-0.01	-0.01	-0.01
MSK4-8	0.00	0.00	-0.01	0.00	0.00	0.00	0.00	0.01
MSK4-9	0.00	0.00	-0.01	0.00	0.00	0.00	0.00	0.01
MSK4 (2 cycles Bl→3 m 23°C)	0.00	-0.01	-0.01	0.00	0.00	0.00	0.00	0.00
MSK4-10	0.00	-0.08	-0.07	-0.07	-0.05	-0.06	-0.07	-0.04
MSK4-11	0.00	-0.01	-0.01	-0.01	-0.01	-0.01	0.00	0.01
MSK4-12	0.00	-0.01	-0.02	-0.01	-0.01	-0.01	0.00	0.00
MSK4 (2 cycles Px)	0.00	-0.04	-0.03	-0.03	-0.02	-0.03	-0.02	-0.01
MSK4-13	0.00	-0.02	-0.02	-0.01	-0.01	-0.01	-0.01	0.00
MSK4-14	0.00	-0.01	-0.01	-0.01	-0.01	0.00	0.01	0.02
MSK4-15	0.00	-0.01	-0.01	-0.01	0.00	0.00	-0.01	0.01
MSK4 (2 cycles Px→3 m 8°C)	0.00	-0.01	-0.01	-0.01	-0.01	0.00	0.00	0.01
MSK4-16	0.00	-0.01	-0.02	-0.01	0.00	0.00	0.00	0.01
MSK4-17	0.00	-0.01	-0.02	-0.01	0.03	0.05	0.08	0.09
MSK4-18	0.00	-0.01	-0.02	-0.01	-0.01	0.00	0.01	0.01
MSK4 (2 cycles Px→3 m 23°C)	0.00	-0.01	-0.02	-0.01	0.01	0.01	0.03	0.04
MSK6-1	0.00	-0.03	-0.03	-0.02	-0.02	-0.03	-0.03	-0.04
MSK6-2	0.00	-0.03	-0.03	-0.02	-0.02	-0.02	-0.03	-0.03
MSK6-3	0.00	-0.03	-0.03	-0.02	-0.02	-0.02	-0.03	-0.03
MSK6 (no cycling)	0.00	-0.03	-0.03	-0.02	-0.02	-0.02	-0.03	-0.03

Table B6 (continued): Expansion values (%) of Set 4 and Set 6 mortar bars.

Mortar bars	Expansion (%) as a function of time (days)							
	60	71	78	89	102	116	134	151
MSK4-1	0.01	0.00	0.00	0.01	0.01	0.02	0.02	0.03
MSK4-2	0.01	0.00	0.00	0.01	0.01	0.02	0.02	0.02
MSK4-3	0.01	0.00	0.00	0.00	0.01	0.02	0.01	0.02
MSK4 (2 cycles Bl)	0.01	0.00	0.00	0.01	0.01	0.02	0.02	0.02
MSK4-4	0.02	0.02	0.02	0.02	0.08			
MSK4-5	0.00	0.00	0.00	0.00	0.03			
MSK4-6	0.09	0.08	0.08	0.09	0.19			
MSK4 (2 cycles Bl→3 m 8°C)	0.04	0.03	0.03	0.04	0.10			
MSK4-7	-0.01	-0.01	0.00	0.00	0.01	0.01	0.00	0.01
MSK4-8	0.01	0.00	0.00	0.00	0.01	0.01	0.01	0.01
MSK4-9	0.01	0.00	0.00	0.00	0.01	0.01	0.01	0.01
MSK4 (2 cycles Bl→3 m 23°C)	0.01	0.00	0.00	0.00	0.01	0.01	0.01	0.01
MSK4-10	-0.05	-0.05	-0.06	-0.06	-0.05	-0.06	-0.06	-0.06
MSK4-11	0.01	0.00	-0.01	0.00	0.00	0.00	0.00	0.01
MSK4-12	0.00	-0.01	-0.02	0.00	0.00	-0.01	-0.01	-0.01
MSK4 (2 cycles Px)	-0.01	-0.02	-0.03	-0.02	-0.02	-0.02	-0.02	-0.02
MSK4-13	0.00	-0.01	-0.02	-0.01	0.00	0.00	0.00	0.00
MSK4-14	0.02	0.01	0.00	0.01	0.02	0.02	0.02	0.01
MSK4-15	0.01	0.00	-0.01	0.00	0.01	0.01	0.01	0.01
MSK4 (2 cycles Px→3 m 8°C)	0.01	0.00	-0.01	0.00	0.01	0.01	0.01	0.01
MSK4-16	0.00	-0.01	-0.01	0.00	0.00	-0.01	-0.01	-0.01
MSK4-17	0.09	0.09	0.09	0.11	0.13	0.13	0.13	0.13
MSK4-18	0.02	0.03	0.04	0.07	0.08	0.08	0.09	0.09
MSK4 (2 cycles Px→3 m 23°C)	0.04	0.04	0.04	0.06	0.07	0.06	0.07	0.07
MSK6-1	-0.03	-0.04	-0.04	-0.05	-0.05	-0.04	-0.04	-0.04
MSK6-2	-0.03	-0.04	-0.04	-0.05	-0.05	-0.04	-0.04	-0.04
MSK6-3	-0.03	-0.04	-0.04	-0.05	-0.05	-0.04	-0.04	-0.04
MSK6 (no cycling)	-0.03	-0.04	-0.04	-0.05	-0.05	-0.04	-0.04	-0.04

Table B6 (continued): Expansion values (%) of Set 4 and Set 6 mortar bars

Mortar bars	Expansion (%) as a function of time (days)						
	166	187	215	246	264	299	327
MSK4-1	0.03	0.04	0.04	0.04	0.05	0.08	0.13
MSK4-2	0.02	0.03	0.03	0.04	0.05	0.05	0.08
MSK4-3	0.02	0.03	0.03	0.04	0.05	0.05	0.09
MSK4 (2 cycles Bl)	0.02	0.03	0.03	0.04	0.05	0.06	0.10
MSK4-4							
MSK4-5							
MSK4-6							
MSK4 (2 cycles Bl→3 m 8°C)							
MSK4-7	0.01	0.00	0.00	-0.01	-0.01	0.00	0.00
MSK4-8	0.01	0.01	0.01	0.01	0.01	0.02	0.02
MSK4-9	0.01	0.01	0.01	0.01	0.01		
MSK4 (2 cycles Bl→3 m 23°C)	0.01	0.01	0.01	0.00	0.00		
MSK4-10	-0.06	-0.05	-0.05	-0.03			
MSK4-11	0.00	0.02	0.04	0.06			
MSK4-12	-0.01	-0.02	-0.01	-0.02			
MSK4 (2 cycles Px)	-0.02	-0.02	0.00	0.00			
MSK4-13	0.00	0.00	0.00	-0.01	0.00	0.00	0.00
MSK4-14	0.01	0.01	0.02	0.00	0.00	0.01	0.01
MSK4-15	0.01	0.01	0.01	0.00	0.00	0.01	0.01
MSK4 (2 cycles Px→3 m 8°C)	0.01	0.01	0.01	0.00	0.00	0.01	0.01
MSK4-16	-0.02						
MSK4-17	0.13						
MSK4-18	0.09						
MSK4 (2 cycles Px→3 m 23°C)	0.07						
MSK6-1	-0.04	-0.04	-0.04	-0.04	-0.04		
MSK6-2	-0.04	-0.05	-0.04	-0.02	0.03		
MSK6-3	-0.04	-0.04	-0.04	-0.03	-0.03		
MSK6 (no cycling)	-0.04	-0.04	-0.04	-0.03	-0.02		

Table B.7: Expansion values (%) of Set 7 (MSK7) mortar specimens stored at 38°C/60% RH, with immersion (twice per week) in bleach (6%) (Bl) solution; the bars were then transferred at 23°C/60% RH after 3 months, while pursuing the immersion (twice per week) in bleach (6%). A sub-set of mortar specimens was kept for long-term monitoring at 38°C/60% without immersion (no cycling). Average values for each series of 3 bars in grey.

Mortar bars	Expansion (%) as a function of time (days)							
	0	7	15	22	29	39	47	53
MSK7-1	0.00	-0.01	-0.05	-0.05	-0.06	-0.06	-0.07	-0.06
MSK7-2	0.00	-0.01	0.02	0.01	-0.01	-0.03	-0.11	-0.11
MSK7-3	0.00	-0.01	-0.13	-0.13	-0.11	-0.10	-0.08	-0.07
MSK7 (2 cycles Bl 3m→23°C)	0.00	-0.01	-0.06	-0.06	-0.06	-0.06	-0.09	-0.08
MSK7-4	0.00	-0.02	-0.03	-0.04	-0.03	-0.03	-0.03	-0.04
MSK7-5	0.00	-0.02	-0.03	-0.04	-0.04	-0.04	-0.04	-0.04
MSK7-6	0.00	-0.02	-0.03	-0.04	-0.04	-0.04	-0.01	0.00
MSK7 (no cycling)	0.00	-0.02	-0.03	-0.04	-0.04	-0.04	-0.03	-0.03

Table B7 (continued): Expansion values (%) of Set 7 mortar bars.

Mortar bars	Expansion (%) as a function of time (days)							
	60	71	78	89	102	116	134	151
MSK7-1	-0.07	-0.09	-0.10	-0.07	-0.06	-0.06	-0.07	-0.06
MSK7-2	-0.12	-0.15	-0.15	-0.12	-0.11	-0.11	-0.11	-0.11
MSK7-3	-0.08	-0.11	-0.12	-0.09	-0.09	-0.09	-0.09	-0.09
MSK7 (2 cycles Bl 3m→23°C)	-0.09	-0.12	-0.12	-0.09	-0.09	-0.09	-0.09	-0.09
MSK7-4	-0.06	-0.08	-0.08	-0.05	-0.05	-0.05	-0.05	-0.05
MSK7-5	-0.06	-0.09	-0.08	-0.06	-0.05	-0.05	-0.05	-0.05
MSK7-6	-0.03	-0.06	-0.06	-0.04	-0.03	-0.04	-0.04	-0.04
MSK7 (no cycling)	-0.05	-0.07	-0.07	-0.05	-0.04	-0.04	-0.05	-0.04

Table B7 (continued): Expansion values (%) of Set 7 mortar bars.

Mortar bars	Expansion (%) as a function of time (days)		
	166	187	215
MSK7-1	-0.06	-0.08	-0.17
MSK7-2	-0.11	-0.12	-0.12
MSK7-3	-0.09	-0.10	-0.10
MSK7 (2 cycles Bl 3m→23°C)	-0.09	-0.10	-0.13
MSK7-4	-0.04	-0.05	-0.04
MSK7-5	-0.05	-0.05	-0.04
MSK7-6	-0.04	-0.05	-0.04
MSK7 (no cycling)	-0.04	-0.05	-0.04

Table B.8: Expansion values (%) of Set 8 (HPL8) mortar specimens stored at 60°C/60% RH, while pursuing the immersion (twice per week) in bleach (6%) (Bl) or hydrogen peroxide (3%) (Px). Set 9 (HPL9): mortar specimens stored at 60°C/60% RH without immersion (no cycling). Set 10 (HPL10): mortar specimens stored at 8°C/60% RH without immersion (no cycling). Average values for each series of 3 bars in grey.

Mortar bars	Expansion (%) as a function of time (days)							
	7	10	20	28	35	42	52	60
HPL8-1	-0.01	-0.02	-0.02	-0.02	-0.02	-0.01	-0.02	-0.02
HPL8-2	-0.02	0.00	0.02	-0.02	-0.02	-0.02	-0.03	-0.04
HPL8-3	-0.01	-0.01	-0.02	-0.02	-0.01	-0.01	-0.02	-0.02
HPL8 (2 cycles Bl)	-0.01	-0.01	0.00	-0.02	-0.02	-0.02	-0.02	-0.03
HPL8-4	-0.03	-0.03	-0.03	-0.03	-0.03	-0.03	-0.04	-0.04
HPL8-5	-0.03	-0.03	-0.03	-0.03	-0.03	-0.03	-0.04	-0.04
HPL8-6	-0.03	-0.04	-0.03	-0.03	-0.03	-0.03	-0.04	-0.05
HPL8 (2 cycles Px)	-0.03	-0.03	-0.03	-0.03	-0.03	-0.03	-0.04	-0.04
HPL9-1	-0.04	-0.03	-0.05	-0.04	-0.05	-0.05	-0.06	-0.06
HPL9-2	-0.04	-0.03	-0.05	-0.05	-0.05	-0.05	-0.06	-0.06
HPL9-3	-0.03	-0.03	-0.05	-0.04	-0.05	-0.05	-0.06	-0.06
HPL9 (no cycling)	-0.04	-0.03	-0.05	-0.05	-0.05	-0.05	-0.06	-0.06
HPL10-1	-0.03	-0.02	-0.02	-0.01	-0.01	-0.01	-0.02	-0.02
HPL10-2	-0.03	-0.02	-0.02	-0.01	-0.01	-0.01	-0.02	-0.02
HPL10-3	-0.03	-0.02	-0.02	-0.01	-0.01	-0.01	-0.02	-0.02
HPL10 (no cycling)	-0.03	-0.02	-0.02	-0.01	-0.01	-0.01	-0.02	-0.02

Table B8 (continued): Expansion values (%) of Sets 8, 9 and 10 mortar bars.

Mortar bars	Expansion (%) as a function of time (days)							
	66	73	91	102	115	129	147	164
HPL8-1	-0.02	-0.02	-0.03	-0.01	-0.01	-0.01	-0.02	-0.02
HPL8-2	-0.04	-0.04	-0.03	-0.05	-0.07	-0.07	-0.08	-0.08
HPL8-3	-0.02	-0.02	-0.01	-0.01	-0.01	-0.01	-0.01	-0.01
HPL8 (2 cycles Bl)	-0.03	-0.03	-0.02	-0.02	-0.03	-0.03	-0.03	-0.04
HPL8-4	-0.04	-0.03	-0.03	-0.03	-0.03	-0.03	-0.04	-0.04
HPL8-5	-0.04	-0.03	-0.03	-0.03	-0.03	-0.03	-0.04	-0.04
HPL8-6	-0.04	-0.03	-0.03	-0.03	-0.03	-0.04	-0.04	-0.04
HPL8 (2 cycles Px)	-0.04	-0.03	-0.03	-0.03	-0.03	-0.03	-0.04	-0.04
HPL9-1	-0.06	-0.06	-0.05	-0.05	-0.05	-0.05	-0.05	-0.06
HPL9-2	-0.06	-0.06	-0.05	-0.05	-0.05	-0.05	-0.05	-0.05
HPL9-3	-0.05	-0.06	-0.05	-0.05	-0.05	-0.05	-0.05	-0.05
HPL9 (no cycling)	-0.06	-0.06	-0.05	-0.05	-0.05	-0.05	-0.05	-0.05
HPL10-1	-0.02	-0.02	-0.01	-0.01	-0.01	-0.01	-0.01	-0.02
HPL10-2	-0.01	-0.01	0.00	0.00	0.00	0.00	0.00	-0.01
HPL10-3	-0.02	-0.01	-0.01	-0.01	-0.01	-0.01	-0.01	-0.02
HPL10 (no cycling)	-0.01	-0.01	-0.01	-0.01	-0.01	-0.01	-0.01	-0.01

Table B8 (continued): Expansion values (%) of Sets 8, 9 and 10 mortar bars.

Mortar bars	Expansion (%) as a function of time (days)		
	200	228	250
HPL8-1	-0.02	-0.01	-0.01
HPL8-2	-0.09	-0.05	0.01
HPL8-3	-0.01	0.00	0.00
HPL8 (2 cycles Bl)	-0.04	-0.02	0.00
HPL8-4	-0.04	-0.04	-0.04
HPL8-5	-0.04	-0.04	-0.04
HPL8-6	-0.04	-0.05	-0.04
HPL8 (2 cycles Px)	-0.04	-0.04	-0.04
HPL9-1	-0.06	-0.04	-0.05
HPL9-2	-0.05	-0.05	-0.05
HPL9-3	-0.05	-0.05	-0.05
HPL9 (no cycling)	-0.05	-0.05	-0.05
HPL10-1	-0.02	-0.02	-0.02
HPL10-2	-0.01	-0.01	-0.01
HPL10-3	-0.02	-0.02	-0.02
HPL10 (no cycling)	-0.02	-0.01	-0.02

B4.4.2 Expansion as a function of time graphs (first series)

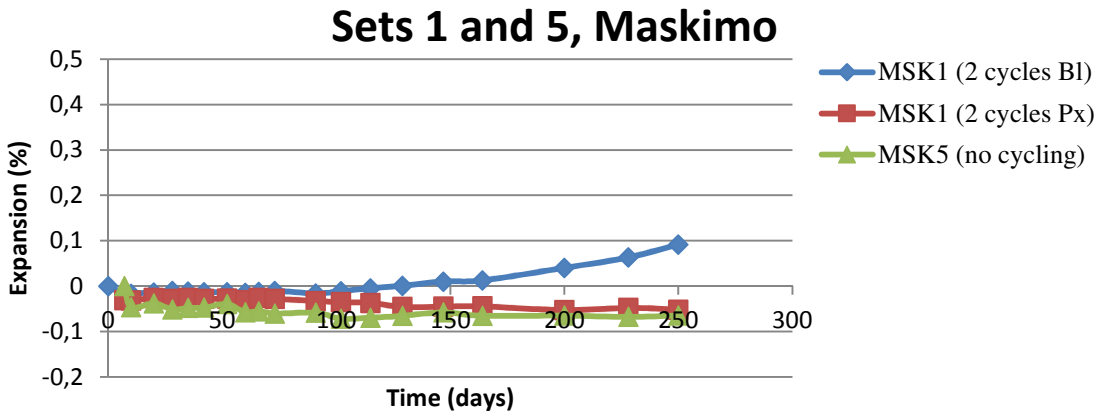


Figure B.3: Expansion values (%) of Set 1 (MSK1) mortar specimens stored at 60°C/60% RH, with immersion (twice per week) in bleach (6%) (BI) or hydrogen peroxide (3%) (Px) solutions. Set 5 (MSK5) mortar specimens are stored at 60°C/60% RH, without immersion (no cycling). Each curve in this figure corresponds to the average values obtained from a set of three bars.

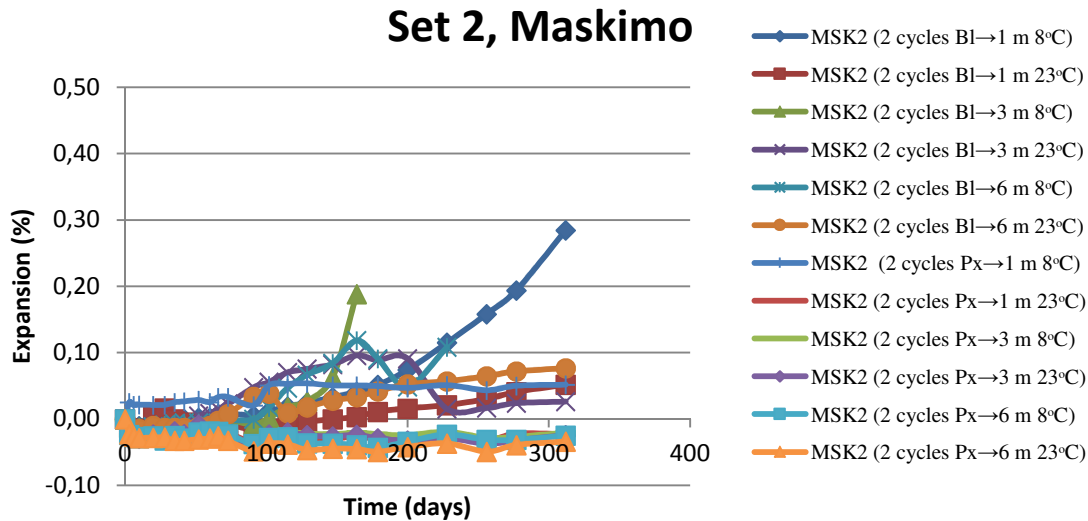


Figure B.4: Expansion values (%) of Set 1 (MSK1) mortar specimens stored at 60°C/60% RH, with immersion (twice per week) in bleach (6%) (BI) or hydrogen peroxide (3%) (Px) solutions. Set 5 (MSK5) mortar specimens are stored at 60°C/60% RH, without immersion (no cycling). Each curve in this figure corresponds to the average values obtained from a set of three bars.

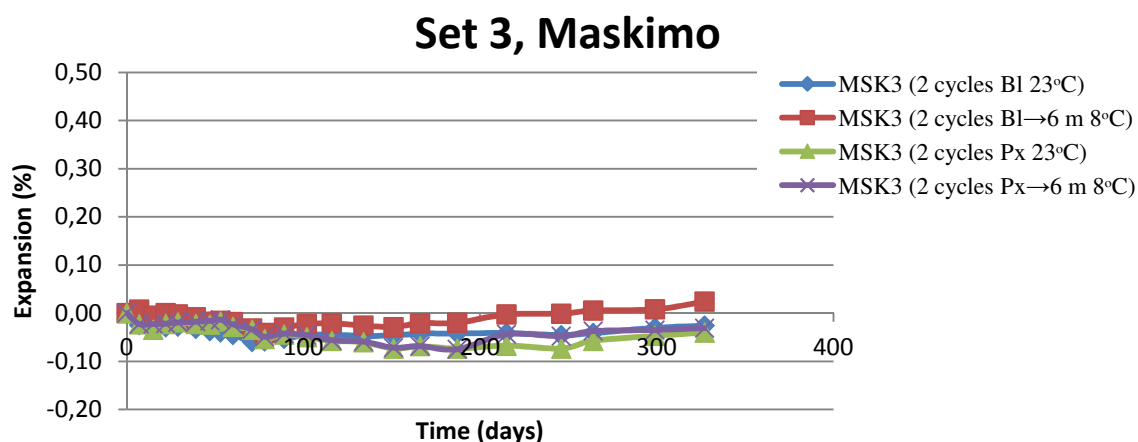


Figure B.5: Expansion values (%) of Set 3 (MSK3) mortar specimens stored at 23°C/60% RH, with immersion (twice per week) in bleach (6%) (BI) or hydrogen peroxide (3%) (Px) solutions. Two sub-sets of mortar bars were kept for long-term monitoring in the above conditions. The other two sub-sets of bars were transferred at 8°C/60% RH after 6 months, while pursuing the immersion (twice per week) in bleach (6%) or hydrogen peroxide (3%) (i.e. same immersion solution as before the temperature transfer). Each curve in this figure corresponds to the average values obtained from a set of three bars.

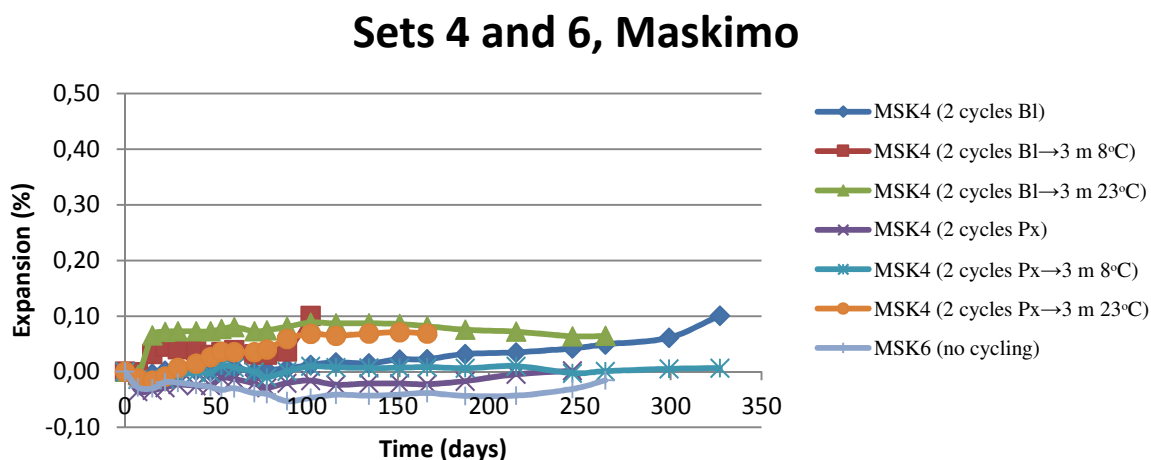


Figure B. 6: Expansion values (%) of Set 4 (MSK4) mortar specimens stored at 60°C/80% RH, with immersion (twice per week) in bleach (6%) (BI) or hydrogen peroxide (3%) (Px) solutions. Two sub-sets of mortar bars were kept for long-term monitoring in the above conditions. The other series of bars were transferred at either 8°C/60% RH or at 23°C/60% after 3 months, while pursuing the immersion (twice per week) in bleach (6%) or hydrogen peroxide (3%) (i.e. same immersion solution as before the temperature transfer). Set 6 (MSK6): mortar specimens stored at 60°C/80% RH without immersion (no cycling). Each curve in this figure corresponds to the average values obtained from a set of three bars.

Set 7 MSK

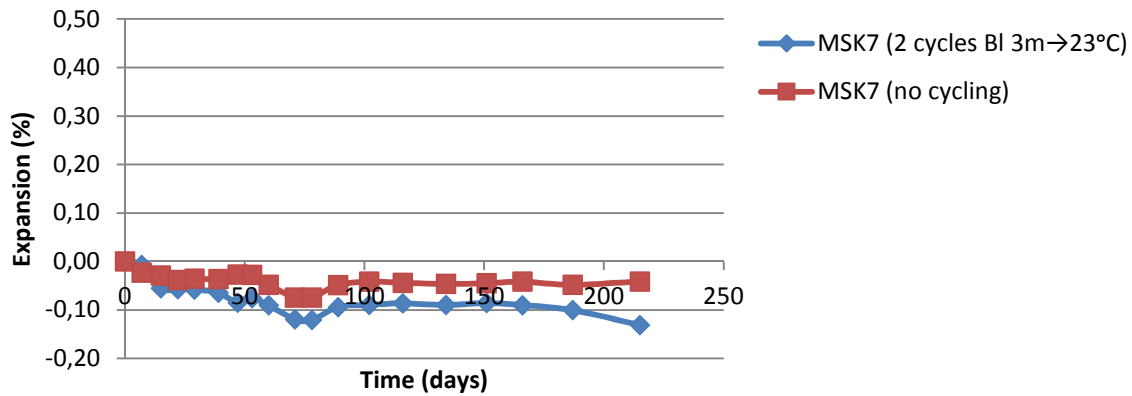


Figure B. 7: Expansion values (%) of Set 7 (MSK7) mortar specimens stored at 38°C/60% RH, with immersion (twice per week) in bleach (6%) (BI) solution; the bars were then transferred at 23°C/60% RH after 3 months, while pursuing the immersion (twice per week) in bleach (6%). A sub-set of mortar specimens was kept for long-term monitoring at 38°C/60% without immersion (no cycling). Each curve in this figure corresponds to the average values obtained from a set of three bars.

Sets 8, 9, 10, HPL

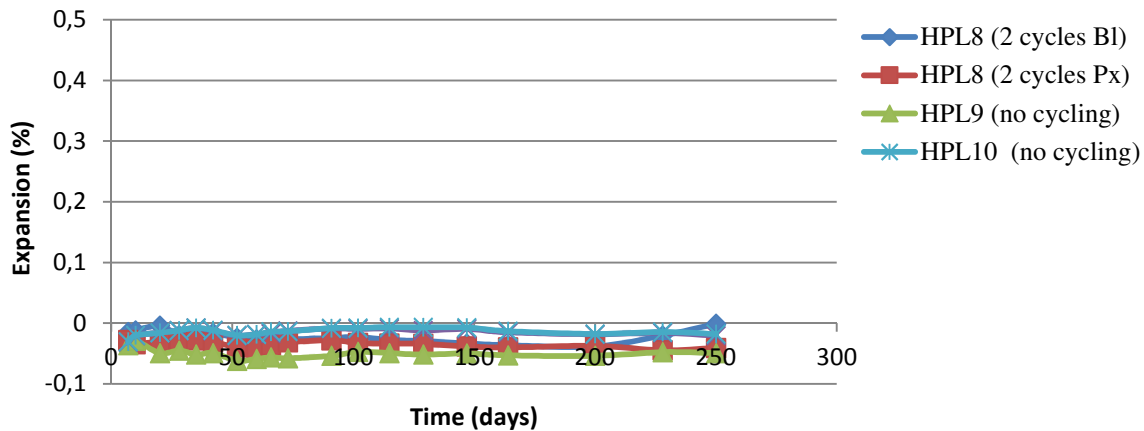


Figure B.8: Expansion values (%) of Set 8 (HPL8) mortar specimens stored at 60°C/60% RH, while pursuing the immersion (twice per week) in bleach (6%) (BI) or hydrogen peroxide (3%) (Px). Set 9 (HPL9): mortar specimens stored at 60°C/60% RH without immersion (no cycling). Set 10 (HPL10): mortar specimens stored at 8°C/60% RH without immersion (no cycling). Each curve in this figure corresponds to the average values obtained from a set of three bars.

B5 Preliminary tests: series 2

B5.1 Test conditions:

- Temperature: 4°C, 60°C, 80°C
- Relative humidity (RH): 80%
- Immersion solutions: bleach (6%)

B5.2 Aggregates tested:

- MSK
- SBR
- PKA (control aggregate)

B5.3 Storage conditions

- 4°C/80% RH: bars stored above oversaturated solution of cane sugar in air-tight container
- 60°C/80% RH: bars stored above oversaturated solution of KCl in air-tight container
- 80°C/80% RH: bars stored above oversaturated solution of NaCl in air-tight container

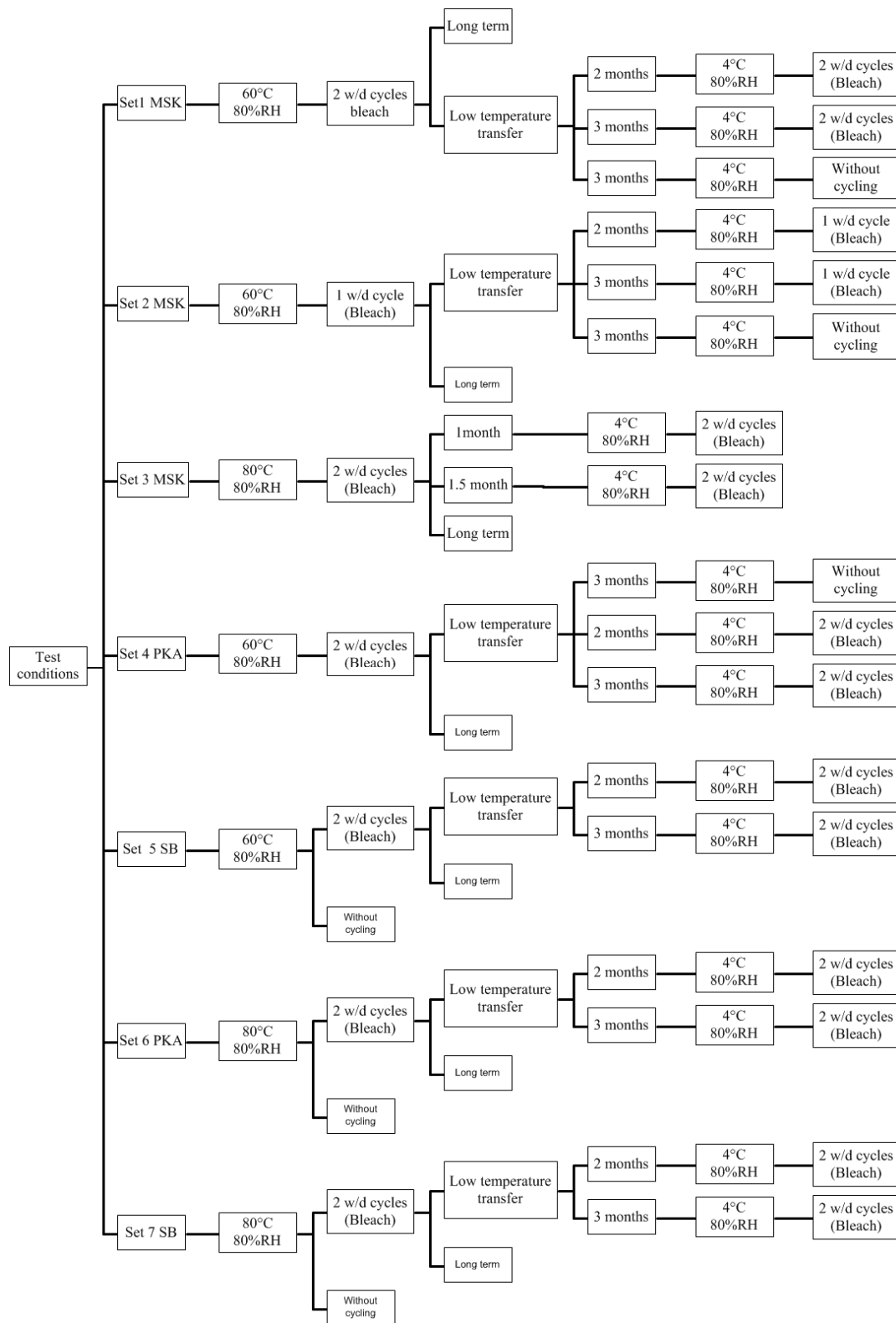


Figure B.9: Experimental program flowchart - testing conditions for the second series.

B5.4 Results

B5.4.1 Expansion values (%) second series

Table B. 9: Expansion values (%) of Set 1 (MSK1) mortar specimens stored at 60°C/80% RH, with immersion (twice per week) in bleach (6%) (Bl) solution. The first sub-set of mortar specimens was kept for long-term monitoring in the above conditions. The other sub-sets of mortar bars were transferred at low temperature (4°C/80% RH) after 2 or 3 months, while pursuing the immersion (twice per week) in bleach (6%), or without immersion (no cycling). Average values for each series of 3 bars in grey.

Mortar bars	Expansion (%) as a function of time (days)							
	0	11	18	25	38	41	51	55
MSK1-1	0.00	-0.01	0.00	0.00	0.00	0.00	0.02	0.02
MSK1-2	0.00	-0.01	0.00	0.01	0.01	0.01	0.02	0.02
MSK1-3	0.00	-0.01	0.00	0.00	0.00	0.00	0.02	0.02
MSK1(2 cycles Bl)	0.00	-0.01	0.00	0.00	0.00	0.00	0.02	0.02
MSK1-4	0.00	0.00	0.00	0.00	0.00	0.00	0.02	0.02
MSK1-5	0.00	-0.01	0.00	0.00	0.00	0.00	0.02	0.02
MSK1-6	0.00	-0.01	0.00	0.00	0.00	0.00	0.03	0.03
MSK1 (→2 m 4°C 2 cycles Bl)	0.00	-0.01	0.00	0.00	0.00	0.00	0.02	0.02
MSK1-7	0.00	0.00	0.00	0.00	0.00	0.01	0.02	0.02
MSK1-8	0.00	0.00	0.00	0.01	0.00	0.00	0.03	0.03
MSK1-9	0.00	-0.01	0.00	0.00	0.00	0.00	0.02	0.02
MSK1 (→3 m 4°C 2 cycles Bl)	0.00	0.00	0.00	0.01	0.00	0.01	0.02	0.02
MSK1-10	0.00	-0.03	-0.03	-0.02	-0.01	-0.02	-0.03	-0.04
MSK1-11	0.00	-0.03	-0.02	-0.03	-0.01	-0.02	-0.03	-0.04
MSK1-12	0.00	-0.03	-0.02	-0.02	0.00	-0.01	-0.04	-0.04
MSK1(→3 m 4°C no cycling)	0.00	-0.03	-0.02	-0.03	-0.01	-0.02	-0.03	-0.04

Table B9 (continued): Expansion values (%) of Set 1 mortar bars.

Mortar bars	Expansion (%) as a function of time (days)							
	62	69	76	83	90	118	125	139
MSK1-1	0.02	0.01	0.02	0.02	0.02	0.02	0.02	0.02
MSK1-2	0.02	0.02	0.02	0.02	0.02	0.02	0.03	0.02
MSK1-3	0.02	0.02	0.02	0.02	0.02	0.03	0.03	0.02
MSK1(2 cycles Bl)	0.02	0.02	0.02	0.02	0.02	0.03	0.03	0.02
MSK1-4	0.02	0.02	0.02	0.03	0.04	0.10	0.12	0.18
MSK1-5	0.03	0.03	0.03	0.03	0.03	0.04	0.04	0.03
MSK1-6	0.03	0.03	0.03	0.03	0.03	0.05	0.05	0.05
MSK1 (→2 m 4°C 2 cycles Bl)	0.03	0.03	0.03	0.03	0.03	0.06	0.07	0.09
MSK1-7	0.02	0.02	0.02	0.02	0.03	0.05	0.04	0.04
MSK1-8	0.03	0.03	0.03	0.03	0.03	0.07	0.08	0.11
MSK1-9	0.02	0.02	0.02	0.02	0.03	0.05	0.05	0.04
MSK1 (→3 m 4°C 2 cycles Bl)	0.02	0.02	0.02	0.03	0.03	0.05	0.06	0.06
MSK1-10	-0.03	-0.04	-0.04	-0.04	-0.03	-0.02	-0.02	-0.03
MSK1-11	-0.03	-0.04	-0.04	-0.04	-0.03	-0.02	-0.02	-0.04
MSK1-12	-0.03	-0.04	-0.04	-0.04	-0.03	-0.02	-0.02	-0.03
MSK1(→3 m 4°C no cycling)	-0.03	-0.04	-0.04	-0.04	-0.03	-0.02	-0.02	-0.03

Table B9 (continued): Expansion values (%) of Set 1 mortar bars

Mortar bars	Expansion (%) as a function of time (days)							
	153	167	174	203	217	231	245	259
MSK1-1	0.02	0.01	0.01	0.03	0.05	0.09	0.13	0.16
MSK1-2	0.02	0.01	0.01	0.03	0.03	0.07	0.09	0.12
MSK1-3	0.02	0.02	0.02	0.02	0.03	0.07	0.09	0.13
MSK1(2 cycles Bl)	0.02	0.01	0.01	0.03	0.04	0.08	0.10	0.14
MSK1-4	0.28	0.38						
MSK1-5	0.04	0.04						
MSK1-6	0.05	0.06						
MSK1 (→2 m 4°C 2 cycles Bl)	0.12	0.16						
MSK1-7	0.05	0.05	0.05					
MSK1-8	0.18	0.23	0.26					
MSK1-9	0.05	0.05	0.05					
MSK1 (→3 m 4°C 2 cycles Bl)	0.09	0.11	0.12					
MSK1-10	-0.03	-0.03	-0.04	-0.03	-0.04	-0.04	-0.04	-0.04
MSK1-11	-0.04	-0.04	-0.04	-0.03	-0.04	-0.04	-0.04	-0.05
MSK1-12	-0.03	-0.03	-0.03	-0.02	-0.04	-0.03	-0.04	-0.04
MSK1(→3 m 4°C no cycling)	-0.03	-0.03	-0.04	-0.03	-0.04	-0.03	-0.04	-0.04

Table B9 (continued): Expansion values (%) of Set 1 mortar bars.

Mortar bars	Expansion (%) as a function of time (days)						
	266	273	287	302	315	330	351
MSK1-1	0.20	0.23	0.25	0.27	0.31	0.34	0.38
MSK1-2	0.16	0.20	0.23	0.26	0.29	0.34	0.37
MSK1-3	0.16	0.19	0.21	0.23	0.27	0.30	0.33
MSK1(2 cycles Bl)	0.17	0.21	0.23	0.25	0.29	0.33	0.36
MSK1-4							
MSK1-5							
MSK1-6							
MSK1 (→2 m 4°C 2 cycles Bl)							
MSK1-7							
MSK1-8							
MSK1-9							
MSK1 (→3 m 4°C 2 cycles Bl)							
MSK1-10	-0.04	-0.04	-0.04	-0.04	-0.03	-0.04	-0.03
MSK1-11	-0.05	-0.04	-0.04	-0.05	-0.04	-0.04	-0.03
MSK1-12	-0.04	-0.04	-0.04	-0.04	-0.03	-0.03	-0.02
MSK1(→3 m 4°C no cycling)	-0.04	-0.04	-0.04	-0.04	-0.03	-0.04	-0.03

Table B. 10: Expansion values (%) of Set 2 (MSK2) mortar specimens stored at 60°C/80% RH, with immersion (once per week) in bleach (6%) (Bl) solution. The first sub-set of mortar specimens was kept for long-term monitoring in the above conditions. The other sub-sets of mortar bars were transferred at low temperature (4°C/80% RH) after 2 or 3 months, while pursuing the immersion (once per week) in bleach (6%), or without immersion (no cycling). Average values for each series of 3 bars in grey.

Mortar bars	Expansion (%) as a function of time (days)							
	0	11	18	25	38	41	51	55
MSK2-1	0.00	-0.01	-0.01	-0.01	0.00	0.00	0.02	0.02
MSK2-2	0.00	-0.01	0.00	0.00	0.00	0.00	0.01	0.01
MSK2-3	0.00	0.00	0.00	-0.01	0.00	0.01	0.00	0.00
MSK2 (1 cycle Bl)	0.00	-0.01	0.00	-0.01	0.00	0.00	0.01	0.01
MSK2-4	0.00	-0.02	0.00	0.00	0.00	0.00	0.02	0.02
MSK2-5	0.00	0.00	0.00	0.01	0.01	0.01	0.02	0.02
MSK2-6	0.00	-0.01	0.00	0.00	0.00	0.01	0.02	0.02
MSK2 (→2 m 4°C 1 cycle Bl)	0.00	-0.01	0.00	0.00	0.00	0.01	0.02	0.02
MSK2-7	0.00	-0.01	0.00	0.00	0.00	0.01	0.02	0.02
MSK2-8	0.00	-0.01	0.00	0.00	0.00	0.00	0.02	0.02
MSK2-9	0.00	-0.01	0.00	0.00	0.00	0.00	0.02	0.02
MSK2 (→3 m 4°C 1 cycle Bl)	0.00	-0.01	0.00	0.00	0.00	0.00	0.02	0.02
MSK2-10	0.00	0.00	-0.02	-0.02	0.00	0.01	-0.03	-0.03
MSK2-11	0.00	0.00	-0.02	-0.02	-0.02	0.01	-0.03	-0.03
MSK2-12	0.00	0.00	-0.01	-0.02	0.00	0.01	-0.03	-0.03
MSK2 (→3 m 4°C no cycling)	0.00	0.00	-0.02	-0.02	-0.01	0.01	-0.03	-0.03

Table B10 (continued): Expansion values (%) of Set 2 mortar bars.

Mortar bars	Expansion (%) as a function of time (days)							
	62	69	76	83	90	118	125	139
MSK2-1	0.02	0.02	0.02	0.02	0.03	0.03	0.03	0.02
MSK2-2	0.02	0.01	0.02	0.02	0.01	0.03	0.03	0.02
MSK2-3	0.01	0.00	0.01	0.01	0.01	0.02	0.01	0.01
MSK2 (1 cycle Bl)	0.02	0.01	0.02	0.02	0.02	0.03	0.02	0.02
MSK2-4	0.02	0.02	0.02	0.02	0.02	0.04	0.04	0.03
MSK2-5	0.02	0.02	0.02	0.03	0.03	0.06	0.06	0.06
MSK2-6	0.02	0.02	0.02	0.03	0.03	0.05	0.05	0.04
MSK2 (→2 m 4°C 1 cycle Bl)	0.02	0.02	0.02	0.03	0.03	0.05	0.05	0.04
MSK2-7	0.02	0.02	0.02	0.02	0.02	0.04	0.04	0.03
MSK2-8	0.02	0.01	0.02	0.02	0.02	0.03	0.03	0.03
MSK2-9	0.02	0.02	0.02	0.02	0.03	0.04	0.04	0.03
MSK2 (→3 m 4°C 1 cycle Bl)	0.02	0.02	0.02	0.02	0.02	0.04	0.04	0.03
MSK2-10	-0.03	-0.03	-0.03	-0.04	-0.03	-0.01	-0.01	-0.02
MSK2-11	-0.03	-0.04	-0.04	-0.04	-0.04	-0.01	-0.02	-0.03
MSK2-12	-0.03	-0.03	-0.03	-0.04	-0.03	-0.01	-0.01	-0.02
MSK2 (→3 m 4°C no cycling)	-0.03	-0.03	-0.03	-0.04	-0.04	-0.01	-0.01	-0.02

Table B10 (continued): Expansion values (%) of Set 2 mortar bars.

Mortar bars	Expansion (%) as a function of time (days)							
	153	167	174	203	217	231	245	259
MSK2-1	0.02	0.01	0.01	0.02	0.02	0.04	0.05	0.07
MSK2-2	0.03	0.01	0.01	0.02	0.03	0.04	0.05	0.07
MSK2-3	0.01	0.00	0.00	0.01	0.01	0.03	0.03	0.05
MSK2 (1 cycle Bl)	0.02	0.01	0.01	0.02	0.02	0.04	0.04	0.06
MSK2-4	0.03	0.03	0.03	0.03	0.03	0.04	0.04	0.04
MSK2-5	0.08	0.10	0.11	0.15	0.18	0.23	0.28	0.35
MSK2-6	0.05	0.05	0.04	0.05	0.05	0.06	0.06	0.25
MSK2 (→2 m 4°C 1 cycle Bl)	0.05	0.06	0.06	0.08	0.08	0.11	0.13	0.21
MSK2-7	0.03	0.03	0.03	0.03	0.02	0.03	0.03	0.03
MSK2-8	0.03	0.03	0.03	0.03	0.02	0.03	0.03	0.03
MSK2-9	0.04	0.04	0.03	0.04	0.03	0.04	0.04	0.05
MSK2 (→3 m 4°C 1 cycle Bl)	0.03	0.04	0.03	0.03	0.03	0.04	0.04	0.04
MSK2-10	0.00	-0.02	-0.03	-0.02	-0.03	-0.03	-0.03	-0.03
MSK2-11	0.00	-0.02	-0.03	-0.02	-0.03	-0.03	-0.03	-0.03
MSK2-12	0.00	-0.02	-0.03	-0.02	-0.03	-0.03	-0.03	-0.03
MSK2 (→3 m 4°C no cycling)	0.00	-0.02	-0.03	-0.02	-0.03	-0.03	-0.03	-0.03

Table B10 (continued): Expansion values (%) of Set 2 mortar bars.

Mortar bars	Expansion (%) as a function of time (days)						
	266	273	287	302	315	330	351
MSK2-1	0.09	0.12	0.13	0.16	0.20	0.24	0.28
MSK2-2	0.10	0.13	0.15	0.18	0.22	0.27	0.31
MSK2-3	0.07	0.10	0.11	0.14	0.18	0.22	0.26
MSK2 (1 cycle Bl)	0.09	0.12	0.13	0.16	0.20	0.24	0.28
MSK2-4							
MSK2-5							
MSK2-6							
MSK2 (\rightarrow 2 m 4°C 1 cycle Bl)							
MSK2-7	0.04	0.05	0.03	0.04	0.06	0.08	0.10
MSK2-8	0.04	0.04	0.04	0.05	0.07	0.09	0.10
MSK2-9	0.05	0.06	0.05	0.06	0.09	0.11	0.14
MSK2 (\rightarrow 3 m 4°C 1 cycle Bl)	0.04	0.05	0.04	0.05	0.07	0.09	0.11
MSK2-10	-0.03	-0.03	-0.04	-0.04	-0.02	-0.02	-0.02
MSK2-11	-0.04	-0.03	-0.04	-0.04	-0.02	-0.03	-0.02
MSK2-12	-0.04	-0.03	-0.04	-0.04	-0.03	-0.03	-0.02
MSK2 (\rightarrow 3 m 4°C no cycling)	-0.03	-0.03	-0.04	-0.04	-0.02	-0.03	-0.02

Table B.11: Expansion values (%) of Set 3 (MSK3) mortar specimens stored at 80°C/80% RH, with immersion (twice per week) in bleach (Bl) (6%) solution. The first sub-set of mortar specimens was kept for long-term monitoring in the above conditions. The other sub-sets of mortar bars were transferred at low temperature (4°C/80% RH) after 1 or 1.5 months, while pursuing the immersion (twice per week) in bleach (6%). Average values for each series of 3 bars in grey.

Mortar bars	Expansion (%) as a function of time (days)							
	0	11	18	25	38	41	51	55
MSK3-1	0.00	-0.01	0.00	0.01	0.04	0.05	0.11	0.11
MSK3-2	0.00	-0.01	0.00	0.01	0.04	0.04	0.10	0.11
MSK3-3	0.00	-0.01	0.00	0.01	0.04	0.04	0.10	0.11
MSK3 (2 cycles Bl)	0.00	-0.01	0.00	0.01	0.04	0.05	0.10	0.11
MSK3-4	0.00	-0.01	0.00	0.01	0.04	0.04	0.07	0.07
MSK3-5	0.00	-0.01	0.00	0.02	0.04	0.04	0.05	0.05
MSK3-6	0.00	0.00	0.00	0.01	0.03	0.03	0.05	0.05
MSK3 (\rightarrow 1 m 4°C 2 cycles Bl)	0.00	-0.01	0.00	0.01	0.04	0.03	0.06	0.05
MSK3-7	0.00	-0.01	0.00	0.01	0.04	0.05	0.10	0.11
MSK3-8	0.00	-0.02	-0.01	0.00	0.03	0.04	0.10	0.10
MSK3-9	0.00	-0.01	0.00	0.02	0.05	0.09	0.10	0.11
MSK3 (\rightarrow 1.5 m 4°C 2 cycles Bl)	0.00	-0.01	-0.01	0.01	0.04	0.06	0.10	0.11

Table B11 (continued): Expansion values (%) of Set 3 mortar bars.

Mortar bars	Expansion (%) as a function of time (days)							
	62	69	76	83	90	118	125	139
MSK3-1	0.14	0.16	0.18	0.19	0.21	0.27	0.29	0.29
MSK3-2	0.14	0.15	0.18	0.19	0.21	0.28	0.28	0.30
MSK3-3	0.14	0.15	0.17	0.19	0.21	0.28	0.29	0.30
MSK3 (2 cycles Bl)	0.14	0.15	0.18	0.19	0.21	0.28	0.28	0.30
MSK3-4	0.07	0.07	0.07	0.09	0.13			
MSK3-5	0.06	0.07	0.07	0.14	0.31			
MSK3-6	0.05	0.06	0.06	0.09	0.14			
MSK3 (→1 m 4°C 2 cycles Bl)	0.06	0.07	0.07	0.11	0.20			
MSK3-7	0.13	0.13	0.14	0.15	0.16	0.46		
MSK3-8	0.12	0.13	0.13	0.15	0.16	0.59		
MSK3-9	0.13	0.14	0.14	0.16	0.17	0.61		
MSK3 (→1.5 m 4°C 2 cycles Bl)	0.13	0.13	0.14	0.15	0.16	0.55		

Table B11 (continued): Expansion values (%) of Set 3 mortar bars.

Mortar bars	Expansion (%) as a function of time (days)							
	153	167	174	203	217	231	245	259
MSK3-1	0.31	0.30	0.31	0.34	0.36	0.40	0.41	0.43
MSK3-2	0.31	0.30	0.31	0.34	0.36	0.40	0.42	0.43
MSK3-3	0.34	0.31	0.32	0.35	0.37	0.41	0.42	0.44
MSK3 (2 cycles Bl)	0.32	0.30	0.31	0.34	0.36	0.40	0.42	0.43
MSK3-4								
MSK3-5								
MSK3-6								
MSK3 (→1 m 4°C 2 cycles Bl)								
MSK3-7								
MSK3-8								
MSK3-9								
MSK3 (→1.5 m 4°C 2 cycles Bl)								

Table B11 (continued): Expansion values (%); Set 3 mortar bars.

Mortar bars	Expansion (%) as a function of time (days)						
	266	273	287	302	315	330	351
MSK3-1	0.44	0.46	0.45	0.46	0.48	0.50	0.51
MSK3-2	0.44	0.45	0.45	0.47	0.49	0.50	0.52
MSK3-3	0.45	0.46	0.45	0.48	0.50	0.51	0.52
MSK3 (2 cycles BI)	0.44	0.46	0.45	0.47	0.49	0.50	0.52
MSK3-4							
MSK3-5							
MSK3-6							
MSK3 (→1 m 4°C 2 cycles BI)							
MSK3-7							
MSK3-8							
MSK3-9							
MSK3 (→1.5 m 4°C 2 cycles BI)							

Table B.12: Expansion values (%) of Set 4 (PKA1) mortar specimens stored at 60°C/80% RH, with immersion (twice per week) in bleach (BI) (6%) solution. The first sub-set of mortar specimens was kept for long-term monitoring in the above conditions. The other sub-sets of mortar bars were transferred at low temperature (4°C/80% RH) after 2 or 3 months, while pursuing the immersion (twice per week) in bleach (6%) or without immersion (no cycling). Average values for each series of 3 bars in grey.

Mortar bars	Expansion (%) as a function of time (days)							
	0	4	11	18	31	38	48	52
PKA1-1	-0.07	-0.06	-0.06	-0.05	-0.06	-0.04	-0.04	-0.04
PKA1-2	0.00	-0.08	-0.07	-0.07	-0.06	-0.07	-0.05	-0.05
PKA1-3	-0.02	-0.01	-0.01	0.00	-0.01	0.01	0.01	0.01
PKA1(2 cycles BI)	-0.03	-0.05	-0.04	-0.04	-0.04	-0.03	-0.03	-0.03
PKA1-4	0.00	-0.01	0.00	0.00	0.01	0.00	0.02	0.02
PKA1-5	0.00	-0.01	0.00	0.00	0.00	0.00	0.02	0.02
PKA1-6	0.00	-0.02	-0.01	0.00	0.00	0.00	0.01	0.01
PKA1(→2 m 4°C 2 cycles BI)	0.00	-0.01	0.00	0.00	0.00	0.00	0.02	0.02
PKA1-7	0.00	-0.01	0.00	0.00	0.00	0.00	0.01	0.01
PKA1-8	0.00	-0.01	-0.01	-0.01	-0.01	-0.01	0.01	0.01
PKA1-9	0.00	-0.01	0.00	0.00	0.00	0.00	0.01	0.01
PKA1(→3 m 4°C 2 cycles BI)	0.00	-0.01	0.00	0.00	0.00	0.00	0.01	0.01
PKA1-10	0.00	-0.03	-0.03	-0.03	-0.01	-0.01	-0.03	-0.03
PKA1-11	0.00	-0.02	-0.03	-0.03	-0.01	-0.02	-0.03	-0.03
PKA1-12	0.00	-0.03	-0.03	-0.03	-0.01	-0.02	-0.03	-0.04
PKA1(→3 m 4°C no cycling)	0.00	-0.03	-0.03	-0.03	-0.01	-0.02	-0.03	-0.03

Table B12 (continued): Expansion values (%) of Set 4 mortar bars.

Mortar bars	Expansion (%) as a function of time (days)							
	59	65	72	79	90	114	121	135
PKA1-1	-0.04	-0.04	-0.04	-0.04	-0.03	-0.04	-0.04	-0.04
PKA1-2	-0.05	-0.05	-0.05	-0.05	-0.05	-0.05	-0.05	-0.06
PKA1-3	0.01	0.01	0.01	0.01	0.01	0.01	0.01	0.01
PKA1(2 cycles Bl)	-0.03	-0.03	-0.03	-0.03	-0.02	-0.02	-0.03	-0.03
PKA1-4	0.02	0.02	0.02	0.02	0.02	0.03	0.03	0.02
PKA1-5	0.02	0.02	0.02	0.01	0.01	0.02	0.02	0.01
PKA1-6	0.01	0.01	0.01	0.01	0.01	0.02	0.02	0.01
PKA1(→2 m 4°C 2 cycles Bl)	0.02	0.02	0.01	0.01	0.02	0.02	0.02	0.01
PKA1-7	0.01	0.00	0.00	0.01	0.00	0.02	0.01	0.01
PKA1-8	0.01	0.01	0.01	0.01	0.01	0.02	0.02	0.01
PKA1-9	0.02	0.01	0.01	0.01	0.02	0.03	0.03	0.02
PKA1(→3 m 4°C 2 cycles Bl)	0.01	0.01	0.01	0.01	0.01	0.02	0.02	0.01
PKA1-10	-0.03	-0.04	-0.04	-0.04	-0.04	-0.02	-0.03	-0.03
PKA1-11	-0.03	-0.04	-0.04	-0.04	-0.04	-0.03	-0.03	-0.04
PKA1-12	-0.03	-0.04	-0.04	-0.04	-0.04	-0.02	-0.02	-0.04
PKA1(→3 m 4°C no cycling)	-0.03	-0.04	-0.04	-0.04	-0.04	-0.02	-0.03	-0.04

Table B12 (continued): Expansion values (%) of Set 4 mortar bars.

Mortar bars	Expansion (%) as a function of time (days)							
	149	163	170	200	214	228	242	256
PKA1-1	-0.05	-0.05	-0.05	-0.05	-0.03	-0.03	-0.03	-0.02
PKA1-2	-0.06	-0.06	-0.07	-0.06	-0.06	-0.05	-0.05	-0.05
PKA1-3	0.00	0.00	0.01	0.00	0.02	0.02	0.02	0.03
PKA1(2 cycles Bl)	-0.04	-0.04	-0.04	-0.03	-0.03	-0.02	-0.02	-0.01
PKA1-4	0.02	0.00	0.00	0.01	0.00	0.01	0.00	0.00
PKA1-5	0.01	0.00	0.00	0.00	-0.01	0.00	0.00	0.00
PKA1-6	0.01	0.00	-0.01	0.00	-0.01	0.00	0.00	-0.01
PKA1(→2 m 4°C 2 cycles Bl)	0.01	0.00	0.00	0.00	-0.01	0.00	0.00	0.00
PKA1-7	0.00	0.00	0.00	0.00	-0.01	0.00	0.00	-0.01
PKA1-8	0.01	0.01	0.00	0.00	-0.01	0.00	0.00	-0.01
PKA1-9	0.02	0.02	0.01	0.01	0.00	0.01	0.01	0.01
PKA1(→3 m 4°C 2 cycles Bl)	0.01	0.01	0.01	0.00	-0.01	0.01	0.00	0.00
PKA1-10	-0.03	-0.04	-0.04	-0.03	-0.04	-0.04	-0.04	-0.05
PKA1-11	-0.04	-0.04	-0.05	-0.04	-0.05	-0.04	-0.05	-0.05
PKA1-12	-0.03	-0.03	-0.04	-0.03	-0.04	-0.04	-0.04	-0.04
PKA1(→3 m 4°C no cycling)	-0.03	-0.04	-0.04	-0.03	-0.04	-0.04	-0.04	-0.05

Table B12 (continued): Expansion values (%) of Set 4 mortar bars.

Mortar bars	Expansion (%) as a function of time (days)					
	262	269	283	298	311	326
PKA1-1	-0.01	-0.01	0.01	0.01	0.04	-0.06
PKA1-2	-0.04	-0.03	-0.03	-0.01	0.00	0.02
PKA1-3	0.04	0.04	0.06	0.07	0.09	0.09
PKA1(2 cycles Bl)	0.00	0.00	0.02	0.02	0.04	0.02
PKA1-4	0.00	0.00	-0.01	0.00	0.00	0.01
PKA1-5	-0.01	0.00	-0.01	0.00	0.00	0.00
PKA1-6	0.00	0.00	-0.01	0.00	0.00	0.01
PKA1(→2 m 4°C 2 cycles Bl)	0.00	0.00	-0.01	0.00	0.00	0.01
PKA1-7	0.00	0.00	-0.01	0.00	0.02	0.02
PKA1-8	0.00	0.00	-0.02	-0.01	0.01	0.01
PKA1-9	0.01	0.01	0.00	0.01	0.03	0.03
PKA1(→3 m 4°C 2 cycles Bl)	0.00	0.01	-0.01	0.00	0.04	0.02
PKA1-10	-0.04	-0.04	-0.05	-0.03	-0.04	-0.03
PKA1-11	-0.05	-0.05	-0.06	-0.05	-0.04	-0.04
PKA1-12	-0.04	-0.04	-0.05	-0.04	-0.04	-0.03
PKA1(→3 m 4°C no cycling)	-0.05	-0.04	-0.05	-0.04	-0.04	-0.03

Table B.13: Expansion values (%) of Set 5 (SBR1) mortar specimens stored at 60°C/80% RH, without immersion (no cycling) or with immersion (twice per week) in bleach (6%) solution. The first sub-set of mortar bars that was subjected to cycling in bleach was kept for long term monitoring in this condition, while the other two sub-sets were transferred at low temperature (4°C/80% RH) after 2 or 3 months while pursuing the immersion (twice per week) in bleach (6%). Average values for each series of 3 bars in grey.

Mortar bars	Expansion (%) as a function of time (days)							
	0	4	11	18	31	38	48	52
SBR1-1	0.00	-0.01	0.03	0.12	0.24	0.27	0.37	0.40
SBR1-2	0.00	-0.01	0.02	0.12	0.24	0.28	0.39	0.42
SBR1-3	0.00	-0.01	0.02	0.11	0.23	0.27	0.37	0.41
SBR1(2 cycles Bl)	0.00	-0.01	0.02	0.12	0.24	0.27	0.38	0.41
SBR1-4	0.00	-0.01	0.02	0.11	0.23	0.27	0.37	0.41
SBR1-5	0.00	-0.01	0.02	0.11	0.23	0.27	0.37	0.40
SBR1-6	0.00	-0.01	0.02	0.11	0.23	0.26	0.36	0.39
SBR1(→2 m 4°C 2 cycles Bl)	0.00	-0.01	0.02	0.11	0.23	0.27	0.37	0.40
SBR1-7	0.00	-0.01	0.02	0.11	0.23	0.26	0.36	0.39
SBR1-8	0.00	0.00	0.02	0.11	0.23	0.26	0.36	0.40
SBR1-9	0.00	0.01	0.02	0.10	0.21	0.25	0.35	0.38
SB1(2 cycles Bl→3 m 4°C)	0.00	0.00	0.02	0.11	0.22	0.26	0.36	0.39
SBR1-10	0.00	-0.02	-0.02	-0.02	0.00	-0.01	-0.03	-0.03
SBR1-11	0.00	-0.02	0.00	-0.02	0.00	-0.01	-0.04	-0.04
SBR1-12	0.00	-0.02	-0.03	-0.02	-0.01	-0.01	-0.03	-0.03
SBR1(no cycling)	0.00	-0.02	-0.02	-0.02	-0.01	-0.01	-0.03	-0.03

Table B13 (continued): Expansion values (%) of Set 5 mortar bars.

Mortar bars	Expansion (%) as a function of time (days)							
	59	65	72	79	86	114	121	135
SBR1-1	0.47	0.53	0.58	0.63	0.66	0.75	0.75	0.77
SBR1-2	0.49	0.55	0.61	0.66	0.69	0.79	0.78	0.80
SBR1-3	0.48	0.53	0.59	0.63	0.68	0.78	0.78	0.69
SB1(2 cycles Bl)	0.48	0.54	0.60	0.64	0.67	0.77	0.77	0.76
SBR1-4	0.47	0.54	0.54	0.55	0.56	0.60	0.60	0.61
SBR1-5	0.48	0.54	0.55	0.56	0.57	0.61	0.62	0.63
SBR1-6	0.46	0.51	0.52	0.53	0.54	0.58	0.59	0.60
SBR1(→2 m 4°C 2 cycles Bl)	0.47	0.53	0.54	0.55	0.55	0.60	0.60	0.61
SBR1-7	0.46	0.51	0.52	0.53	0.54	0.58	0.59	0.60
SBR1-8	0.46	0.52	0.57	0.61	0.64	0.76	0.77	0.78
SBR1-9	0.45	0.50	0.55	0.59	0.62	0.74	0.74	0.75
SBR1(2 cycles Bl→3 m 4°C)	0.46	0.51	0.55	0.58	0.60	0.69	0.70	0.71
SBR1-10	-0.03	-0.03	-0.03	-0.04	-0.04	-0.03	-0.03	-0.05
SBR1-11	-0.04	-0.04	-0.04	-0.04	-0.05	-0.04	-0.04	-0.05
SBR1-12	-0.03	-0.03	-0.04	-0.04	-0.04	-0.03	-0.04	-0.05
SBR1(no cycling)	-0.03	-0.04	-0.04	-0.04	-0.04	-0.04	-0.04	-0.05

Table B13 (continued): Expansion values (%) of Set 5 mortar bars.

Mortar bars	Expansion (%) as a function of time (days)							
	149	163	170	200	214	228	242	256
SBR1-1	0.77	0.76	0.77	0.79	0.80	0.84	0.87	0.89
SBR1-2	0.80	0.79	0.79	0.80	0.80	0.83	0.84	0.84
SBR1-3	0.81	0.80	0.80	0.83	0.85	0.90	0.91	0.92
SBR1(2 cycles Bl)	0.80	0.78	0.79	0.81	0.82	0.86	0.87	0.88
SBR1-4	0.63	0.65	0.65	0.68	0.69	0.75	0.79	
SBR1-5	0.65	0.67	0.67	0.69	0.70	0.75	0.79	
SB1-6	0.62	0.63	0.63	0.64	0.65	0.68	0.70	
SBR1(→2 m 4°C 2 cycles Bl)	0.63	0.65	0.65	0.67	0.68	0.72	0.76	
SBR1-7	0.62	0.63	0.63	0.64	0.65	0.68	0.70	
SBR1-8	0.80	0.82	0.83	0.86	0.88	0.93	0.99	
SBR1-9	0.77	0.80	0.80	0.82	0.84	0.88	1.21	
SBR1(2 cycles Bl→3 m 4°C)	0.73	0.75	0.75	0.78	0.79	0.83	0.97	
SBR1-10	-0.05	-0.05	-0.06	-0.05	-0.05	-0.05	-0.06	-0.06
SBR1-11	-0.05	-0.06	-0.06	-0.06	-0.06	-0.06	-0.06	-0.06
SBR1-12	-0.06	-0.06	-0.06	-0.06	-0.06	-0.05	-0.06	-0.06
SBR1(no cycling)	-0.05	-0.06	-0.06	-0.06	-0.06	-0.05	-0.06	-0.06

Table B13 (continued): Expansion values (%) of Set 5 mortar bars.

Mortar bars	Expansion (%) as a function of time (days)					
	262	269	283	298	311	326
SBR1-1	0.91	0.91	0.91	0.94	0.95	0.96
SBR1-2	0.85	0.86	0.84	0.86	0.86	0.87
SBR1-3	0.93	0.94	0.94	0.96	0.96	0.98
SBR1(2 cycles Bl)	0.90	0.90	0.90	0.92	0.92	0.94
SBR1-4						
SBR1-5						
SBR1-6						
SBR1(→2 m 4°C 2 cycles Bl)						
SBR1-7						
SBR1-8						
SBR1-9						
SBR1(2 cycles Bl→3 m 4°C)						
SBR1-10	-0.06	-0.05	-0.06	-0.05	-0.05	-0.04
SBR1-11	-0.06	-0.06	-0.06	-0.05	-0.05	-0.05
SBR1-12	-0.07	-0.06	-0.07	-0.06	-0.06	-0.05
SBR1(no cycling)	-0.06	-0.06	-0.07	-0.05	-0.05	-0.05

Table B.14: Expansion values (%) of Set 6 (PKA2) mortar specimens stored at 80°C/80% RH, without immersion (no cycling) or with immersion (twice per week) in bleach (6%) solution. The first sub-set of mortar bars that was subjected to cycling in bleach was kept for long term monitoring in this condition, while the other two sub-sets were transferred at low temperature (4°C/80% RH) after 2 or 3 months while pursuing the immersion (twice per week) in bleach (6%). Average values for each series of 3 bars in grey.

Mortar bars	Expansion (%) as a function of time (days)							
	0	4	11	18	31	38	48	52
PKA2-1	0.00	-0.02	-0.01	0.00	0.01	0.00	0.02	0.03
PKA2-2	0.00	-0.02	-0.01	-0.01	0.01	0.00	0.03	0.03
PKA2-3	0.00	-0.02	-0.01	0.00	0.01	0.00	0.02	0.03
PKA2 (2 cycles Bl)	0.00	-0.02	-0.01	0.00	0.01	0.00	0.02	0.03
PKA2-4	0.00	-0.02	0.00	0.00	0.01	0.00	0.00	0.00
PKA2-5	0.00	-0.02	-0.01	0.00	0.01	0.01	0.02	0.03
PKA2-6	0.00	-0.02	-0.01	0.00	0.01	0.01	0.03	0.03
PKA2 (→2 m 4°C 2 cycles Bl)	0.00	-0.02	-0.01	0.00	0.01	0.01	0.02	0.02
PKA2-7	0.00	-0.02	-0.01	0.00	0.01	0.01	0.02	0.03
PKA2-8	0.00	-0.01	-0.01	0.00	0.00	0.00	0.03	0.03
PKA2-9	0.00	-0.02	-0.01	0.00	0.00	0.00	0.03	0.03
PKA2 (→3 m 4°C 2 cycles Bl)	0.00	-0.02	-0.01	0.00	0.00	0.01	0.03	0.03
PKA2-10	0.00	0.00	-0.03	-0.01	-0.01	-0.01	-0.03	-0.03
PKA2-11	0.00	0.00	-0.02	0.00	-0.01	-0.01	-0.04	-0.04
PKA2-12	0.00	0.00	-0.03	-0.01	-0.01	-0.01	-0.02	-0.03
PKA2 (no cycling)	0.00	0.00	-0.03	-0.01	-0.01	-0.01	-0.03	-0.03

Table B14 (continued): Expansion values (%) of Set 6 mortar bars.

Mortar bars	Expansion (%) as a function of time (days)							
	59	65	72	79	86	114	121	135
PKA2-1	0.03	0.03	0.03	0.03	0.03	0.05	0.05	0.05
PKA2-2	0.03	0.03	0.03	0.03	0.03	0.05	0.05	0.05
PKA2-3	0.03	0.03	0.03	0.03	0.04	0.05	0.05	0.05
PKA2 (2 cycles Bl)	0.03	0.03	0.03	0.03	0.03	0.05	0.05	0.05
PKA2-4	0.00	0.01	0.01	0.02	0.02	0.03	0.03	0.02
PKA2-5	0.03	0.04	0.03	0.04	0.04	0.05	0.04	0.04
PKA2-6	0.03	0.04	0.04	0.05	0.05	0.06	0.06	0.05
PKA2 (→2 m 4°C 2 cycles Bl)	0.02	0.03	0.03	0.03	0.03	0.05	0.04	0.04
PKA2-7	0.03	0.03	0.04	0.04	0.04	0.05	0.06	0.05
PKA2-8	0.04	0.03	0.04	0.04	0.04	0.06	0.06	0.05
PKA2-9	0.04	0.03	0.04	0.04	0.04	0.07	0.06	0.05
PKA2 (→3 m 4°C 2 cycles Bl)	0.04	0.03	0.04	0.04	0.04	0.06	0.06	0.05
PKA2-10	-0.03	-0.03	-0.03	-0.03	-0.04	-0.03	-0.03	-0.04
PKA2-11	-0.04	-0.04	-0.04	-0.04	-0.04	-0.03	-0.03	-0.04
PKA2-12	-0.02	-0.03	-0.03	-0.03	-0.04	-0.03	-0.03	-0.04
PKA2 (no cycling)	-0.03	-0.03	-0.03	-0.04	-0.04	-0.03	-0.03	-0.04

Table B14 (continued): Expansion values (%) of Set 6 mortar bars.

Mortar bars	Expansion (%) as a function of time (days)							
	149	163	170	200	214	228	242	256
PKA2-1	0.05	0.04	0.04	0.05	0.04	0.07	0.07	0.07
PKA2-2	0.05	0.04	0.04	0.05	0.04	0.06	0.07	0.07
PKA2-3	0.05	0.04	0.04	0.05	0.05	0.06	0.06	0.07
PKA2 (2 cycles Bl)	0.05	0.04	0.04	0.05	0.04	0.06	0.07	0.07
PKA2-4	0.02	0.02	0.02	0.02	0.01	0.02	0.02	0.01
PKA2-5	0.03	0.03	0.04	0.03	0.02	0.03	0.03	0.03
PKA2-6	0.05	0.05	0.04	0.04	0.03	0.04	0.04	0.03
PKA2 (→2 m 4°C 2 cycles Bl)	0.03	0.03	0.03	0.03	0.02	0.03	0.03	0.02
PKA2-7	0.04	0.05	0.04	0.04	0.03	0.04	0.03	0.03
PKA2-8	0.05	0.05	0.04	0.04	0.03	0.04	0.03	0.03
PKA2-9	0.05	0.05	0.04	0.04	0.03	0.05	0.04	0.04
PKA2 (→3 m 4°C 2 cycles Bl)	0.05	0.05	0.04	0.04	0.03	0.04	0.04	0.03
PKA2-10	-0.04	-0.05	-0.05	-0.04	-0.05	-0.05	-0.05	-0.06
PKA2-11	-0.04	-0.05	-0.05	-0.04	-0.05	-0.05	-0.05	-0.05
PKA2-12	-0.04	-0.05	-0.05	-0.04	-0.05	-0.05	-0.05	-0.05
PKA2 (no cycling)	-0.04	-0.05	-0.05	-0.04	-0.05	-0.05	-0.05	-0.05

Table B14 (continued): Expansion values (%) of Set 6 mortar bars.

Mortar bars	Expansion (%) as a function of time (days)					
	262	269	283	298	311	326
PKA2-1	0.07	0.08	0.08	0.09	0.10	0.13
PKA2-2	0.07	0.08	0.08	0.10	0.11	0.12
PKA2-3	0.07	0.08	0.07	0.09	0.10	0.12
PKA2 (2 cycles Bl)	0.07	0.08	0.07	0.09	0.10	0.12
PKA2-4	0.01	0.02	0.04	0.02	0.02	0.04
PKA2-5	0.03	0.03	0.02	0.04	0.04	0.04
PKA2-6	0.04	0.04	0.03	0.04	0.04	0.04
PKA2 (→2 m 4°C 2 cycles Bl)	0.03	0.03	0.03	0.03	0.03	0.04
PKA2-7	0.04	0.04	0.02	0.04	0.05	0.05
PKA2-8	0.04	0.04	0.02	0.03	0.05	0.05
PKA2-9	0.04	0.04	0.03	0.04	0.04	0.05
PKA2 (→3 m 4°C 2 cycles Bl)	0.04	0.04	0.02	0.04	0.05	0.05
PKA2-10	-0.06	-0.05	-0.06	-0.05	-0.04	-0.04
PKA2-11	-0.05	-0.05	-0.06	-0.04	-0.04	-0.04
PKA2-12	-0.06	-0.05	-0.06	-0.04	-0.04	-0.04
PKA2 (no cycling)	-0.06	-0.05	-0.06	-0.04	-0.04	-0.04

Table B.15: Expansion values (%) of Set 7 (SBR2) mortar specimens stored at 80°C/80% RH, without immersion (no cycling) or with immersion (twice per week) in bleach (6%) solution. The first sub-set of mortar bars that were subjected to cycling in bleach was kept for long term monitoring in this condition, while the other two sub-sets were transferred at low temperature (4°C/80% RH) after 2 or 3 months while pursuing the immersion (twice per week) in bleach (6%). Average values for each series of 3 bars in grey.

Mortar bars	Expansion (%) as a function of time (days)							
	0	4	11	18	31	38	48	52
SBR2-1	0.00	-0.01	0.10	0.40	0.60	0.72	0.87	0.95
SBR2-2	0.00	-0.01	0.09	0.39	0.59	0.71	0.87	0.94
SBR2-3	0.00	-0.02	0.09	0.40	0.61	0.74	0.90	0.98
SBR2 (2 cycles Bl)	0.00	-0.01	0.09	0.40	0.60	0.72	0.88	0.96
SBR2-4	0.00	-0.01	0.09	0.38	0.58	0.70	0.86	0.92
SBR2-5	0.00	-0.01	0.10	0.38	0.56	0.67	0.82	0.88
SBR2-6	0.00	0.04	0.09	0.23	0.56	0.67	0.84	0.89
SBR2 (→2 m 4°C 2 cycles Bl)	0.00	0.01	0.10	0.33	0.57	0.68	0.84	0.90
SBR2-7	0.00	0.03	0.10	0.38	0.53	0.69	0.84	0.91
SBR2-8	0.00	-0.03	0.12	0.39	0.59	0.70	0.83	0.90
SBR2-9	0.00	-0.01	0.10	0.37	0.55	0.66	0.81	0.87
SBR2 (→3 m 4°C 2 cycles Bl)	0.00	0.00	0.11	0.38	0.56	0.68	0.83	0.89
SBR2-10	0.00	0.00	-0.01	0.00	0.00	-0.01	-0.02	-0.03
SBR2-11	0.00	-0.01	-0.01	0.00	0.00	0.00	-0.02	-0.03
SBR2-12	0.00	0.00	-0.01	0.00	0.00	0.00	-0.03	-0.03
SBR2 (no cycling)	0.00	0.00	-0.01	0.00	0.00	0.00	-0.02	-0.03

Table B15 (continued): Expansion values (%) of Set 7 mortar bars.

Mortar bars	Expansion (%) as a function of time (days)							
	59	65	72	79	86	114	121	135
SBR2-1	1.00	1.05	1.10	1.15	1.17	1.30	1.31	1.39
SBR2-2	0.99	1.05	1.09	1.14	1.16	1.28	1.29	1.36
SBR2-3	1.03	1.09	1.14	1.19	1.21	1.33	1.34	1.43
SBR2 (2 cycles Bl)	1.01	1.07	1.11	1.16	1.18	1.30	1.31	1.39
SBR2-4	0.97	1.07	1.10	1.11	1.11	1.13	1.13	1.13
SBR2-5	0.95	1.05	1.06	1.07	1.07	1.09	1.09	1.09
SBR2-6	0.96	1.06	1.07	1.08	1.08	1.10	1.10	1.10
SBR2 (→2 m 4°C 2 cycles Bl)	0.96	1.06	1.08	1.09	1.09	1.11	1.11	1.10
SBR2-7	0.98	1.05	1.09	1.13	1.15	1.29	1.28	1.28
SBR2-8	0.97	1.04	1.08	1.13	1.15	1.29	1.29	1.29
SBR2-9	0.94	1.00	1.04	1.09	1.11	1.23	1.23	1.23
SBR2 (→3 m 4°C 2 cycles Bl)	0.97	1.03	1.07	1.11	1.14	1.27	1.27	1.27
SBR2-10	-0.02	-0.03	-0.03	-0.03	-0.03	-0.03	-0.03	-0.03
SBR2-11	-0.03	-0.03	-0.03	-0.04	-0.03	-0.03	-0.03	-0.04
SBR2-12	-0.03	-0.03	-0.03	-0.03	-0.03	-0.03	-0.03	-0.03
SBR2 (no cycling)	-0.03	-0.03	-0.03	-0.03	-0.03	-0.03	-0.03	-0.03

Table B15 (continued): Expansion values (%) of Set 7 mortar bars.

Mortar bars	Expansion (%) as a function of time (days)							
	149	163	170	200	214	228	242	256
SBR2-1	1.41	1.40	1.40	1.40	1.40	1.42	1.42	1.42
SBR2-2	1.37	1.36	1.36	1.36	1.36	1.37	1.37	1.37
SBR2-3	1.44	1.44	1.43	1.44	1.44	1.46	1.46	1.46
SBR2 (2 cycles Bl)	1.41	1.40	1.40	1.40	1.40	1.42	1.41	1.42
SBR2-4	1.13	1.14	1.14	1.14	1.14	1.16	1.18	
SBR2-5	1.09	1.10	1.09	1.09	1.09	1.11	1.13	
SBR2-6	1.10	1.11	1.10	1.11	1.11	1.14	1.16	
SBR2 (→2 m 4°C 2 cycles Bl)	1.11	1.11	1.11	1.11	1.11	1.14	1.16	
SBR2-7	1.28	1.29	1.29	1.29	1.28	1.30	1.30	
SBR2-8	1.29	1.30	1.30	1.30	1.30	1.32	1.33	
SBR2-9	1.24	1.24	1.24	1.24	1.24	1.26	1.27	
SBR2 (→3 m 4°C 2 cycles Bl)	1.27	1.28	1.28	1.28	1.27	1.29	1.30	
SBR2-10	-0.04	-0.04	-0.05	-0.04	-0.05	-0.05	-0.05	-0.05
SBR2-11	-0.04	-0.05	-0.05	-0.04	-0.05	-0.05	-0.06	-0.06
SBR2-12	-0.04	-0.04	-0.05	-0.04	-0.05	-0.05	-0.05	-0.05
SBR2 (no cycling)	-0.04	-0.05	-0.05	-0.04	-0.05	-0.05	-0.05	-0.05

Table B15 (continued): Expansion values (%) of Set 7 mortar bars.

Mortar bars	Expansion (%) as a function of time (days)					
	262	269	283	298	311	326
SBR2-1	1.43	1.44	1.44	1.46	1.46	1.47
SBR2-2	1.37	1.38	1.37	1.39	1.39	1.41
SBR2-3	1.47	1.47	1.48	1.50	1.50	1.52
SBR2 (2 cycles BI)	1.42	1.43	1.43	1.45	1.45	1.47
SBR2-4						
SBR2-5						
SBR2-6						
SBR2 (→2 m 4°C 2 cycles BI)						
SBR2-7						
SBR2-8						
SBR2-9						
SBR2 (→3 m 4°C 2 cycles BI)						
SBR2-10	-0.06	-0.05	-0.06	-0.02	-0.04	-0.03
SBR2-11	-0.06	-0.05	-0.06	-0.05	-0.05	-0.04
SBR2-12	-0.06	-0.05	-0.06	-0.04	-0.04	-0.03
SBR2 (no cycling)	-0.06	-0.05	-0.06	-0.04	-0.04	-0.03

B5.4.2 Expansion as a function of time graphs (second series)

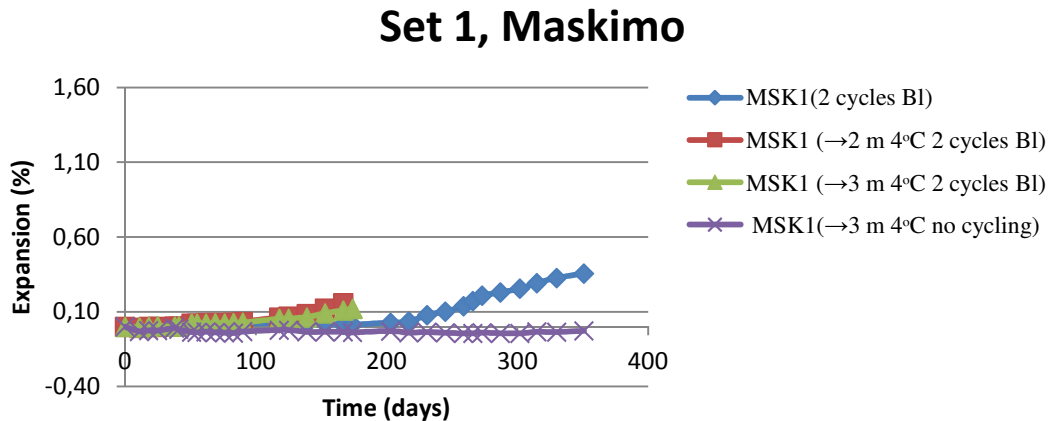


Figure B. 10: Expansion values (%) of Set 1 (MSK1) mortar specimens stored at 60°C/80% RH, with immersion (twice per week) in bleach (6%) (BI) solution. The first sub-set of mortar specimens was kept for long-term monitoring in the above conditions. The other sub-sets of mortar bars were transferred at low temperature (4°C/80% RH) after 2 or 3 months, while pursuing the immersion (twice per week) in bleach (6%), or without immersion (no cycling). Each curve in this figure corresponds to the average values obtained from a set of three bars.

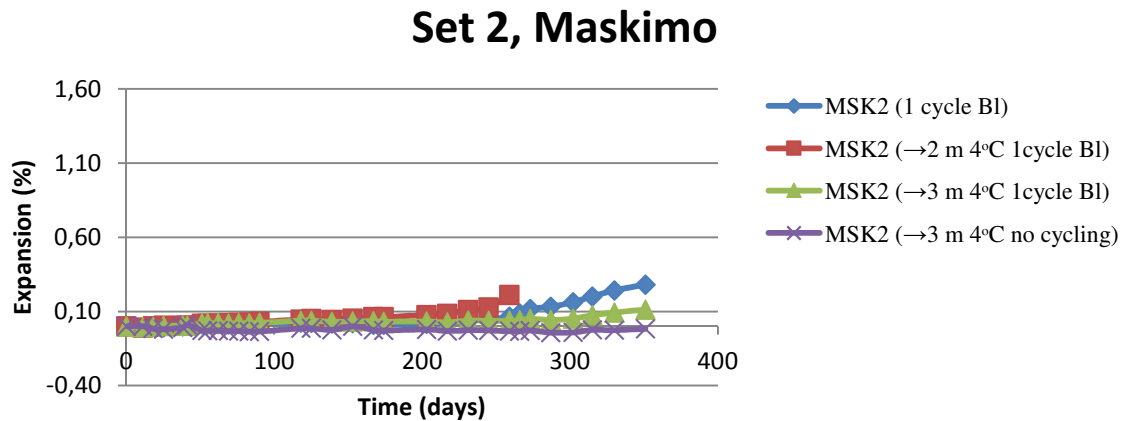


Figure B.11: Expansion values (%) of Set 2 (MSK2) mortar specimens stored at 60°C/80% RH, with immersion (once per week) in bleach (6%) (BI) solution. The first sub-set of mortar specimens was kept for long-term monitoring in the above conditions. The other sub-sets of mortar bars were transferred at low temperature (4°C/80% RH) after 2 or 3 months, while pursuing the immersion (once per week) in bleach (6%), or without immersion (no cycling). Each curve in this figure corresponds to the average values obtained from a set of three bars.

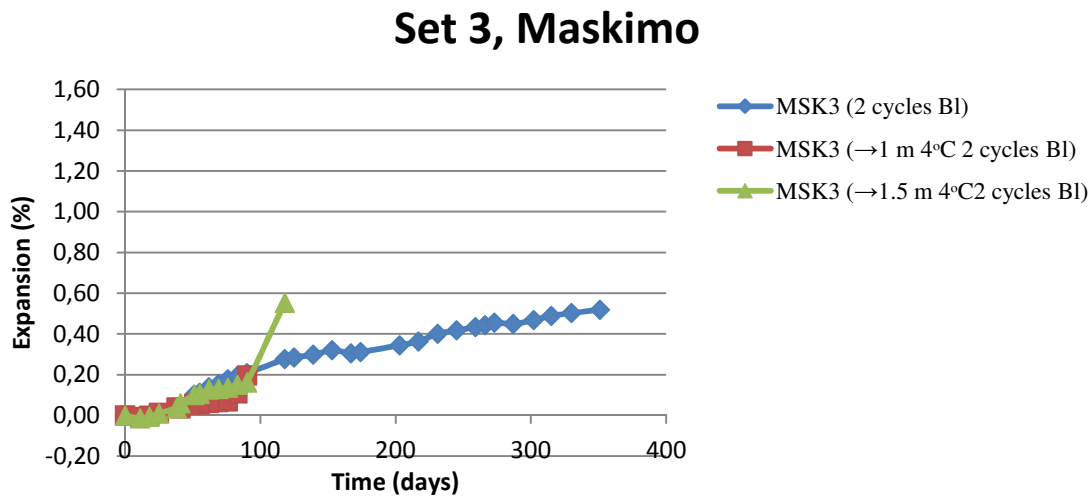


Figure B.12: Expansion values (%) of Set 3 (MSK3) mortar specimens stored at 80°C/80% RH, with immersion (twice per week) in bleach (BI) (6%) solution. The first sub-set of mortar specimens was kept for long-term monitoring in the above conditions. The other sub-sets of mortar bars were transferred at low temperature (4°C/80% RH) after 1 or 1.5 months, while pursuing the immersion (twice per week) in bleach (6%). Each curve in this figure corresponds to the average values obtained from a set of three bars.

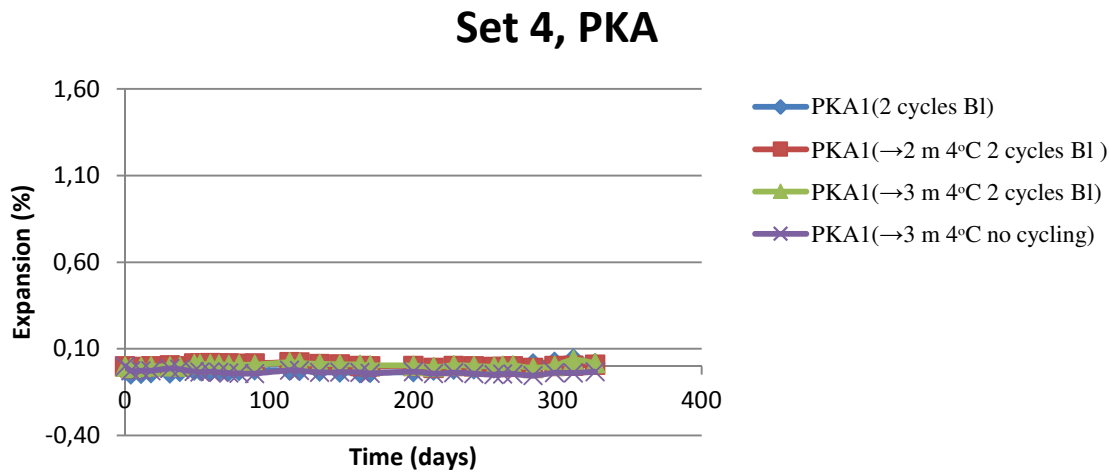


Figure B.13: Expansion values (%) of Set 4 (PKA1) mortar specimens stored at 60°C/80% RH, with immersion (twice per week) in bleach (BI) (6%) solution. The first sub-set of mortar specimens was kept for long-term monitoring in the above conditions. The other sub-sets of mortar bars were transferred at low temperature (4°C/80% RH) after 2 or 3 months, while pursuing the immersion (twice per week) in bleach (6%) or without immersion (no cycling). Each curve in this figure corresponds to the average values obtained from a set of three bars.

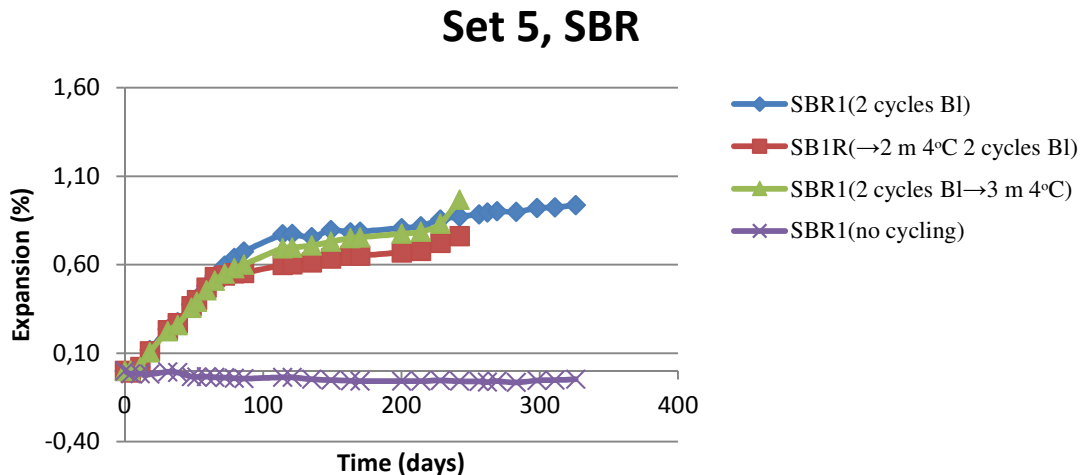


Figure B.14: Expansion values (%) of Set 5 (SBR1) mortar specimens stored at 60°C/80% RH, without immersion (no cycling) or with immersion (twice per week) in bleach (6%) solution. The first sub-set of mortar bars that was subjected to cycling in bleach was kept for long term monitoring in this condition, while the other two sub-sets were transferred at low temperature (4°C/80% RH) after 2 or 3 months while pursuing the immersion (twice per week) in bleach (6%). Each curve in this figure corresponds to the average values obtained from a set of three bars.

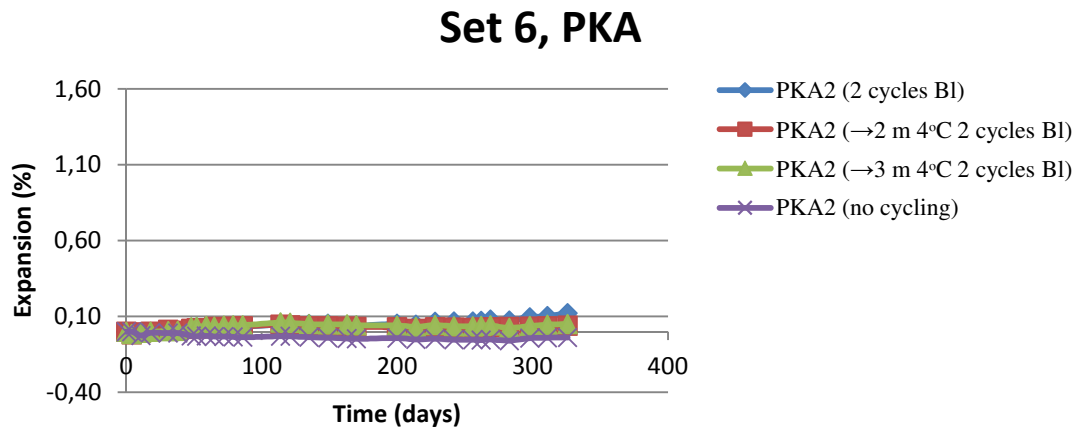


Figure B.15: Expansion values (%) of Set 6 (PKA2) mortar specimens stored at 80°C/80% RH, without immersion (no cycling) or with immersion (twice per week) in bleach (6%) solution. The first sub-set of mortar bars that was subjected to cycling in bleach was kept for long term monitoring in this condition, while the other two sub-sets were transferred at low temperature (4°C/80% RH) after 2 or 3 months while pursuing the immersion (twice per week) in bleach (6%). Each curve in this figure corresponds to the average values obtained from a set of three bars.

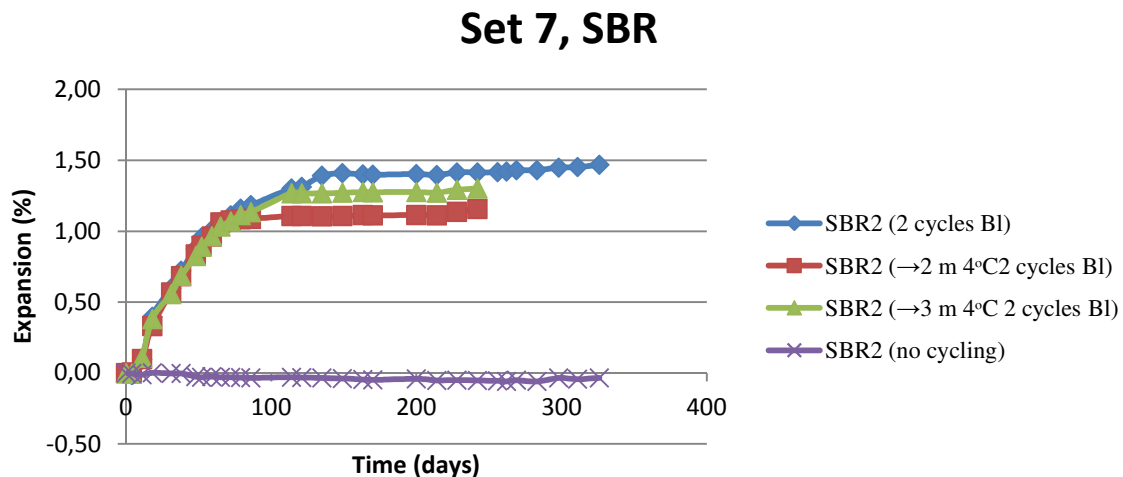


Figure B. 16: Expansion values (%) of Set 7 (SBR2) mortar specimens stored at 80°C/80% RH, without immersion (no cycling) or with immersion (twice per week) in bleach (6%) solution. The first sub-set of mortar bars that were subjected to cycling in bleach was kept for long term monitoring in this condition, while the other two sub-sets were transferred at low temperature (4°C/80% RH) after 2 or 3 months while pursuing the immersion (twice per week) in bleach (6%). Each curve in this figure corresponds to the average values obtained from a set of three bars.

B6 Preliminary tests: series 3

B6.1 Test conditions:

- Temperature: 4°C, 80°C
- Relative humidity (RH): 80%, 100%
- Immersion solutions: bleach (6%), tap water

B6.2 Aggregates tested:

- MSK
- SBR
- GGP
- HPL (control aggregate)
- PKA (control aggregate)

B6.3 Storage conditions

- 4°C/80% RH: bars stored above oversaturated solution of cane sugar in air-tight container
- 4°C/100% RH: bars stored above tap water in air-tight container
- 80°C/80% RH: bars stored above oversaturated solution of NaCl in air-tight container

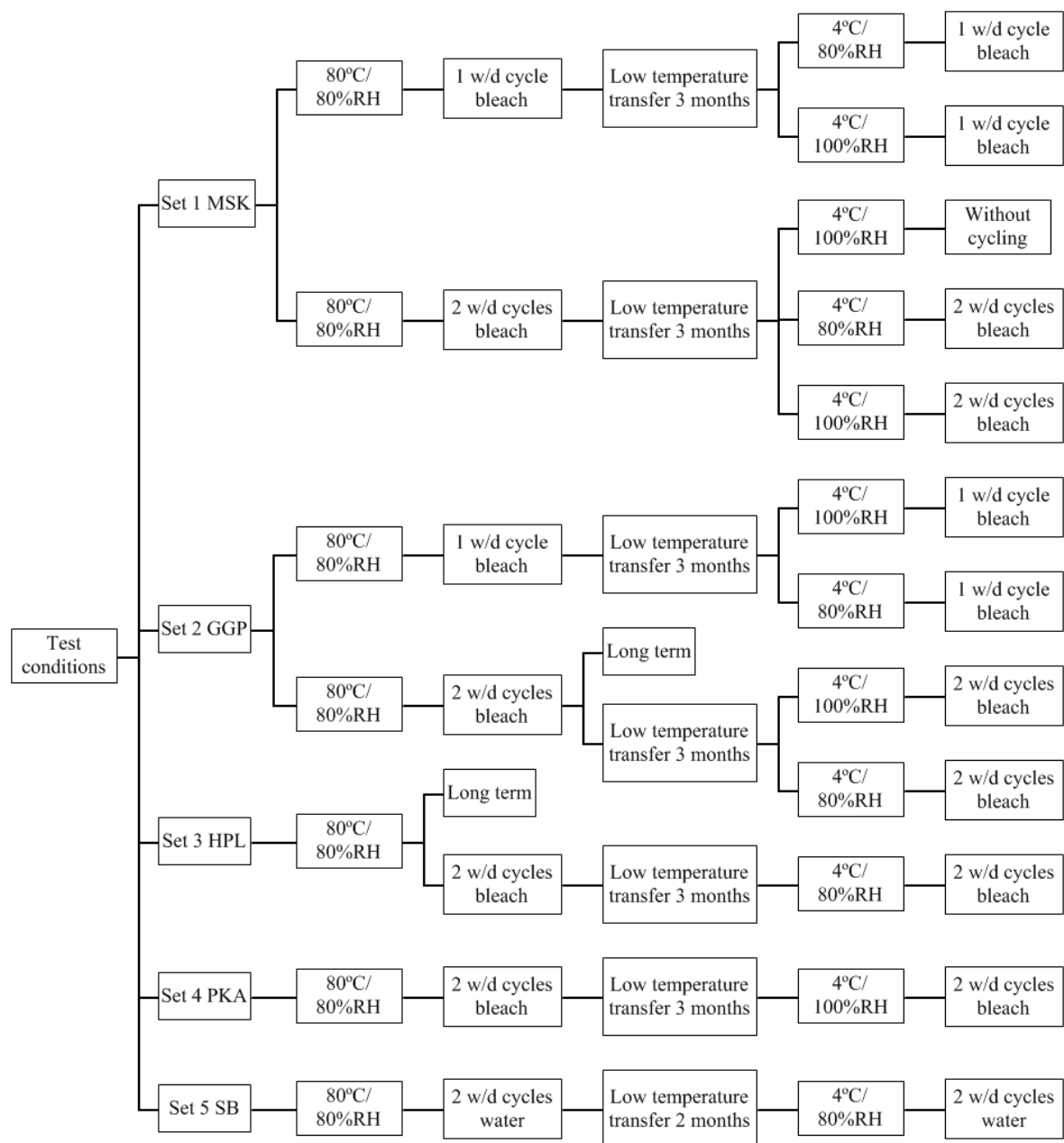


Figure B.17: Experimental program flowchart - testing conditions for the third series.

B6.5 Results

B6.5.1 Expansion values (%) - third series

Table B.16: Expansion values (%) of Set 1 (MSK) mortar specimens stored at 80°C/80% RH, with immersion (once or twice per week) in bleach (Bl) (6%) solution. The different sub-sets of mortar bars were transferred at low temperature (4°C) after 3 months, either at 80% RH or 100% RH, while pursuing the immersion (once or twice per week) in bleach (6%), or without immersion (nc). Average values for each series of 3 bars in grey.

Mortar bars	Expansion (%) as a function of time (days)							
	3	10	17	24	31	56	63	70
MSK-1	-0.01	0.00	-0.01	0.00	0.00	0.07	0.07	0.09
MSK-2	-0.01	0.00	0.00	0.00	0.01	0.05	0.07	0.09
MSK-3	0.00	0.00	-0.01	0.00	0.00	0.06	0.08	0.10
MSK (2cy Bl → 3m 4°C/80%RH Bl)	-0.01	0.00	0.00	0.00	0.00	0.06	0.07	0.09
MSK-4	-0.01	0.00	0.00	0.00	0.01	0.06	0.08	0.10
MSK-5	-0.01	0.00	0.00	0.00	0.01	0.07	0.08	0.09
MSK-6	-0.01	-0.01	-0.01	0.00	0.00	0.07	0.08	0.10
MSK2 (2cy Bl → 3m 4°C/100%RH Bl)	-0.01	0.00	0.00	0.00	0.01	0.07	0.08	0.09
MSK-7	-0.01	0.00	0.00	0.01	0.01	0.06	0.08	0.10
MSK-8	-0.01	0.00	0.00	0.00	0.01	0.06	0.07	0.10
MSK-9	-0.01	0.00	0.00	0.00	0.00	0.06	0.07	0.09
MSK (2cy Bl → 3m 4°C/100%RH nc)	-0.01	0.00	0.00	0.00	0.01	0.06	0.07	0.10
MSK-10	-0.01	0.00	-0.01	-0.01	0.00	0.03	0.05	0.06
MSK-11	-0.01	0.00	-0.01	-0.01	-0.01	0.03	0.05	0.06
MSK-12	0.00	0.00	-0.01	-0.01	0.00	0.03	0.05	0.06
MSK (1cy Bl → 3m 4°C/80%RH Bl)	-0.01	0.00	-0.01	-0.01	0.00	0.03	0.05	0.06
MSK-13	-0.01	-0.01	-0.01	-0.01	0.00	0.03	0.04	0.06
MSK-14	-0.01	0.00	-0.01	-0.01	0.00	0.04	0.06	0.07
MSK-15	-0.01	0.00	-0.01	-0.01	-0.01	0.03	0.05	0.06
MSK (1cy Bl → 3m 4°C/100%RH Bl)	-0.01	0.00	-0.01	-0.01	0.00	0.03	0.05	0.06

Table B16 (continued): Expansion values (%) of Set 1 mortar bars.

Mortar bars	Expansion (%) as a function of time (days)							
	77	84	91	98	105	112	120	127
MSK-1	0.13	0.16	0.17	0.19	0.19	0.21	0.21	0.21
MSK-2	0.13	0.15	0.17	0.18	0.19	0.20	0.20	0.21
MSK-3	0.14	0.17	0.19	0.20	0.20	0.21	0.22	0.22
MSK (2cy Bl → 3m 4°C/80%RH Bl)	0.13	0.16	0.18	0.19	0.20	0.20	0.21	0.21
MSK-4	0.14	0.16	0.18	0.21	0.22	0.23	0.24	0.25
MSK-5	0.13	0.15	0.17	0.19	0.20	0.21	0.21	0.22
MSK-6	0.13	0.16	0.18	0.19	0.20	0.21	0.22	0.23
MSK2 (2cy Bl → 3m 4°C/100%RH Bl)	0.13	0.16	0.18	0.19	0.20	0.22	0.23	0.24
MSK-7	0.13	0.16	0.18	0.19	0.19	0.20	0.20	0.20
MSK-8	0.13	0.15	0.17	0.17	0.18	0.19	0.19	0.19
MSK-9	0.12	0.14	0.16	0.17	0.18	0.19	0.19	0.19
MSK (2cy Bl → 3m 4°C/100%RH nc)	0.13	0.15	0.17	0.18	0.18	0.19	0.19	0.20
MSK-10	0.08	0.10	0.12	0.12	0.12	0.13	0.13	0.13
MSK-11	0.09	0.11	0.13	0.13	0.13	0.14	0.14	0.14
MSK-12	0.10	0.11	0.14	0.13	0.14	0.15	0.16	0.15
MSK (1cy Bl → 3m 4°C/80%RH Bl)	0.09	0.11	0.13	0.13	0.13	0.14	0.14	0.14
MSK-13	0.09	0.11	0.13	0.13	0.14	0.14	0.15	0.15
MSK-14	0.10	0.12	0.14	0.14	0.15	0.16	0.16	0.17
MSK-15	0.09	0.11	0.14	0.14	0.14	0.15	0.15	0.16
MSK (1cy Bl → 3m 4°C/100%RH Bl)	0.09	0.11	0.14	0.14	0.14	0.15	0.15	0.16

Table B16 (continued): Expansion values (%) of Set 1 mortar bars.

Mortar bars	Expansion (%) as a function of time (days)							
	134	141	148	155	170	183	190	198
MSK-1	0.22	0.24	0.24	0.25	0.32	0.38	0.44	0.50
MSK-2	0.22	0.23	0.23	0.24	0.31	0.36	0.40	0.45
MSK-3	0.23	0.24	0.25	0.26	0.34	0.39	0.45	0.51
MSK (2cy B1 → 3m 4°C/80%RH B1)	0.22	0.24	0.24	0.25	0.32	0.38	0.43	0.49
MSK-4	0.27	0.30	0.32	0.36	0.50	0.59	0.67	0.74
MSK-5	0.24	0.27	0.28	0.30	0.40	0.47	0.51	0.56
MSK-6	0.26	0.30	0.30	0.32	0.43	0.52	0.57	0.65
MSK2 (2cy B1 → 3m 4°C/100%RH B1)	0.26	0.29	0.30	0.33	0.44	0.53	0.58	0.65
MSK-7	0.22	0.22	0.20	0.20	0.22	0.23	0.22	0.24
MSK-8	0.20	0.20	0.19	0.19	0.21	0.22	0.21	0.22
MSK-9	0.19	0.20	0.18	0.18	0.20	0.22	0.21	0.22
MSK (2cy B1 → 3m 4°C/100%RH nc)	0.20	0.21	0.19	0.19	0.21	0.22	0.22	0.23
MSK-10	0.13	0.14	0.13	0.13	0.15	0.17	0.17	0.19
MSK-11	0.15	0.15	0.15	0.15	0.18	0.19	0.20	0.22
MSK-12	0.16	0.17	0.15	0.15	0.19	0.19	0.19	0.21
MSK (1cy B1 → 3m 4°C/80%RH B1)	0.15	0.15	0.14	0.14	0.17	0.18	0.19	0.21
MSK-13	0.16	0.17	0.16	0.17	0.21	0.22	0.24	0.26
MSK-14	0.17	0.18	0.18	0.18	0.22	0.25	0.26	0.29
MSK-15	0.16	0.17	0.17	0.17	0.22	0.24	0.26	0.29
MSK (1cy B1 → 3m 4°C/100%RH B1)	0.16	0.17	0.17	0.17	0.22	0.24	0.25	0.28

Table B16 (continued): Expansion values (%) of Set 1 mortar bars.

Mortar bars	Expansion (%) as a function of time (days)							
	205	212	220	227	233	240	247	254
MSK-1	0.54	0.61	0.71	0.81	0.89	0.94	1.02	1.11
MSK-2	0.48	0.53	0.62	0.71	0.78	0.82	0.90	0.97
MSK-3	0.50	0.61	0.71	0.81	0.90	0.95	1.03	1.12
MSK (2cy Bl → 3m 4°C/80%RH Bl)	0.50	0.58	0.68	0.77	0.86	0.91	0.98	1.07
MSK-4	0.78	0.84	0.92	0.98				
MSK-5	0.60	0.64	0.72	0.75				
MSK-6	0.68	0.73	0.81	0.98				
MSK2 (2cy Bl → 3m 4°C/100%RH Bl)	0.69	0.74	0.82	0.91				
MSK-7	0.24	0.24	0.25	0.26	0.26	0.26	0.25	0.25
MSK-8	0.23	0.23	0.24	0.24	0.24	0.25	0.24	0.24
MSK-9	0.22	0.22	0.23	0.24	0.24	0.24	0.23	0.24
MSK (2cy Bl → 3m 4°C/100%RH nc)	0.23	0.23	0.24	0.25	0.25	0.25	0.24	0.25
MSK-10	0.20	0.21	0.22	0.23	0.27	0.28	0.29	0.32
MSK-11	0.23	0.25	0.27	0.26	0.32	0.34	0.35	0.38
MSK-12	0.23	0.24	0.27	0.29	0.33	0.34	0.34	0.37
MSK (1cy Bl → 3m 4°C/80%RH Bl)	0.22	0.23	0.25	0.26	0.31	0.32	0.33	0.36
MSK-13	0.27	0.27	0.30	0.32	0.33	0.35	0.35	0.37
MSK-14	0.30	0.31	0.34	0.35	0.38	0.40	0.40	0.42
MSK-15	0.30	0.31	0.34	0.36	0.37	0.39	0.39	0.42
MSK (1cy Bl → 3m 4°C/100%RH Bl)	0.29	0.30	0.33	0.34	0.36	0.38	0.38	0.40

Table B16 (continued): Expansion values (%) of Set 1 mortar bars.

Mortar bars	Expansion (%) as a function of time (days)							
	261	268	275	283	317	324	331	339
MSK-1	1.21	1.30	1.39	1.48				
MSK-2	1.05	1.12	1.20	1.26				
MSK-3	1.21	1.29	1.38	1.46				
MSK (2cy B1 → 3m 4°C/80%RH B1)	1.16	1.24	1.32	1.40				
MSK-4								
MSK-5								
MSK-6								
MSK2 (2cy B1 → 3m 4°C/100%RH B1)								
MSK-7	0.25	0.25	0.26	0.26	0.26	0.26	0.26	0.27
MSK-8	0.24	0.24	0.25	0.25	0.24	0.24	0.25	0.25
MSK-9	0.24	0.24	0.24	0.24	0.24	0.24	0.24	0.24
MSK (2cy B1 → 3m 4°C/100%RH nc)	0.24	0.24	0.25	0.25	0.25	0.25	0.25	0.25
MSK-10	0.33	0.36	0.38	0.40	0.50	0.51	0.54	0.56
MSK-11	0.40	0.42	0.45	0.47	0.59	0.62	0.64	0.67
MSK-12	0.39	0.41	0.44	0.46	0.57	0.59	0.62	0.65
MSK (1cy B1 → 3m 4°C/80%RH B1)	0.37	0.39	0.42	0.44	0.55	0.57	0.60	0.63
MSK-13	0.39	0.39	0.41	0.43	0.50	0.51	0.52	0.54
MSK-14	0.44	0.45	0.46	0.48	0.54	0.55	0.57	0.59
MSK-15	0.43	0.44	0.46	0.47	0.54	0.55	0.56	0.58
MSK (1cy B1 → 3m 4°C/100%RH B1)	0.42	0.43	0.45	0.46	0.53	0.54	0.55	0.57

Table B16 (continued): Expansion values (%) of Set 1 mortar bars.

Mortar bars	Expansion (%) as a function of time (days)							
	345	352	359	366	373	380	394	408
MSK-1								
MSK-2								
MSK-3								
MSK (2cy B1 → 3m 4°C/80%RH B1)								
MSK-4								
MSK-5								
MSK-6								
MSK2 (2cy B1 → 3m 4°C/100%RH B1)								
MSK-7	0.27	0.26	0.27	0.27	0.28	0.27	0.27	0.27
MSK-8	0.25	0.25	0.25	0.26	0.26	0.26	0.26	0.26
MSK-9	0.24	0.24	0.25	0.25	0.26	0.25	0.25	0.26
MSK (2cy B1 → 3m 4°C/100%RH nc)	0.25	0.25	0.25	0.26	0.26	0.26	0.26	0.26
MSK-10	0.59	0.61	0.63	0.65	0.68	0.70	0.75	0.81
MSK-11	0.70	0.72	0.75	0.77	0.80	0.82	0.88	0.94
MSK-12	0.68	0.70	0.72	0.75	0.78	0.81	0.86	0.93
MSK (1cy B1 → 3m 4°C/80%RH B1)	0.65	0.68	0.70	0.72	0.75	0.78	0.83	0.89
MSK-13	0.56	0.57	0.59	0.60	0.62	0.63	0.67	0.71
MSK-14	0.60	0.62	0.63	0.65	0.66	0.68	0.71	0.75
MSK-15	0.59	0.61	0.62	0.63	0.65	0.67	0.70	0.73
MSK (1cy B1 → 3m 4°C/100%RH B1)	0.59	0.60	0.62	0.63	0.65	0.66	0.69	0.73

Table B16 (continued): Expansion values (%) of Set 1 mortar bars.

Mortar bars	Expansion (%) as a function of time (days)							
	415	422	437	444	451	458	465	472
MSK-1								
MSK-2								
MSK-3								
MSK (2cy B1 → 3m 4°C/80%RH B1)								
MSK-4								
MSK-5								
MSK-6								
MSK2 (2cy B1 → 3m 4°C/100%RH B1)								
MSK-7	0.27	0.28	0.27	0.28	0.27	0.27	0.27	0.28
MSK-8	0.26	0.27	0.26	0.26	0.26	0.26	0.26	0.26
MSK-9	0.25	0.26	0.26	0.26	0.26	0.26	0.25	0.26
MSK (2cy B1 → 3m 4°C/100%RH nc)	0.26	0.27	0.26	0.27	0.27	0.26	0.26	0.27
MSK-10	0.84	0.87	0.93	0.96	0.98			
MSK-11	0.97	1.00	1.08	1.11	1.13			
MSK-12	0.96	0.99	1.09	1.16	1.24			
MSK (1cy B1 → 3m 4°C/80%RH B1)	0.92	0.95	1.03	1.08	1.12			
MSK-13	0.73	0.74	0.79	0.81	0.82	0.84	0.88	0.91
MSK-14	0.76	0.78	0.82	0.84	0.85	0.87	0.89	0.90
MSK-15	0.75	0.76	0.80	0.82	0.83	0.85	0.87	0.88
MSK (1cy B1 → 3m 4°C/100%RH B1)	0.75	0.76	0.80	0.82	0.84	0.85	0.88	0.90

Table B16 (continued): Expansion values (%) of Set 1 mortar bars.

Mortar bars	Expansion (%) as a function of time (days)
	479
MSK-1	
MSK-2	
MSK-3	
MSK (2cy B1 → 3m 4°C/80%RH B1)	
MSK-4	
MSK-5	
MSK-6	
MSK2 (2cy B1 → 3m 4°C/100%RH B1)	
MSK-7	0.28
MSK-8	0.26
MSK-9	0.26
MSK (2cy B1 → 3m 4°C/100%RH nc)	0.27
MSK-10	
MSK-11	
MSK-12	
MSK (1cy B1 → 3m 4°C/80%RH B1)	
MSK-13	0.93
MSK-14	0.92
MSK-15	0.90
MSK (1cy B1 → 3m 4°C/100%RH B1)	0.92

Table B.17: Expansion values (%) of Set 2 (GGP) mortar specimens stored at 80°C/80% RH, with immersion (once or twice per week) in bleach (Bl) (6%) solution. Four sub-sets of mortar bars were transferred at low temperature (4°C) after 3 months, either at 80% RH or 100% RH, while pursuing the immersion (once or twice per week) in bleach (6%). One subset of mortar bars was kept at 80°C/80% RH, while pursuing immersion twice per week in bleach (Bl) (6%) solution (no low-temperature transfer). Average values for each series of 3 bars in grey.

Mortar bars	Expansion (%) as a function of time (days)							
	3	10	17	24	31	56	63	70
GGP-1	-0.01	0.00	-0.01	0.00	0.01	0.08	0.09	0.11
GGP-2	-0.01	-0.01	-0.01	0.00	0.00	0.07	0.08	0.09
GGP-3	-0.01	0.00	0.00	0.00	0.01	0.07	0.08	0.09
GGP (2cy Bl → 3m 4°C/80%RH Bl)	-0.01	0.00	-0.01	0.00	0.01	0.07	0.08	0.10
GGP-4	-0.01	-0.01	-0.01	0.00	0.00	0.08	0.09	0.10
GGP-5	-0.01	0.00	0.00	0.00	0.01	0.08	0.09	0.11
GGP-6	-0.01	0.00	0.00	0.00	0.01	0.08	0.09	0.10
GGP (2cy Bl → 3m 4°C/100%RH Bl)	-0.01	-0.01	0.00	0.00	0.01	0.08	0.09	0.10
GGP-7	0.00	0.00	0.00	0.01	0.08	0.09	0.10	0.14
GGP-8	-0.01	-0.01	0.00	0.00	0.08	0.09	0.11	0.14
GGP-9	-0.01	-0.01	-0.01	0.00	0.07	0.08	0.09	0.12
GGP long term	-0.01	-0.01	0.00	0.01	0.08	0.09	0.10	0.13
GGP-10	0.00	-0.01	-0.01	0.00	0.03	0.04	0.05	0.08
GGP-11	0.00	-0.01	-0.01	0.00	0.04	0.05	0.06	0.09
GGP-12	0.00	-0.01	0.00	0.00	0.04	0.06	0.07	0.10
GGP (1cy Bl → 3m 4°C/80%RH Bl)	0.00	-0.01	-0.01	0.00	0.04	0.05	0.06	0.09
GGP-13	0.00	-0.01	-0.01	0.00	0.04	0.06	0.07	0.10
GGP-14	-0.01	-0.01	-0.01	0.00	0.04	0.06	0.07	0.10
GGP-15	-0.01	-0.01	-0.01	0.00	0.05	0.07	0.07	0.11
GGP (1cy Bl → 3m 4°C/100%RH Bl)	-0.01	-0.01	-0.01	0.00	0.05	0.06	0.07	0.10

Table B17 (continued): Expansion values (%) of Set 2 mortar bars.

Mortar bars	Expansion (%) as a function of time (days)							
	77	84	91	98	105	112	120	127
GGP-1	0.15	0.16	0.18	0.19	0.19	0.19	0.20	0.20
GGP-2	0.12	0.14	0.16	0.17	0.17	0.17	0.17	0.17
GGP-3	0.13	0.15	0.16	0.17	0.17	0.17	0.18	0.18
GGP (2cy Bl → 3m 4°C/80%RH Bl)	0.13	0.15	0.17	0.17	0.18	0.18	0.18	0.18
GGP-4	0.13	0.15	0.16	0.18	0.18	0.19	0.19	0.19
GGP-5	0.13	0.15	0.16	0.17	0.17	0.18	0.18	0.18
GGP-6	0.13	0.15	0.16	0.17	0.17	0.17	0.18	0.18
GGP (2cy Bl → 3m 4°C/100%RH Bl)	0.13	0.15	0.16	0.17	0.18	0.18	0.18	0.18
GGP-7	0.16	0.17	0.19	0.20	0.22	0.23	0.24	0.26
GGP-8	0.16	0.18	0.19	0.21	0.23	0.24	0.25	0.27
GGP-9	0.15	0.17	0.18	0.20	0.22	0.23	0.24	0.26
GGP long term	0.16	0.17	0.19	0.20	0.22	0.23	0.25	0.26
GGP-10	0.10	0.12	0.13	0.13	0.13	0.14	0.14	0.14
GGP-11	0.11	0.13	0.14	0.14	0.14	0.14	0.14	0.14
GGP-12	0.12	0.14	0.14	0.15	0.15	0.15	0.15	0.15
GGP (1cy Bl → 3m 4°C/80%RH Bl)	0.11	0.13	0.14	0.14	0.14	0.14	0.14	0.14
GGP-13	0.12	0.13	0.14	0.15	0.15	0.15	0.15	0.15
GGP-14	0.11	0.13	0.14	0.14	0.15	0.15	0.15	0.15
GGP-15	0.13	0.14	0.15	0.16	0.16	0.16	0.17	0.17
GGP (1cy Bl → 3m 4°C/100%RH Bl)	0.12	0.14	0.14	0.15	0.15	0.16	0.16	0.16

Table B17 (continued): Expansion values (%) of Set 2 mortar bars.

Mortar bars	Expansion (%) as a function of time (days)							
	134	141	148	155	170	183	190	198
GGP-1	0.20	0.20	0.20	0.19	0.21	0.22	0.22	0.22
GGP-2	0.17	0.18	0.17	0.16	0.18	0.19	0.19	0.19
GGP-3	0.18	0.19	0.17	0.17	0.18	0.19	0.20	0.19
GGP (2cy Bl → 3m 4°C/80%RH Bl)	0.18	0.19	0.18	0.17	0.19	0.20	0.20	0.20
GGP-4	0.19	0.20	0.20	0.19	0.20	0.22	0.22	0.22
GGP-5	0.19	0.19	0.19	0.18	0.20	0.21	0.21	0.22
GGP-6	0.18	0.19	0.18	0.18	0.19	0.20	0.20	0.21
GGP (2cy Bl → 3m 4°C/100%RH Bl)	0.19	0.19	0.19	0.18	0.20	0.21	0.21	0.22
GGP-7	0.28	0.28	0.29	0.31	0.32	0.34	0.39	0.38
GGP-8	0.28	0.28	0.30	0.31	0.33	0.34	0.38	0.37
GGP-9	0.27	0.27	0.29	0.30	0.32	0.35	0.38	0.36
GGP long term	0.28	0.27	0.29	0.31	0.32	0.34	0.38	0.37
GGP-10	0.14	0.13	0.13	0.14	0.14	0.15	0.16	0.15
GGP-11	0.15	0.14	0.13	0.14	0.15	0.15	0.16	0.15
GGP-12	0.15	0.15	0.14	0.14	0.15	0.17	0.17	0.16
GGP (1cy Bl → 3m 4°C/80%RH Bl)	0.15	0.14	0.13	0.14	0.14	0.15	0.16	0.15
GGP-13	0.16	0.15	0.15	0.15	0.16	0.16	0.18	0.17
GGP-14	0.16	0.15	0.15	0.16	0.16	0.16	0.18	0.17
GGP-15	0.17	0.16	0.16	0.17	0.17	0.18	0.20	0.19
GGP (1cy Bl → 3m 4°C/100%RH Bl)	0.16	0.16	0.15	0.16	0.16	0.17	0.19	0.18

Table B17 (continued): Expansion values (%) of Set 2 mortar bars.

Mortar bars	Expansion (%) as a function of time (days)							
	205	212	220	227	233	240	247	254
GGP-1	0.23	0.22	0.23	0.23	0.25	0.25	0.25	0.25
GGP-2	0.21	0.20	0.21	0.20	0.23	0.22	0.22	0.23
GGP-3	0.21	0.20	0.20	0.22	0.22	0.23	0.22	0.23
GGP (2cy Bl → 3m 4°C/80%RH Bl)	0.21	0.20	0.21	0.22	0.23	0.23	0.23	0.23
GGP-4	0.23	0.19	0.23	0.23	0.25	0.25	0.25	0.25
GGP-5	0.23	0.22	0.24	0.24	0.25	0.25	0.25	0.25
GGP-6	0.22	0.21	0.23	0.21	0.24	0.24	0.23	0.24
GGP (2cy Bl → 3m 4°C/100%RH Bl)	0.22	0.21	0.23	0.23	0.25	0.25	0.24	0.25
GGP-7	0.40	0.39	0.41	0.41	0.40	0.41	0.41	0.41
GGP-8	0.38	0.40	0.40	0.41	0.40	0.40	0.40	0.40
GGP-9	0.40	0.40	0.41	0.41	0.40	0.40	0.40	0.40
GGP long term	0.40	0.40	0.41	0.41	0.40	0.41	0.41	0.41
GGP-10	0.16	0.16	0.17	0.18	0.16	0.17	0.17	0.17
GGP-11	0.16	0.17	0.17	0.18	0.16	0.17	0.17	0.17
GGP-12	0.17	0.17	0.18	0.18	0.17	0.18	0.18	0.18
GGP (1cy Bl → 3m 4°C/80%RH Bl)	0.16	0.17	0.17	0.18	0.16	0.17	0.17	0.17
GGP-13	0.18	0.19	0.19	0.20	0.18	0.19	0.19	0.19
GGP-14	0.18	0.19	0.19	0.20	0.18	0.19	0.19	0.19
GGP-15	0.20	0.21	0.21	0.22	0.21	0.21	0.22	0.21
GGP (1cy Bl → 3m 4°C/100%RH Bl)	0.19	0.19	0.20	0.20	0.19	0.20	0.20	0.20

Table B17 (continued): Expansion values (%) of Set 2 mortar bars.

Mortar bars	Expansion (%) as a function of time (days)							
	261	268	275	283	289	296	303	310
GGP-1	0.25	0.25	0.26	0.25	0.26	0.26	0.26	0.26
GGP-2	0.23	0.23	0.24	0.23	0.24	0.24	0.24	0.24
GGP-3	0.22	0.23	0.23	0.23	0.23	0.23	0.23	0.23
GGP (2cy Bl → 3m 4°C/80%RH Bl)	0.23	0.24	0.24	0.24	0.24	0.24	0.24	0.25
GGP-4	0.25	0.26	0.22	0.26	0.26	0.27	0.26	0.27
GGP-5	0.26	0.26	0.27	0.27	0.27	0.27	0.26	0.27
GGP-6	0.24	0.25	0.25	0.25	0.25	0.26	0.25	0.26
GGP (2cy Bl → 3m 4°C/100%RH Bl)	0.25	0.26	0.25	0.26	0.26	0.27	0.26	0.27
GGP-7	0.41	0.41	0.42	0.41	0.43	0.42	0.41	0.42
GGP-8	0.40	0.40	0.41	0.40	0.42	0.41	0.40	0.42
GGP-9	0.40	0.40	0.41	0.40	0.41	0.40	0.40	0.41
GGP long term	0.41	0.41	0.42	0.41	0.42	0.41	0.40	0.42
GGP-10	0.17	0.17	0.17	0.17	0.17	0.17	0.16	0.17
GGP-11	0.17	0.17	0.17	0.17	0.17	0.17	0.16	0.17
GGP-12	0.18	0.18	0.18	0.17	0.18	0.17	0.17	0.17
GGP (1cy Bl → 3m 4°C/80%RH Bl)	0.17	0.17	0.17	0.17	0.17	0.17	0.16	0.17
GGP-13	0.19	0.19	0.20	0.19	0.20	0.20	0.19	0.20
GGP-14	0.19	0.20	0.20	0.20	0.20	0.20	0.20	0.20
GGP-15	0.22	0.22	0.22	0.22	0.22	0.23	0.22	0.23
GGP (1cy Bl → 3m 4°C/100%RH Bl)	0.20	0.20	0.21	0.20	0.21	0.21	0.20	0.21

Table B17 (continued): Expansion values (%) of Set 2 mortar bars.

Mortar bars	Expansion (%) as a function of time (days)							
	317	324	331	339	345	352	359	366
GGP-1	0.26	0.26	0.26	0.26	0.27	0.28	0.27	0.28
GGP-2	0.24	0.25	0.25	0.25	0.25	0.26	0.26	0.26
GGP-3	0.24	0.24	0.24	0.24	0.24	0.25	0.25	0.25
GGP (2cy Bl → 3m 4°C/80%RH Bl)	0.25	0.25	0.25	0.25	0.26	0.26	0.26	0.26
GGP-4	0.27	0.27	0.27	0.28	0.28	0.29	0.29	0.28
GGP-5	0.27	0.28	0.28	0.29	0.29	0.29	0.30	0.29
GGP-6	0.26	0.27	0.27	0.27	0.28	0.28	0.29	0.29
GGP (2cy Bl → 3m 4°C/100%RH Bl)	0.27	0.27	0.28	0.28	0.28	0.29	0.29	0.29
GGP-7	0.42	0.42	0.43	0.44	0.43	0.43	0.43	0.43
GGP-8	0.41	0.41	0.42	0.42	0.42	0.42	0.42	0.42
GGP-9	0.40	0.40	0.41	0.42	0.41	0.41	0.41	0.41
GGP long term	0.41	0.41	0.42	0.43	0.42	0.42	0.42	0.42
GGP-10	0.17	0.16	0.16	0.17	0.17	0.17	0.17	0.17
GGP-11	0.17	0.17	0.17	0.17	0.17	0.17	0.17	0.17
GGP-12	0.17	0.17	0.17	0.18	0.18	0.17	0.18	0.18
GGP (1cy Bl → 3m 4°C/80%RH Bl)	0.17	0.17	0.17	0.17	0.17	0.17	0.17	0.17
GGP-13	0.20	0.20	0.20	0.21	0.21	0.21	0.22	0.22
GGP-14	0.21	0.21	0.21	0.21	0.21	0.22	0.22	0.22
GGP-15	0.23	0.23	0.24	0.24	0.25	0.25	0.25	0.25
GGP (1cy Bl → 3m 4°C/100%RH Bl)	0.21	0.21	0.22	0.22	0.22	0.22	0.23	0.23

Table B17 (continued): Expansion values (%) of Set 2 mortar bars.

Mortar bars	Expansion (%) as a function of time (days)							
	373	380	394	408	415	422	437	444
GGP-1	0.27	0.27	0.28	0.28	0.28	0.28	0.29	0.30
GGP-2	0.27	0.27	0.28	0.28	0.28	0.29	0.29	0.30
GGP-3	0.25	0.25	0.26	0.27	0.27	0.27	0.28	0.29
GGP (2cy Bl → 3m 4°C/80%RH Bl)	0.27	0.26	0.27	0.28	0.28	0.28	0.29	0.30
GGP-4	0.29	0.29	0.30	0.30	0.30	0.31	0.31	0.32
GGP-5	0.30	0.30	0.31	0.32	0.32	0.32	0.33	0.33
GGP-6	0.29	0.29	0.30	0.30	0.31	0.31	0.32	0.32
GGP (2cy Bl → 3m 4°C/100%RH Bl)	0.30	0.30	0.30	0.31	0.31	0.31	0.32	0.33
GGP-7	0.43	0.44	0.43	0.43	0.44	0.44	0.44	0.44
GGP-8	0.42	0.42	0.42	0.43	0.42	0.43	0.43	0.43
GGP-9	0.42	0.42	0.41	0.44	0.43	0.44	0.44	0.44
GGP long term	0.42	0.43	0.42	0.43	0.43	0.43	0.44	0.44
GGP-10	0.17	0.17	0.16	0.17	0.17	0.17	0.17	0.17
GGP-11	0.17	0.17	0.17	0.17	0.17	0.17	0.17	0.18
GGP-12	0.18	0.18	0.17	0.18	0.18	0.18	0.18	0.18
GGP (1cy Bl → 3m 4°C/80%RH Bl)	0.17	0.17	0.17	0.17	0.17	0.17	0.17	0.18
GGP-13	0.22	0.22	0.22	0.23	0.23	0.24	0.24	0.24
GGP-14	0.23	0.23	0.23	0.23	0.24	0.24	0.25	0.25
GGP-15	0.26	0.26	0.26	0.27	0.28	0.28	0.28	0.29
GGP (1cy Bl → 3m 4°C/100%RH Bl)	0.24	0.24	0.24	0.24	0.25	0.25	0.25	0.26

Table B17 (continued): Expansion values (%) of Set 2 mortar bars.

Mortar bars	Expansion (%) as a function of time (days)							
	451	458	465	472	479	486	495	508
GGP-1	0.30	0.30	0.30	0.30	0.30	0.31	0.31	0.32
GGP-2	0.30	0.30	0.31	0.31	0.31	0.32	0.32	0.32
GGP-3	0.29	0.29	0.29	0.30	0.30	0.31	0.30	0.31
GGP (2cy Bl \rightarrow 3m 4°C/80%RH Bl)	0.29	0.30	0.30	0.30	0.31	0.31	0.31	0.32
GGP-4	0.32	0.33	0.33	0.33	0.33	0.34	0.34	0.34
GGP-5	0.33	0.34	0.34	0.34	0.35	0.35	0.35	0.37
GGP-6	0.33	0.33	0.33	0.34	0.34	0.35	0.35	0.35
GGP (2cy Bl \rightarrow 3m 4°C/100%RH Bl)	0.33	0.33	0.33	0.34	0.34	0.35	0.35	0.35
GGP-7	0.44	0.44	0.44	0.44	0.44	0.44	0.44	0.44
GGP-8	0.43	0.43	0.43	0.44	0.44	0.44	0.44	0.44
GGP-9	0.44	0.44	0.44	0.44	0.44	0.45	0.45	0.45
GGP long term	0.44	0.43	0.44	0.44	0.44	0.44	0.44	0.44
GGP-10	0.18	0.17	0.18	0.18	0.18	0.18	0.18	0.18
GGP-11	0.18	0.18	0.18	0.18	0.18	0.19	0.18	0.18
GGP-12	0.18	0.21	0.18	0.18	0.18	0.19	0.19	0.18
GGP (1cy Bl \rightarrow 3m 4°C/80%RH Bl)	0.18	0.19	0.18	0.18	0.18	0.18	0.18	0.18
GGP-13	0.25	0.25	0.25	0.26	0.26	0.27	0.27	0.26
GGP-14	0.26	0.25	0.26	0.34	0.26	0.27	0.27	0.27
GGP-15	0.30	0.30	0.30	0.31	0.31	0.32	0.32	0.32
GGP (1cy Bl \rightarrow 3m 4°C/100%RH Bl)	0.27	0.27	0.27	0.30	0.28	0.28	0.28	0.28

Table B17 (continued): Expansion values (%) of Set 2 mortar bars.

Mortar bars	Expansion (%) as a function of time (days)			
	523	530	536	543
GGP-1	0.31	0.33	0.31	0.32
GGP-2	0.32	0.33	0.33	0.34
GGP-3	0.31	0.32	0.32	0.33
GGP (2cy Bl → 3m 4°C/80%RH Bl)	0.32	0.33	0.32	0.33
GGP-4	0.34	0.34	0.34	0.35
GGP-5	0.36	0.37	0.37	0.38
GGP-6	0.36	0.36	0.37	0.37
GGP (2cy Bl → 3m 4°C/100%RH Bl)	0.36	0.36	0.36	0.37
GGP-7	0.44	0.44	0.44	0.45
GGP-8	0.44	0.45	0.45	0.47
GGP-9	0.45	0.45	0.45	0.47
GGP long term	0.44	0.44	0.45	0.46
GGP-10	0.18	0.18	0.17	0.18
GGP-11	0.18	0.18	0.18	0.19
GGP-12	0.18	0.19	0.18	0.19
GGP (1cy Bl → 3m 4°C/80%RH Bl)	0.18	0.18	0.18	0.19
GGP-13	0.27	0.27	0.27	0.28
GGP-14	0.27	0.28	0.28	0.28
GGP-15	0.32	0.33	0.32	0.33
GGP (1cy Bl → 3m 4°C/100%RH Bl)	0.29	0.29	0.29	0.30

Table B.18: Expansion values (%) of Set 3 (HPL) mortar specimens stored at 80°C/80% RH with immersion (twice per week) in bleach (Bl) (6%) solution; that sub-set of mortar bars was transferred at low temperature (4°C/80% RH) after 3 months, while pursuing the immersion (twice per week) in bleach (6%). One subset of mortar bars was kept at 80°C/80% RH for long term monitoring, with no immersion. Average values for each series of 3 bars in grey.

Mortar bars	Expansion (%) as a function of time (days)							
	3	10	17	24	31	56	63	70
HPL-1	0.00	0.00	-0.01	0.00	-0.01	0.00	-0.01	-0.01
HPL-2	-0.01	0.00	-0.01	-0.01	-0.01	0.00	-0.01	-0.02
HPL-3	-0.01	-0.01	-0.01	-0.01	-0.01	0.00	-0.01	-0.02
HPL (2cy Bl → 3m 4°C/80%RH Bl)	-0.01	0.00	-0.01	0.00	-0.01	0.00	-0.01	-0.02
HPL-4	0.00	0.00	-0.01	-0.01	-0.01	-0.01	0.00	-0.01
HPL-5	-0.01	0.00	-0.01	0.00	-0.01	0.00	-0.01	-0.02
HPL-6	-0.01	0.00	-0.01	0.00	-0.01	0.00	-0.01	-0.02
HPL long term	-0.01	0.00	-0.01	0.00	-0.01	0.00	-0.01	-0.02

Table B18 (continued): Expansion values (%) of Set 3 mortar bars.

Mortar bars	Expansion (%) as a function of time (days)							
	77	84	91	98	105	112	120	127
HPL-1	-0.01	-0.01	0.00	-0.02	-0.02	-0.01	-0.01	0.00
HPL-2	-0.01	-0.01	-0.01	-0.01	-0.01	-0.01	-0.01	-0.01
HPL-3	-0.01	-0.01	-0.01	-0.02	-0.02	-0.01	-0.01	-0.01
HPL (2cy Bl → 3m 4°C/80%RH Bl)	-0.01	-0.01	-0.01	-0.01	-0.01	-0.01	-0.01	-0.01
HPL-4	-0.01	-0.01	-0.01	-0.02	-0.02	-0.02	-0.02	-0.02
HPL-5	-0.01	0.00	-0.01	-0.01	-0.02	-0.02	-0.02	-0.02
HPL-6	-0.01	-0.01	-0.01	-0.01	-0.02	-0.02	-0.02	-0.02
HPL long term	-0.01	-0.01	-0.01	-0.01	-0.02	-0.02	-0.02	-0.02

Table B18 (continued): Expansion values (%) of Set 3 mortar bars.

Mortar bars	Expansion (%) as a function of time (days)							
	134	141	148	155	170	183	190	198
HPL-1	0.00	-0.01	-0.02	-0.03	-0.03	-0.01	-0.01	0.00
HPL-2	-0.01	-0.01	-0.02	-0.03	-0.03	-0.01	-0.01	0.00
HPL-3	-0.01	-0.01	-0.01	-0.03	-0.03	-0.01	-0.01	0.00
HPL (2cy Bl → 3m 4°C/80%RH Bl)	-0.01	-0.01	-0.02	-0.03	-0.03	-0.01	-0.01	0.00
HPL-4	-0.02	-0.02	-0.03	-0.03	-0.03	-0.02	-0.02	-0.01
HPL-5	-0.02	-0.01	-0.02	-0.03	-0.03	-0.02	-0.02	-0.01
HPL-6	-0.02	-0.02	-0.02	-0.03	-0.03	-0.02	-0.02	-0.01
HPL long term	-0.02	-0.02	-0.03	-0.03	-0.03	-0.02	-0.02	-0.01

Table B18 (continued): Expansion values (%) of Set 3 mortar bars.

Mortar bars	Expansion (%) as a function of time (days)							
	205	212	220	227	233	240	247	254
HPL-1	0.00	-0.01	-0.01	0.03	0.01	0.01	0.00	0.00
HPL-2	0.00	-0.02	0.00	0.00	0.01	0.01	0.00	0.00
HPL-3	0.00	-0.02	0.00	0.00	0.01	0.01	-0.01	0.00
HPL(2cy Bl → 3m 4°C/80%RH Bl)	0.00	-0.02	0.00	0.01	0.01	0.01	0.00	0.00
HPL-4	-0.01	-0.02	-0.01	0.00	0.00	0.00	-0.02	-0.01
HPL-5	-0.01	-0.02	-0.01	0.00	0.00	0.00	-0.01	0.00
HPL-6	0.00	-0.02	-0.01	0.00	0.00	0.00	-0.01	0.00
HPL long term	-0.01	-0.02	-0.01	0.00	0.00	0.00	-0.01	0.00

Table B18 (continued): Expansion values (%) of Set 3 mortar bars.

Mortar bars	Expansion (%) as a function of time (days)							
	261	268	275	283	289	296	303	310
HPL-1	0.00	0.00	0.00	0.00	0.00	0.00	-0.01	-0.01
HPL-2	0.00	0.00	0.00	0.00	0.00	0.00	-0.01	-0.01
HPL-3	0.00	0.00	0.00	0.00	0.00	0.00	-0.01	0.00
HPL (2cy Bl → 3m 4°C/80%RH Bl)	0.00	0.00	0.00	0.00	0.00	0.00	-0.01	-0.01
HPL-4	-0.01	-0.01	-0.01	-0.01	-0.01	-0.01	-0.02	-0.02
HPL-5	-0.01	-0.01	0.00	-0.01	-0.01	-0.01	-0.02	-0.01
HPL-6	0.00	-0.01	0.00	0.00	-0.01	-0.01	-0.01	-0.01
HPL long term	-0.01	-0.01	0.00	-0.01	-0.01	-0.01	-0.02	-0.01

Table B18 (continued): Expansion values (%) of Set 3 mortar bars.

Mortar bars	Expansion (%) as a function of time (days)							
	317	324	331	339	345	352	359	366
HPL-1	-0.01	-0.01	-0.01	-0.01	-0.01	-0.01	-0.01	-0.01
HPL-2	-0.01	-0.01	-0.01	-0.01	-0.01	-0.01	-0.01	-0.01
HPL-3	-0.01	0.00	-0.01	0.00	0.00	0.00	0.00	0.00
HPL (2cy Bl → 3m 4°C/80%RH Bl)	-0.01	-0.01	-0.01	0.00	0.00	-0.01	-0.01	-0.01
HPL-4	-0.02	-0.02	-0.02	-0.01	-0.01	-0.02	-0.02	-0.02
HPL-5	-0.01	-0.01	-0.01	-0.01	-0.01	-0.01	-0.01	-0.01
HPL-6	-0.01	-0.01	-0.01	-0.01	-0.01	-0.01	-0.01	-0.01
HPL long term	-0.01	-0.01	-0.01	-0.01	-0.01	-0.01	-0.01	-0.01

Table B18 (continued): Expansion values (%) of Set 3 mortar bars.

Mortar bars	Expansion (%) as a function of time (days)							
	373	380	394	408	415	422	437	444
HPL-1	0.00	-0.01	-0.01	-0.01	-0.01	0.00	-0.01	0.00
HPL-2	0.00	-0.01	-0.01	-0.01	-0.01	0.00	-0.01	0.00
HPL-3	0.00	0.00	0.00	0.00	0.00	0.00	0.00	0.00
HPL (2cy B1 → 3m 4°C/80%RH B1)	0.00	-0.01	-0.01	-0.01	0.00	0.00	-0.01	0.00
HPL-4	-0.01	-0.02	-0.02	-0.01	-0.01	-0.01	-0.01	-0.01
HPL-5	-0.01	-0.01	-0.01	-0.01	-0.01	-0.01	-0.01	-0.01
HPL-6	-0.01	-0.01	-0.01	-0.01	-0.01	-0.01	-0.01	-0.01
HPL long term	-0.01	-0.01	-0.01	-0.01	-0.01	-0.01	-0.01	-0.01

Table B18 (continued): Expansion values (%) of Set 3 mortar bars.

Mortar bars	Expansion (%) as a function of time (days)							
	451	458	465	472	479	486	495	508
HPL-1	-0.01	0.00	0.00	0.00	0.00	0.00	0.00	-0.01
HPL-2	-0.01	0.00	0.00	0.00	0.00	0.00	0.00	-0.01
HPL-3	0.00	0.00	0.00	0.00	0.00	0.00	0.00	0.00
HPL (2cy B1 → 3m 4°C/80%RH B1)	-0.01	0.00	0.00	0.00	0.00	0.00	0.00	-0.01
HPL-4	-0.01	-0.01	-0.01	-0.01	-0.01	-0.05	-0.01	-0.01
HPL-5	-0.01	-0.01	-0.01	-0.01	-0.01	-0.01	-0.01	-0.01
HPL-6	-0.01	-0.01	0.00	0.00	-0.01	-0.07	0.00	-0.01
HPL long term	-0.01	-0.01	-0.01	-0.01	-0.01	-0.04	-0.01	-0.01

Table B18 (continued): Expansion values (%) of Set 3 mortar bars.

Mortar bars	Expansion (%) as a function of time (days)			
	523	530	536	543
HPL-1	-0.01	-0.01	-0.01	0.00
HPL-2	-0.01	-0.01	-0.01	0.00
HPL-3	-0.01	-0.01	-0.01	0.00
HPL (2cy B1 → 3m 4°C/80%RH B1)	-0.01	-0.01	-0.01	0.00
HPL-4	-0.01	-0.02	-0.02	-0.01
HPL-5	-0.02	-0.01	-0.01	-0.01
HPL-6	-0.01	-0.01	-0.01	-0.03
HPL long term	-0.01	-0.01	-0.01	-0.02

Table B. 19: Expansion values (%) of Set 4 PKA mortar specimens stored at 80°C/80% RH with immersion (twice per week) in bleach (Bl) (6%) solution; the mortar bars were transferred at low temperature (4°C/100% RH) after 3 months, while pursuing the immersion (twice per week) in bleach (6%). Average values for each series of 3 bars in grey.

Mortar bars	Expansion (%) as a function of time (days)							
	3	10	35	42	49	56	63	70
PKA-1	-0.02	-0.01	0.01	0.01	0.01	0.02	0.01	0.01
PKA-2	-0.02	-0.01	0.01	0.01	0.00	0.01	0.01	0.01
PKA-3	-0.02	-0.01	0.01	0.00	0.01	0.02	0.02	0.02
PKA (2cy Bl → 3m 4°C/80%RH Bl)	-0.02	-0.01	0.01	0.01	0.01	0.02	0.01	0.01

Table B19 (continued): Expansion values (%) of Set 4 mortar bars.

Mortar bars	Expansion (%) as a function of time (days)							
	77	84	91	98	105	112	119	126
PKA-1	0.01	0.01	0.00	0.01	0.01	0.01	0.02	0.01
PKA-2	0.01	0.01	0.01	0.02	0.02	0.02	0.02	0.01
PKA-3	0.01	0.01	0.01	0.02	0.02	0.02	0.02	0.02
PKA (2cy Bl → 3m 4°C/80%RH Bl)	0.01	0.01	0.01	0.02	0.02	0.02	0.02	0.01

Table B19 (continued): Expansion values (%) of Set 4 mortar bars.

Mortar bars	Expansion (%) as a function of time (days)							
	133	141	148	155	161	168	176	183
PKA-1	0.00	0.00	0.00	0.02	0.02	0.02	0.02	0.03
PKA-2	0.00	0.01	0.01	0.02	0.02	0.02	0.03	0.03
PKA-3	0.01	0.02	0.02	0.02	0.03	0.02	0.03	0.04
PKA (2cy Bl → 3m 4°C/80%RH Bl)	0.00	0.01	0.01	0.02	0.02	0.02	0.03	0.03

Table B19 (continued): Expansion values (%) of Set 4 mortar bars.

Mortar bars	Expansion (%) as a function of time (days)							
	190	198	205	211	218	225	232	239
PKA-1	0.02	0.03	0.03	0.04	0.04	0.03	0.04	0.04
PKA-2	0.03	0.03	0.03	0.04	0.04	0.03	0.04	0.04
PKA-3	0.03	0.03	0.03	0.04	0.05	0.03	0.04	0.04
PKA (2cy Bl → 3m 4°C/80%RH Bl)	0.02	0.03	0.03	0.04	0.04	0.03	0.04	0.04

Table B19 (continued): Expansion values (%) of Set 4 mortar bars.

Mortar bars	Expansion (%) as a function of time (days)							
	246	253	261	267	274	281	289	296
PKA-1	0.04	0.04	0.04	0.04	0.04	0.03	0.03	0.03
PKA-2	0.04	0.04	0.04	0.04	0.04	0.03	0.04	0.03
PKA-3	0.04	0.04	0.04	0.04	0.04	0.03	0.04	0.04
PKA (2cy Bl → 3m 4°C/80%RH Bl)	0.04	0.04	0.04	0.04	0.04	0.03	0.04	0.04

Table B19 (continued): Expansion values (%) of Set 4 mortar bars.

Mortar bars	Expansion (%) as a function of time (days)							
	303	310	318	324	331	338	345	352
PKA-1	0.03	0.03	0.03	0.04	0.03	0.04	0.03	0.04
PKA-2	0.03	0.03	0.03	0.04	0.04	0.04	0.04	0.04
PKA-3	0.04	0.03	0.03	0.03	0.04	0.04	0.04	0.04
PKA (2cy Bl → 3m 4°C/80%RH Bl)	0.03	0.03	0.03	0.04	0.04	0.04	0.04	0.04

Table B19: Expansion values (%) Set 4 (continuation)

Mortar bars	Expansion (%) as a function of time (days)							
	359	366	373	387	394	401	416	423
PKA-1	0.03	0.03	0.03	0.04	0.03	0.03	0.04	0.04
PKA-2	0.04	0.04	0.04	0.04	0.04	0.04	0.04	0.04
PKA-3	0.04	0.04	0.04	0.04	0.04	0.04	0.04	0.04
PKA (2cy Bl → 3m 4°C/80%RH Bl)	0.04	0.03	0.04	0.04	0.04	0.04	0.04	0.04

Table B19 (continued): Expansion values (%) of Set 4 mortar bars.

Mortar bars	Expansion (%) as a function of time (days)							
	430	437	444	451	458	465	472	485
PKA-1	0.03	0.04	0.04	0.04	0.04	0.04	0.04	0.04
PKA-2	0.04	0.04	0.04	0.04	0.04	0.04	0.04	0.04
PKA-3	0.04	0.04	0.04	0.04	0.04	0.04	0.04	0.04
PKA (2cy Bl → 3m 4°C/80%RH Bl)	0.04	0.04	0.04	0.04	0.04	0.04	0.04	0.04

Table B19 (continued): Expansion values (%) of Set 4 mortar bars.

Mortar bars	Expansion (%) as a function of time (days)			
	500	507	512	519
PKA-1	0.03	0.04	0.03	0.04
PKA-2	0.03	0.04	0.03	0.04
PKA-3	0.04	0.04	0.04	0.04
PKA (2cy Bl → 3m 4°C/80%RH Bl)	0.04	0.04	0.03	0.04

Table B. 20: Expansion values (%) of Set 5 SBR mortar specimens stored at 80°C/80% RH with immersion (twice per week) in tap water (Tw); the mortar bars were transferred at low temperature (4°C/80% RH) after 3 months, while pursuing the immersion (twice per week) in tap water.

Mortar bars	Expansion (%) as a function of time (days)							
	3	10	17	24	31	56	63	70
SBR-1	0.00	0.00	-0.01	-0.01	-0.01	0.00	0.00	0.00
SBR-2	0.00	0.00	-0.01	-0.01	-0.01	0.00	0.00	0.00
SBR-3	0.00	0.00	-0.01	-0.01	-0.01	0.00	0.00	0.01
SBR 2(2cy Bl → 3m 4°C/80%RH Tw)	0.00	0.00	-0.01	-0.01	-0.01	0.00	0.00	0.00

Table B20 (continued): Expansion values (%) of Set 5 mortar bars.

Mortar bars	Expansion (%) as a function of time (days)							
	77	84	91	98	105	112	120	127
SBR-1	0.01	0.01	0.02	0.01	0.01	0.01	0.01	0.01
SBR-2	0.01	0.01	0.01	0.01	0.01	0.02	0.01	0.01
SBR-3	0.02	0.02	0.02	0.02	0.01	0.02	0.02	0.02
SBR 2 (2cy Bl → 3m 4°C/80%RH Tw)	0.01	0.01	0.02	0.01	0.01	0.02	0.01	0.02

Table B20 (continued): Expansion values (%) of Set 5 mortar bars.

Mortar bars	Expansion (%) as a function of time (days)							
	134	141	148	155	170	183	190	198
SBR-1	0.01	0.02	0.01	0.01	0.00	0.01	0.02	0.02
SBR-2	0.01	0.02	0.01	0.01	0.01	0.02	0.02	0.03
SBR-3	0.02	0.03	0.02	0.02	0.02	0.02	0.02	0.03
SBR 2 (2cy Bl → 3m 4°C/80%RH Tw)	0.02	0.02	0.01	0.01	0.01	0.02	0.02	0.03

Table B20 (continued): Expansion values (%) of Set 5 mortar bars.

Mortar bars	Expansion (%) as a function of time (days)							
	205	212	220	227	233	240	247	254
SBR-1	0.03	0.03	0.03	0.03	0.04	0.03	0.02	0.03
SBR-2	0.04	0.03	0.03	0.04	0.04	0.03	0.02	0.03
SBR-3	0.03	-0.25	0.03	0.03	0.04	0.04	0.02	0.03
SBR 2 (2cy Bl → 3m 4°C/80%RH Tw)	0.03	-0.06	0.03	0.04	0.04	0.04	0.02	0.03

Table B20 (continued): Expansion values (%) of Set 5 mortar bars.

Mortar bars	Expansion (%) as a function of time (days)							
	261	268	275	283	289	296	303	310
SBR-1	0.03	0.03	0.03	0.02	0.02	0.02	0.02	0.02
SBR-2	0.03	0.03	0.03	0.03	0.03	0.03	0.02	0.03
SBR-3	0.03	0.03	0.03	0.03	0.03	0.10	0.03	0.03
SBR 2 (2cy B1 → 3m 4°C/80%RH Tw)	0.03	0.03	0.03	0.03	0.03	0.05	0.02	0.03

Table B20 (continued): Expansion values (%) of Set 5 mortar bars.

Mortar bars	Expansion (%) as a function of time (days)							
	317	324	331	339	345	352	359	366
SBR-1	0.02	0.02	0.02	0.02	0.02	0.02	0.02	0.02
SBR-2	0.03	0.02	0.02	0.02	0.03	0.03	0.03	0.02
SBR-3	0.03	0.03	0.03	0.03	0.03	0.03	0.03	0.03
SBR 2 (2cy B1 → 3m 4°C/80%RH Tw)	0.02	0.02	0.02	0.02	0.03	0.02	0.02	0.02

Table B20 (continued): Expansion values (%) of Set 5 mortar bars.

Mortar bars	Expansion (%) as a function of time (days)							
	373	380	394	408	415	422	437	444
SBR-1	0.02	0.02	0.02	0.02	0.02	0.03	0.02	0.02
SBR-2	0.03	0.02	0.02	0.02	0.02	0.03	0.02	0.03
SBR-3	0.03	0.02	0.03	0.03	0.02	0.03	0.02	0.03
SBR 2 (2cy B1 → 3m 4°C/80%RH Tw)	0.03	0.02	0.02	0.02	0.02	0.03	0.02	0.03

Table B20 (continued): Expansion values (%) of Set 5 mortar bars.

Mortar bars	Expansion (%) as a function of time (days)							
	451	458	465	472	479	486	495	508
SBR-1	0.02	0.02	0.02	0.02	0.02	0.03	0.02	0.02
SBR-2	0.02	0.03	0.03	0.03	0.03	0.03	0.03	0.02
SBR-3	0.10	0.03	0.03	0.03	0.03	0.03	0.03	0.03
SBR 2 (2cy B1 → 3m 4°C/80%RH Tw)	0.05	0.03	0.02	0.02	0.02	0.03	0.03	0.02

Table B20 (continued): Expansion values (%) of Set 5 mortar bars.

Mortar bars	Expansion (%) as a function of time (days)			
	523	530	536	543
SBR-1	0.01	0.02	0.01	0.02
SBR-2	0.02	0.02	0.02	0.02
SBR-3	0.03	0.03	0.02	0.02
SBR 2 (2cy B1 → 3m 4°C/80%RH Tw)	0.02	0.02	0.02	0.02

B6.5.2 Expansion (%) as a function of time (days) graphs (third series)

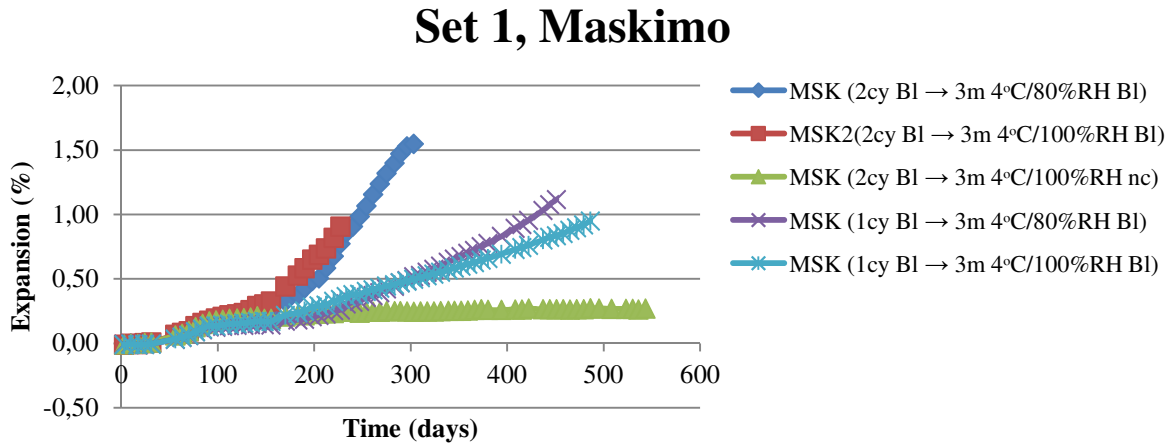


Figure B.18: Expansion values (%) of Set 1 (MSK) mortar specimens stored at 80°C/80% RH, with immersion (once or twice per week) in bleach (BI) (6%) solution. The different sub-sets of mortar bars were transferred at low temperature (4°C) after 3 months, either at 80% RH or 100% RH, while pursuing the immersion (once or twice per week) in bleach (6%), or without immersion (nc). Each curve in this figure corresponds to the average values obtained from a set of three bars.

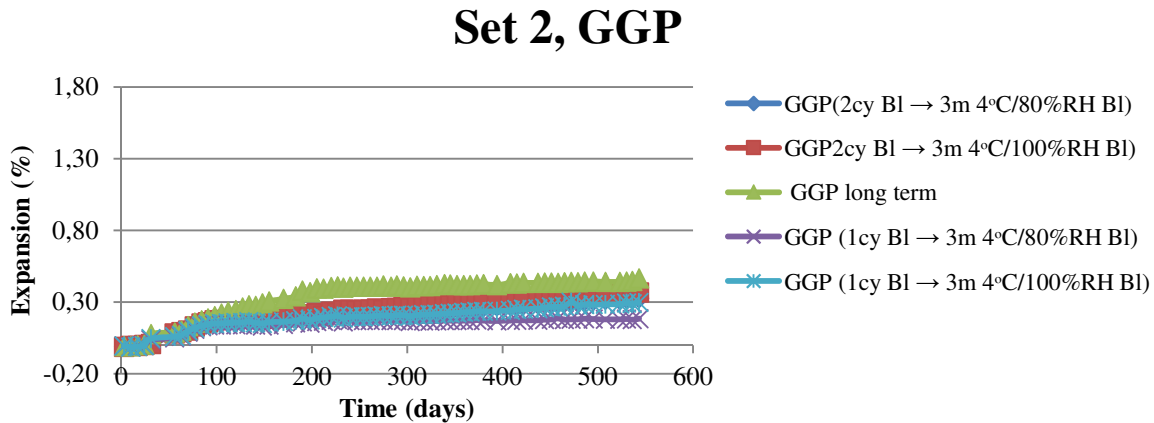


Figure B.19: Expansion values (%) of Set 2 (GGP) mortar specimens stored at 80°C/80% RH, with immersion (once or twice per week) in bleach (BI) (6%) solution. Four sub-sets of mortar bars were transferred at low temperature (4°C) after 3 months, either at 80% RH or 100% RH, while pursuing the immersion (once or twice per week) in bleach (6%). One subset of mortar bars was kept at 80°C/80% RH, while pursuing immersion twice per week in bleach (BI) (6%) solution (no low-temperature transfer). Each curve in this figure corresponds to the average values obtained from a set of three bars.

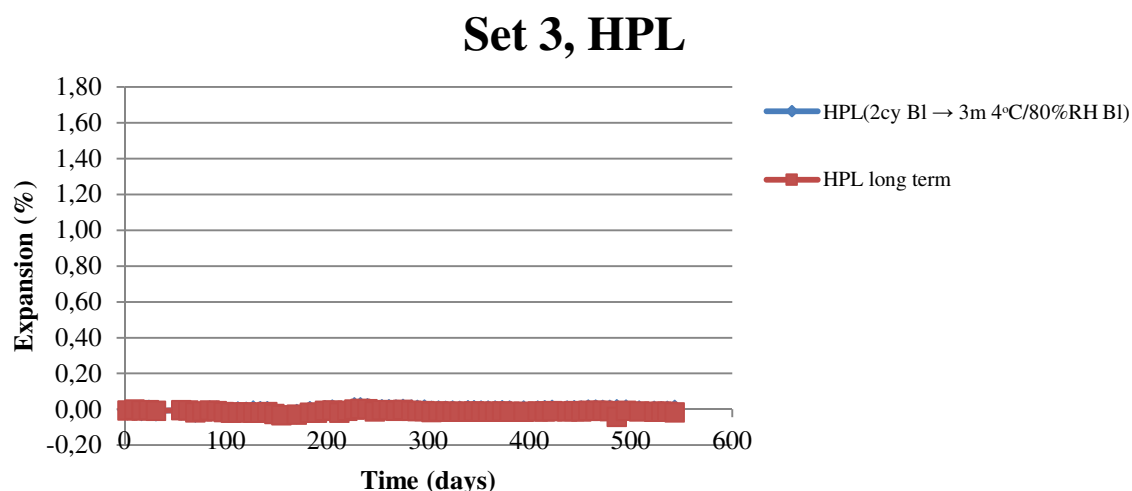


Figure B.20: Expansion values (%) of Set 3 (HPL) mortar specimens stored at 80°C/80% RH with immersion (twice per week) in bleach (BI) (6%) solution; that sub-set of mortar bars were transferred at low temperature (4°C/80% RH) after 3 months, while pursuing the immersion (twice per week) in bleach (6%). One subset of mortar bars was kept at 80°C/80% RH for long term monitoring, with no immersion. Each curve in this figure corresponds to the average values obtained from a set of three bars.

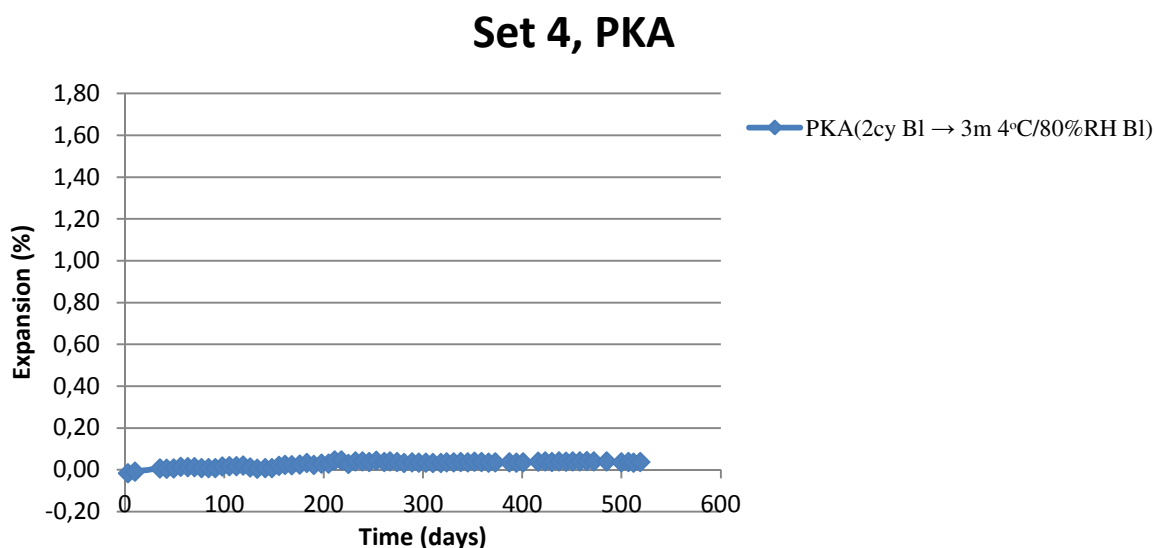


Figure B.21: Expansion values (%) of Set 4 PKA mortar specimens stored at 80°C/80% RH with immersion (twice per week) in bleach (BI) (6%) solution; the mortar bars were transferred at low temperature (4°C/100% RH) after 3 months, while pursuing the immersion (twice per week) in bleach (6%). Each curve in this figure corresponds to the average values obtained from a set of three bars.

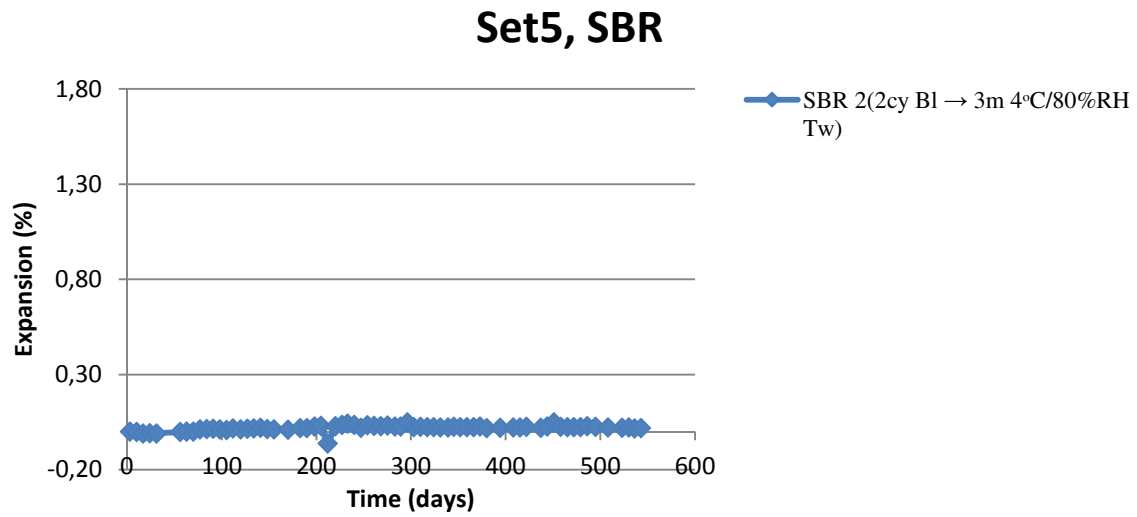


Figure B.22: Expansion values (%) of Set 5 SB mortar specimens stored at 80°C/80% RH with immersion (twice per week) in tap water (Tw); the mortar bars were transferred at low temperature (4°C/80% RH) after 3 months, while pursuing the immersion (twice per week) in tap water. Each curve in this figure corresponds to the average values obtained from a set of three bars.

B7 Optimized test conditions

B7.1 Test conditions:

- *Phase 1*: 80°C/ 80% RH for a 90-day period, with two 3-h immersion periods in a 6% bleach solution per week.
- *Phase 2*: 4°C/ 100% RH for a 90-day period, with two 3-h immersion periods in a 6% bleach solution per week.

B7.2 Aggregates tested:

- MSK
- GGP
- B&B
- SDBR
- SW
- SPH
- DLS
- HPL (control aggregate)
- PKA (control aggregate)

B7.3 Storage conditions

- 4°C/100% RH: bars stored above tap water in air-tight container
- 80°C/80% RH: bars stored above oversaturated solution of NaCl in air-tight container

B7.4 Results

B7.4.1 Expansion values (%) optimized conditions

Table B.21: Expansion values (%) of mortar specimens stored at 80°C/80% RH, with immersion (twice per week) in bleach (6%) solution. The mortar bars were transferred at low temperature (4°C/100% RH) after 90 days, while pursuing the immersion (twice per week) in bleach (6%). Average values for each series of 3 bars in grey.

Mortar bars	Expansion (%) as a function of time (days)							
	3	10	17	24	31	38	45	52
MSK-1	-0.02	-0.01	-0.01	0.01	0.02	0.05	0.08	0.08
MSK-2	-0.02	-0.01	-0.01	0.01	0.02	0.04	0.07	0.08
MSK-3	0.00	-0.01	-0.01	0.00	0.02	0.03	0.06	0.07
MSK	-0.01	-0.01	-0.01	0.01	0.02	0.04	0.07	0.08
B&B-1	-0.01	0.00	0.01	0.01	0.02	0.02	0.03	0.03
B&B-2	-0.01	0.00	0.01	0.01	0.02	0.02	0.03	0.02
B&B-3	-0.01	0.00	0.01	0.01	0.02	0.02	0.03	0.02
***B&B	-0.01	0.00	0.01	0.01	0.02	0.02	0.03	0.02
DLS-1	0.00	0.00	0.02	0.06	0.11	0.16	0.20	0.23
DLS-2	0.00	0.00	0.02	0.05	0.10	0.15	0.19	0.22
DLS-3	0.00	0.00	0.02	0.05	0.09	0.13	0.18	0.20
DLS	0.00	0.00	0.02	0.05	0.10	0.15	0.19	0.22
GGP-1	-0.02	0.02	0.07	0.14	0.20	0.25	0.30	0.35
GGP-2	-0.02	0.02	0.07	0.14	0.20	0.25	0.31	0.35
GGP-3	-0.02	0.02	0.08	0.15	0.21	0.27	0.33	0.37
GGP	-0.02	0.02	0.08	0.15	0.20	0.26	0.32	0.35
SPH-1	-0.02	-0.01	0.02	0.12	0.25	0.39	0.49	0.59
SPH-2	-0.02	-0.02	0.01	0.10	0.22	0.35	0.45	0.54
SPH-3	-0.02	-0.01	0.02	0.12	0.25	0.37	0.48	0.56
SPH	-0.02	-0.01	0.02	0.11	0.24	0.37	0.47	0.56
GGP-1	-0.02	-0.01	0.00	0.01	0.02	0.05	0.07	0.09
GGP-2	-0.02	-0.01	0.00	0.01	0.02	0.05	0.07	0.08
GGP-3	-0.02	-0.02	-0.01	0.00	0.02	0.04	0.06	0.07
GGP	-0.02	-0.01	-0.01	0.01	0.02	0.04	0.07	0.08
PKA-1	-0.01	-0.01	-0.01	-0.01	-0.01	0.00	0.00	-0.01
PKA-2	-0.01	-0.01	-0.01	0.00	0.00	0.00	0.00	-0.01
PKA-3	-0.01	-0.01	-0.01	-0.01	-0.01	0.00	0.00	-0.01
PKA	-0.01	-0.01	-0.01	-0.01	-0.01	0.00	0.00	-0.01
SDBR-1	0.00	0.00	0.01	0.02	0.03	0.03	0.03	0.05
SDBR-2	0.00	0.01	0.02	0.02	0.03	0.04	0.04	0.05
SDBR-3	0.00	0.01	0.02	0.02	0.03	0.04	0.04	0.06
***SDBR	0.00	0.00	0.06	0.12	0.17	0.19	0.22	0.23

Table B21 (continued): Expansion values (%) with optimized conditions.

Mortar bars	Expansion (%) as a function of time (days)							
	59	66	74	81	87	90	94	102
MSK-1	0.12	0.15	0.15	0.17	0.20	0.21	0.22	0.23
MSK-2	0.11	0.15	0.15	0.17	0.20	0.20	0.22	0.23
MSK-3	0.10	0.14	0.14	0.16	0.18	0.19	0.21	0.22
MSK	0.11	0.15	0.14	0.17	0.19	0.20	0.22	0.23
B&B-1	0.03	0.05	0.03	0.04	0.05	0.06	0.07	0.09
B&B-2	0.03	0.04	0.03	0.04	0.05	0.05	0.07	0.07
B&B-3	0.03	0.05	0.03	0.04	0.05	0.05	0.06	0.08
***B&B	0.03	0.05	0.03	0.04	0.05	0.06	0.07	0.08
DLS-1	0.27	0.31	0.31	0.33	0.35	0.35	0.37	0.38
DLS-2	0.25	0.30	0.29	0.31	0.33	0.34	0.36	0.36
DLS-3	0.23	0.28	0.27	0.29	0.31	0.32	0.34	0.35
DLS	0.25	0.29	0.29	0.31	0.33	0.34	0.36	0.36
GGP-1	0.41	0.46	0.49	0.53	0.55	0.56	0.63	0.65
GGP-2	0.39	0.46	0.49	0.52	0.55	0.56	0.62	0.64
GGP-3	0.41	0.50	0.52	0.55	0.59	0.60	0.66	0.68
GGP	0.41	0.47	0.50	0.53	0.56	0.58	0.64	0.66
SPH-1	0.70	0.81	0.86	0.89	0.93	0.94	1.06	1.10
SPH-2	0.65	0.75	0.79	0.83	0.85	0.86	0.98	1.01
SPH-3	0.66	0.74	0.78	0.82	0.84	0.85	0.95	0.99
SPH	0.67	0.77	0.81	0.85	0.87	0.88	1.00	1.03
GGP-1	0.13	0.16	0.17	0.20	0.22	0.23	0.24	0.25
GGP-2	0.11	0.15	0.16	0.19	0.21	0.22	0.23	0.24
GGP-3	0.10	0.14	0.14	0.16	0.19	0.19	0.20	0.21
GGP	0.11	0.15	0.16	0.18	0.20	0.21	0.22	0.24
PKA-1	-0.02	0.01	-0.02	-0.01	0.00	0.00	0.01	0.01
PKA-2	-0.02	0.01	-0.01	0.00	0.01	0.00	0.01	0.02
PKA-3	-0.01	0.01	-0.01	-0.01	0.00	0.00	0.01	0.01
PKA	-0.02	0.01	-0.01	-0.01	0.00	0.00	0.01	0.02
SBR-1	0.06	0.05	0.06	0.06	0.07	0.07	0.09	0.10
SBR-2	0.06	0.06	0.07	0.08	0.09	0.09	0.11	0.12
SBR-3	0.07	0.07	0.08	0.09	0.10	0.10	0.13	0.14
***SDBR	0.06	0.06	0.07	0.08	0.08	0.09	0.11	0.12

Table B21 (continued): Expansion values (%) with optimized conditions.

Mortar bars	Expansion (%) as a function of time (days)							
	109	116	124	131	137	144	151	158
MSK-1	0.25	0.24	0.26	0.27	0.29	0.29	0.30	0.31
MSK-2	0.24	0.24	0.26	0.27	0.29	0.29	0.29	0.30
MSK-3	0.23	0.22	0.24	0.25	0.27	0.27	0.27	0.28
MSK	0.24	0.23	0.25	0.26	0.28	0.29	0.28	0.30
B&B-1	0.11	0.12	0.17	0.18	0.22	0.24	0.24	0.27
B&B-2	0.09	0.10	0.13	0.14	0.17	0.19	0.19	0.21
B&B-3	0.10	0.11	0.15	0.17	0.21	0.23	0.23	0.26
***B&B	0.10	0.11	0.15	0.17	0.20	0.22	0.22	0.25
DLS-1	0.39	0.37	0.40	0.39	0.40	0.40	0.38	0.39
DLS-2	0.37	0.36	0.38	0.38	0.39	0.39	0.37	0.38
DLS-3	0.36	0.35	0.36	0.34	0.37	0.37	0.36	0.37
DLS	0.38	0.36	0.38	0.37	0.39	0.39	0.37	0.38
GGP-1	0.66	0.66	0.67	0.67	0.69	0.69	0.68	0.69
GGP-2	0.66	0.66	0.67	0.67	0.68	0.68	0.67	0.68
GGP-3	0.70	0.70	0.71	0.71	0.72	0.72	0.71	0.72
GGP	0.67	0.67	0.68	0.68	0.70	0.70	0.68	0.70
SPH-1	1.11	1.10	1.13	1.13	1.14	1.14	1.13	1.14
SPH-2	1.03	1.02	1.03	1.05	1.06	1.06	1.05	1.06
SPH-3	1.00	0.99	1.01	1.01	1.03	1.03	1.01	1.03
SPH	1.04	1.04	1.06	1.06	1.08	1.08	1.06	1.07
GGP-1	0.25	0.24	0.26	0.26	0.27	0.27	0.27	0.27
GGP-2	0.24	0.24	0.26	0.26	0.26	0.27	0.26	0.26
GGP-3	0.22	0.21	0.22	0.23	0.23	0.23	0.23	0.23
GGP	0.24	0.23	0.25	0.25	0.26	0.26	0.25	0.26
PKA-1	0.02	0.02	0.03	0.03	0.04	0.04	0.02	0.03
PKA-2	0.02	0.03	0.03	0.03	0.04	0.04	0.03	0.04
PKA-3	0.02	0.02	0.03	0.03	0.04	0.04	0.02	0.03
PKA	0.02	0.02	0.03	0.03	0.04	0.04	0.02	0.03
SDBR-1	0.10	0.11	0.11	0.11	0.12	0.12	0.12	0.12
SDBR-2	0.13	0.13	0.13	0.14	0.15	0.15	0.15	0.15
SDBR-3	0.15	0.15	0.15	0.16	0.16	0.17	0.17	0.17
***SDBR	0.13	0.13	0.13	0.14	0.14	0.15	0.15	0.15

Table B21 (continued): Expansion values (%) with optimized conditions.

Mortar bars	Expansion (%) as a function of time (days)							
	165	172	179	187	193	200	207	214
MSK-1	0.33	0.34	0.35	0.36	0.38	0.39	0.40	0.42
MSK-2	0.32	0.33	0.34	0.35	0.37	0.38	0.38	0.40
MSK-3	0.29	0.30	0.31	0.32	0.33	0.34	0.35	0.37
MSK	0.31	0.32	0.34	0.35	0.36	0.37	0.38	0.40
B&B-1	0.29	0.31	0.33	0.34	0.36	0.37	0.38	0.40
B&B-2	0.23	0.25	0.27	0.28	0.30	0.31	0.32	0.34
B&B-3	0.28	0.30	0.32	0.34	0.35	0.37	0.38	0.39
***B&B	0.27	0.29	0.31	0.32	0.34	0.35	0.36	0.38
DLS-1	0.39	0.39	0.40	0.39	0.39	0.39	0.39	0.39
DLS-2	0.38	0.38	0.38	0.38	0.38	0.38	0.37	0.38
DLS-3	0.37	0.37	0.37	0.37	0.37	0.37	0.36	0.37
DLS	0.38	0.38	0.38	0.38	0.38	0.38	0.37	0.38
GGP-1	0.69	0.69	0.70	0.69	0.69	0.69	0.69	0.69
GGP-2	0.68	0.68	0.68	0.68	0.68	0.69	0.67	0.68
GGP-3	0.72	0.72	0.73	0.72	0.72	0.73	0.71	0.72
GGP	0.70	0.70	0.70	0.70	0.70	0.70	0.69	0.70
SPH-1	1.14	1.14	1.14	1.14	1.14	1.14	1.14	1.14
SPH-2	1.06	1.06	1.07	1.07	1.06	1.07	1.06	1.06
SPH-3	1.02	1.03	1.03	1.03	1.03	1.03	1.02	1.03
SPH	1.07	1.08	1.08	1.08	1.08	1.08	1.07	1.08
GGP-1	0.27	0.27	0.28	0.27	0.27	0.28	0.27	0.28
GGP-2	0.26	0.26	0.27	0.26	0.26	0.26	0.26	0.27
GGP-3	0.23	0.23	0.23	0.23	0.23	0.23	0.23	0.23
GGP	0.26	0.26	0.26	0.26	0.26	0.26	0.26	0.26
PKA-1	0.03	0.03	0.04	0.03	0.03	0.03	0.03	0.03
PKA-2	0.04	0.04	0.04	0.04	0.04	0.04	0.03	0.03
PKA-3	0.03	0.03	0.03	0.03	0.03	0.03	0.03	0.03
PKA	0.03	0.03	0.04	0.03	0.03	0.03	0.03	0.03
SDBR-1	0.13	0.13	0.14	0.14	0.14	0.15	0.15	0.16
SDBR-2	0.16	0.17	0.17	0.18	0.18	0.18	0.19	0.20
SDBR-3	0.19	0.19	0.19	0.20	0.20	0.21	0.21	0.22
***SDBR	0.16	0.17	0.17	0.17	0.18	0.18	0.18	0.19

Table B21 (continued): Expansion values (%) with optimized conditions.

Mortar bars	Expansion (%) as a function of time (days)							
	221	228	235	243	249	256	263	270
MSK-1	0.43	0.44	0.46	0.47	0.49	0.51	0.52	0.54
MSK-2	0.42	0.43	0.44	0.46	0.48	0.49	0.50	0.52
MSK-3	0.38	0.39	0.41	0.42	0.45	0.46	0.48	0.50
MSK	0.41	0.42	0.44	0.45	0.47	0.48	0.50	0.52
B&B-1	0.42	0.43	0.44	0.45	0.47	0.49	0.50	0.51
B&B-2	0.35	0.36	0.38	0.39	0.41	0.43	0.45	0.46
B&B-3	0.41	0.42	0.44	0.45	0.47	0.49	0.51	0.52
***B&B	0.39	0.40	0.42	0.43	0.45	0.47	0.48	0.50
DLS-1	0.39	0.39	0.39	0.39				
DLS-2	0.38	0.38	0.38	0.38				
DLS-3	0.36	0.37	0.37	0.37				
DLS	0.38	0.38	0.38	0.38				
GGP-1	0.69	0.69	0.69	0.69	0.69	0.69	0.68	0.69
GGP-2	0.68	0.67	0.68	0.67	0.68	0.68	0.67	0.67
GGP-3	0.72	0.72	0.72	0.72	0.72	0.72	0.72	0.72
GGP	0.70	0.69	0.69	0.69	0.70	0.70	0.69	0.70
SPH-1	1.14	1.14	1.14	1.14	1.14	1.15	1.15	1.14
SPH-2	1.07	1.06	1.06	1.07	1.06	1.06	1.06	1.07
SPH-3	1.03	1.03	1.03	1.03	1.03	1.03	1.03	1.03
SPH	1.08	1.08	1.08	1.08	1.08	1.08	1.08	1.08
GGP-1	0.28	0.28	0.28	0.28	0.29	0.28	0.28	0.29
GGP-2	0.27	0.27	0.27	0.27	0.27	0.27	0.27	0.27
GGP-3	0.23	0.23	0.23	0.24	0.24	0.24	0.24	0.24
GGP	0.26	0.26	0.26	0.26	0.27	0.26	0.26	0.27
PKA-1	0.03	0.03	0.03	0.03	0.03	0.03	0.04	0.03
PKA-2	0.03	0.03	0.03	0.04	0.04	0.04	0.04	0.04
PKA-3	0.03	0.03	0.03	0.03	0.03	0.03	0.03	0.04
PKA	0.03	0.03	0.03	0.03	0.03	0.03	0.04	0.04
SDBR-1	0.15	0.16	0.16	0.16	0.16	0.18	0.18	0.18
SDBR-2	0.19	0.20	0.20	0.21	0.21	0.22	0.22	0.23
SDBR-3	0.22	0.23	0.23	0.23	0.23	0.25	0.25	0.25
***SDBR	0.19	0.20	0.20	0.20	0.20	0.21	0.22	0.22

Table B21 (continued): Expansion values (%) with optimized conditions.

Mortar bars	Expansion (%) as a function of time (days)							
	277	284	291	298	304	312	319	326
MSK-1	0.56	0.57	0.58	0.60	0.62	0.63	0.65	0.67
MSK-2	0.54	0.55	0.56	0.57	0.59	0.60	0.62	0.64
MSK-3	0.52	0.53	0.55	0.56	0.59	0.61	0.65	0.71
MSK	0.54	0.55	0.56	0.58	0.60	0.61	0.64	0.67
B&B-1	0.54	0.55	0.57	0.59	0.62	0.63	0.66	0.69
B&B-2	0.48	0.50	0.52	0.54	0.57	0.59	0.61	0.64
B&B-3	0.55	0.56	0.58	0.61	0.63	0.66	0.68	0.72
***B&B	0.52	0.54	0.56	0.58	0.61	0.63	0.65	0.68
DLS-1								
DLS-2								
DLS-3								
DLS								
GGP-1	0.69	0.69	0.69	0.69	0.69	0.69	0.69	0.69
GGP-2	0.68	0.67	0.67	0.67	0.67	0.67	0.67	0.67
GGP-3	0.72	0.72	0.72	0.72	0.72	0.72	0.72	0.72
GGP	0.70	0.69	0.69	0.69	0.69	0.70	0.69	0.70
SPH-1	1.15	1.14	1.14	1.15	1.15	1.15	1.15	1.15
SPH-2	1.07	1.06	1.06	1.07	1.06	1.07	1.07	1.08
SPH-3	1.04	1.03	1.03	1.03	1.04	1.04	1.04	1.04
SPH	1.08	1.08	1.08	1.08	1.08	1.08	1.08	1.09
GGP-1	0.29	0.29	0.29	0.29	0.29	0.29	0.29	0.29
GGP-2	0.28	0.27	0.27	0.27	0.28	0.28	0.28	0.28
GGP-3	0.24	0.24	0.24	0.24	0.25	0.25	0.25	0.25
GGP	0.27	0.27	0.27	0.27	0.27	0.27	0.27	0.27
PKA-1	0.04	0.04	0.04	0.04	0.04	0.04	0.04	0.04
PKA-2	0.04	0.04	0.04	0.04	0.04	0.04	0.04	0.04
PKA-3	0.04	0.04	0.04	0.04	0.04	0.04	0.04	0.04
PKA	0.04	0.04	0.04	0.04	0.04	0.04	0.04	0.04
SDBR-1	0.19	0.19	0.19	0.19	0.20			
SDBR-2	0.23	0.23	0.23	0.24	0.25			
SDBR-3	0.26	0.27	0.26	0.27	0.28			
***SDBR	0.23	0.23	0.23	0.23	0.24			

B7.5.2 Expansion (%) as a function of time (days).

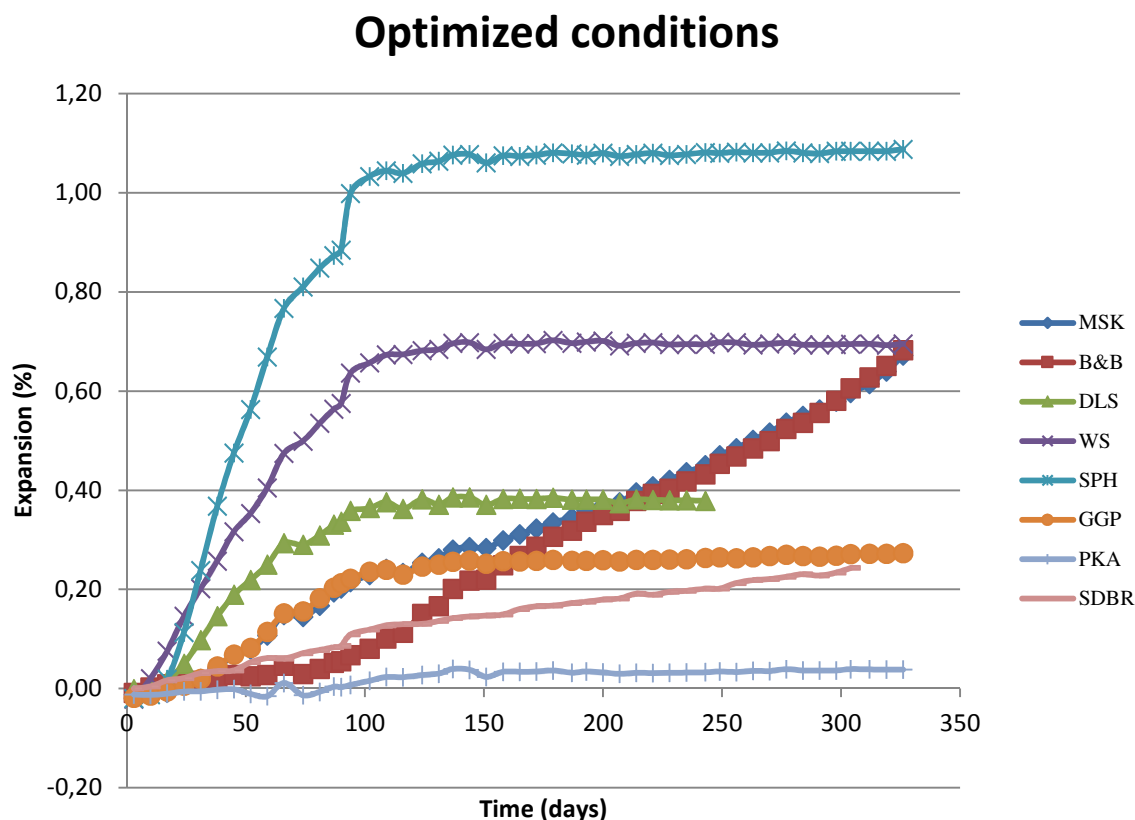


Figure B.23: Expansion of mortar specimens stored at 80°C/80% RH, with immersion (twice per week) in bleach (6%) solution. The specimens are transferred at low temperature (4°C/100%RH) after 90 days, while pursuing immersion (twice per week) in bleach (6%) solution. Each curve in this figure corresponds to the average values obtained from a set of three bars.

***The expansion observed for the mortar bars specimens elaborated with **B&B aggregate** and **SDBR aggregate** do not express correctly the deterioration that occurs in such aggregates. Those aggregates, due to their high content in iron sulfides, after a few wetting and drying cycles, start to lose the oxidized particles instead of expand (Figure: B.23 and B.24). This trend is observed for specimens manufactured with the SDBR aggregate during the two phases of the test. The specimens manufactured with the B&B aggregate show very low expansion values during the first phase of the test, but after transfer to low temperature there is an increase of the expansion values, overlaying the expansion values obtained with the MSK aggregate.

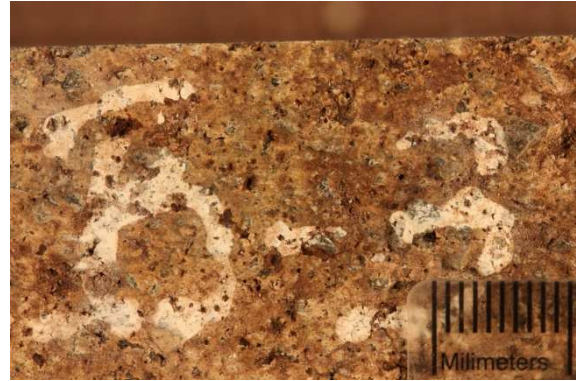


Figure B.24: Mortar bar made with B&B riche aggregate at 90 days before being transferred to low temperature, soaked 2 times per week in a bleach (6%) solution and stored at 80°C/80%RH.

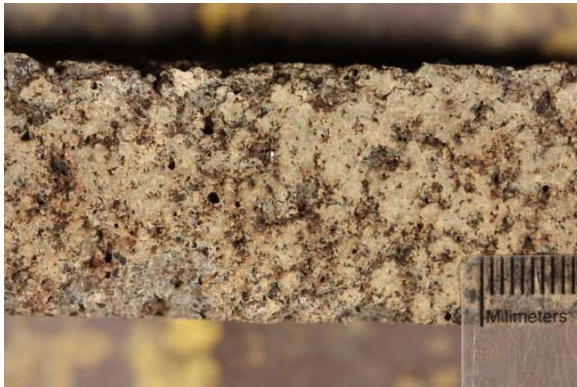


Figure B.25: The same mortar bar made with B&B riche aggregate at 300 days of testing.



Figure B. 26: The same mortar bar made with B&B riche aggregate at 438 days of testing.



Figure B. 27: Mortar bar made with SDBR aggregate after 90 days before being transferred to low temperature, soaked 2 times per week in a bleach (6%) solution and stored at 80°C/80%RH.

Appendix C
Petrographic description of the rock facies from Maskimo and
B&B of Saint-Boniface quarries.

C1: Introduction


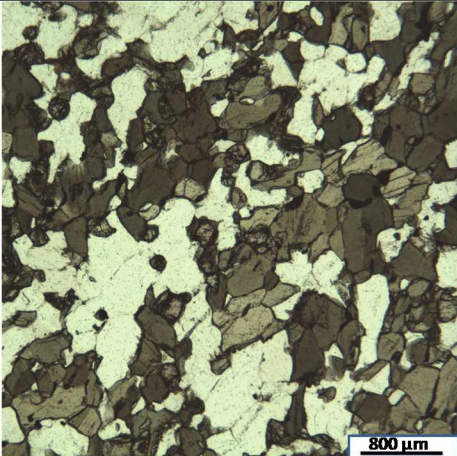
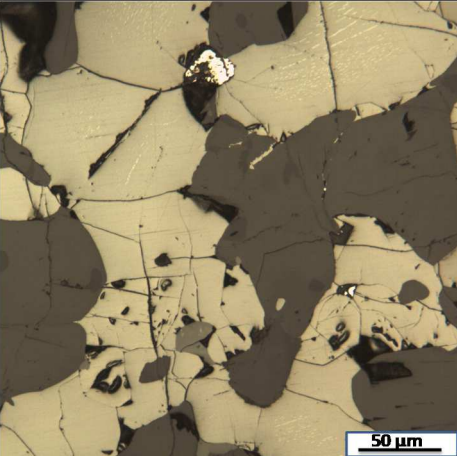
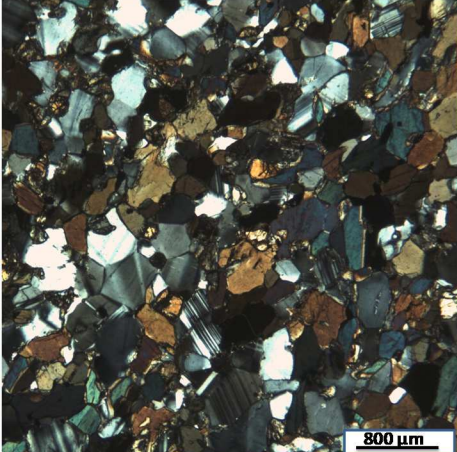

Samples from all the different geological facies present in the Maskimo and B&B quarries were identified and collected for posterior petrographic classification and chemical analysis.

The microscopic analysis was made using polished thin sections (25mm x 45 mm). For each different facies one or two polished thin sections were produced. The thin sections were polished using SiC (silicon carbide) and loose alumina as abrasive powders. The thin sections were examined using a transmitted and reflected light microscope (Nikon Eclipse E600 Pol).


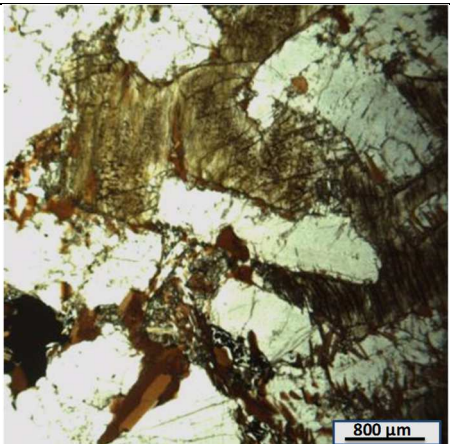
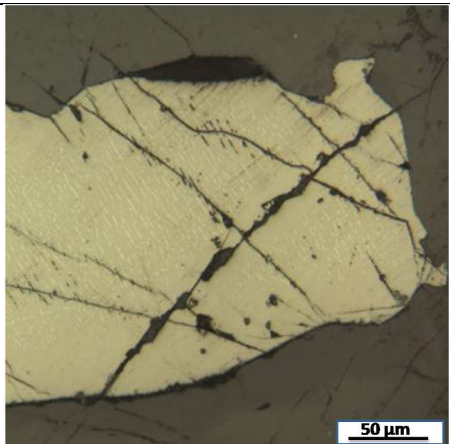
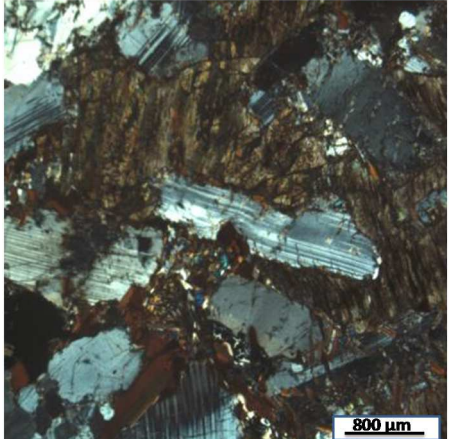
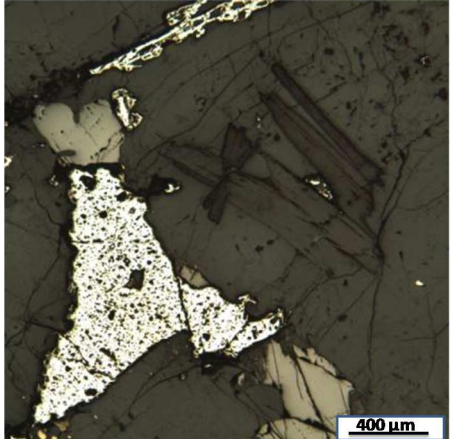
The percentage of minerals was calculated using a point counter.

C1.1 Rock facies classification: Maskimo quarry


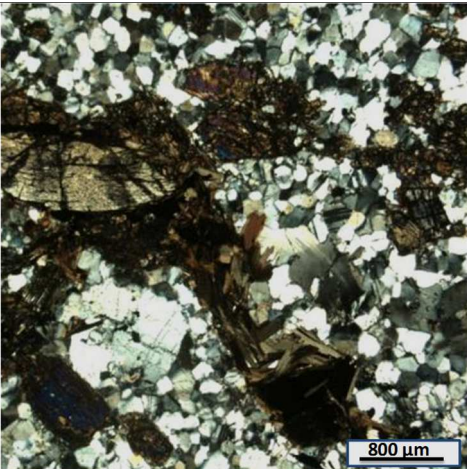
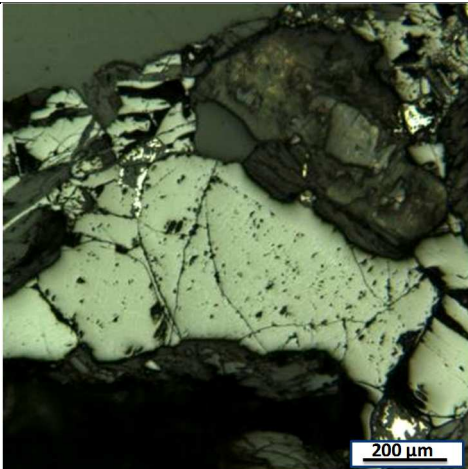
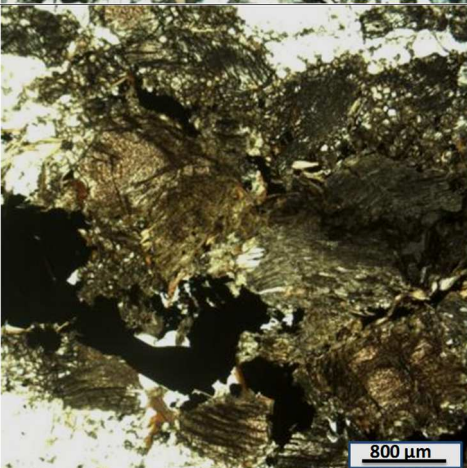
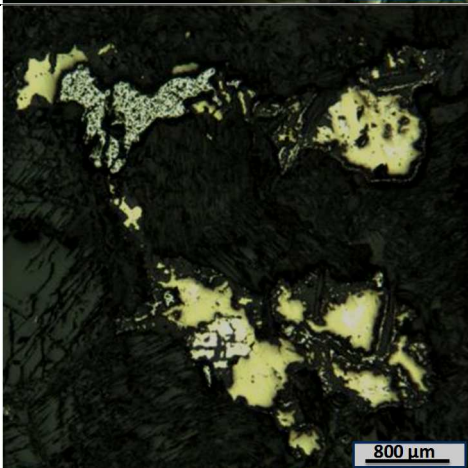
C1.1.1MSK-1: Granodiorite

Macroscopic description	
	<p>Grain size: fine grained</p> <p>Colour: dark gray</p> <p>Structure: massive</p>
Microscopic description	
Mineralogy (%)	Opaque minerals: 6.2%
<p>Plagioclase: 25.2%</p> <p>Amphibole: 49.0%</p> <p>Pyroxene: 5.5%</p> <p>Quartz: 12.9%</p> <p>Opaque: 6.2%</p> <p>Feldspar: 12%</p>	<p>Pyrrhotite: 95%</p> <p>Pyrite: 4%</p> <p>Chalcopyrite: 1%</p> <p>Pentlandite</p>
	
	


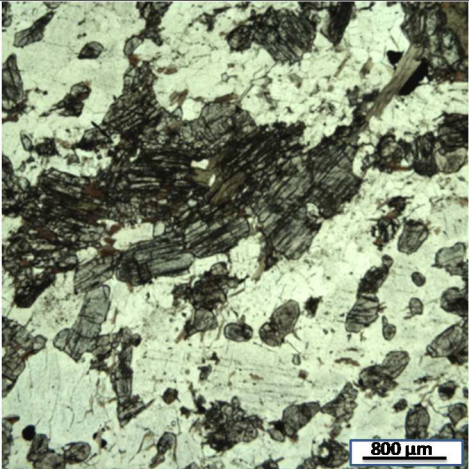
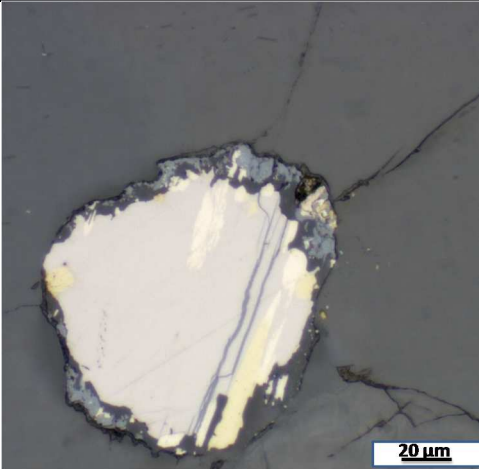
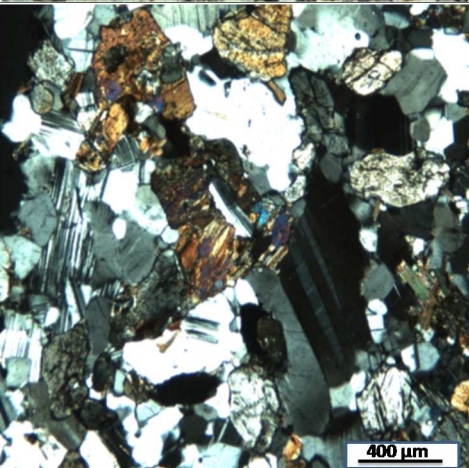
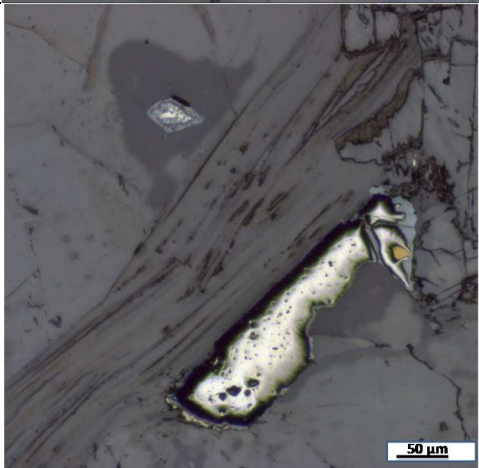
C1.1.2 MSK-2: Gabbro

Macroscopic description	
	<p>Grain size: medium grained</p> <p>Colour: dark gray</p>
Microscopic description	
Mineralogy (%)	Opaque minerals: 1.4%
<p>Plagioclase: 70.8%</p> <p>Pyroxene (altered): 16.0%</p> <p>Quartz: 4.4%</p> <p>Opaque: 1.4%</p> <p>Feldspar: 3.3%</p> <p>Biotite: 3.9%</p> <p>Carbonates/others: 0.2%</p>	<p>Pyrrhotite: 45%</p> <p>Pyrite: 50%</p> <p>Chalcopyrite: 5%</p> <p>Pentlandite</p>
	
	


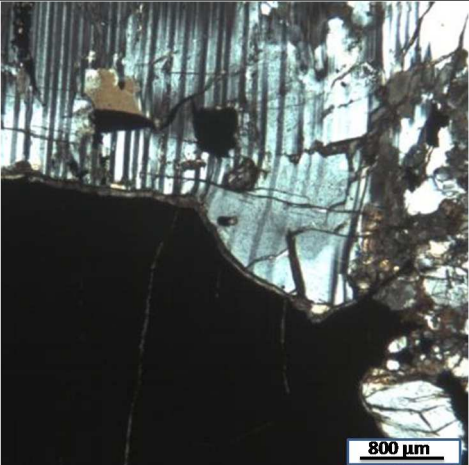
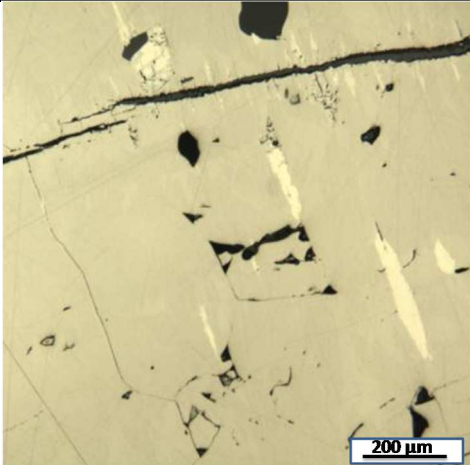

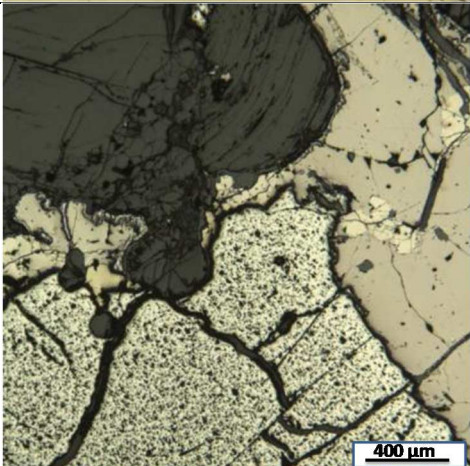
C1.1.3MSK-3 Metagabbro

Macroscopic description	
	Grain size: medium grained Colour: dark greenish-gray
Microscopic description	
Mineralogy (%)	Opaque minerals: 4.3%
Plagioclase: 27.4% Pyroxenes and pyroxenes altered to amphibole: 37.9% Quartz: 16.8% Opaque: 4.3% Biotite: 6% Epidote: 2%	Pyrite : 95% Chalcopyrite : 3% Magnetite : 2%
	
	

C1.1.4 MSK-4 Granodiorite


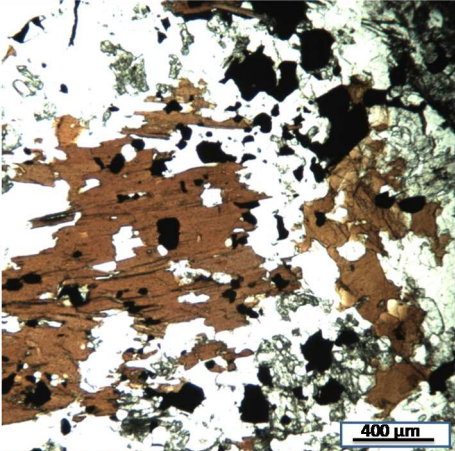
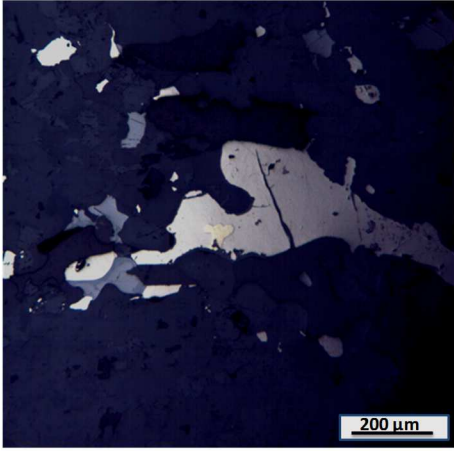
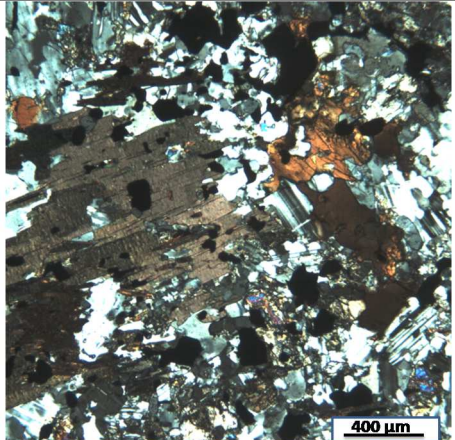
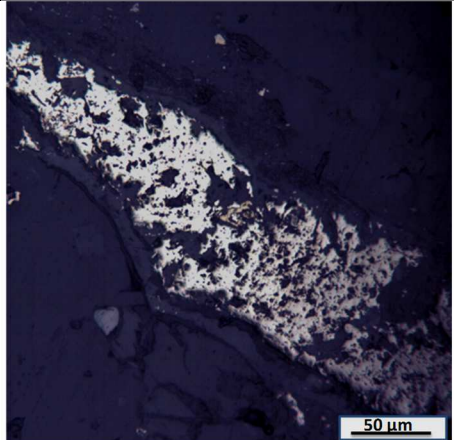
Macroscopic description	
	Grain size: Fine grained Colour: brownish gray
Microscopic description	
Mineralogy (%) Plagioclase: 37.7% Pyroxenes: 34.1% Quartz :16.8% Opaque: 0.5% Biotite: 4.9%	Opaque minerals: 0.5 % Pentlandite Pyrite Chalcopyrite
	
	

C1.1.5 MSK-5 Anorthosite


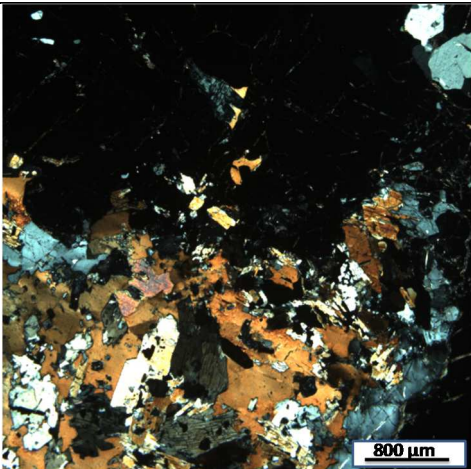
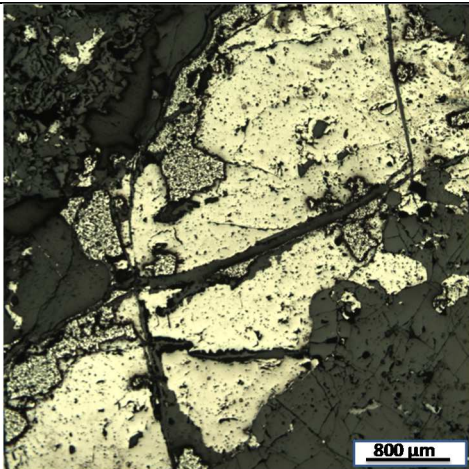
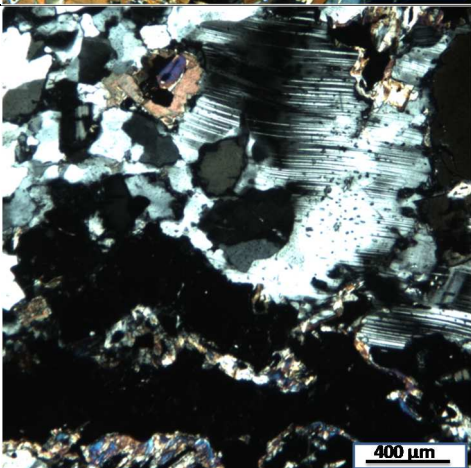
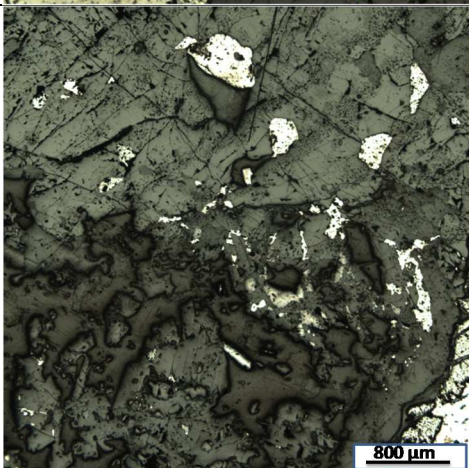
Macroscopic description	
	Grain size: Fine grained Colour: dark gray
Microscopic description	
Mineralogy (%)	Opaque minerals: 43%
Plagioclase: 14.9% Pyroxene: 38% Quartz: 0% Opaque: 43.0% Biotite: 1.6% Feldspar: 0.8% Carbonates: 2%	65% pyrrhotite 32% pyrite 3% chalcopyrite pentlandite
	
	

C1.2 Rock facies classification: B&B quarry


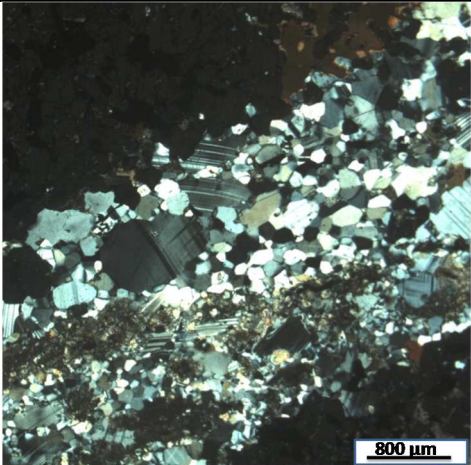
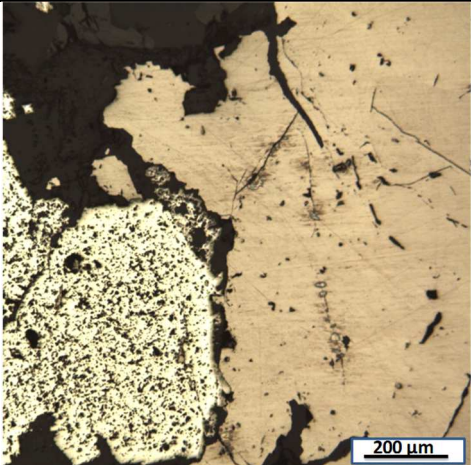
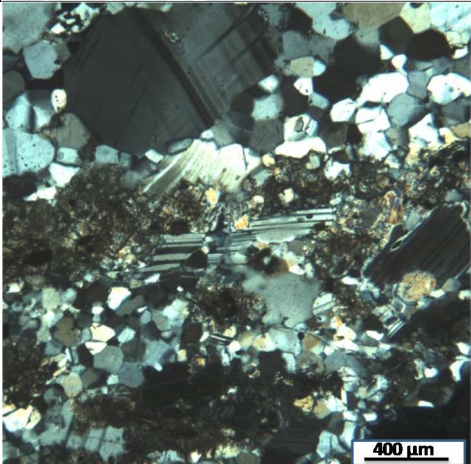
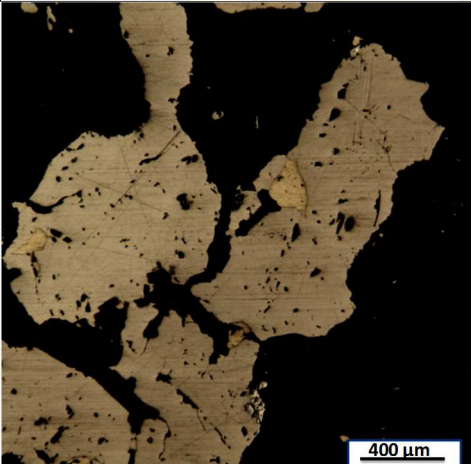
C1.2.1 B&B-1: Gabbro

Macroscopic description	
	Grain size: Fine grained Colour: dark gray
Microscopic description	
Mineralogy (%)	Opaque minerals: 10.3 %
Pyroxenes: 45.1% Plagioclase: 26.8% Quartz: 10.8% Opaque :10.3% Biotite: 4.7% K Feldspar: 1.6% Carbonates: 0.7%	Pyrrhotite: 50% Pyrite: 45% Chalcopyrite: 5%
	
	


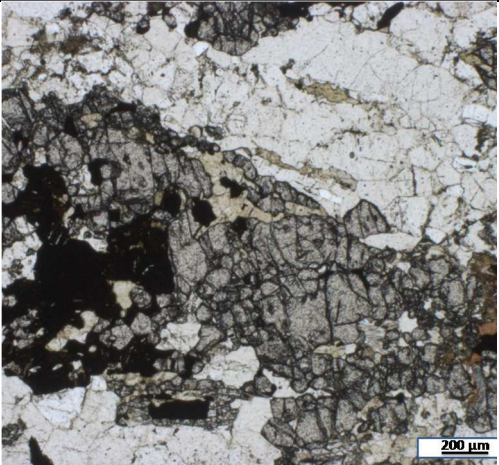
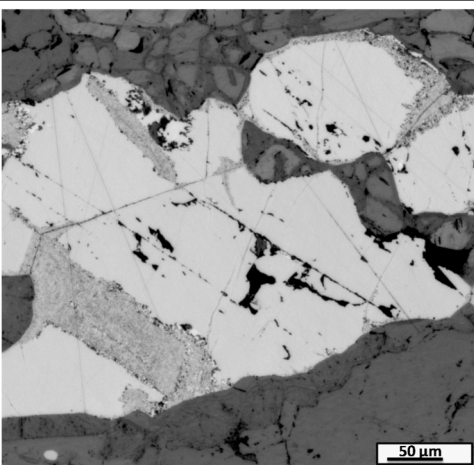

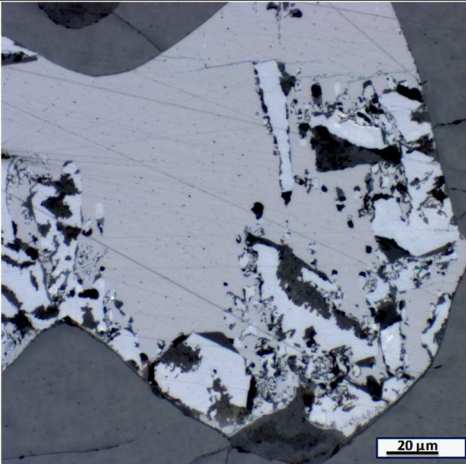
C1.2.2 B&B-2 Anorthositic metagabbro

Macroscopic description	
	Grain size: coarse Colour: medium gray and dark pink (garnet)
Microscopic description	
Mineralogy (%)	Opaque minerals: 7.7 %
Quartz 54.4% Garnet 19.7% Opaque 7.7% Pyroxenes 7% Plagioclase 4.3% Biotite 4.3% Feldspar 1,8% Carbonates 0,8%	Pyrrhotite 90% Pyrite 8% Chalcopyrite 2%
	
	


C1.2.3 B&B-3 Garnet metagabbro

Macroscopic description	
	Grain size: medium Colour: pink medium gray
Microscopic description	
Mineralogy (%)	Opaque mineral: 12.4 %
Granet : 29.3% Amphibole : 17.2% Quartz : 17.0% Plagioclase : 15.8% Opaque : 12.4% Biotite : 6.3% Feldspar : 1.8% Chlorite : 0.2%	Pyrrhotite: 55% Pyrite: 40% Chalcocopyrite: 5%
	
	

C1.2.4 B&B-4 Granodiorite

Macroscopic description		
		Grain size: Fine grained Colour: dark gray
Microscopic description		
Mineralogy (%)	Opaque minerals: 20 %	
Pyroxene : 34.8% Plagioclase : 26.5% Opaque : 17.8% Quartz : 14.3% Calcite : 3.9% Biotite: 1.8% Feldspar: 0.9%	Pyrrhotite : 50% Pyrite : 45% Chalcopyrite : 5% Pentlandite : traces	
		
		

C1.2.5 B&B-5 Metamorphosed granodiorite

Macroscopic description	
	Grain size: Fine grained Colour: greenish gray
Microscopic description	
Mineralogy (%)	Opaque minerals: 2.7 %
Quartz 67.6% Granet 17.2 Plagioclase 7.4% Opaque 2.7% Chlorite 1.4% Biotite 1.8% Carbonates 0.7% Pyroxenes 0.6% K Feldspar 0.6%	Pyrite : 95% Chalcopyrite : 3% Pentlandite : 2%
